

FINAL REPORT

Volume 1: Main Report

Dynamic Stability Analysis of Estates Dam

Oakland, California

NOVEMBER 2006



Prepared for
East Bay Municipal
Utility District
375 Eleventh Street
Oakland, CA 94607



URS

URS Corporation
1333 Broadway, Suite 800
Oakland, CA 94612

26814957.E0000



November 3, 2006

Mr. Dar Chen, Project Manager
East Bay Municipal Utility District
375 – 11th Street
Oakland, CA 94607-4240

**Subject: Dynamic Stability Analysis of Estates Dam
Final Engineering Report**

Dear Mr. Chen:

In accordance with the requirements of our contract with the District, dated 2 November 2004, we are pleased to submit herewith our final engineering report on the dynamic stability analysis of Estates Dam. We previously submitted the report in draft final form on March 28, 2006, for review by the District. The District's comments have been addressed and incorporated into the final report.

The report is submitted in two volumes as follows:

- Volume 1 - Main report
- Volume 2 - Appendices

The study was carried out by URS with support from our subconsultants Robert Y. Chew Geotechnical Inc., HQE Inc., John Wakabayashi, and DotDat.inc.

It has been a pleasure working with you on this interesting assignment and we look forward to continuing to serve the District on future projects. If you have any questions regarding the report or if we can be of any other service, please do not hesitate to contact the undersigned.

Yours truly,

URS Corporation


Lelio H. Mejia, PhD, GE
Project Manager



Enclosures: Final Engineering Report, Volumes 1 and 2 (14 copies)

FINAL REPORT

VOLUME 1

**DYNAMIC STABILITY ANALYSIS
OF ESTATES DAM**

OAKLAND, CALIFORNIA

Prepared for

East Bay Municipal Utility District
375 Eleventh Street
Oakland, California 94607

November, 2006

URS

URS Corporation
1333 Broadway, Suite 800
Oakland, California 94612

26814957.E0000

TABLE OF CONTENTS

VOLUME 1

Executive Summary	ES-1
Section 1 Introduction	1-1
1.1 Background.....	1-1
1.2 Purpose and Objectives.....	1-1
1.3 Previous Investigations.....	1-1
1.4 Report Organization.....	1-1
Section 2 Scope of Work	2-1
Section 3 Project Description	3-1
3.1 Site Setting.....	3-1
3.2 Description of Dam.....	3-1
3.3 Appurtenant Facilities.....	3-1
3.4 Construction History.....	3-1
3.5 Performance and Monitoring.....	3-2
Section 4 Field and Laboratory Investigations	4-1
4.1 Field Investigations.....	4-1
4.1.1 Rotary Wash Drilling.....	4-1
4.1.2 Hammer Energy Measurements.....	4-2
4.1.3 Downhole Geophysical Surveys.....	4-2
4.2 Laboratory Testing.....	4-2
Section 5 Geological Setting	5-1
5.1 Regional Geology	5-1
5.2 Site Geology.....	5-1
5.3 Fault Rupture	5-2
Section 6 Site - Specific Earthquake Ground Motions	6-1
6.1 General Approach.....	6-1
6.2 Seismic Sources	6-1
6.3 Design Response Spectra.....	6-2
6.3.1 Site Conditions.....	6-2
6.3.2 Attenuation Relationships.....	6-2
6.3.3 Deterministic Ground Motion Analysis.....	6-2
6.3.4 Fault Rupture Directivity Effects.....	6-3
6.3.5 Design Response Spectra.....	6-3
6.4 Spectrum-Compatible Acceleration Time Histories.....	6-4

TABLE OF CONTENTS

Section 7	Embankment and Foundation Conditions.....	7-1
7.1	Dam Materials and Zonation	7-1
7.2	Embankment Conditions.....	7-2
7.2.1	1903 Fill.....	7-2
7.2.2	1938-39 Fill.....	7-3
7.3	Foundation Conditions.....	7-5
7.3.1	Foundation Soils	7-5
7.3.2	Bedrock.....	7-6
7.4	Groundwater Conditions.....	7-6
Section 8	General Analysis Approach.....	8-1
Section 9	Limit Equilibrium Stability Analyses.....	9-1
9.1	Analytical Procedures	9-1
9.2	Cross Sections.....	9-1
9.3	Material Properties.....	9-1
9.4	Analysis Results.....	9-1
Section 10	Dynamic Response Analyses.....	10-1
10.1	Methodology.....	10-1
10.2	Dynamic Material Properties	10-1
10.2.1	Shear Wave Velocities.....	10-2
10.2.2	Modulus Reduction and Damping Relationships	10-2
10.3	Analysis Results.....	10-2
10.3.1	1989 Loma Prieta Earthquake.....	10-3
10.3.2	Hayward-Rogers Creek Fault Mce	10-3
10.3.3	San Andreas Fault Mce.....	10-4
Section 11	Seismic Stability Analyses	11-1
11.1	Approach.....	11-1
11.2	Evaluation of Potential Strength Loss in Embankment and Foundation Soils	11-1
11.2.1	Evaluation Procedures	11-1
11.2.2	Potential for Strength Loss.....	11-3
11.3	Post-Earthquake Slope Stability	11-3
11.4	Deformation Analyses	11-3
11.4.1	Methodology.....	11-3
11.4.2	Yield Acceleration Evaluation.....	11-3
11.4.3	Analysis Results.....	11-4
11.5	Sensitivity of Calculated Deformations to Ground Motion Time Histories	11-5
11.5.1	Additional Ground Motion Time Histories.....	11-5
11.5.2	Simplified Newmark Analysis.....	11-5

TABLE OF CONTENTS

Section 12	Nonlinear Analyses	12-1
12.1	Methodology	12-1
12.2	Material Properties.....	12-1
12.3	Analysis Results.....	12-2
12.3.1	1989 Loma Prieta Earthquake.....	12-2
12.3.2	Hayward-Rogers Creek Fault Mce	12-2
12.3.3	San Andreas Fault Mce.....	12-3
Section 13	Three Dimensional Stability Effects.....	13-1
13.1	Approach.....	13-1
13.2	Three Dimensional Slope Stability Analysis	13-1
13.3	Dynamic Response Analysis.....	13-2
13.4	Deformation Analysis Results	13-3
Section 14	Expected Dam Performance	14-1
Section 15	Conclusions	15-1
Section 16	References	16-1

Tables

Table 3-1	Existing Piezometers at Estates Dam
Table 4-1	Summary of Borings
Table 6-1	Main Earthquake Sources in the Region
Table 6-2	Selected Attenuation Relationships
Table 6-3	Calculated Horizontal Peak Ground Acceleration
Table 6-4	Recommended Design Response Spectral Values
Table 6-5	Earthquake Records Used to Develop Time Histories for Hayward-Rodgers Creek Fault and San Andreas Fault MCEs
Table 7-1	Representative Index Properties of Embankment and Foundation Materials(1)
Table 7-2	Strength Parameters for Embankment and Foundation Soils
Table 7-3	Comparison of Effective Stress Strength Parameters Between This and Previous Studies
Table 7-4	Comparison of Total Stress Strength Parameters Between This and Previous Studies
Table 9-1	UTEXAS3 Input Parameters for Static Stability Analysis - Long Term Condition
Table 9-2	UTEXAS3 Input Parameters for Seismic Stability Analysis - Pre-Earthquake Condition
Table 10-1	Material Parameters for Dynamic Response Analysis
Table 11-1	UTEXAS3 Input Parameters for Seismic Stability Analysis – Post-Earthquake Condition
Table 11-2	Yield Acceleration Coefficients of Selected Sliding Blocks
Table 11-3	Calculated Horizontal Displacement in Newmark-type Analyses
Table 11-4	Calculated Horizontal Displacements in Newmark-type and Simplified Newmark Analyses
Table 12-1	Material Properties for Static Stress Analysis
Table 12-2	Material Properties for Dynamic Analysis
Table 12-3	Calculated Downstream Slope Horizontal Displacements (in feet)
Table 12-4	Calculated Crest Vertical Displacements (in feet)
Table 13-1	Calculated Factors of Safety and Yield Acceleration Coefficients
Table 13-2	Calculated Downstream Horizontal Displacements (in feet)

List of Tables, Figures and Appendices

Figures

- Figure 1-1 Site Location Map
- Figure 3-1 Location of Estates Dam and Reservoir
- Figure 3-2 Site Plan
- Figure 4-1 Locations of Previous Field Explorations
- Figure 4-2 Locations of Field Explorations
- Figure 5-1 Geological Map of the Estates Reservoir Area
- Figure 6-1 Map of Regional Seismic Sources
- Figure 6-2 Calculated 84th-percentile Acceleration Response Spectra for Hayward-Rodgers Creek Fault MCE
- Figure 6-3 Calculated 84th-percentile Acceleration Response Spectra for San Andreas Fault MCE
- Figure 6-4 Design Acceleration Response Spectra for Hayward-Rodgers Creek Fault MCE
- Figure 6-5 Design Acceleration Response Spectra for San Andreas Fault MCE
- Figure 6-6 Recorded Time History, 1992 Landers, CA, Earthquake at Lucerne Valley Station, Horizontal Component, 270 deg.
- Figure 6-7 Acceleration Response Spectra, 1992 Landers, CA, Earthquake at Lucerne Valley Station, Horizontal Component 270 deg.
- Figure 6-8 Recorded Time History, 1995 Kobe, Japan Earthquake at KJMA Station, Horizontal Component, 142 deg. (Rotated)
- Figure 6-9 Acceleration Response Spectra, 1995 Kobe, Japan Earthquake at KJMA Station, Horizontal Component, 142 deg.
- Figure 6-10 Recorded Time History, 2002 Denali, Alaska, Earthquake at Carlo, Alaska Station, Horizontal Component, 360 deg.
- Figure 6-11 Acceleration Response Spectra, 2002 Denali, Alaska, Earthquake at Carlo, Alaska Station, Horizontal Component 360 deg.
- Figure 6-12 Hayward-Rodgers Creek Fault Event, Recommended Time History # 1
- Figure 6-13 Hayward-Rodgers Creek Fault Event, Recommended Time History # 2
- Figure 6-14 Comparison of Acceleration Response Spectra for Hayward-Rodgers Creek Fault Event
- Figure 6-15 San Andreas Fault Event, Recommended Time History
- Figure 6-16 Comparison of Acceleration Response Spectra for San Andreas Fault Event
- Figure 7-1 Locations of Field Explorations
- Figure 7-2 GIS Model – Isometric View of Dam with Sample Classifications
- Figure 7-3 Cross Section A-A'

List of Tables, Figures and Appendices

Figure 7-4	Cross Section B-B'
Figure 7-5	Fines Content Data From Current and Previous Investigations
Figure 7-6	Gravel Content Data From Current and Previous Investigations
Figure 7-7	Blow Counts Data From Current and Previous Investigations
Figure 7-8	Gradation of 1903 Fill
Figure 7-9	Fines Content of Embankment and Foundation Materials
Figure 7-10	Gravel Content of Embankment and Foundation Materials
Figure 7-11	Atterberg Limits of Embankment and Foundation Materials
Figure 7-12	Water Content of Embankment and Foundation Materials
Figure 7-13	Dry Density of Embankment and Foundation Materials
Figure 7-14	Total Density of Embankment and Foundation Materials
Figure 7-15	Effective Stress Strength Data from Current and Previous Investigations
Figure 7-16	Total Stress Strength Data from Current and Previous Investigations
Figure 7-17	Effective Stress Strength of Embankment and Foundation Materials
Figure 7-18	Total Stress Strength of Embankment and Foundation Materials
Figure 7-19	Liquefaction Susceptibility Chart for Embankment and Foundation Materials
Figure 7-20	Gradation of 1938–1939 Fill
Figure 7-21	Gradation of Foundation Soil
Figure 9-1	Plan View of Analysis Section A-A'
Figure 9-2	Idealized Section A-A' For Slope Stability Analysis
Figure 9-3	Modified Section A-A' For Slope Stability Analysis
Figure 9-4	Slope Stability Analysis Long-Term Condition
Figure 9-5	Slope Stability Analysis Pre-Earthquake Condition
Figure 9-6	Slope Stability Analysis Selected Critical Sliding Blocks Section A-A'
Figure 9-7	Slope Stability Analysis Selected Critical Sliding Blocks Modified Section A-A'
Figure 10-1	Finite Element Mesh for Cross-Section A-A', QUAD4M Analysis
Figure 10-2	Recorded Time History, 1989 Loma Prieta, CA Earthquake at Piedmont Jr. High School Station, Horizontal Component, 045 deg.
Figure 10-3	Seismic Wave Velocity Profile and Stratigraphy from Borings B1, 2, and 3
Figure 10-4	Seismic Wave Velocity Profiles and Stratigraphy from Boring VQ-38
Figure 10-5	Seismic Wave Velocity Profile and Stratigraphy from Boring VQ-40
Figure 10-6	Selected Element Locations For Stress Time-history Plots QUAD4M Analysis
Figure 10-7	Selected Nodal Points For Acceleration Outputs QUAD4M Analysis

List of Tables, Figures and Appendices

- Figure 10-8 Sliding Blocks for Newmark Deformation Analyses Cross Section A-A'
- Figure 10-9 Peak Horizontal Acceleration QUAD4M Analysis, 1989 Loma Prieta Earthquake
- Figure 10-10 Average Mass Acceleration QUAD4M Analysis, 1989 Loma Prieta Earthquake
- Figure 10-11 Peak Horizontal Acceleration, QUAD4M Analysis, Cross-Section A-A', Hayward Fault Event TH #1
- Figure 10-12 Acceleration Time History, 175 FT Offset Upstream, QUAD4M Analysis, Hayward Fault Event TH #1
- Figure 10-13 Average Mass Acceleration, QUAD4M Analysis, Hayward Fault MCE TH #1
- Figure 10-14 Shear Stress Time History Beneath Crest, Elements 465, 469, and 475, Hayward Fault MCE TH #1
- Figure 10-15 Peak Horizontal Acceleration, QUAD4M Analysis, Cross-Section A-A', Hayward Fault Event TH #2
- Figure 10-16 Shear Stress Time History Beneath Crest, Elements 465, 469, and 475, Hayward Fault MCE TH #2
- Figure 10-17 Peak Horizontal Acceleration, QUAD4M Analysis, San Andreas Fault MCE
- Figure 10-18 Shear Stress Time History Beneath Crest, Elements 465, 469, and 475, San Andreas Fault MCE
- Figure 11-1 Cyclic Strength and Undrained Strength Degradation of Saturated Embankment Fills and Foundation Soils
- Figure 11-2 Total Stress Strength Data from Post-Cyclic Consolidated Undrained Triaxial Tests
- Figure 11-3 Slope Stability Analysis Selected Critical Sliding Blocks Post-Earthquake Conditions
- Figure 11-4 Newmark Deformation Analysis, Calculated Displacement, U/S Block #1, Hayward Fault MCE TH #1
- Figure 11-5 Newmark Deformation Analysis, Calculated Displacement, D/S Block #2, Hayward Fault MCE TH #1
- Figure 11-6 Newmark Deformation Analysis, Calculated Displacement, D/S Block #3, Hayward Fault MCE TH #1
- Figure 11-7 Newmark Deformation Analysis, Calculated Displacement, U/S Block #1, Hayward Fault MCE TH #2
- Figure 11-8 Newmark Deformation Analysis, Calculated Displacement, C/S Block #2, Hayward Fault Event TH #2
- Figure 11-9 Newmark Deformation Analysis, Calculated Displacement, D/S Block #3, Hayward Fault Event TH #2
- Figure 11-10 Hayward-Rodgers Creek Fault MCE, Recommended Time History #3

List of Tables, Figures and Appendices

- Figure 11-11 Comparison of Acceleration Response Spectra for Hayward-Rodgers Creek Fault MCE, Time History #3
- Figure 11-12 Hayward-Rodgers Creek Fault MCE, Recommended Time History #4
- Figure 11-13 Comparison of Acceleration Response Spectra for Hayward-Rodgers Creek Fault MCE, Time History #4
- Figure 11-14 Recorded Time History 1978 Tabas, Iran Earthquake at Tabas Station, Horizontal Component, 344 deg.
- Figure 11-15 1978 Tabas, Iran Earthquake at Tabas Station, Horizontal Component, 344 Degree
- Figure 11-16 Recorded Time History 1989 Loma Prieta, CA Earthquake at UCSC – LGPC Station, Horizontal Component, 000 deg.
- Figure 11-17 1989 Loma Prieta, CA Earthquake at UCSC – LGPC Station, Horizontal 000 deg Component
- Figure 11-18 Simplified Newmark Analysis, Calculated Displacement, Assumed $K_y = 0.05$, Hayward Fault MCE TH #1
- Figure 11-19 Simplified Newmark Analysis, Calculated Displacement, Assumed $K_y = 0.05$, Hayward Fault MCE TH #2
- Figure 11-20 Simplified Newmark Analysis, Calculated Displacement, Assumed $K_y = 0.05$, Hayward Fault MCE TH #3
- Figure 11-21 Simplified Newmark Analysis, Calculated Displacement, Assumed $K_y = 0.05$, Hayward Fault MCE TH #4
- Figure 11-22 Simplified Newmark Analysis, Calculated Displacement, Assumed $K_y = 0.05$, San Andreas Fault MCE
- Figure 11-23 Simplified Newmark Analysis, Calculated Displacement, Assumed $K_y = 0.05$, Tabas Earthquake, Tabas 344
- Figure 11-24 Simplified Newmark Analysis, Calculated Displacement, Assumed $K_y = 0.05$, Loma Prieta EQ, LGPC 000
- Figure 11-25 Simplified Newmark Analysis, Calculated Displacement, Assumed $K_y = 0.05$, Loma Prieta Earthquake
- Figure 12-1 Finite Difference Mesh for Cross-Section A-A', FLAC Analysis
- Figure 12-2 FLAC Analysis, Pore Pressure Generation Model
- Figure 12-3 Cyclic Strength and Undrained Strength Degradation of Saturated Embankment Fills and Foundation Soils
- Figure 12-4 FLAC Static Analysis, Downstream Slope, Pre-Earthquake Stability
- Figure 12-5 FLAC Static Analysis Upstream Slope, Pre-Earthquake Stability
- Figure 12-6 FLAC Static Analysis, Downstream Slope, Post-Earthquake Stability
- Figure 12-7 FLAC Static Analysis, Upstream Slope, Post-Earthquake Stability

List of Tables, Figures and Appendices

- Figure 12-8 FLAC Dynamic Analysis with Assumed Strength Degradation, Permanent Horizontal Displacement, Hayward MCE TH #1
- Figure 12-9 FLAC Dynamic Analysis with Assumed Strength Degradation, Permanent Vertical Displacement, Hayward MCE TH #1
- Figure 12-10 FLAC Dynamic Analysis, Locations of Displacement, Time History
- Figure 12-11 FLAC Dynamic Analysis with Assumed Strength Degradation, Horizontal Displacement Time Histories, Hayward MCE TH #1
- Figure 12-12 FLAC Dynamic Analysis with Assumed Strength Degradation, Vertical Displacement Time Histories, Hayward MCE TH #1
- Figure 12-13 FLAC Dynamic Analysis with Assumed Strength Degradation, Permanent Horizontal Displacement, Hayward MCE TH #2
- Figure 12-14 FLAC Dynamic Analysis with Assumed Strength Degradation, Permanent Vertical Displacement, Hayward MCE TH #2
- Figure 12-15 FLAC Dynamic Analysis with Assumed Strength Degradation, Horizontal Displacement Time Histories, Hayward MCE TH #2
- Figure 12-16 FLAC Dynamic Analysis with Assumed Strength Degradation, Vertical Displacement Time Histories, Hayward MCE TH #2
- Figure 12-17 FLAC Dynamic Analysis with Cyclic Degradation Model, Permanent Horizontal Displacement, Hayward MCE TH #1
- Figure 12-18 FLAC Dynamic Analysis with Cyclic Degradation Model, Permanent Vertical Displacement, Hayward MCE TH #1
- Figure 12-19 FLAC Dynamic Analysis with Cyclic Degradation Model, Deformed Mesh, Hayward MCE TH #1
- Figure 12-20 FLAC Dynamic Analysis with Cyclic Degradation Model, Horizontal Displacement Time Histories, Hayward MCE TH #1
- Figure 12-21 FLAC Dynamic Analysis with Cyclic Degradation Model, Vertical Displacement Time Histories, Hayward MCE TH #1
- Figure 12-22 FLAC Dynamic Analysis with Cyclic Degradation Model, Excess Pore Pressure Ratio Contour, Hayward MCE TH #1
- Figure 12-23 FLAC Dynamic Analysis with Cyclic Degradation Model, Cyclic Degradation Contour, Hayward MCE TH #1
- Figure 12-24 FLAC Dynamic Analysis with Cyclic Degradation Model, Locations of Cyclic Degradation TH
- Figure 12-25 FLAC Dynamic Analysis with cyclic Degradation Model, Cyclic Degradation Time Histories, Hayward MCE TH #1
- Figure 13-1 Isometric View of Dam Geometry and Sections A-A' and C-C'
- Figure 13-2 Isometric View of the 3-D Dam Model 3-D Slope Stability Analysis

List of Tables, Figures and Appendices

- Figure 13-3 Example of Interpolated Transverse Cross Section From CLARA 3-D Slope Stability Analysis
- Figure 13-4 Example of Interpolated Longitudinal Cross Section From CLARA 3-D Slope Stability Analysis
- Figure 13-5 Profile of Critical 3-D Sliding Block on Cross-Section A-A', 3-D Slope Stability Analysis, Post-Earthquake Conditions
- Figure 13-6 Profile of Critical 3-D Sliding Block on Cross Section C-C', 3-D Slope Stability Analysis, Post-Earthquake Conditions
- Figure 13-7 Profile of Critical 3-D Sliding Block on Longitudinal Section at Offset = 0, 3-D Slope Stability Analysis
- Figure 13-8 Profile of Critical 3-D Sliding Block on Longitudinal Section at Offset = 40 ft, 3-D Slope Stability Analysis
- Figure 13-9 Profile of Critical 3-D Sliding Block on Longitudinal Section at Offset = 110 ft, 3-D Slope Stability Analysis
- Figure 13-10 Finite Element Mesh for QUAD4M Analysis, Cross-Section A-A' and Critical 3-D Sliding Surface
- Figure 13-11 Finite Element Mesh for QUAD4M Analysis, Additional Cross-Section C-C' and Critical 3-D Sliding Surface
- Figure 13-12 Average Seismic Coefficient Downstream Blocks, QUAD4M Analysis, Hayward Fault MCE TH #1
- Figure 13-13 Average Seismic Coefficient Downstream Blocks, QUAD4M Analysis, Hayward Fault MCE TH #2
- Figure 13-14 Newmark Deformation Analysis, Calculated Displacement, Critical 3-D D/S Sliding Block, Hayward Fault MCE TH #1
- Figure 13-15 Newmark Deformation Analysis Calculated Displacement, Critical 3-D D/S Sliding Block, Hayward Fault MCE TH #2

VOLUME 2

Appendices

- Appendix A Exploratory Drilling
- Appendix B SPT Energy Measurements
- Appendix C Downhole Geophysical Survey
- Appendix D Laboratory Testing
- Appendix E Site Geology

This report presents the results of a dynamic stability study of Estates Dam. The dam and reservoir are located just west of Estates Drive in Oakland, Alameda County, California. The site is on the East Bay hills, approximately 0.3 kilometers (km) southwest of the Hayward fault. Estates Dam is owned and operated by the East Bay Municipal Utility District (EBMUD).

The dam is an earth embankment approximately 90 feet high and 300 feet long with a 15-foot-wide crest. The dam crest elevation is 774¹ and the maximum reservoir storage elevation is 770 (the minimum elevation of the spillway crest). At the latter elevation, the reservoir capacity is about 54 acre-feet. The reservoir is commonly operated between elevations 764 and 768.

The main body of the dam was placed and compacted by teams of horses and wagons to a crest elevation of 765 in 1903. Additional fill was placed along the upstream and downstream slopes and the crest was raised to the current elevation of 774 between 1938 and 1939. Because the dam is located in a relatively narrow ravine, the height and cross-section geometry of the embankment vary markedly across the site between abutments.

In September 2003, the California Department of Water Resources, Division of Safety of Dams (DSOD) conducted a simplified dynamic analysis of Estates Dam, as part of a reevaluation of dams located near active faults. The study presented herein was conducted in response to a directive from DSOD to EBMUD to evaluate the dynamic stability of the dam. The purpose of the study was to evaluate the seismic hazard at the site and to re-evaluate the seismic stability of the dam using current state-of-the-practice techniques. The scope of work included reviewing the existing project data, performing field and laboratory investigations, developing site-specific earthquake design criteria, evaluating the dynamic stability and deformations of the dam, and preparing a report summarizing the analysis results and conclusions.

Field explorations were carried out including geologic mapping, exploratory drilling, and downhole geophysical surveys. Soil and rock samples retrieved from the field were subsequently examined in the URS Pleasant Hill Laboratory and tested for engineering properties and shear strengths. The subsurface data obtained from this study and from previous investigations were entered into a three-dimensional Geographic Information System (GIS) database and were used to develop representative embankment cross-sections.

The study included development of site-specific earthquake ground motions for use in the dam stability analysis. The controlling seismic sources were determined to be the Hayward-Rodgers Creek and San Andreas faults. The maximum credible earthquake (MCE) on the Hayward-Rodgers Creek fault was determined to be a magnitude 7.25 earthquake with a peak horizontal ground acceleration (PGA) of 1.06 g. The MCE on the San Andreas fault was found to be a magnitude 8 event with a PGA of 0.35 g. Multiple acceleration time-histories were developed to represent the earthquake ground motions for dynamic stability analysis under the Hayward fault MCE, and one time history was developed for the San Andreas fault MCE.

There is no evidence of Holocene activity in possible minor faults or shears in the Franciscan rock units at the site, either as independent faults or as structures that exhibit coseismic movement with earthquakes on the Hayward fault. Accordingly, the potential for fault rupture at the dam site is judged to be very small.

¹ Unless otherwise noted, all elevations in this report are given in feet and refer to USGS datum.

The cyclic and post-cyclic strength of the embankment and foundation soils was evaluated based on the results of laboratory cyclic and post-cyclic triaxial tests previously performed by others, and on published data for similar materials. Based on the results of the laboratory tests and on the index properties of the materials, it is concluded that the embankment and foundation soils are not susceptible to liquefaction. However, the materials may develop excess pore pressures and undergo strength loss under strong earthquake shaking.

The approach to evaluate the seismic stability of the dam consisted of evaluating the dynamic response of the dam to the design earthquake motions, evaluating the potential for strength loss of the embankment and foundation materials under the earthquake shaking, estimating the deformations likely to be induced by the earthquake, and assessing the post-earthquake stability of the dam and its overall condition after the earthquake. The seismic response and deformations of the dam were also evaluated using a nonlinear analysis approach in which the above steps are coupled in a single analysis. The nonlinear analyses were performed with the computer program FLAC. The analyses were performed for a two-dimensional (2-D) model idealized from the maximum transverse section of the dam.

The design earthquake was defined as the MCE on the Hayward-Rodgers Creek fault since this earthquake is likely to generate the strongest ground motions at the site. Because the MCE on the San Andreas fault could result in strong shaking of long duration, the seismic stability of the dam was also evaluated for that earthquake. As a check of the analysis procedures, the dynamic response and deformations of the dam were also analyzed for motions representative of the 1989 Loma Prieta earthquake, for which the general performance of the dam is known.

The analyses results for the 1989 Loma Prieta earthquake are consistent with the known performance of the dam and indicate that the dam should perform satisfactorily during small to moderate earthquakes. The analyses for the San Andreas fault MCE result in calculated dam deformations that are lower than those calculated for the Hayward event. Thus, the results of the analyses indicate that the San Andreas event is less critical than the Hayward event regarding the seismic stability of the dam.

The dam deformations calculated for the Hayward fault MCE are sensitive to the details of the input time histories used to represent the earthquake ground motions. Accordingly, sensitivity analyses were performed to estimate the range of potential deformations and the average deformation response of the dam. Three-dimensional stability analyses were performed to assess the effects of the dam's narrow-site geometry on the calculated deformations. Such analyses result in calculated downstream horizontal displacements that are on the average about two-thirds of those calculated from 2-D analyses.

Based on the analysis results and considering the limitations of the methods of analysis, the best estimate of the maximum crest vertical displacement for the Hayward fault MCE is between 3 and 4 feet. Likewise the best estimate of the maximum horizontal displacement of the downstream slope is about 6 feet. The principal mechanism of embankment deformation is downstream block displacement resulting from shear within a relatively thin zone in the 1903 fill and foundation soil just above the bedrock contact. This mechanism seems intuitive in view of the fact that the bedrock surface slopes downstream beneath the embankment. No upstream displacements of the embankment are expected to develop. The estimated settlements and horizontal deformations will likely result in cracking of the upstream face lining, and possibly transverse cracking of the dam embankment near the crest. In view of the estimated crest

settlements, the minimum available dam freeboard of 4 feet is not judged to provide an adequate margin against potential overtopping of the embankment, if the reservoir were to be full during the design earthquake.

The downstream displacements of the embankment may affect the spillway overflow and inlet/outlet pipes and nearby subsurface drains. The spillway overflow pipe is located near the right abutment. Based on its location, it seems unlikely that the pipe will be subjected to large ground displacements. However, small displacements are possible in response to the estimated displacements of the downstream slope. Because of its steel construction, the pipe is likely to be capable of withstanding displacements of a few inches, although an in-depth assessment of this issue has not been made.

The inlet/outlet pipe is located near the left abutment. The available construction records indicate that the pipe was laid in a trench through the embankment and foundation materials and was encased in concrete from the reservoir inlet to the pumping plant. In view of its location, it seems unlikely that the pipe will be subjected to large displacements. However, small displacements are possible in response to the estimated displacements of the downstream slope, particularly where the pipe approaches the pumping plant. Because the pipe is of cast iron construction, it may not be able to tolerate displacements greater than a few inches without damage. Although rupture of the pipe is possible, the extent of damage to the pipe would be limited by the concrete encasement, and potential erosion from pipe leakage would likely be localized to the near-surface materials in the area of the pumping plant.

In view of the available dam freeboard, it may be concluded that the potential crest settlements and horizontal embankment displacements during the design earthquake represent a significant risk regarding the safety of the structure. Damage to the embankment is likely to require drawdown of the reservoir immediately after the earthquake. The significance of the risk associated with the expected embankment damage and potential damage to the inlet/outlet pipe is to be further considered by EBMUD.

1.1 BACKGROUND

This report presents the results of a dynamic stability study of Estates Dam, located in the City of Oakland in Alameda County, California (Figure 1-1). The dam and reservoir were initially constructed in 1903 and were enlarged to their current configuration in 1938-39. Estates Dam is owned and operated by the East Bay Municipal Utility District (EBMUD).

1.2 PURPOSE AND OBJECTIVES

The stability of Estates Dam has been the subject of several previous investigations, including those by Shannon and Wilson (S&W) (1965) and Wahler Associates (1980). Those studies are briefly described below.

In 2003, the California Department of Water Resources, Division of Safety of Dams (DSOD) conducted a simplified dynamic analysis of the dam as part of a statewide reevaluation of dams located near high-slip rate faults (Jones, 2003). On that basis, the DSOD asked EBMUD to perform a more detailed seismic stability study of the dam. The study presented herein was conducted in response to DSOD's request. The purpose of the study was to evaluate the seismic hazard at the site based on the current understanding of the tectonic and geologic setting of the region, evaluate the strengths of the embankment and foundation materials, and reevaluate the seismic stability of the dam using current state-of-practice analytical techniques.

1.3 PREVIOUS INVESTIGATIONS

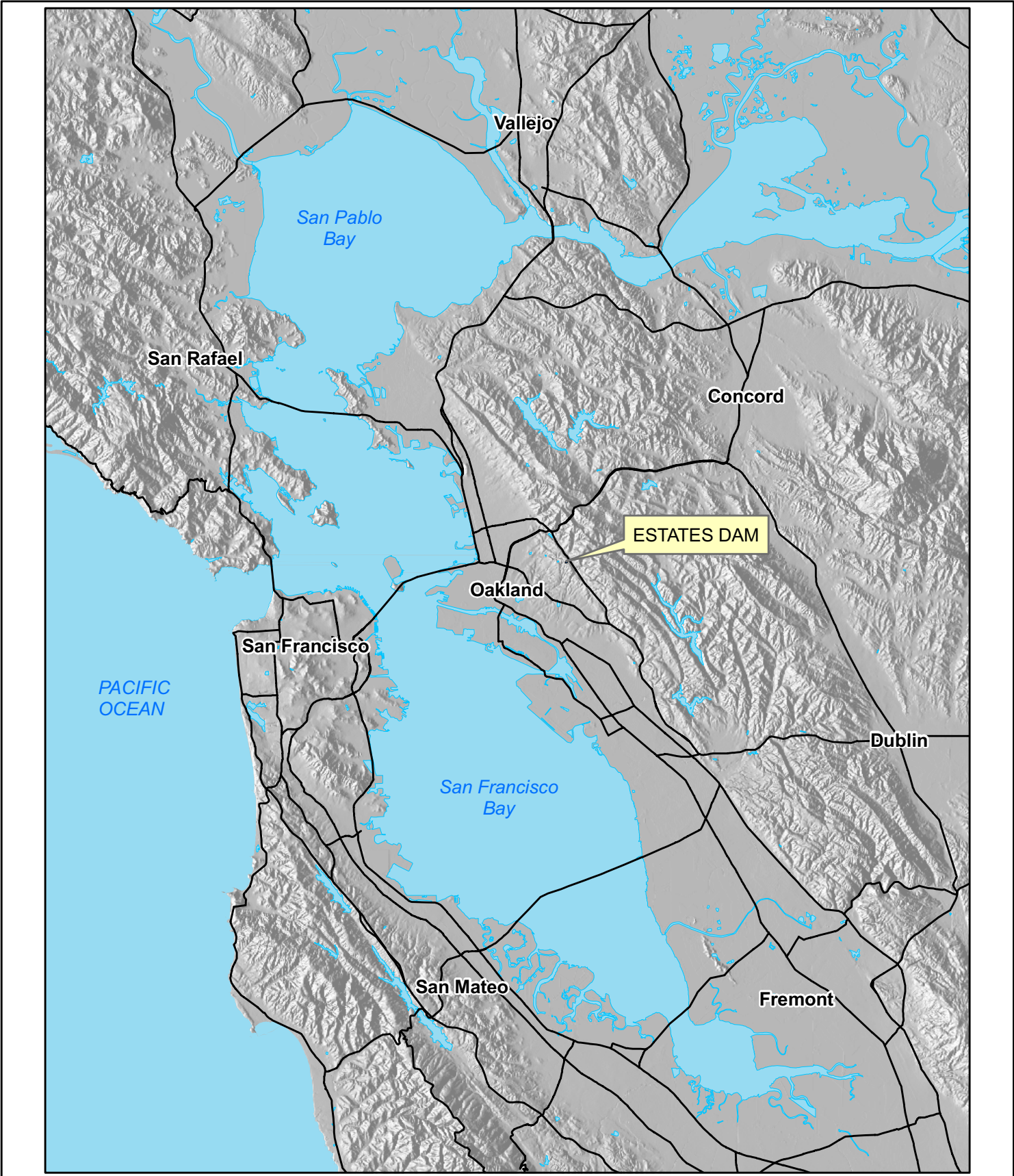
Shannon and Wilson investigated the dam and performed stability analyses in 1965. EBMUD and S&W drilled 27 borings within the reservoir area and on the crest and downstream slope of the dam. The slope stability of the dam was analyzed under steady seepage conditions, pseudo-static conditions, and rapid drawdown conditions, using limit-equilibrium methods. The study concluded that the dam had adequate factors of safety, but made recommendations for installation of subdrains to lower the ground water table in the abutments. Following the S&W study, EBMUD installed a subdrain system consisting of 6-inch perforated AC pipes within 10-foot-deep trenches along both groins of the downstream slope.

Wahler Associates performed an evaluation of the seismic stability of the dam in 1980. EBMUD and Wahler drilled eight borings in the upstream and downstream shells of the dam. The soil samples were tested for index properties and static and cyclic shear strengths. The dynamic response of the dam was evaluated using the finite element method. The investigation predicted limited overall deformation of the dam during San Andreas and Hayward earthquake events, but indicated the possibility of high strain zones near the upstream toe.

1.4 REPORT ORGANIZATION

This report is organized into sixteen sections and six appendices. After this introductory section, Section 2 presents the scope of work of this study. A brief description of the project and information on the construction and performance of the dam are summarized in Section 3. Section 4 summarizes the field and laboratory investigations performed for the study. The geological setting of the dam is discussed in Section 5, followed by a discussion of site-specific

earthquake ground motions in Section 6. Characterizations of the embankment and foundation conditions are presented in Section 7. Section 8 discusses the general analysis approach. The details of the limit-equilibrium stability analyses, dynamic response analyses, seismic stability analyses, and non-linear analyses are presented in Sections 9 through 12. The results of analyses to evaluate 3-dimensional effects on dam stability and seismic deformation are presented in Section 13. Section 14 summarizes the expected seismic performance of the dam whereas Section 15 summarizes the main conclusions and recommendations from the study. The references cited in the report are listed in Section 16. Appendices A through F present supporting documentation including field and laboratory data as well as geologic and seismologic reports produced for the study.



Estates Dam
 Seismic Stability
 26814957

Site Location Map

Figure
 1-1

This study was performed in accordance with the Agreement between URS and EBMUD dated November 2, 2004. The main technical tasks of the scope of work are summarized below.

Data Review

This task consisted of reviewing existing information on the reservoir site geology and on the design, construction, and instrumentation monitoring of the dam. The reliability of the existing field and laboratory test data for use in the stability analysis of the dam was evaluated, and the issues to be addressed in the field exploration and laboratory testing and in the analysis of the dam were identified. The existing boring data was entered into a geographic information system (GIS) database to help assess the distribution of soils and their characteristics within the embankment and the foundation.

Geologic Mapping

This task consisted of developing an understanding of the site geology and the stratigraphy of the dam foundation, based on ground reconnaissance and available boring information.

Simplified Stability Check

This task consisted of characterizing the engineering properties of the embankment and foundation materials using existing information, performing stability analyses using limit-equilibrium methods, and estimating seismic deformations of the embankment using a Newmark-type rigid-block deformation analysis.

Develop Site-Specific Earthquake Ground Motions

This task included reviewing recent information on the regional seismic environment and the characteristics of faults that could affect the dam to determine the maximum credible earthquake (MCE) on the controlling faults. Site-specific acceleration response spectra were developed using well-established attenuation relationships and up-to-date procedures that account for near-field and directivity effects. Acceleration time histories were developed for use in the analysis of the dam.

Field Exploration and Laboratory Testing

This task included drilling four rotary-wash borings through the embankment and foundation soils and into bedrock. Samples were retrieved with a Standard Penetration Test (SPT) sampler and other types of samplers for laboratory testing. Geophysical surveys were performed in selected borings to measure the shear wave velocity of the embankment and foundation materials. The hammer energy efficiency was measured and calibrated during the SPT sampling. Laboratory tests were performed to characterize and evaluate the geotechnical properties of the materials for use in dynamic stability analyses.

Analysis of Dam Stability and Deformations

This task included developing representative cross-sections and material properties for analysis of dam stability. The seismic stability and deformations of the critical section of the dam were evaluated using up-to-date two-dimensional finite element analysis and Newmark-type deformation analysis procedures. In addition, non-linear analyses were performed with the two-dimensional finite difference computer code FLAC. The sensitivity of the calculated seismic deformations to the input ground motions and the effects of three-dimensional behavior on slope stability were also evaluated. The overall performance and seismic stability of the dam were evaluated and assessed based on the results of the analyses.

3.1 SITE SETTING

The dam and reservoir are situated at the head of a narrow ravine, at the intersection of Estates Drive and Bullard Drive, a few hundred yards west of state highway 13, in the Oakland hills. The site location is shown on Figure 3-1.

3.2 DESCRIPTION OF DAM

The dam is approximately 90 feet high and 300 feet long and has a 15-foot-wide crest. The dam crest elevation is 774² and the minimum spillway crest elevation is 770. At this elevation, the reservoir capacity is about 54 acre-feet. The reservoir is commonly operated between elevations 764 and 768. The upstream and downstream slopes are 2:1 (H:V). A 4-inch-thick reinforced concrete lining covers the reservoir slopes and floor. The main body of the dam is composed of clayey sandy soil placed in 1903 by horse-drawn equipment. On the crest and downstream slope, the 1903 fill is overlain by newer fill placed between 1938 and 1939. The dam layout is shown in Figure 3-2.

3.3 APPURTENANT FACILITIES

The project appurtenant facilities include the spillway, the inlet-outlet system, and a wooden roof. The spillway is a side channel type. It drains through a 24-inch mortar-lined and coated steel pipe, located near the right abutment, into a stilling basin at the downstream toe. The inlet-outlet system consists of a 20-inch cast iron pipe passing through a trench excavated in the embankment near the left abutment and control inlet/outlet valving. The pipe connects to the Montclair pumping plant located on the left abutment about halfway on the downstream slope. The reservoir is covered with a wooden roof that supports two fountains and a planter structure.

3.4 CONSTRUCTION HISTORY

Construction of the dam started in 1903 by the Syndicate Water Company. The reservoir was constructed by excavating a basin at the head of a ravine and placing the excavated material to form the embankment. The original dam was about 280 feet long, 50 feet high, and 15 feet wide at the crest. About 24,000 cubic yards of material were excavated from the reservoir and placed in the embankment using horse-drawn equipment. A concrete core wall was built along the centerline of the dam. In their review memorandum, DSOD indicates that the wall is about 1 foot thick and extends about 15 feet into the embankment (Jones, 2003). However, none of the available documents provide the depth or lateral extent of the wall into the foundation.

The original outlet reportedly consisted of 4-inch and 8-inch pipes through the dam. In 1934, a new outlet system was installed and the reservoir basin was enlarged. The new outlet system consisted of a 20-inch cast iron pipe passing through a trench excavated in the embankment. The trench was backfilled in thin lifts compacted with a sheepsfoot roller. A new outlet tower was constructed in the reservoir, and the original outlet pipes were plugged with cement grout. About 8,000 cubic yards of material were excavated from the south slope of the reservoir and used to

² Unless otherwise noted, all elevations in this report are given in feet and refer to USGS datum.

partially backfill the reservoir floor up to the bottom of the new outlet tower at about elevation 742.

In 1938 and 1939, the dam crest was raised about 9 feet (from elevation 765 to 774) by placing excavated material from the reservoir basin on the downstream slope of the dam. The material was spread in about 6-inch-thick layers with a bulldozer, and compacted with a sheepsfoot roller. A short parapet wall (top elevation 775.5) was also added to the crest. A tile drain system was installed at the interface between the new fill and the existing dam to collect seepage from several existing springs near the downstream toe. Reportedly, a “boggy” area at the downstream toe was over-excavated by about 10 to 12 feet, and was backfilled as part of the dam raise construction. A vertical concrete spillway pipe was also added, connecting to a 12-inch overflow pipe routed beneath the north groin to the catch basin at the downstream toe. The slopes within the reservoir were trimmed to about 2H:1V, and a 4-inch-thick reinforced concrete lining was placed over the reservoir floor and slopes. No under-drain system was installed beneath the lining.

In 1968, a new wood roof structure was constructed to completely enclose the reservoir. The roof was supported by columns founded on spread footings. As part of that project, the spillway overflow pipe was abandoned and replaced with a side-channel spillway. The outlet tower was removed and replaced by new inlet-outlet valving. A subdrain system consisting of 6-inch perforated AC pipe was installed in trenches excavated about 10 feet deep on each downstream abutment.

In 1997, the inlet/outlet pipe was relocated away from the upstream toe of the dam. The purpose of that move was to address the possibility for upstream slope instability. The spillway was notched to elevation 770 to provide four feet of freeboard, to account for possible settlement of the embankment under seismic shaking.

3.5 PERFORMANCE AND MONITORING

The performance of Estates Dam is monitored with piezometers, seepage measurement devices, and survey monuments. The instruments are maintained and periodically read by EBMUD personnel. The piezometers are listed in Table 3-1. Seepage through the embankment is monitored at three locations. The embankment and left abutment drain readings are typically less than 1 and 2 gallons per minute (gpm), respectively. The right abutment drain readings show significant greater variation and some large readings, which are mainly due to rain infiltration. A total of twenty-one survey monuments are installed on the embankment.

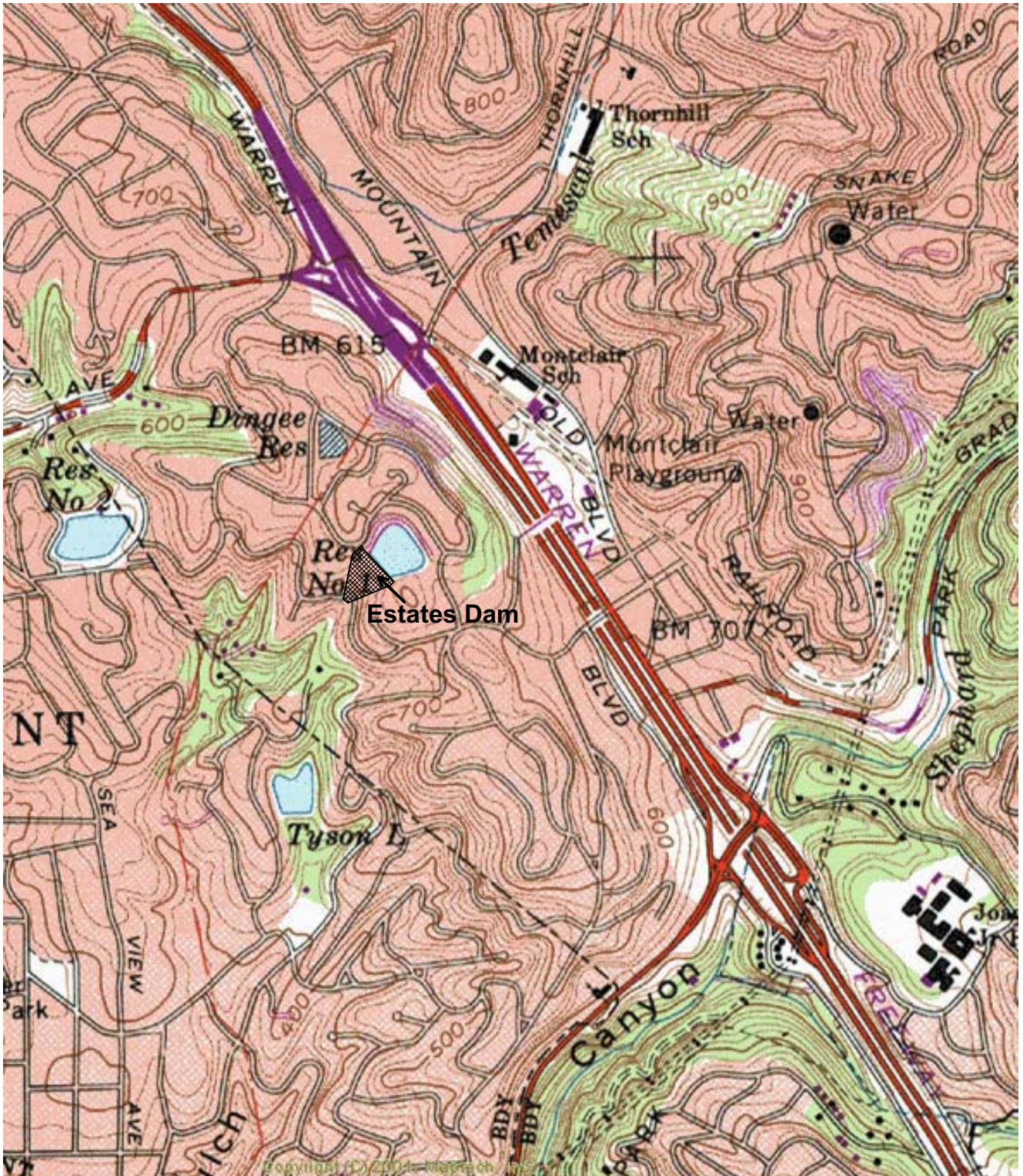
Overall, the dam has performed very well since its construction. Records indicate that the dam performed well during the great San Francisco earthquake of 1906. The dam was inspected following the 1989 Loma Prieta earthquake, and no significant damage or distress was reported. Some post-earthquake photographs of the dam crest show apparent minor deposits of dark colored sand along several preexisting cracks in the asphalt pavement, but the source and transport mechanism for those small sand deposits is unknown. Monitoring data before and after the 1989 Loma Prieta earthquake showed no signs of excessive seepage, phreatic level changes within the dam, or permanent displacement of the embankment.

**Table 3-1
Existing Piezometers at Estates Dam**

Boring No.	Ground Surface Elevation, ft	Piezometer Tip Elevation, ft
VQ-20	731.9	680.0
VQ-21	696.8	675.0
VQ-22	700.2	684.8
VQ-22A	699.9	690.1
VQ-23	732.2	702.7
VQ-24	715.5	695.5
VQ-25	732.1	702.1
VQ-26	701.2	684.2
VQ-28	709.4	701.8
VQ-29	712.3	704.0
VQ-30	709.3	704.3
VQ-31	706.9	701.9
VQ-32	774	707
VQ-33	774	741
VQ-34	774	746
VQ-35	732	694
VQ-36	697	677

Notes:

All piezometers are manually read open standpipes. Boring locations are shown in Figure 4-2.

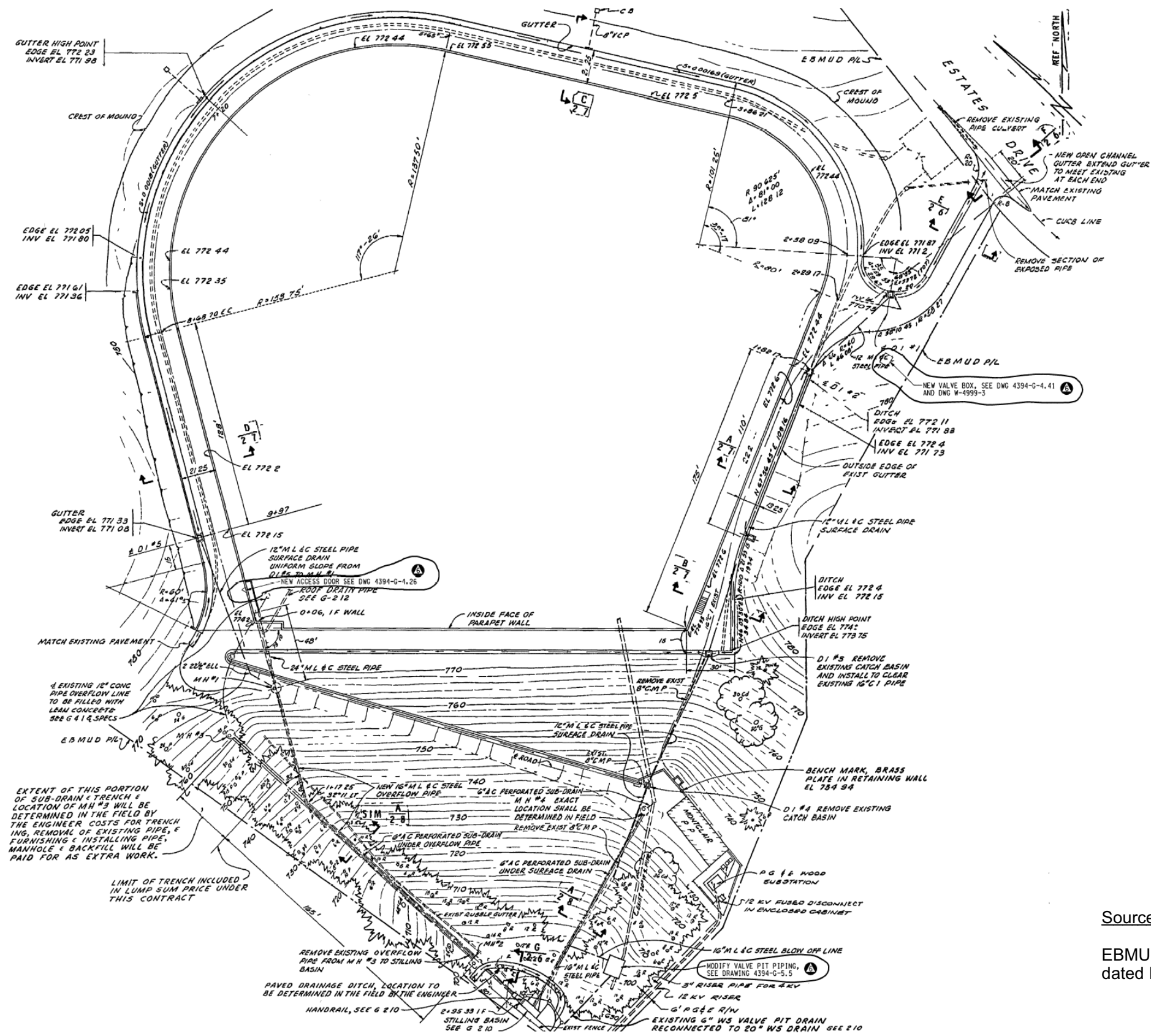


Source: Terrain Navigator, Maptech Inc., 2001



0 200 400 600 Meters

URS	Project No. 26814957	Location of Estates Dam and Reservoir	Figure
	Estates Dam Seismic Stability		3-1



Source:

EBMUD Drawing No. 4394-G-2.6, Roads & Drainage Plan, dated February 11, 1966, last revised on October 17, 1997.

Project No. 26814957	Estates Dam Seismic Stability	Site Plan	FIGURE 3-2
URS			

The objective of the field and laboratory investigations was to supplement the available geotechnical data for the seismic stability re-evaluation of the dam. Previous studies of the dam's stability have also included field and laboratory investigations. The locations of the borings from previous studies are shown in Figure 4-1. Of the existing borings in the embankment, only a few were judged to be reliable. Thus, additional field and laboratory investigations were undertaken for this study to supplement the existing data and to better characterize the materials in the dam and its foundation for the analyses of seismic stability. The investigation program that was carried out for this purpose is described below.

4.1 FIELD INVESTIGATIONS

The field investigation program included exploratory borings, hammer energy measurements, and downhole geophysical surveys. The details of these elements of work are described in the following sections. The boring logs and test data reports are presented in Appendices A through C. The boring depths and materials encountered are summarized in Table 4-1. The locations of the borings drilled for this study are shown in Figure 4-2, along with the locations of previous borings.

The field investigations were carried out between March 28 and April 7, 2005. The drilling program included four rotary-wash borings. Pitcher Drilling Company of East Palo Alto, California performed the drilling work. GEOVision Geophysical Services of Corona, California, performed the downhole geophysical measurements. Energy transfer measurements of hammer efficiency during the SPT testing were obtained by Gregg Drilling and Testing, Inc. Robert Y. Chew Geotechnical supervised the drilling and logged the borings, under the direction of URS. URS reviewed the samples, conducted the laboratory testing, and prepared the final boring logs with assistance from Dot Dat, Inc.

4.1.1 Rotary Wash Drilling

The four rotary-wash borings (designated VQ-37 through VQ-40) were numbered in the order drilled, using nomenclature consistent with borings previously drilled by the District at the site. Borings VQ-37 and VQ-38 were drilled from the crest of the dam. Borings VQ-39 and VQ-40 were drilled from the downstream face access road (Figure 4-2). The boring logs are presented in Appendix A.

The borings were drilled using a truck-mounted Fraste Multi-Drill XL rig (D30) equipped with Failing Exploration Pipe (FEP) drill rods (58 lbs. per 10-foot-length) and a 140-lb. automatic trip hammer. The borings were drilled using a 5-7/8-inch diameter tri-cone bit, and were advanced to depths of 36 to 87 feet. The 5-7/8-inch borehole diameter was selected to allow use of a 4-inch diameter Pitcher Barrel sampler.

The borings were initially located in the field based on tape measurement from available reference points. After drilling, a hand-held Trimble GPS receiver with built-in differential correction capability was used to record the coordinates at each boring location. The horizontal accuracy range for the GPS coordinates is about 5 feet.

4.1.2 Hammer Energy Measurements

The energy transferred from the hammer to the SPT sampler is an important factor in evaluating the SPT resistance of soils. The efficiency of energy transfer is measured by the energy ratio (ER), which is defined as the ratio of energy transferred to the drill rod to the theoretical “free fall” energy. Using the energy correction factor ($C_E = ER/60$), the field SPT blow counts (N) are adjusted to standardized blow counts (N_{60}) corresponding to an average energy ratio of 60 percent.

The SPT hammer energy measurements were obtained during sampling in boring VQ-40 on May 3, 2004. The measurements were obtained with a Pile Dynamics, Inc. Model PAK Pile Driving Analyzer. The measured average ER was about 75%. The complete results of the SPT hammer energy measurements are presented in Appendix B.

4.1.3 Downhole Geophysical Surveys

Downhole seismic wave velocity measurements were made in borings VQ-38 and VQ-40. The surveys were conducted in uncased borings, filled with water and/or drilling fluid, immediately following the completion of the drilling and sampling at each boring. An OYO Model 170 suspension logging probe and recorder were used to measure shear and compression wave (S- and P-wave) velocities at 0.5-meter (m) intervals (1.64 feet). The suspension logger was lowered to the bottom of each boring and velocity measurements were made, as the logger was withdrawn from the hole. The main purpose of the surveys was to obtain shear wave velocity data for the embankment and foundation materials for use in dynamic analysis of the dam. More detailed descriptions of the geophysical survey program and results are presented in Appendix C.

4.2 LABORATORY TESTING

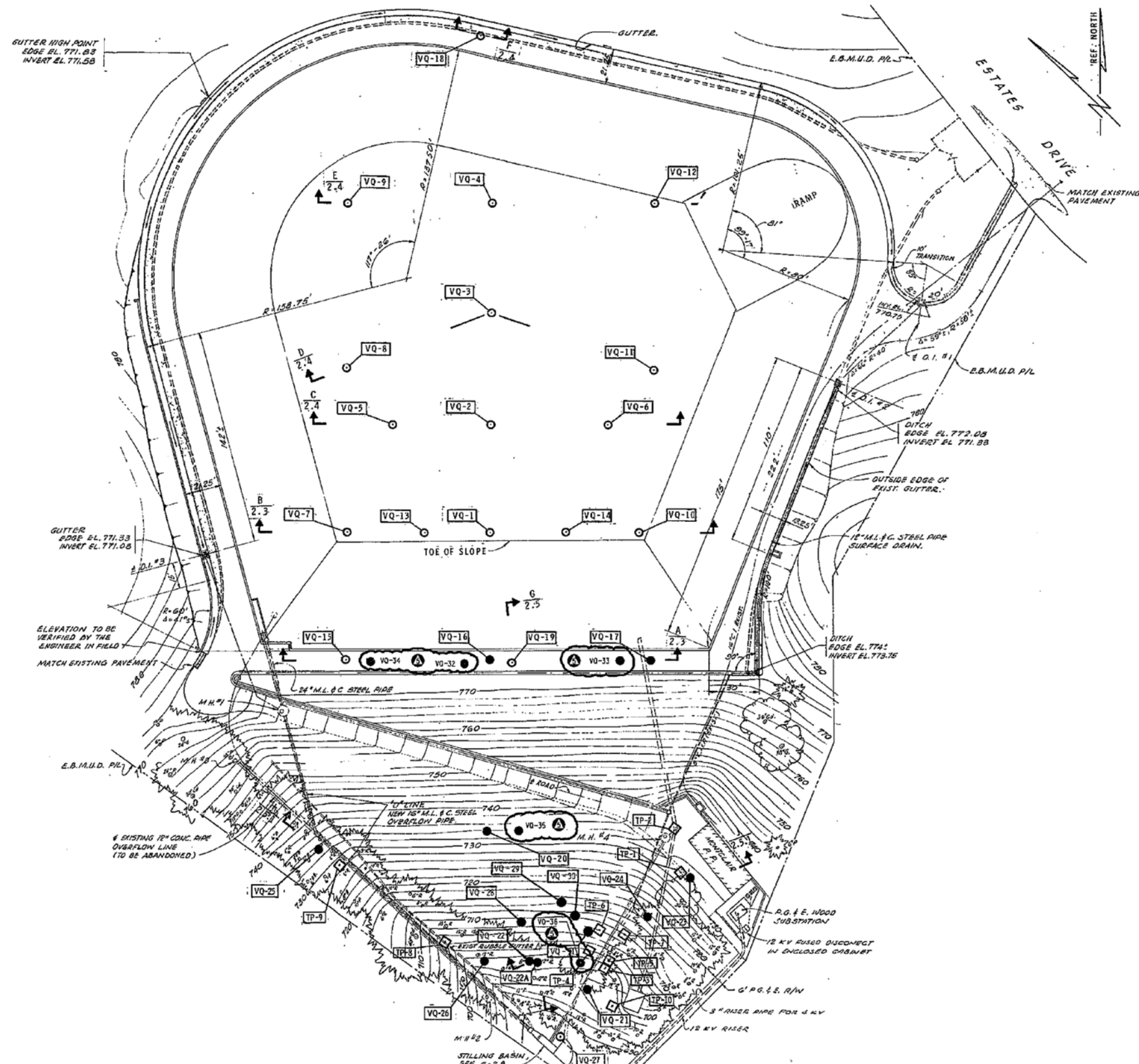
The laboratory test program was conducted at the URS Pleasant Hill laboratory. Prior to finalizing the test program, the soil and rock samples were carefully inspected in the laboratory by the URS team and representatives of the District and the DSOD. Appropriate tests were selected to assist in subsequent evaluation of material properties for use in the stability analyses. The types of tests performed are listed below, along with their ASTM designations.

- In-situ moisture-density (ASTM D2216, D2937)
- Sieve analysis (ASTM D422)
- Hydrometer analysis (ASTM D422)
- Atterberg Limits (ASTM D4318)
- Isotropically consolidated undrained (ICU) triaxial compression tests with pore pressure measurements (ASTM D4267).

The laboratory tests were conducted in accordance with the noted ASTM standards. Consolidation pressures for the ICU tests were selected based on the estimated overburden pressure at each sample depth. The test results are tabulated in Appendix D. Summary plots of the test results are also presented in Appendix D along with the laboratory reports for each test. Abbreviated test results for each sample are also included in the boring logs at the appropriate depths.

**Table 4-1
Summary of Borings**

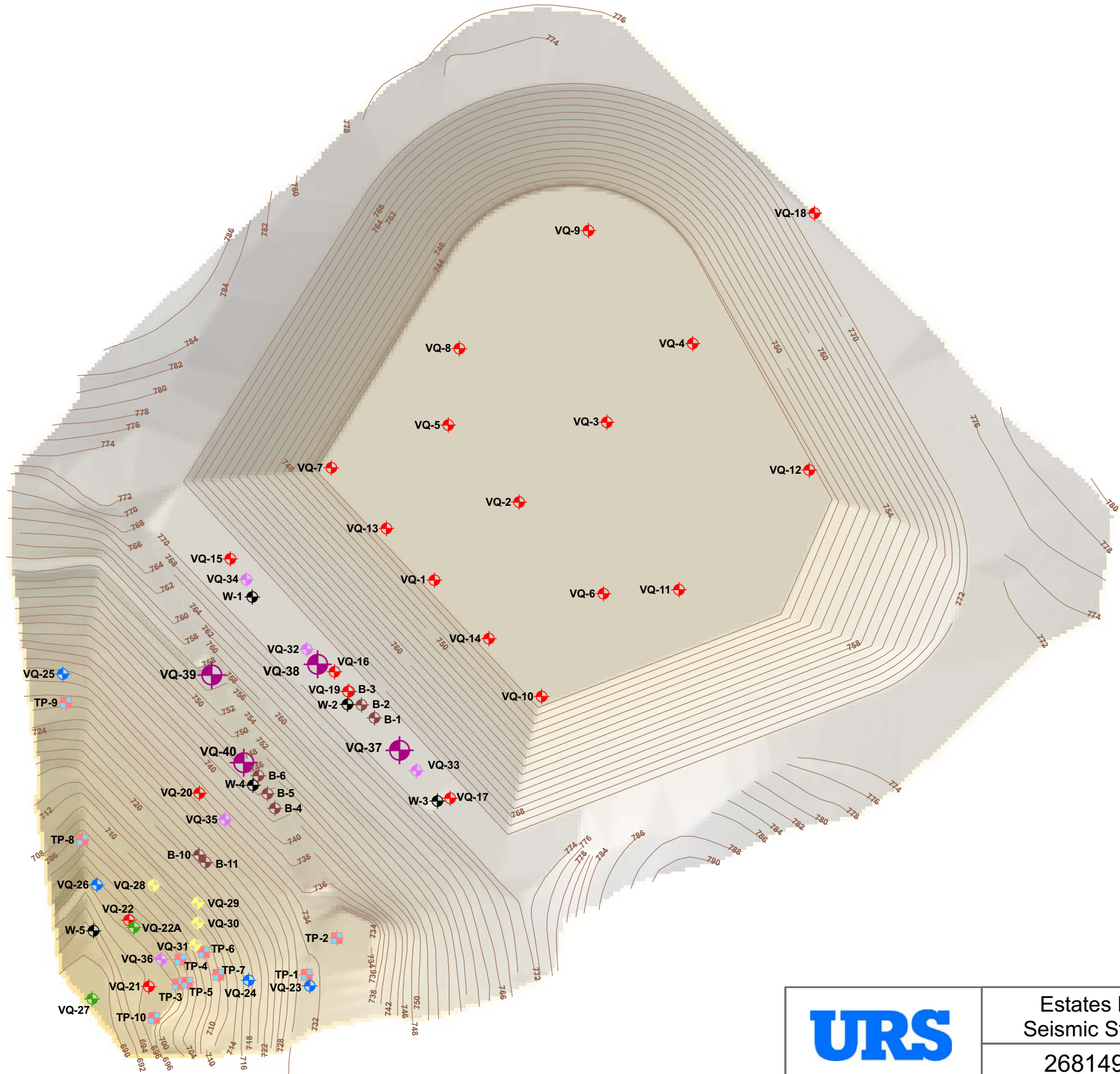
Boring No.	Location	Coordinates (Lat, Long)	Surface Elev. (feet)	Depth (feet)	Materials Encountered (Approximate Depths/Remarks)
VQ-37	Dam Crest	37°49.618' N 122°12.971' W	~774	57.5	0-38 ft. Embankment fill 38-44 ft. Native soil 44-57.5 ft. Meta-volcanic, clayey shale, and meta-sandstone bedrock.
VQ-38	Dam Crest	37°49.624' N 122°12.985' W	~774	87.0	0-51 ft. Embankment fill 51-57 ft. Native soil 57-87 ft. Clayey shale and sandstone bedrock (OYO suspension log)
VQ-39	Downstream Face Access Road	37°49.626' N 122°12.998' W	~755	35.7	0-26 ft. Embankment fill 26-27 ft. Native soil 27-35.7 ft. Clayey shale and meta-volcanic bedrock.
VQ-40	Downstream Face Access Road	37°49.618' N 122°12.993' W	~747	72.0	0-35 ft. Embankment fill 35-41 ft. Native soil 41-72 ft. Clayey shale and sandstone bedrock (SPT energy calibration and OYO suspension log)



Source:

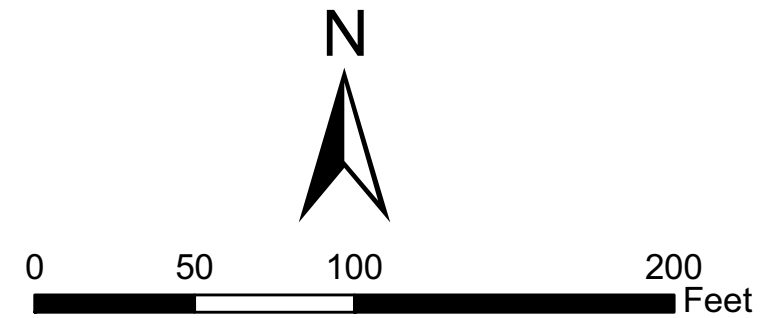
EBMUD Drawing No. 4394-G-2.2, Site Topography - Boring Locations, dated July 12, 1966, last revised in 1999.

Project No. 26814957	Estates Dam Seismic Stability	Locations of Previous Field Explorations	FIGURE 4-1
URS			



Legend

- EBMUD; 1939 (wells)
- EBMUD for S&W study; 1962-1965
- S&W; 1965
- EBMUD for S&W study; 1965 (test pits)
- EBMUD for S&W study; 1965
- EBMUD; 1976
- Wahler Associates; 1978
- EBMUD, 1999 (piezometers)
- URS, 2005



	Estates Dam Seismic Stability	Locations of Field Explorations	Figure 4-2
	26814957		

This study included a review of geologic mapping from previous studies and additional reconnaissance-level geologic mapping in the vicinity of the dam site. This work was conducted by Dr. John Wakabayashi under subcontract to URS. Dr. Wakabayashi's site geology report is included in Appendix E. The seismictectonic environment of the East Bay hills and the characterization of the seismic sources that could affect the dam were recently reviewed and updated by William Lettis & Associates, under subcontract to URS, in a recent seismic study of Chabot dam (URS, 2005).

5.1 REGIONAL GEOLOGY

Estates Dam is located within the seismically active region between the Pacific plate on the west and the Sierra Nevada-Central Valley ("Sierran") microplate on the east. Geodetic data demonstrate that net motion between the two plates is obliquely convergent. The oblique motion of the Sierran microplate relative to the strike of the San Andreas and Hayward faults results in a small component of net convergence normal to these structures, which is accommodated by both strike-slip and thrust faulting in the eastern San Francisco Bay area.

The dam and reservoir are situated in a narrow ravine near the western edge of the East Bay hills, which limit San Francisco Bay on the east. The East Bay hills region is within the central Coast Range geomorphic province of California and is bounded by the Hayward fault on the west and the Northern Calaveras fault on the east.

5.2 SITE GEOLOGY

The site geology in the vicinity of the dam is illustrated in Figure 5-1. The mapping of bedrock contacts and assessment of geomorphology in the site area were difficult because of the modification of land surface by urban development. Only two limited exposures of rock were found during the field reconnaissance and it was not clear whether those two exposures were actually in-place bedrock.

The rock at the dam site and surrounding the reservoir appears to be blueschist-facies metagraywacke of the Franciscan Complex. The Franciscan bedrock units in the vicinity of the dam site include a blueschist-facies metamorphic unit (KJfm), Alcatraz Terrane (Kfa), Mélange including Marin Headlands Terrane rocks (KJfmh), Novato Quarry Terrane (Knq), and undifferentiated mélange (Kjfmel).

The Hayward Fault is located about 1400 feet northeast of Estates Dam (Lienkaemper, 1992) and is the only fault with demonstrated Holocene activity that has been mapped near the reservoir or dam. The Hayward Fault in this area strikes subparallel to the Warren Freeway (State Highway 13) and is located slightly east of the freeway. This fault marks the contact between Franciscan Complex bedrock units to the west and Coast Range ophiolite, Great Valley Group with minor Franciscan Complex rocks to the east. Several different Franciscan Complex rock units crop out west of the Hayward fault and the strikes of their bedding, as well as the strikes of the bounding contacts, are slightly more westerly (by about 15 to 20 degrees) than that of the Hayward fault. This bedrock structural grain and resultant erosional contrasts may have influenced the general shape of the hills in this area because the ridge crests trends have a similar orientation. The Franciscan rock units west of the Hayward fault, including those in the vicinity of the Estates Dam and Reservoir have a northeasterly dip.

5.3 FAULT RUPTURE

There is no positive evidence of Holocene activity in possible minor faults or shears in the Franciscan rock units at the site, either as independent faults or as structures that exhibit coseismic movement with earthquakes on the Hayward fault. Accordingly, the potential for fault rupture at the dam site is judged to be very small.

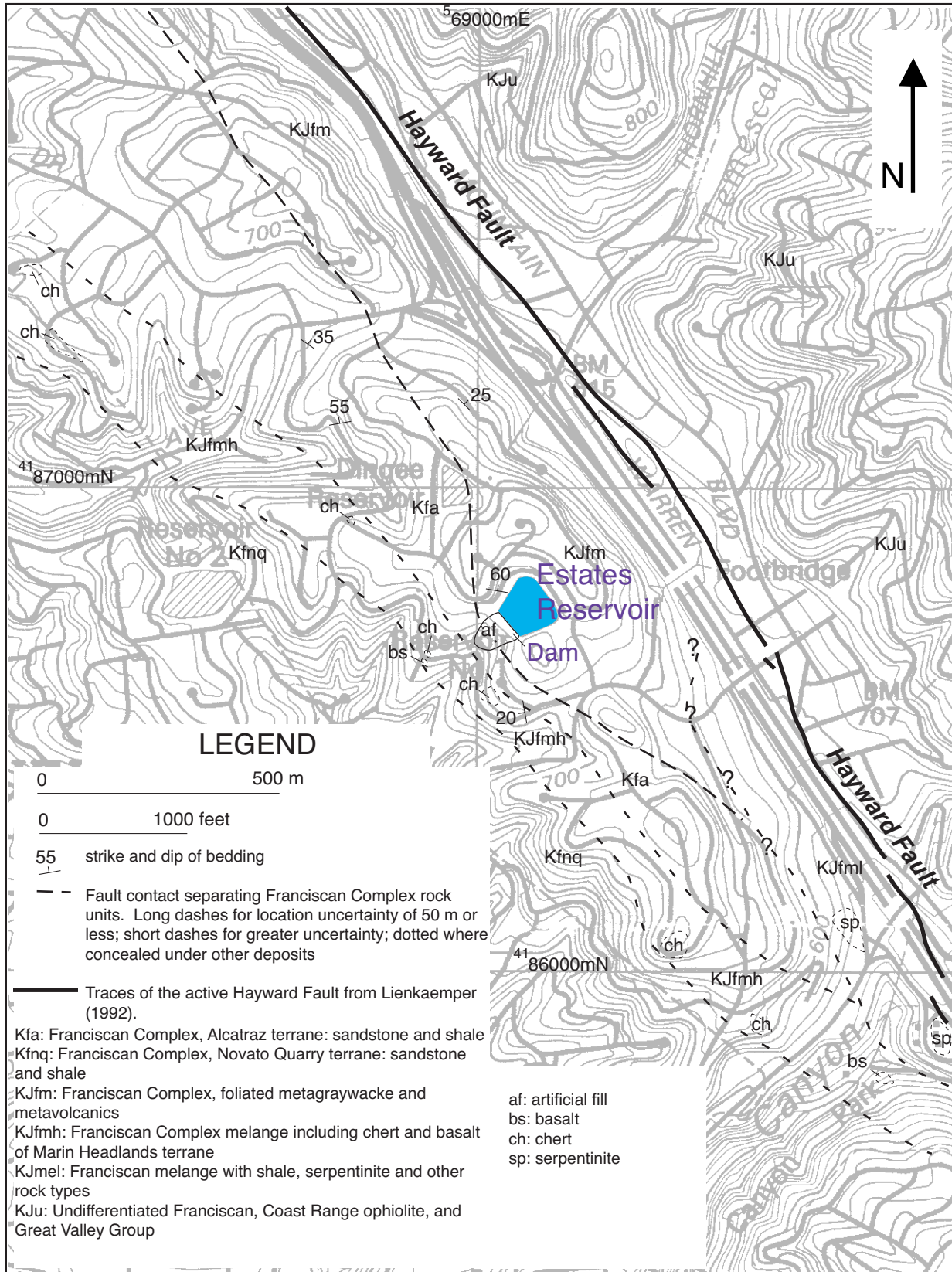


Figure 5-1: Geologic map of the Estates Reservoir area. Geologic mapping by J. Wakabayashi 1984, 2005; Hayward fault traces from Lienkaemper (1992)

6.1 GENERAL APPROACH

The approach used to develop the design acceleration response spectra and corresponding time histories for analysis of Estates Dam consisted of the following steps:

- Identification of the seismic sources that can generate significant earthquake ground motions at the dam site;
- Estimation of the maximum earthquake magnitudes and the closest distances to the dam site for the identified seismic sources;
- Identification of the controlling earthquake sources and the Maximum Credible Earthquake (MCE) on each source;
- Assessment of the site conditions for purpose of estimating earthquake ground motions;
- Selection of appropriate attenuation relationships to estimate ground motions as a function of earthquake magnitude, distance, faulting style, and site condition;
- Development of design acceleration response spectra based on the results of the above steps;
- Adjustment of the design response spectra to include near-field effects;
- Selection of previously recorded time histories that best represent the magnitude, rupture mechanism, distance, site conditions, and other key parameters of the design earthquakes; and
- Modification of the selected time histories to closely match the design response spectra.

6.2 SEISMIC SOURCES

The Hayward-Rodgers Creek fault is located about 0.3 kilometers (km) northeast of the dam site. This fault was the source of an estimated M6.8 earthquake on 21 October 1868. The San Andreas fault, located about 29 km west of the dam, was the source of the 1906 Great San Francisco earthquake. Other active faults within 50 km of the dam that are considered as potential sources of future large earthquakes include the Calaveras, San Gregorio-Seal Cove, Greenville, and Concord-Green Valley faults. The locations of the main potential seismic sources in the region are shown in Figure 6-1.

The maximum magnitudes for each identified seismic source were estimated based on the potential rupture length and seismogenic depth, using an empirical relationship that relates earthquake magnitude and rupture area as proposed by Wells and Coppersmith (1994). Site-to-source distances were measured from the dam site to the main trace of each fault. The estimated maximum earthquake magnitudes and site-to-source distances for each of the main faults in the region are listed in Table 6-1.

Because of its magnitude and site-to-source distance, the Hayward-Rodgers Creek fault is likely to generate the strongest ground motions at the dam site. The estimated maximum magnitude for this fault is $M_w 7\frac{1}{4}$. The San Andreas fault, located about 29 km west of dam, is capable of generating long duration shaking due to its large maximum magnitude ($M_w 8.0$). All other intermediate faults have estimated maximum magnitudes lower than the Hayward-Rodgers

Creek fault. Therefore, the Hayward and San Andreas faults are considered as the controlling earthquake sources for analysis of the dam.

6.3 DESIGN RESPONSE SPECTRA

6.3.1 Site Conditions

Because the dam is underlain predominantly by Franciscan Complex Sandstone, the design ground motions were developed for a rock site condition. This required characterization of the bedrock shear-wave velocity near the surface (top 30 m) and selection of appropriate ground motion attenuation models. The crosshole shear wave velocity measurements performed at the site in 1978 (Wahler, 1980) indicate that the shear wave velocity of the bedrock immediately underlying the dam is about 650 m/second. This velocity was used in developing ground motion estimates.

The shear wave velocity of the bedrock was subsequently measured in the downhole geophysical surveys performed for the present investigation. The measured value is about 610 m/sec (or 2,000 fps), slightly lower than the assumed value. The difference is sufficiently small that no change to the recommended design response spectra was judged necessary.

6.3.2 Attenuation Relationships

To characterize the ground motions at the dam site, empirical attenuation relationships were used to predict peak and spectral accelerations. Three independent relationships were used, to account for epistemic uncertainty. The relationships were selected on the basis of the site conditions and the tectonic environment.

Table 6-2 lists the three selected relationships along with their magnitude and distance definitions and limits of applicability. The site conditions assumed for each relationship are also listed in the table. Use of the relationship by Boore et al. (1997) for the San Andreas fault MCE required slight extrapolation beyond the limits of applicability stated by its authors. The selected attenuation relationships were weighted equally for developing the design ground motions.

6.3.3 Deterministic Ground Motion Analysis

A deterministic analysis was used to estimate the ground motions at the dam site for the MCEs on the two controlling seismic sources. This approach is consistent with current DSOD guidelines (Fraser and Howard, 2002).

Given the estimated slip rates on the Hayward and San Andreas faults (about 9 and 24 mm/year, respectively) and the consequence class weight associated with the dam, the DSOD Consequence Hazard Matrix dictates the use of 84th-percentile ground motions for deterministic analysis. Figure 6-2 shows the 84th-percentile horizontal acceleration response spectra calculated using the three selected attenuation relationships for the MCE on the Hayward-Rodgers Creek fault. A similar plot for the MCE on the San Andreas fault is shown in Figure 6-3.

Figures 6-2 and 6-3 also show the arithmetic mean spectra calculated using the three selected models. The calculated horizontal peak ground accelerations are summarized in Table 6-3.

Because of the short site-to-source distance for the Hayward Fault MCE, the vertical ground motions at the site are expected to be of similar (or possibly higher) intensity as the horizontal motions, at high frequencies. Strong vertical motions are also expected for the San Andreas fault MCE. However, vertical motions induce primarily normal stresses in the body of an embankment (as opposed to shear stresses) and so are not expected to result in development of significant excess pore water pressures or shear deformations. For that reason, vertical motions are not usually input into the dynamic analysis of embankment dams.

6.3.4 Fault Rupture Directivity Effects

Because the dam is located in close proximity to the Hayward and San Andreas faults, the effects of fault rupture directivity were considered in selecting the design ground motions. Fault rupture directivity increases the intensity of long-period motions (periods > 0.6 seconds) when the rupture propagates toward the site (forward directivity), and decreases the intensity of motions when it propagates away from the site. Two types of effects are considered: a) average amplification due to forward directivity, and b) amplification due to orientation with respect to fault strike. The latter effect produces stronger long-period motions in the direction normal to fault strike.

For this study, fault rupture directivity effects for strike-slip faults were accounted for in a manner consistent with DSOD's guidelines (Fraser and Howard, 2002) as follows:

- The directivity effects were applied to the average response spectrum (with no directivity) developed at the appropriate statistical level of design for the project;
- The Somerville et al. (1997) near-source factors, as modified by Abrahamson (2000), were used to develop spectra for average directivity effects and for the fault-normal and fault-parallel components. The portion of the fault that ruptures towards the site was assumed to be 40% of the total rupture length.
- The spectrum for the fault-parallel component was assumed to be no lower than the spectrum for the average component without directivity

The effects of directivity on the duration of strong shaking were accounted for through the selection of time histories for analysis.

6.3.5 Design Response Spectra

The design response spectra for the dam were developed from the results of the deterministic analysis, modified for fault rupture directivity effects. Figures 6-4 and 6-5 show the mean 84th-percentile horizontal acceleration response spectra for MCEs on the Hayward and San Andreas faults, respectively. These figures also show the response spectra modified for average, fault-normal, and fault-parallel directivity. Figure 6-4 shows that the fault-parallel response spectrum calculated for the MCE on the Hayward fault is similar to that without directivity effects. For the MCE on the San Andreas fault, however, the calculated fault-parallel response spectrum is higher than the average spectrum without directivity effects (see Figure 6-5).

Because the transverse axis of the dam is oriented at about 90° with respect to the strike of the Hayward and San Andreas faults, we recommend that the spectrum corresponding to the normal directivity effects be used for dynamic stability analysis of the dam. The recommended spectral

values are tabulated in Table 6-4. The recommended response spectra are applicable to a free-field rock condition and a damping value of 5 percent.

The response spectrum for the MCE on the San Andreas fault is lower than that for the Hayward fault. However, the MCE on the San Andreas fault has a larger magnitude (M_w 8.0) and will produce longer duration shaking.

6.4 SPECTRUM-COMPATIBLE ACCELERATION TIME HISTORIES

Acceleration time histories were developed for each recommended design response spectrum. The time histories were selected from a database of past earthquake records and then modified to match the recommended design response spectra.

To evaluate the sensitivity of the dam's dynamic analysis to the time history details, two acceleration time histories were initially developed for the Hayward fault MCE. The time histories were based on the 270-degree component of the Lucerne Valley record of the 1992 Landers, California earthquake and the 142-degree component of the KJMA record of the 1995 Kobe, Japan earthquake. The 360-degree component of the Carlo record from the 2002 Denali, Alaska earthquake was used for the San Andreas fault MCE. The key characteristics of the recorded time histories are shown in Table 6-5. The recorded acceleration, velocity and displacement time histories and the corresponding 5%-damped acceleration response spectra are plotted in Figures 6-6 through 6-11.

The selected recorded time histories were modified so that their spectra after modification closely match the recommended spectra for each MCE. The records were modified using the procedures developed by Lilhanand and Tseng (1988), as modified by Abrahamson (1993).

In matching the time histories to the target spectra, the following criteria were used:

- For each time history, and over the period range of interest (0.2 to 1.0 seconds), the average of the ratios of the spectral accelerations for the modified time history to the corresponding target spectral accelerations should be approximately equal to 1.0.
- The spectrum for each time history should not be more than about 15 percent lower than the target spectrum at any period over the period range of interest (0.2 to 1.0 seconds).

The recommended time histories and comparisons between their response spectra and the target spectra are shown in Figures 6-12 through 6-16. Figures 6-12 and 6-13 show the two recommended time histories for the Hayward fault MCE. The spectra for those time histories are compared with the target spectrum in Figure 6-14. Figure 6-15 shows the recommended time history for the San Andreas fault MCE. Its spectrum is compared with the target spectrum in Figure 6-16. As shown in Figures 6-14 and 6-16, the spectra for the recommended time histories match the target spectra reasonably well.

These time histories were used in the seismic response and deformation analyses of the dam. These analyses indicated that the calculated seismic deformations of the dam are rather sensitive to the time history details. Thus, additional time histories were developed to represent the motions of the Hayward fault MCE and were used to evaluate the sensitivity of the calculated dam deformations to the ground motions. The additional time histories and the sensitivity analysis results are presented in Section 11.

**Table 6-1
Main Earthquake Sources in the Region**

Fault	Maximum Magnitude, M_w	Site-to-source Distance, km	Activity¹
Hayward-Rodgers Creek	7 ¼	0.3	Active
Mt. Diablo Thrust	6 ¾	17	Active
Concord-Green Valley	6 ¾	22	Active
Northern Calaveras	7	19	Active
San Andreas	8	29	Active
Greenville	7	36	Active
San Gregorio-Seal Cove	7 ½	36	Active

Note:

(1) Defined in accordance with DSOD guidelines.

**Table 6-2
Selected Attenuation Relationships**

Attenuation Relationship	Definitions		Limits of Applicability		Site Condition
	Magnitude	Distance	Magnitude	Distance	
Abrahamson and Silva (1997)	M_w^1	R_{rup}^2	(see note 4)	(see note 4)	Rock
Sadigh et al. (1997)	M_w^1	R_{rup}^2	$4.0 \leq M_w \leq 8+$	$R_{rup} \leq 100$ km	Rock
Boore et al. (1997)	M_w^1	R_{jb}^3	$5.5 \leq M_w \leq 7.5$	$R_{jb} \leq 80$ km	$V_s=650$ m/s

Note:

1 = Moment magnitude.

2 = Closest distance to rupture surface.

3 = Closest horizontal distance to vertical projection of rupture surface.

4 = Not stated by the authors of the relationship; assumed applicable up to M_w 8+, and to the site-to-source distances, based on range of data used for its development.

**Table 6-3
Calculated Horizontal Peak Ground Acceleration**

MCE	M_w	Distance, km	Calculated 84th-% Horizontal Peak Ground Acceleration, g			
			AS 97	SD 97	BR 97	Mean
Hayward-Rodgers Creek	7¼	0.3	1.25	1.10	0.83	1.06
San Andreas	8.0	29	0.33	0.37	0.34	0.35

Note:

AS 97 = Abrahamson and Silva (1997)

SD 97 = Sadigh et al. (1997)

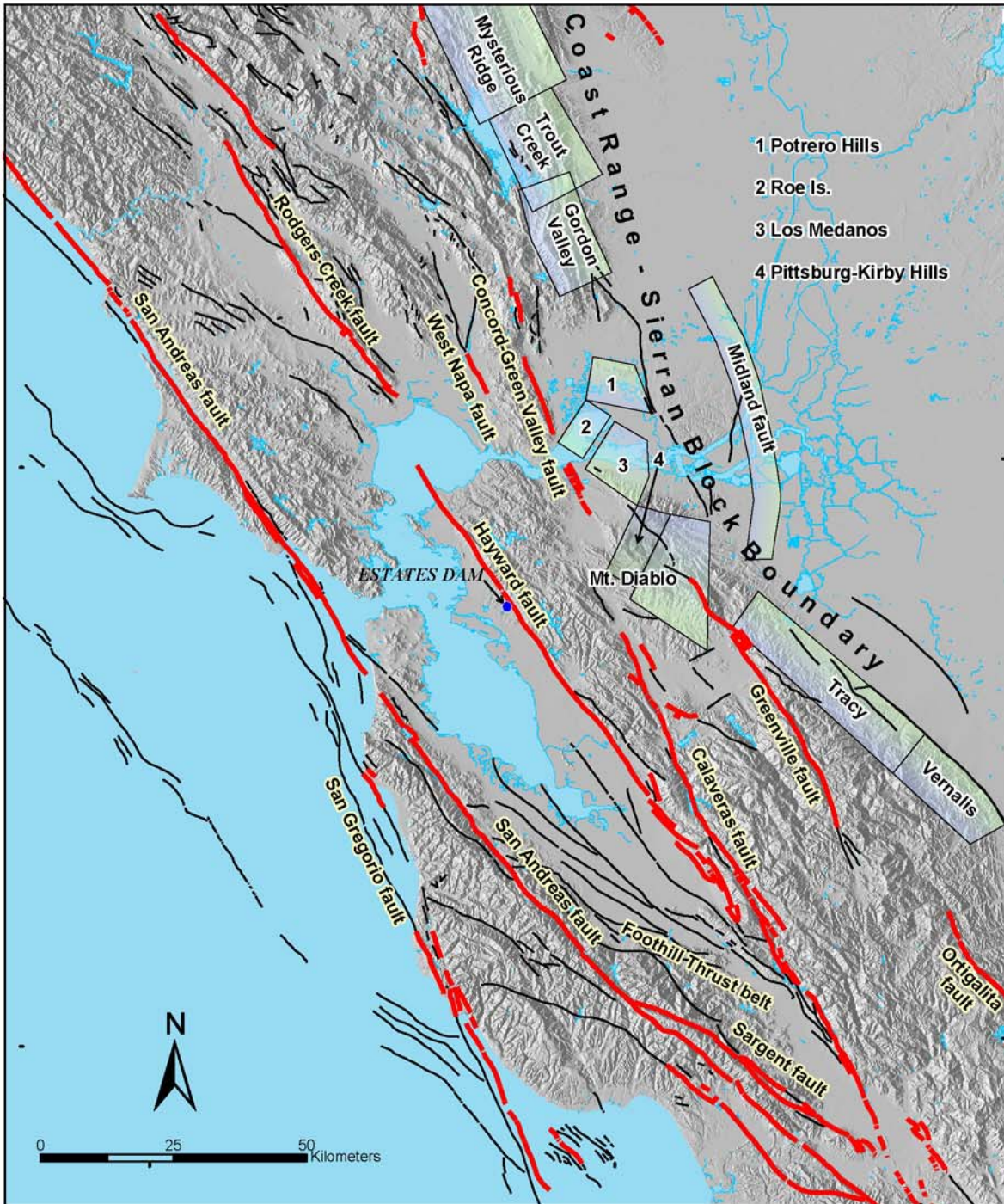
BR 97 = Boore et al. (1997)

**Table 6-4
Recommended Design Response Spectral Values**

Period, seconds	Recommended Design Response Spectral Values, g	
	Hayward-Rodgers Creek Fault MCE	San Andreas Fault MCE
PGA	1.060	0.345
0.02	1.060	0.345
0.05	1.525	0.407
0.075	1.808	0.462
0.10	2.076	0.539
0.15	2.431	0.681
0.20	2.575	0.747
0.30	2.479	0.782
0.40	2.298	0.758
0.50	2.080	0.710
0.75	1.818	0.620
1.0	1.592	0.562
1.5	1.188	0.466
2.0	0.927	0.401
3.0	0.671	0.281
4.0	0.525	0.215

**Table 6-5
Earthquake Records Used to Develop Time Histories
for Hayward-Rodgers Creek Fault and San Andreas Fault MCEs**

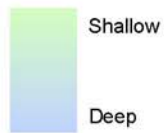
Earthquake	M _w	Recording Station			Component
		Station	Distance (km)	Site Condition	
Hayward fault MCE					
1992 Landers, California	7.3	Lucerne Valley	2	6m Decomposed Granite	270-deg
1995 Kobe, Japan	6.9	KJMA	0.6	Shallow soil over rock	142-deg
San Andreas fault MCE					
2002 Denali, Alaska	7.9	Carlo, Alaska Station	64	Shallow alluvium over rock	360-deg



Legend

- Holocene faults
- Pre-Holocene faults

Blind Thrust Depth



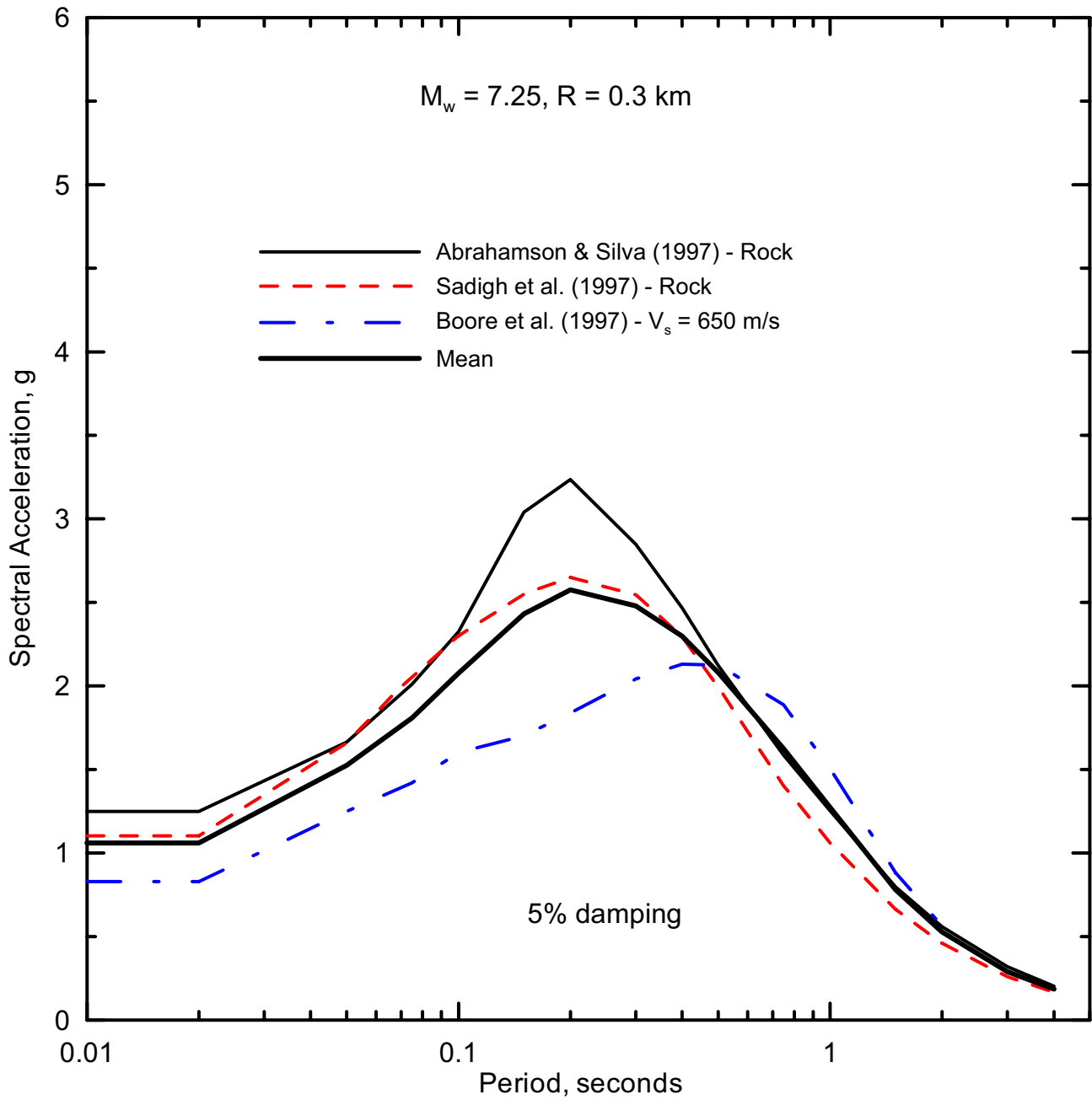
References:
 Jennings 1994
 O'Connell et al., 2001
 Unruh and Hector, 1999



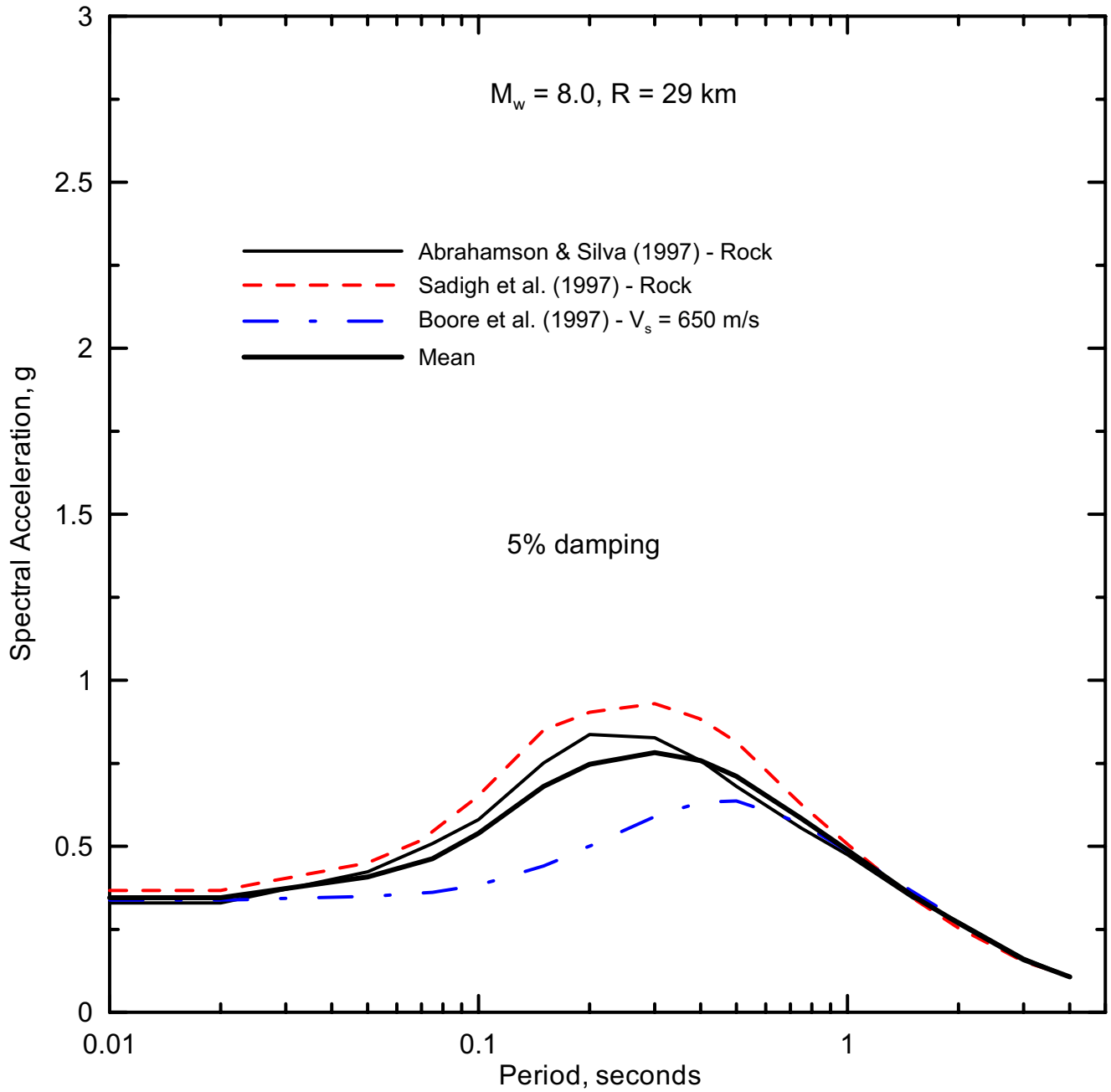
26814957
 Estates Dam
 Seismic Stability Study

Map of Regional
 Seismic Sources

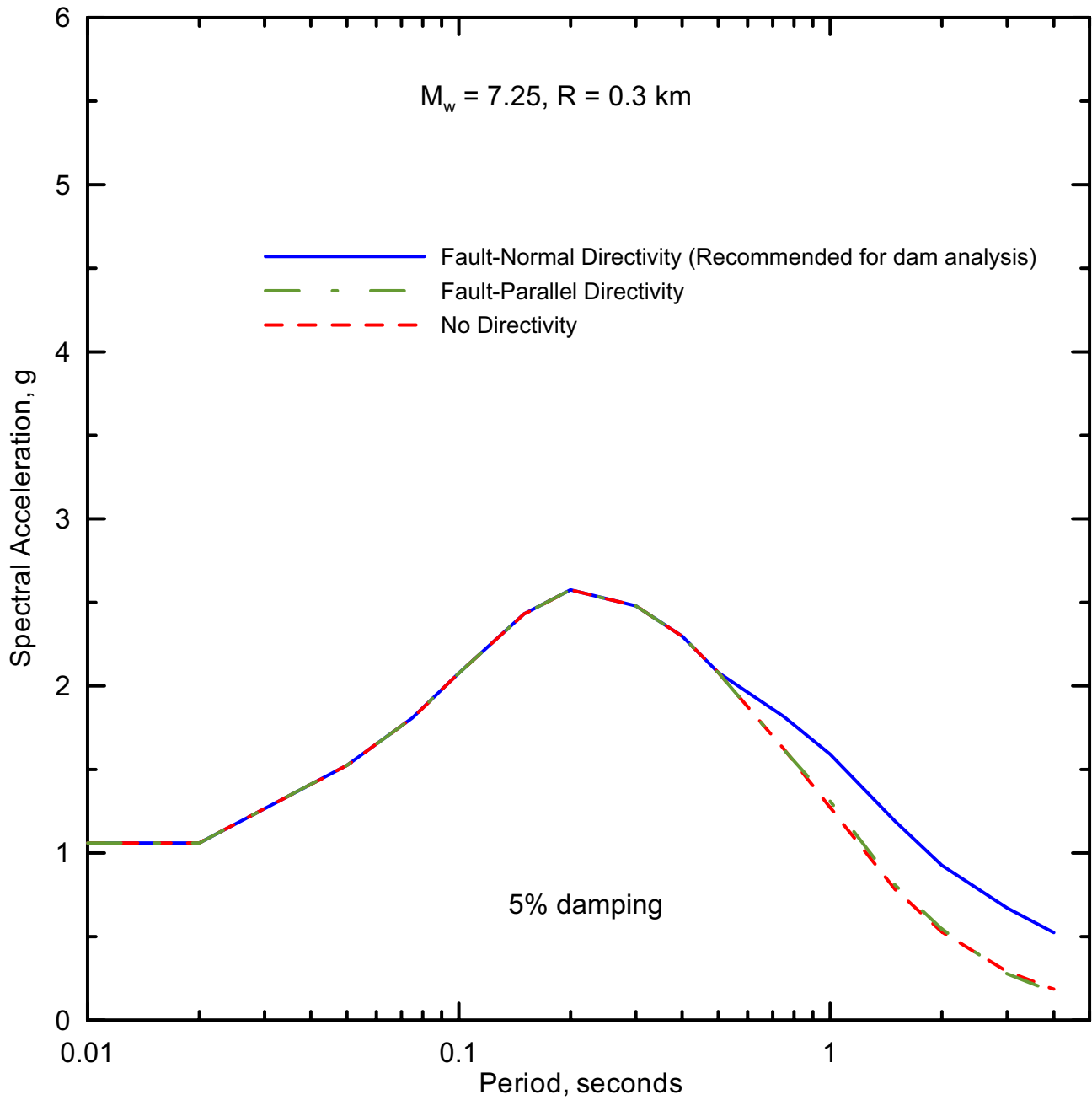
Figure
 6-1



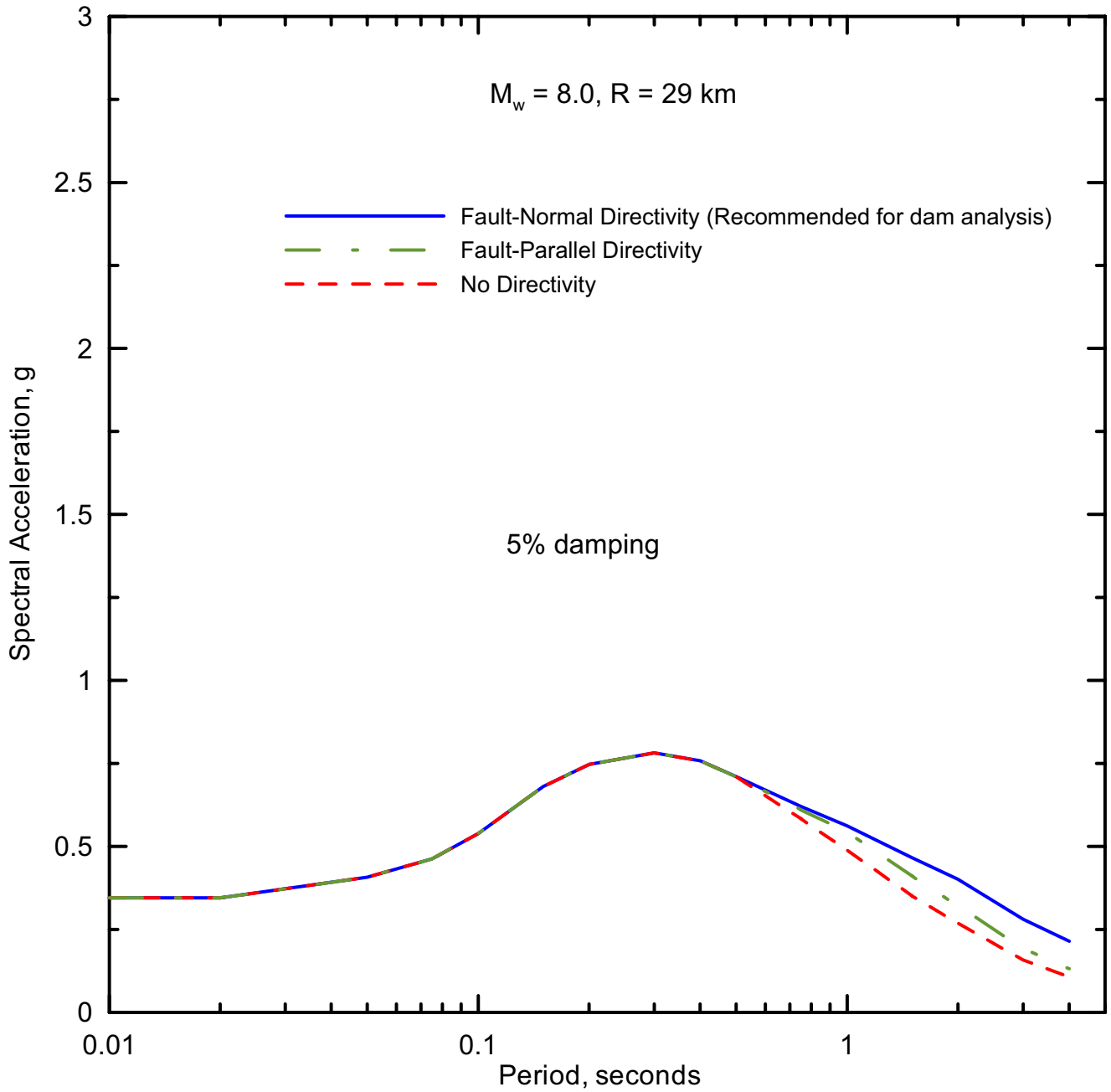
URS	Project No. 26814957	Calculated 84th-percentile Acceleration Response Spectra for Hayward-Rodgers Creek Fault MCE	Figure
	Estates Dam Seismic Stability		6-2



URS	Project No. 26814957	Calculated 84th-percentile Acceleration Response Spectra for San Andreas Fault MCE	Figure
	Estates Dam Seismic Stability		6-3



URS	Project No. 26814957	Design Acceleration Response Spectra for Hayward-Rodgers Creek Fault MCE	Figure
	Estates Dam Seismic Stability		6-4



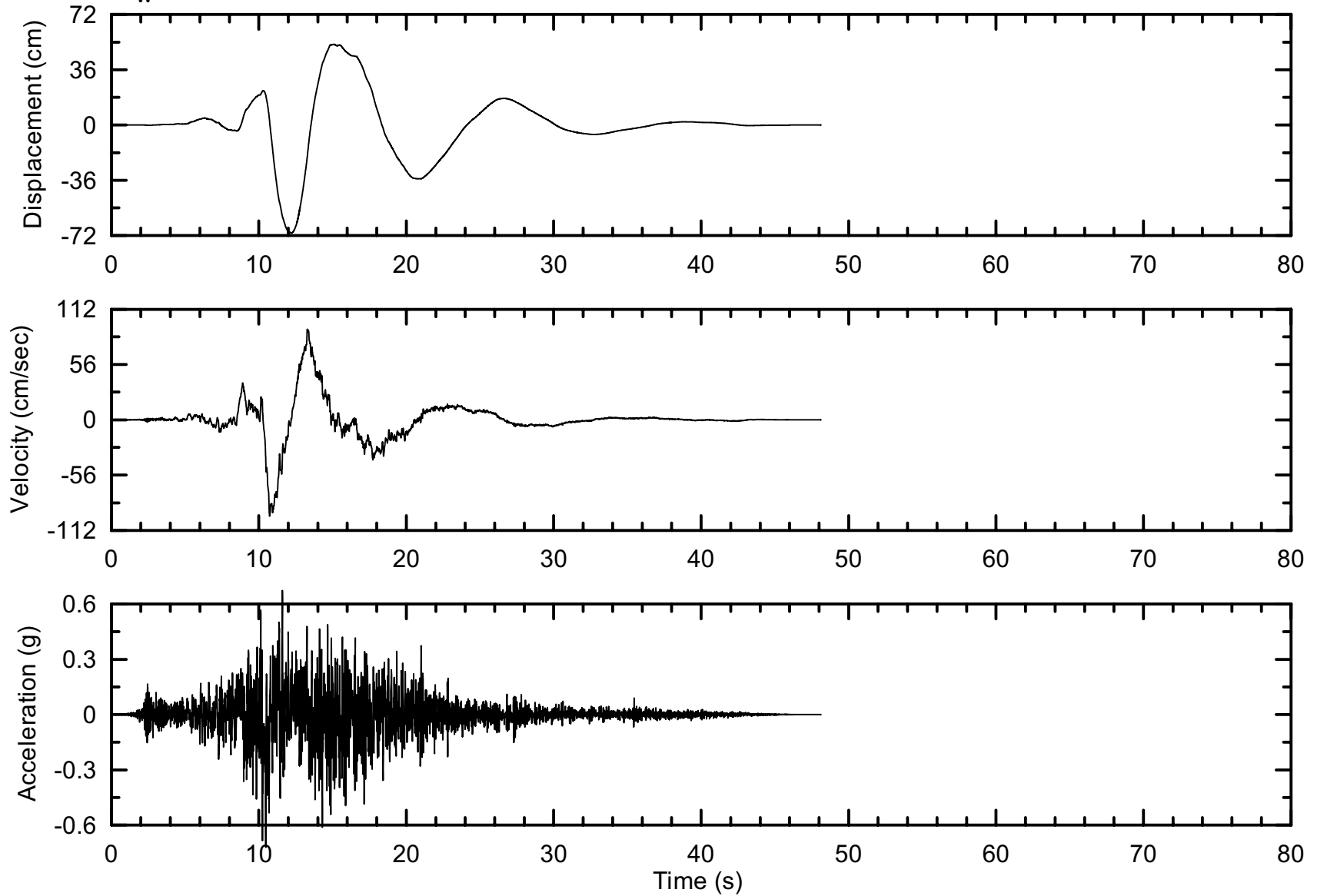
Project No. 26814957

Estates Dam
Seismic Stability

**Design Acceleration Response
Spectra for San Andreas Fault MCE**

Figure
6-5

1992 Landers, CA Earthquake Time History
 at Lucerne Valley Station,
 $M_w = 7.3$, $R = 2.0$ km



Project No.
26814957

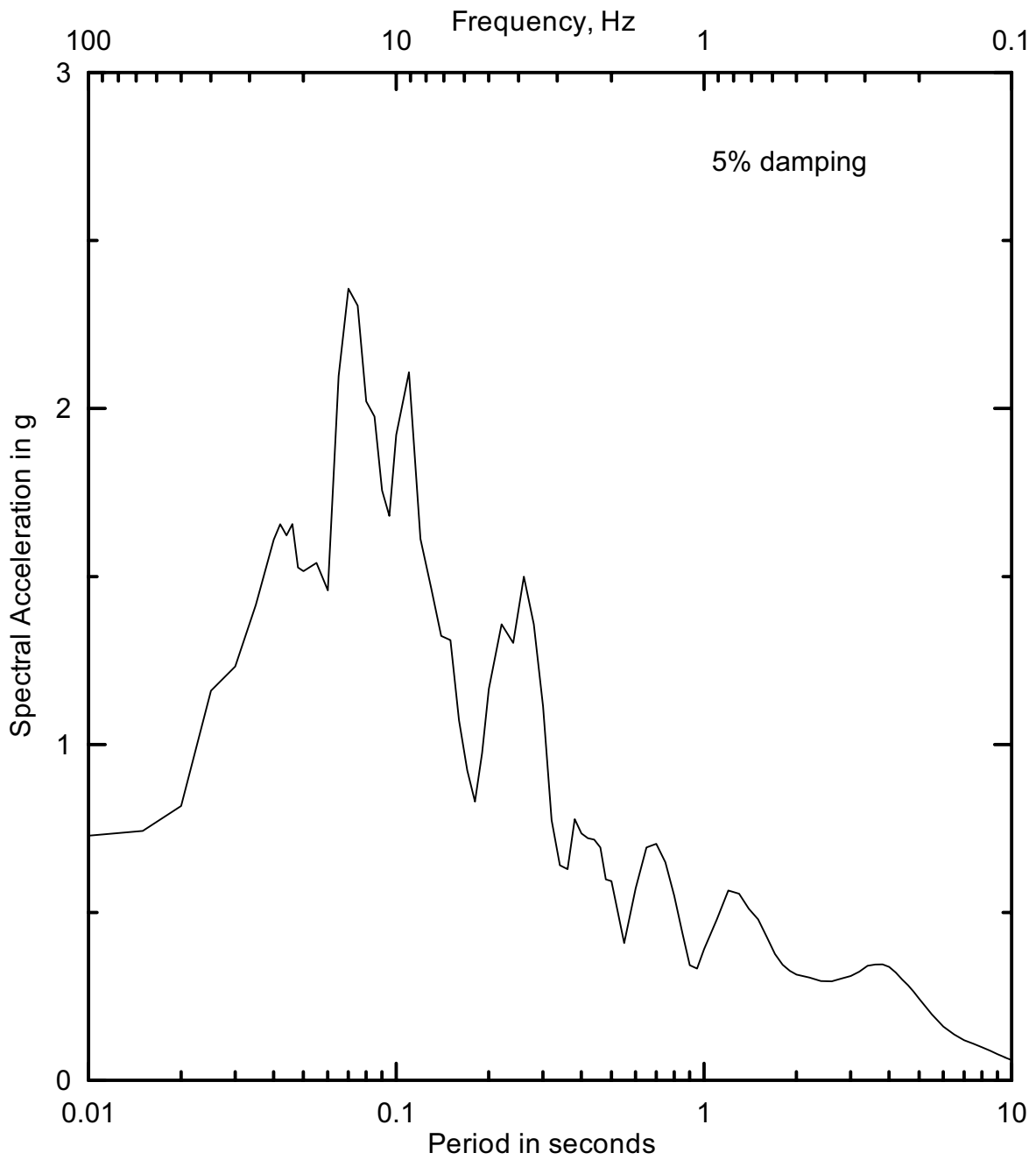
Estates Dam
Seismic Stability

Recorded Time History
1992 Landers, CA Earthquake
at Lucerne Valley Station,
Horizontal Component, 270 deg.

Figure

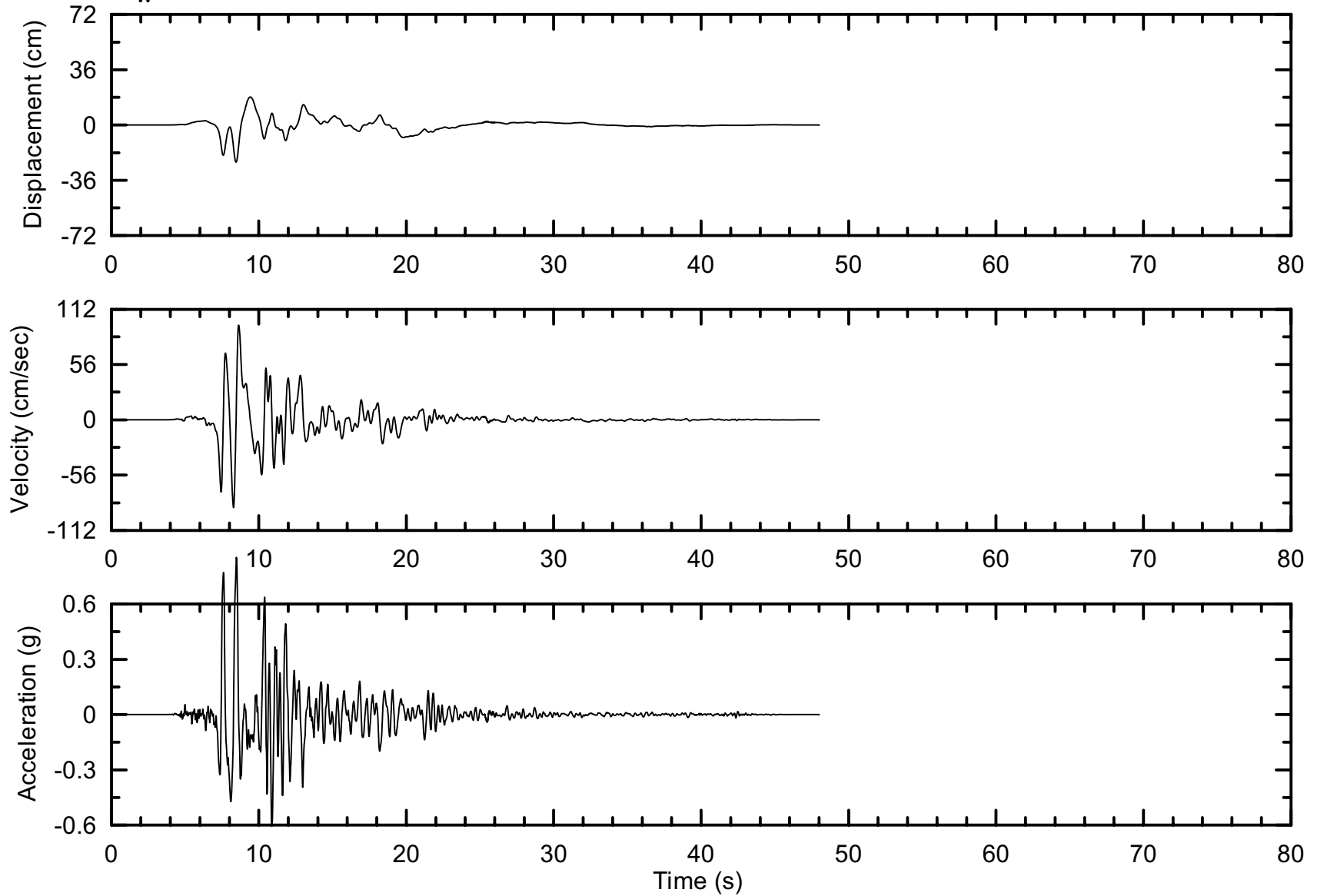
6-6

URS



Project No. 26814957	Estates Dam Seismic Stability	Acceleration Response Spectra 1992 Landers, CA Earthquake at Lucerne Valley Station, Horizontal Component 270 deg.	Figure 6-7
URS			

1995 Kobe, Japan Earthquake Time History
 at KJMA Station,
 $M_w = 6.9$, $R = 0.6$ km



Project No.
26814957

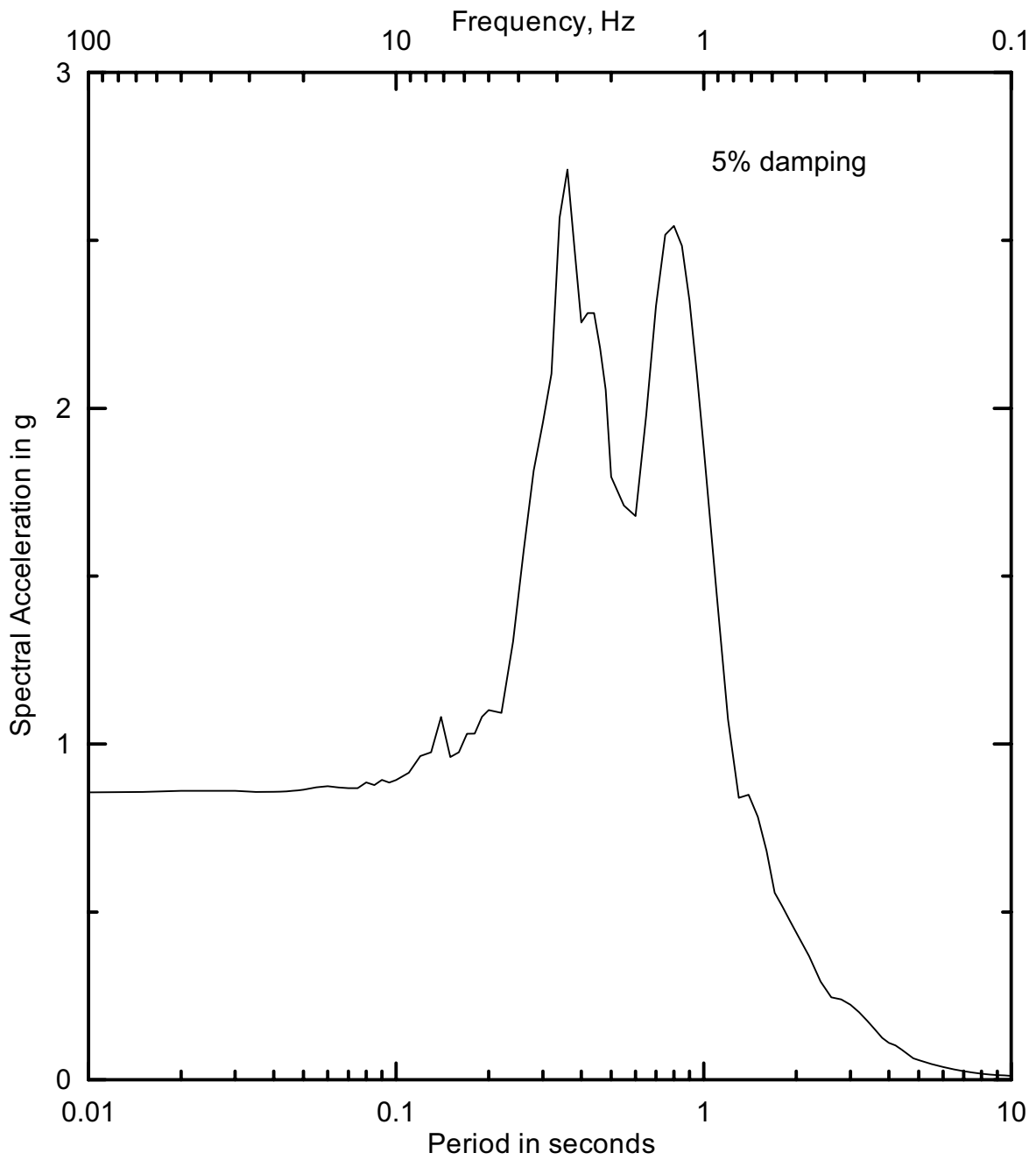
Estates Dam
Seismic Stability

Recorded Time History
1995 Kobe, Japan Earthquake
at KJMA Station,
Horizontal Component, 142 deg (Rotated).

Figure

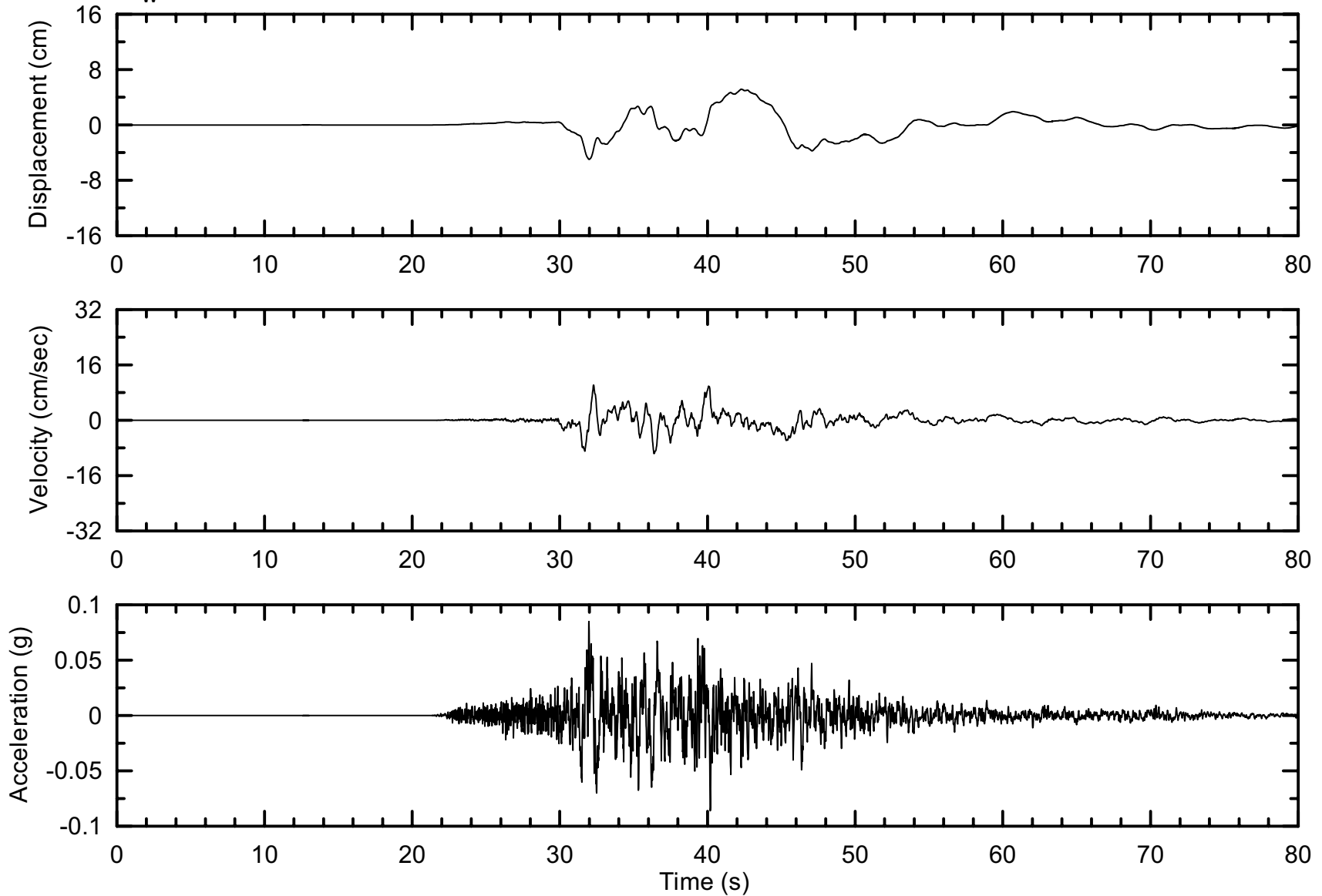
6-8

URS



Project No. 26814957	Estates Dam Seismic Stability	Acceleration Response Spectra 1995 Kobe, Japan Earthquake at KJMA Station, Horizontal Component, 142 deg.	Figure 6-9
URS			

2002 Denali, Alaska Earthquake Time History
 Recorded at Carlo, Alaska Station,
 $M_w = 7.9$, $R = 64$ km



Project No.
26814957

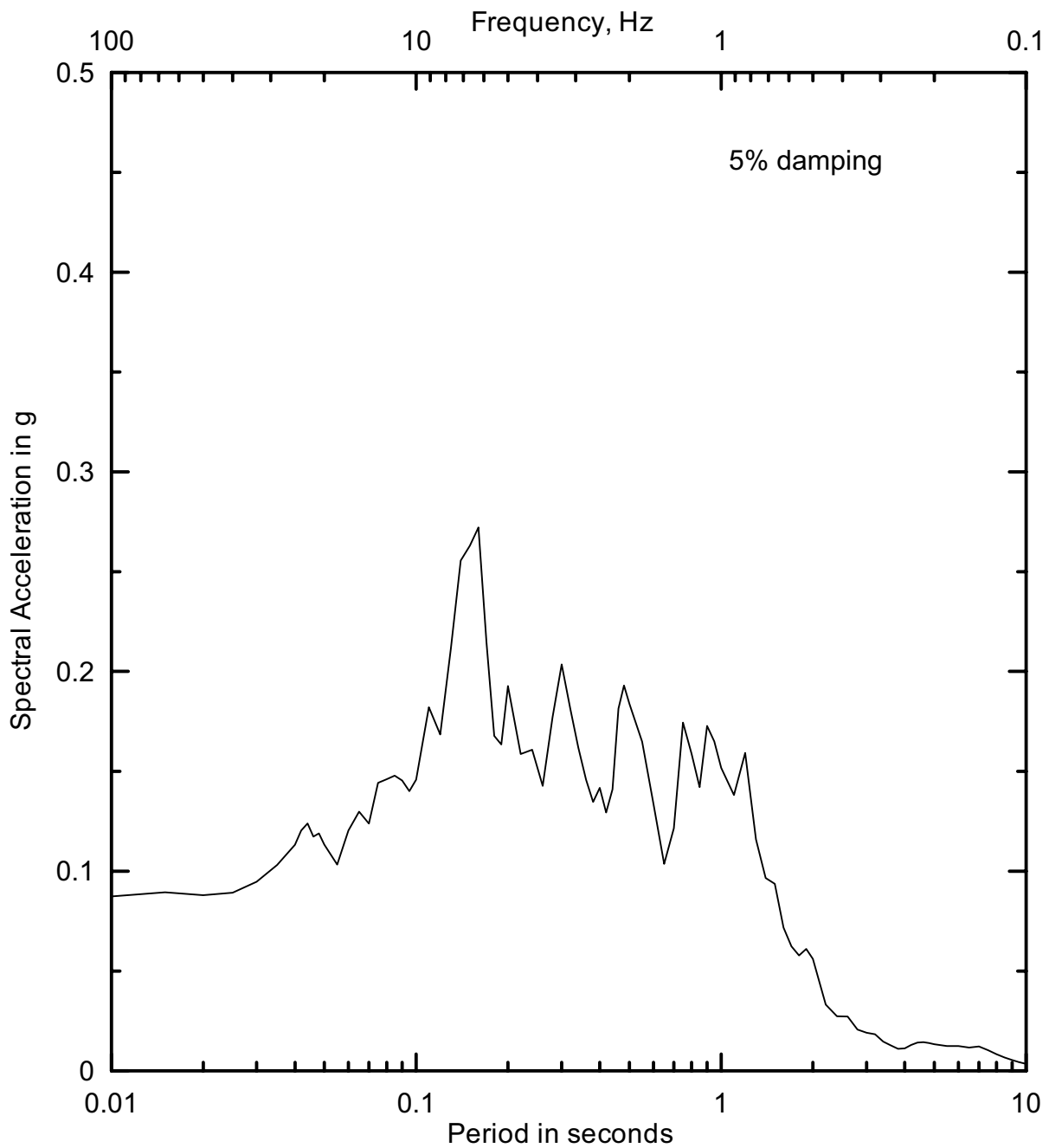
Estates Dam
Seismic Stability

Recorded Time History
2002 Denali, Alaska Earthquake
at Carlo, Alaska Station,
Horizontal Component, 360 deg.

Figure

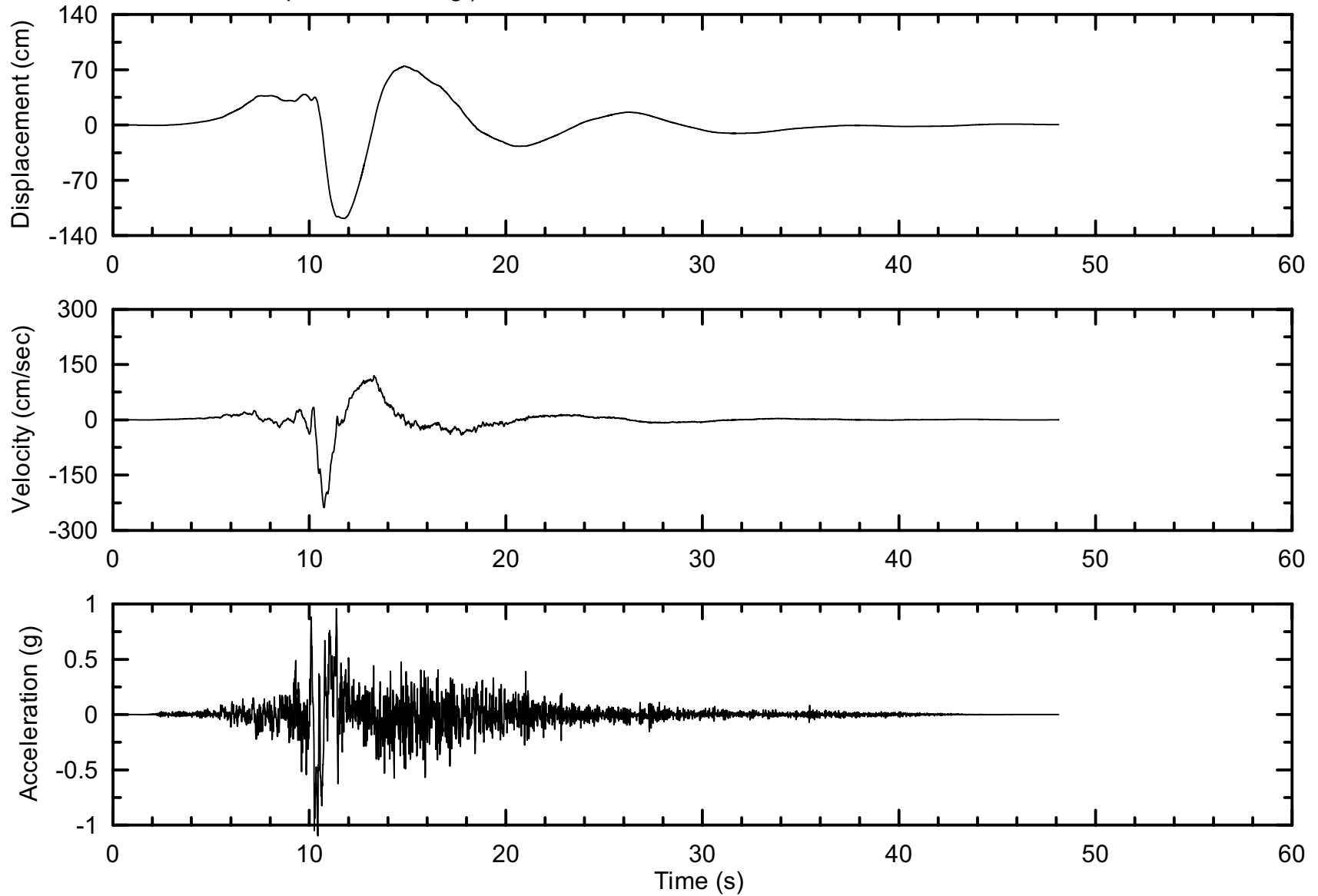
6-10

URS



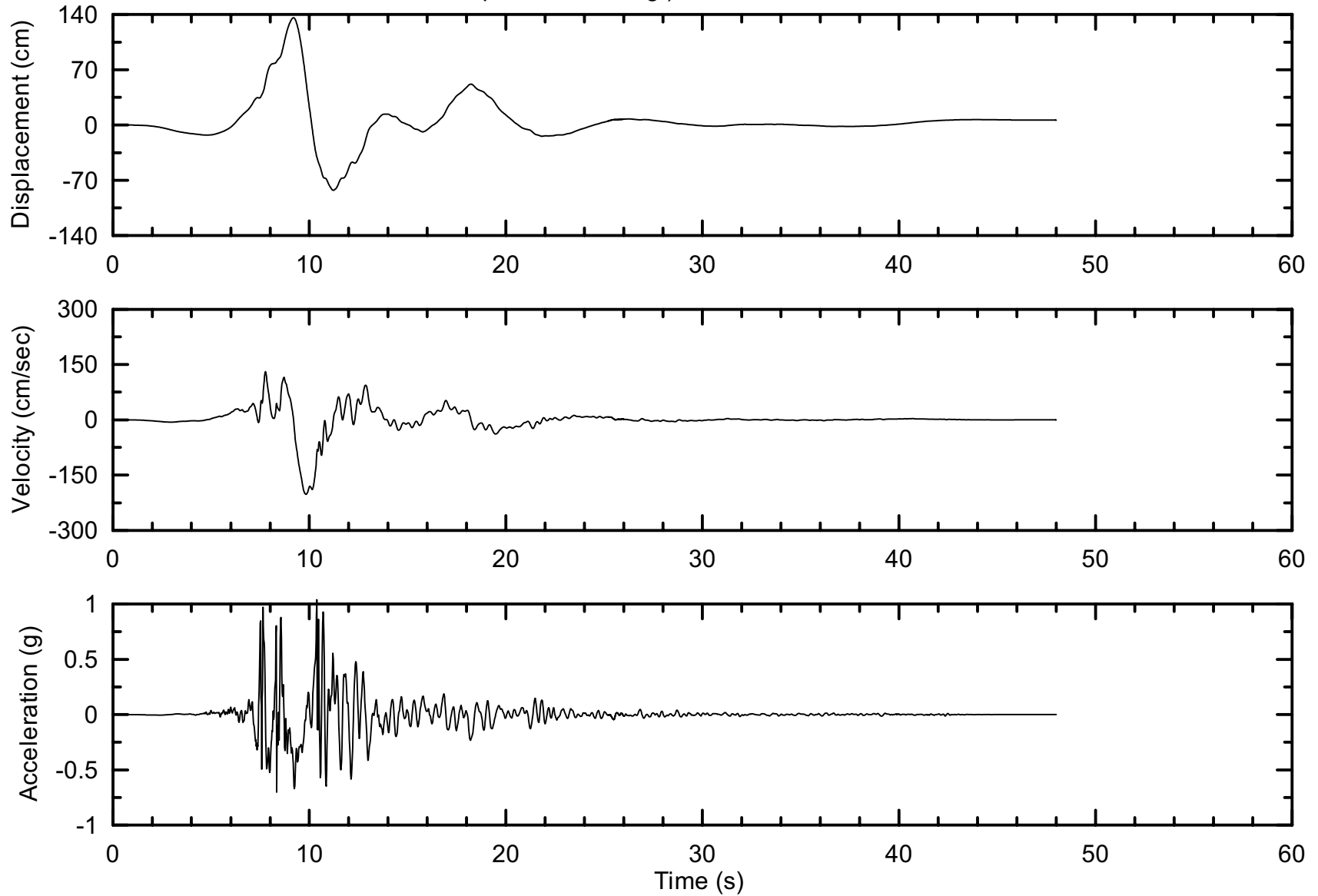
Project No. 26814957	Estates Dam Seismic Stability	Acceleration Response Spectra 2002 Denali, Alaska Earthquake at Carlo, Alaska Station, Horizontal Component 360 deg.	Figure 6-11
URS			

Hayward - Rodgers Creek Fault Event - Recommended Time History #1
 (Modified from 1992 Landers, CA Earthquake - Lucerne Valley Station,
 Horizontal Component, 270 deg.)

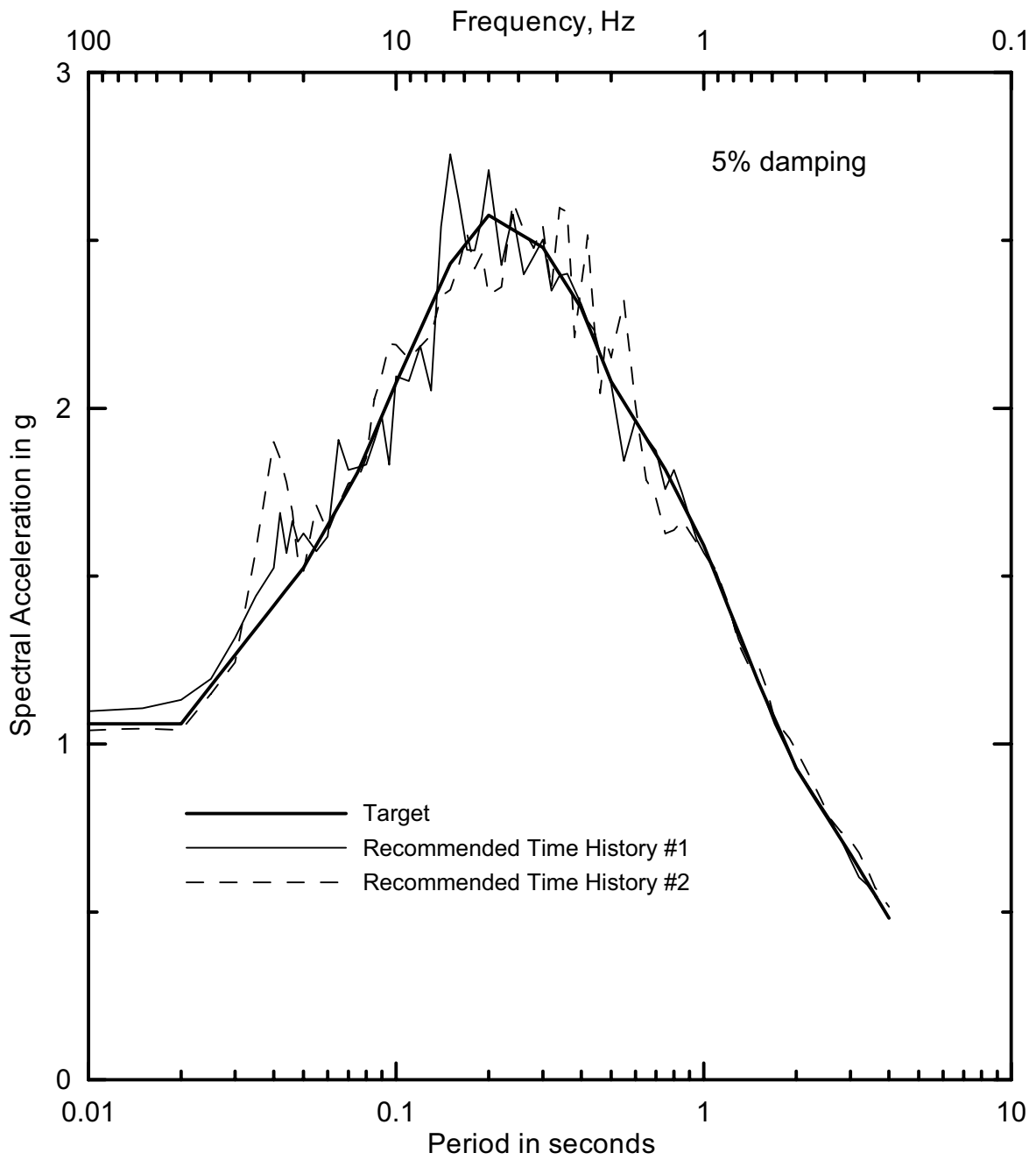


Project No. 26814957	Estates Dam Seismic Stability	Hayward - Rodgers Creek Fault Event Recommended Time History # 1	Figure 6-12
URS			

Hayward - Rodgers Creek Fault Event - Recommended Time History # 2
 (Modified from 1995 Kobe, Japan Earthquake
 at KJMA Station, Horizontal Component, 142 deg.)

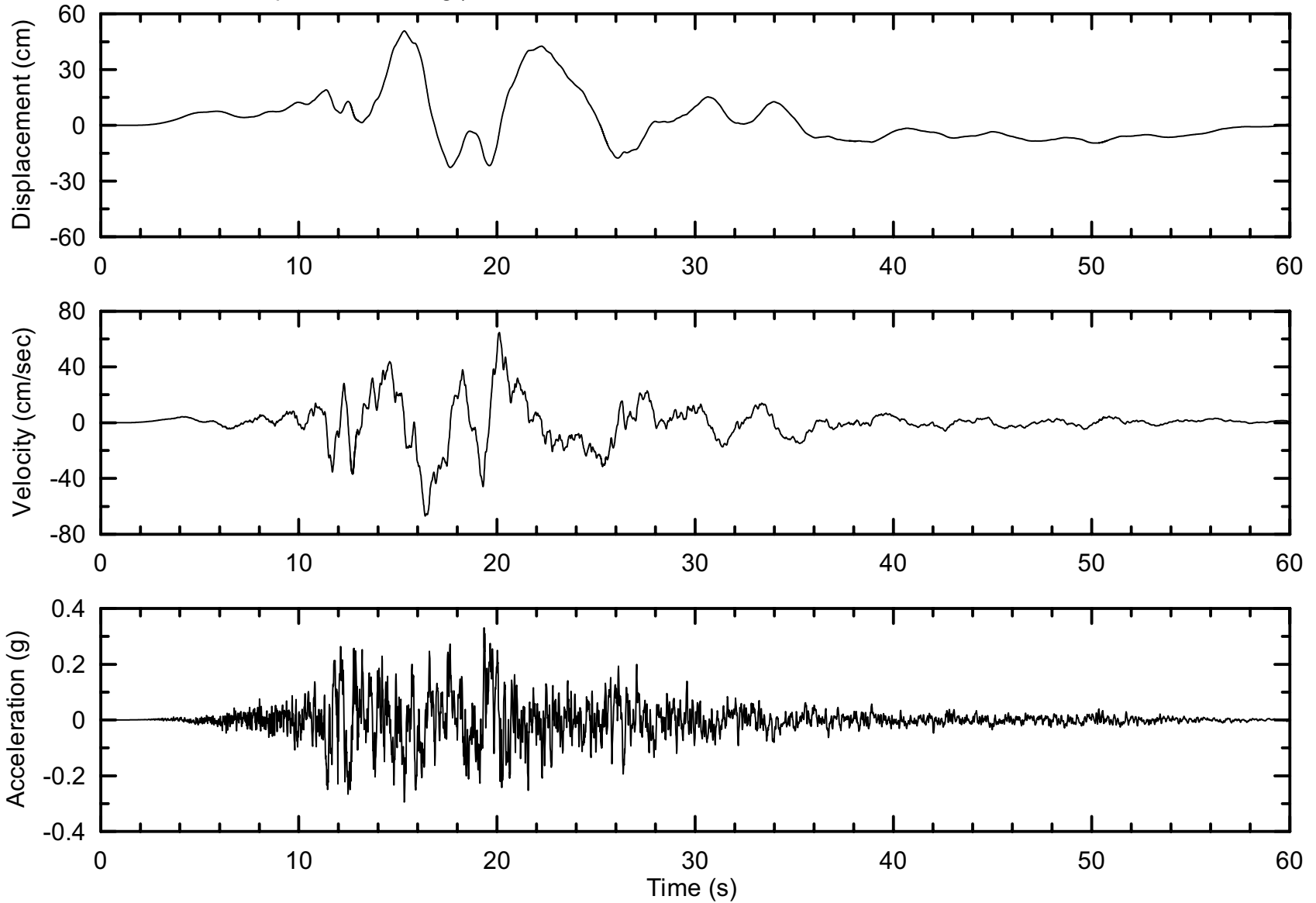


Project No. 26814957	Estates Dam Seismic Stability	Hayward - Rodgers Creek Fault Event Recommended Time History #2	Figure 6-13
URS			

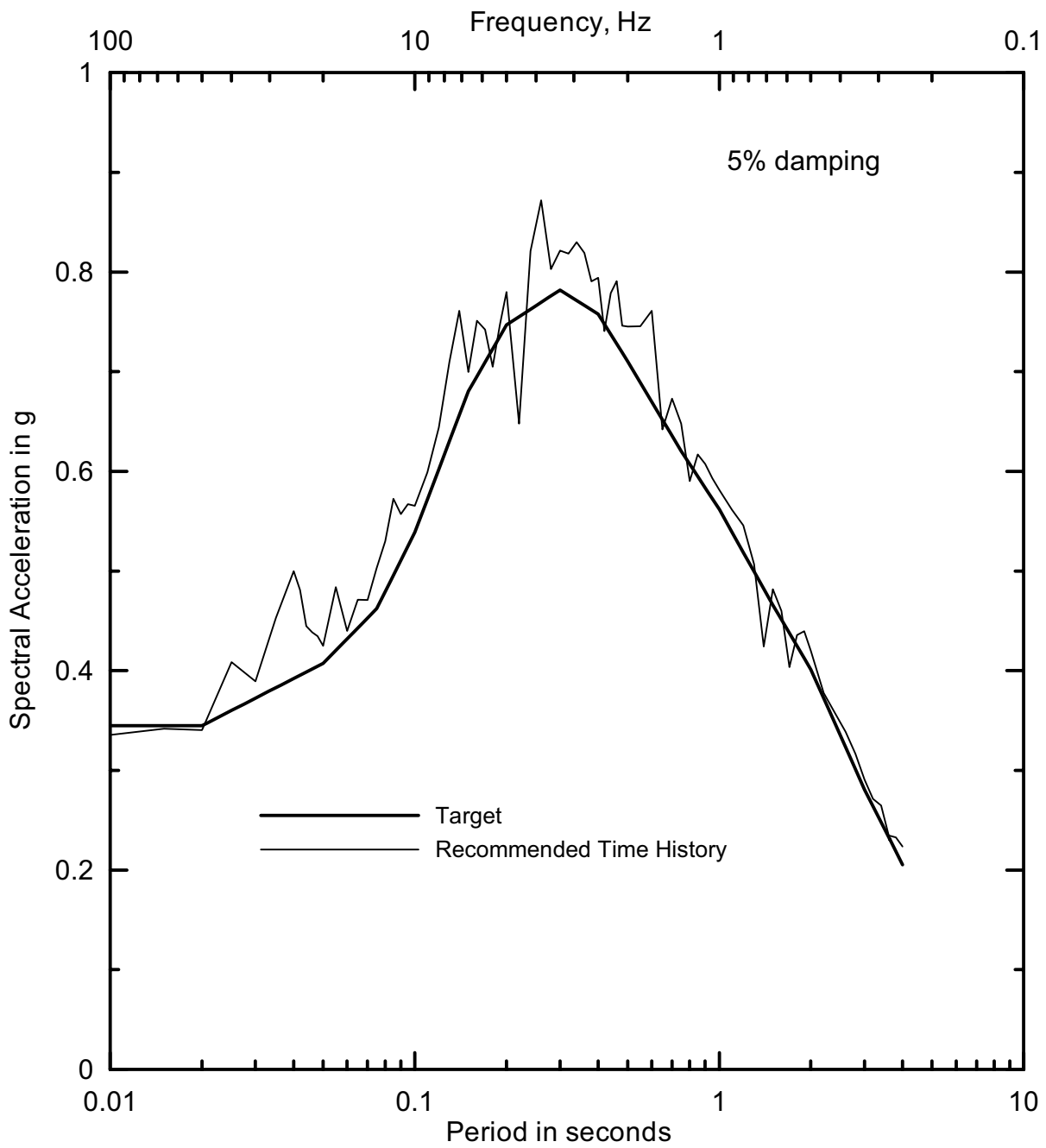


Project No. 26814957	Estates Dam Seismic Stability	Comparison of Acceleration Response Spectra for Hayward - Rodgers Creek Fault Event	Figure 6-14
URS			

San Andreas Fault Event - Recommended Time History
 (Modified from 2002 Denali, Alaska Earthquake - Carlo, Alaska Station,
 Horizontal Component, 360 deg.)



Project No. 26814957	Estates Dam Seismic Stability	San Andreas Fault Event Recommended Time History	Figure 6-15
URS			



Project No. 26814957	Estates Dam Seismic Stability	Comparison of Acceleration Response Spectra for San Andreas Fault Event	Figure
URS			6-16

This section presents the geotechnical characterization of the embankment and foundation conditions. The characterization consisted of three main elements: 1) identifying the material zones that make up the embankment and foundation, 2) characterizing their engineering properties, and 3) defining the groundwater conditions and location of the phreatic surface for analysis. This work was based on the field and laboratory investigations conducted as part of this study, and on the data from previous investigations of the dam. Piezometric data provided by EBMUD were used in characterizing the groundwater conditions within the dam. The locations of the borings and piezometers used to characterize the site conditions are shown in Figure 7-1, along with the locations of two cross-sections used to illustrate the dam conditions.

As part of the geotechnical characterization work, the subsurface data were incorporated into a 3-D GIS model. The GIS model helped visualize the 3-D geometry of the dam, as well as the spatial distribution of the borings and SPT sampling, soil classifications, and foundation soil thickness. A graphical view of the model is presented in Figure 7-2. The electronic data for the model were previously submitted to EBMUD in the form of shape files.

7.1 DAM MATERIALS AND ZONATION

The main body of the embankment was placed in 1903 with material excavated from the upstream basin and compacted by horse-drawn equipment. Additional embankment fill was placed along the downstream slope between 1938 and 1939 to raise the dam. This fill was placed with a bulldozer and compacted with a sheepsfoot roller. Thus, the embankment consists of two main zones: fill of 1903 and fill of 1938-39. The foundation consists of colluvium and residual soils underlain by bedrock.

Based on the data from the new borings and previous borings, two interpretive sections (A-A' and B-B') were developed to illustrate the embankment and foundation conditions. These sections are shown in Figures 7-3 and 7-4. They show the types of materials encountered in the borings in the embankment and foundation. It should be noted that laboratory test data from some of the previous investigations were very limited, and the material classifications of many samples from those investigations are based on visual examination only.

The interpretive sections shown in Figures 7-3 and 7-4 present a best estimate of the zonation within the dam embankment and foundation. It should be noted that some of the zone boundaries shown in these figures cannot be located with certainty. For the most part, the boundary between the 1903 and 1938-39 embankment fills shown in the figures was inferred from the pre-1938 topography of the dam site. However, in the area beneath the downstream slope where the 1903 fill reportedly was over-excavated during the dam raise, the location of this boundary is uncertain. The uncertainty regarding the boundary between the 1903 fill and 1938-39 fill is further discussed in Section 9.

The geotechnical characteristics and engineering properties of the embankment and foundation materials are described in the following sections and are summarized in Tables 7-1 through 7-4. In general, the field and laboratory data obtained from the current investigations are in good agreement with the data obtained from previous investigations, as illustrated in Figures 7-5 through 7-7.

7.2 EMBANKMENT CONDITIONS**7.2.1 1903 Fill*****General Characteristics***

The 1903 fill materials were reportedly excavated from the upper part of the ravine in the upstream basin and compacted by horse-drawn equipment. The records suggest that the materials were placed to form a homogeneous earth fill approximately 280 feet long and 50 feet high. The 1903 fill consists primarily of clayey sands and sandy clays, with gravel. The color of the material varies from yellowish brown and gray to bluish gray and dark gray.

Gradation and Plasticity

The gradations of 1903 fill samples obtained in the exploratory borings for this study are shown in Figure 7-8. The figure shows that the 1903 fill materials have a relatively broad range of gradations. The fines and gravel contents of the material are plotted against elevation in Figures 7-9 and 7-10. Also shown in these figures are the fines and gravel contents of the 1938-39 fill and foundation materials.

Based on those data, the 1903 fill classifies as a clayey sand to sandy clay with gravel. The measured fines content of the material ranges from about 20 to 65 percent, with an average value of about 45 percent. The measured gravel content ranges from about 0 to 25 percent, and averages about 15 percent. Because of the broadly graded nature of the materials, the fines contents are expected to control the overall material behavior under shear and cyclic loading. The results of Atterberg Limits tests from this investigation, shown in Figure 7-11, indicate that the fines are of medium plasticity. The plasticity index for the 1903 fill generally ranges from about 7 to 33 and the liquid limit ranges from about 25 to 50. These ranges are consistent with the data from previous investigations.

Density and Moisture Content

Figure 7-12 presents the water content measurements of the 1903 fill from this investigation. The measured in-situ water content of the 1903 fill ranges from about 10 to 30 percent, and is relatively uniform with elevation. The dry and total densities of the 1903 fill are shown in Figures 7-13 and 7-14. The dry density of the 1903 fill ranges from about 100 to 130 pcf, and the total density of the material ranges from about 120 to 145 pcf. Both types of densities are relatively uniform with elevation.

Shear Strength

As part of this investigation, 16 isotropically consolidated-undrained (ICU) triaxial strength tests with pore pressure measurements were performed on 3- and 4-inch-diameter Pitcher barrel samples. These data, combined with data from previous investigations judged to be of high reliability, were used to evaluate the shear strength of the embankment fill and foundation materials. The strength data from the triaxial tests were taken as one-half the deviator stress at 10% axial strain.

Figures 7-15 and 7-16 show the data by type of test and sample diameter. These figures also compare the data with the strength envelopes used in the analyses by DSOD (Jones, 2003). As shown in these figures, the data from the current and previous investigations are consistent with each other, and there is no significant difference between the strengths measured using 3-inch-diameter samples and those measured from 4-inch samples.

Figure 7-17 shows the strength data for the 1903 fill material, plotted in terms of effective stress-path parameters. The test results are best represented by an effective stress friction angle of 30° and an effective cohesion intercept of 120 pounds per square foot (psf). The strength data in terms of total stress-path parameters are shown in Figure 7-18. Those test results can be represented by a total friction angle of 20° and a cohesion intercept of 380 psf.

Liquefaction Susceptibility

The fines contents of the 1903 fill are sufficiently high such that the behavior of the material under monotonic shear and cyclic loading is expected to be controlled by the fines fraction. Because of the clayey nature of the fines and the moderate water contents and medium plasticity of the materials, the 1903 fill is judged not susceptible to liquefaction. This conclusion was reached by applying the modified Chinese criteria proposed by Seed and Idriss (1982) and the more conservative criteria proposed by Seed et al. (2003). The conclusion is also supported by the criteria recently proposed by Boulanger and Idriss (2004).

As summarized in Table 7-1, on average, the water content of the embankment fill and foundation materials (15 to 18%) is significantly lower than the liquid limit (33 to 37%). Figure 7-19 shows a comparison of the available data on Atterberg limits for the embankment and foundation materials with the liquefaction susceptibility criteria of Seed et al. (2003). It may be seen that the samples tested for this investigation are not susceptible to liquefaction, based on comparison of their water contents and liquid limits with the criteria. The majority of the samples tested in previous investigations are also not susceptible to liquefaction.

Although liquefaction is not expected, the 1903 fill material can develop excess pore pressures during strong earthquake shaking. Such excess pore pressures will result in a reduced undrained strength. The strength loss potential of the material as a result of cyclic loading is discussed in Section 11. The dynamic properties are discussed in Sections 10 and 12.

7.2.2 1938-39 Fill

General

During 1938 and 1939, additional fill was placed on the crest and along the downstream slope of the dam to raise the crest elevation from elevation 765 to the current level of 774. This fill material was excavated from the reservoir, and placed in about 6-inch layers with a bulldozer and compacted with a sheepsfoot roller. During the construction, a wet “boggy” area near the downstream toe, which was caused by a spring, was excavated and drained, and backfilled with new fill material. Tile drains were placed in the trenches to reach the seepage sources. The extent of the excavation area, however, was not documented in detail.

The 1903 and 1938-39 fill materials are similar in appearance, and have been described as “basically indistinguishable” in previous investigations. However, the analysis of the new and

previous data for this study shows that there are differences in the index and strength properties of the materials in these two fill zones.

Gradation and Plasticity

The gradations of 1938-39 fill samples obtained in this investigation are shown in Figure 7-20. The figure shows that the 1938-39 fill material has a broad range of gradations similar to those of the 1903 fill, but tends to be coarser graded.

The fines and gravel contents of the 1938-39 fill material are plotted against elevation in Figures 7-9 and 7-10. Based on these data the 1938-39 fill generally classifies as a clayey sand with gravel. The fines content of the material typically ranges from about 15 to 50 percent, with an average value of about 35 percent. The gravel content ranges from about 10 to 35 percent, and averages about 25 percent. Because of the broadly graded nature of the materials, the fines contents are expected to control the overall material behavior under shear and cyclic loading. The results of Atterberg Limits tests, shown in Figure 7-11, indicate that the fines typically are of medium plasticity. The plasticity index for the 1938-39 fill generally ranges from about 15 to 25 and the liquid limit ranges from about 30 to 47.

Density and Moisture Content

The water contents measured in the 1938-39 fill for this study are shown in Figure 7-12. The in-situ water content of the material ranges from about 10 to 20 percent, and is relatively uniform with elevation. The dry and total densities of the 1938-39 fill are shown in Figures 7-13 and 7-14. The dry density of the material ranges from about 105 to 130 pcf, and the total density ranges from about 120 to 150 pcf. Both densities are relatively uniform with elevation.

Shear Strength

The shear strength data for the 1938-39 fill are shown on Figures 7-17 and 7-18. The effective stress strength envelope is best represented by an effective stress friction angle of 35° and zero cohesion. The total stress strength envelope can be best represented by a total friction angle of 23° and a cohesion intercept of 1250 psf. It is clear from these data that while the effective strength envelopes of the two fill materials are similar, the total strength envelope of the 1938-39 fill is significantly higher than that of the 1903 fill.

Liquefaction Susceptibility

Because the 1938-39 fill has similar index properties to those of the 1903 fill, the 1938-39 fill is also judged to be not susceptible to liquefaction. Nevertheless, when saturated the 1938-39 fill material can develop excess pore pressures during strong earthquake shaking and its undrained strength may be reduced as a result. The potential for strength loss of the material due to cyclic loading is discussed in Section 11. The dynamic properties of the material are discussed in Sections 10 and 12.

7.3 FOUNDATION CONDITIONS

7.3.1 Foundation Soils

General

The depth of foundation excavation and level of preparation prior to placement of the embankment is unknown but thought to be limited. The foundation soils encountered in the recent and previous borings generally consisted of stiff to very stiff sandy clay, silty clay and clay with sand. Medium to stiff dark-colored sandy and silty clay with organics was encountered in a few borings, possibly indicative of an original surface layer that was incompletely removed during original construction. Overall, the data do not indicate the presence of a continuous layer of organic-rich, dark-colored, potentially weak native foundation soil beneath the dam. Based on the boring logs and laboratory tests, the native soils in the dam foundation are stiff and competent. This conclusion is also supported by the downhole geophysical survey results, which do not show lower velocities within the native soils. As discussed below, the index and shear strength properties of the foundation soils are similar to those of the overlying 1903 fill material.

Gradation and Plasticity

The gradations of the foundation soils measured in this study are shown in Figure 7-21. The figure indicates that the foundation soils have a broad range of gradations similar to that of the embankment fill, but somewhat more finely graded.

The measured fines and gravel contents of the foundation soils are plotted against elevation in Figures 7-9 and 7-10. The fines content of the material ranges from about 30 to 70 percent, with an average value of about 60 percent. The gravel content ranges from about 0 to 10 percent, and averages about 5 percent. The fines contents of the foundation soils are generally higher than those of the embankment fill. The Atterberg Limits data for the material, shown in Figure 7-11, fall with the same narrow range as for the embankment fill. The measured plasticity index of the foundation soils generally ranges from about 12 to 22 and the liquid limit ranges from about 30 to 40. The average values of plasticity index and liquid limit are very similar to those of the 1903 fill.

Density and Moisture Content

The water contents of the foundation soils are shown in Figure 7-12. The in-situ water content of the material falls within a narrow range, from about 15 to 22 percent. The dry and total densities of the material are shown in Figures 7-13 and 7-14. The dry density ranges from about 100 to 120 pcf, and the total density ranges from about 125 to 140 pcf. The water contents and the densities are very similar to those of the overlying 1903 fill.

Shear Strength

The shear strength data for the foundation soils are shown on Figures 7-17 and 7-18. At least two of the strength tests from this study were conducted on samples of the dark-colored soils (VQ-38, sample 16, and VQ-40, sample 12). As shown in the figures, the strength data for the foundation

soils and the 1903 fill are very similar. Thus, the same effective and total strength envelopes were used for both the foundation soils and the 1903 fill.

Liquefaction Susceptibility

Overall, the foundation soils are more finely graded than and have similar plasticity characteristics to the 1903 fill. Thus, the foundation soil is also judged to be not susceptible to liquefaction. Nevertheless, excess pore pressures may develop in the foundation soils during strong earthquake shaking and result in a reduction of the undrained strength of the material. The potential for strength loss in the material due to cyclic loading is discussed in Section 11. The dynamic properties of the material are discussed in Sections 10 and 12.

7.3.2 Bedrock

The rock at the dam site and in the area surrounding the reservoir appears to be primarily meta-graywacke of the Franciscan Complex. A detailed description of the geology of the bedrock at the site is included in Appendix E.

The available data on in-situ water content and density of bedrock samples are shown in Figures 7-12 through 7-14. As shown in these figures, laboratory test data are available for only two rock samples. These samples were obtained near the bedrock surface in the more weathered horizons of the formation, and are not likely to be representative of the properties of the less weathered materials at depth. On this basis, a total density of 140 pcf was assumed for the bedrock unit in the dam foundation. The downhole seismic surveys conducted for this study indicate that the shear wave velocity of the materials is about 1,500 feet per second (fps) near the bedrock surface. The measurements also indicate that the shear wave velocity of the materials increases rapidly with depth such that a representative average of the velocities beneath the dam is at least 2,000 fps (see Figures 10-3 through 10-5 and Appendix C).

7.4 GROUNDWATER CONDITIONS

The piezometric data obtained by EBMUD were reviewed to assess the groundwater conditions within the dam and the foundation, and to estimate the location of the phreatic line for analysis. These data are recorded in the piezometers located as shown in Figure 7-1.

The location of the phreatic surface through the dam was estimated based on the piezometric data corresponding to full reservoir level at spillway Elevation 770. The interpreted phreatic surface is shown in the cross-sections in Figures 7-3 and 7-4. The data indicate a relatively steep gradient in the upstream embankment with phreatic levels decreasing from the reservoir level to about Elevation 746 beneath the dam crest. From there, the estimated phreatic line follows a gentle gradient to about Elevation 675 at the downstream toe.

This estimated location of the phreatic surface was used in the stability analysis of the dam.

Table 7-1
Representative Index Properties of Embankment and Foundation Materials⁽¹⁾

Material	Dry Unit Weight (pcf)	Total Unit Weight (pcf)	Liquid Limit (%)	Plasticity Index (%)	Fines Content (%)	Gravel Content (%)
1938-39 Embankment Fill	115 (105 – 130)	133 (120 – 150)	37 (30 – 47)	20 (15 – 25)	35 (15 – 60)	25 (10 – 35)
1903 Embankment Fill	115 (100 – 130)	133 (120 – 150)	35 (25 – 50)	18 (7 – 33)	45 (20 – 65)	15 (0 – 25)
Foundation Soil	112 (100 – 120)	132 (125 – 140)	33 (30 – 40)	17 (12 – 22)	60 (30 – 70)	5 (0 – 10)
Bedrock	(106 – 116) (2)	(128 – 132) (2)	-	-	-	-

Notes:

- (1). Typical range shown in parentheses.
- (2). Only two values reported.

Table 7-2
Strength Parameters for Embankment and Foundation Soils

Material (Zone)	Total Unit Weight	Total Stress Strength Parameters		Effective Stress Strength Parameters	
	γ_t	c	ϕ	c'	ϕ'
	(pcf)	(psf)	(°)	(psf)	(°)
1938-39 Embankment Fill	133	1250	23	0	35
1903 Embankment Fill	133	380	20	120	30
Foundation Soil	133	380	20	120	30

Table 7-3
Comparison of Effective Stress Strength Parameters Between This and Previous Studies

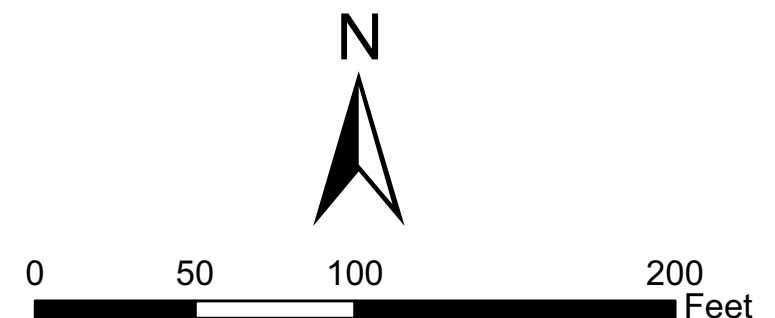
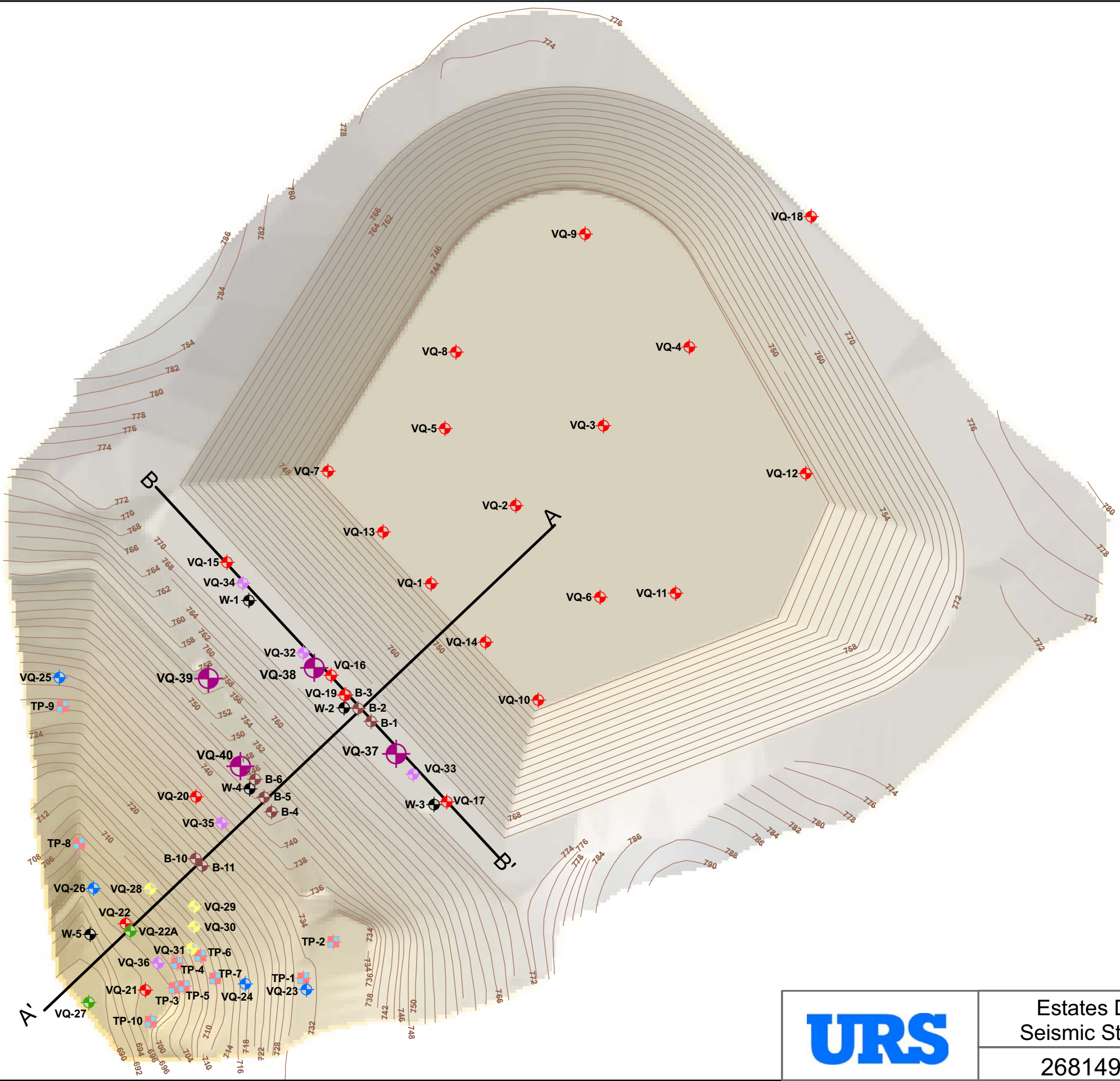
Material (Zone)	This Study		S&W, 1965		Wahler Associates, 1980		DSOD, 2003	
	c'	ϕ'	c'	ϕ'	c'	ϕ'	c'	ϕ'
	(psf)	(°)	(psf)	(°)	(psf)	(°)	(psf)	(°)
1938-39 Embankment Fill	0	35	200	32	420	30	530	23.6
1903 Embankment Fill	120	30	200	32	420	30	530	23.6
Foundation Soil	120	30	-	-	2000	34	-	-

Table 7-4
Comparison of Total Stress Strength Parameters Between This and Previous Studies

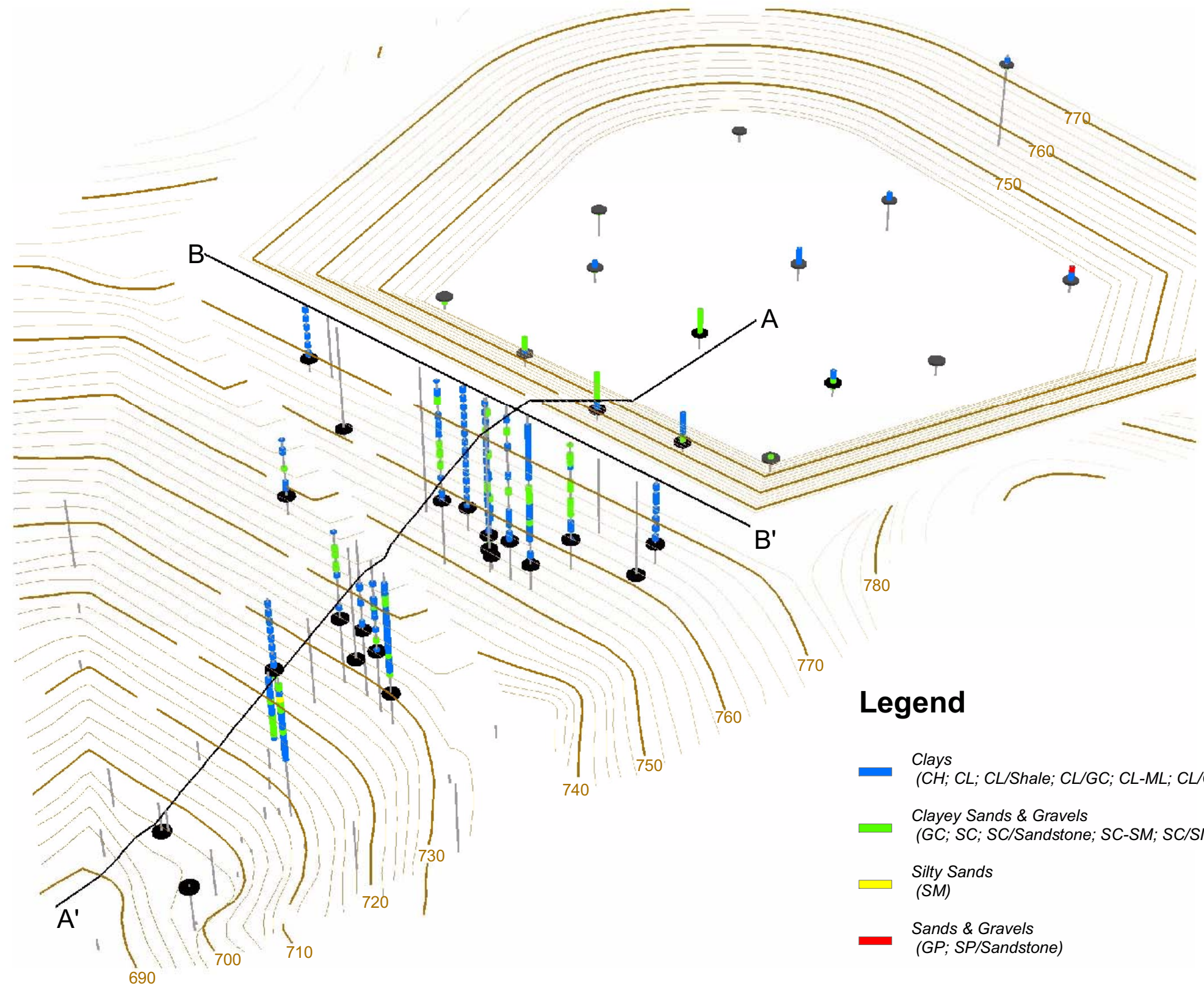
Material (Zone)	This Study		S&W, 1965				Wahler Associates, 1980		DSOD, 2003	
			Normal stress < 2tsf		Normal stress > 2tsf					
	c	φ	c	φ	c	φ	c	φ	c	φ
	(psf)	(°)	(psf)	(°)	(psf)	(°)	(psf)	(°)	(psf)	(°)
1938-39 Embankment Fill	1250	23	1100	8	0	24	-	-	849	13.8
1903 Embankment Fill	380	20	1100	8	0	24	-	-	849	13.8
Foundation Soil	380	20	-	-	-	-	-	-	-	-

Legend

-  EBMUD; 1939 (wells)
-  EBMUD for S&W study; 1962-1965
-  S&W; 1965
-  EBMUD for S&W study; 1965 (test pits)
-  EBMUD for S&W study; 1965
-  EBMUD; 1976
-  Wahler Associates; 1978
-  EBMUD, 1999 (piezometers)
-  URS, 2005

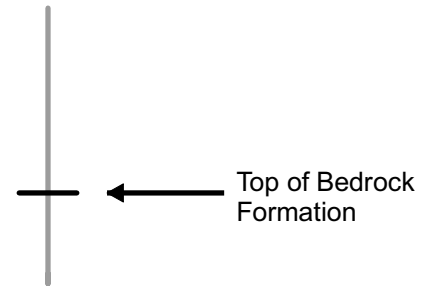


	Estates Dam Seismic Stability	Locations of Field Explorations	Figure 7-1
	26814957		



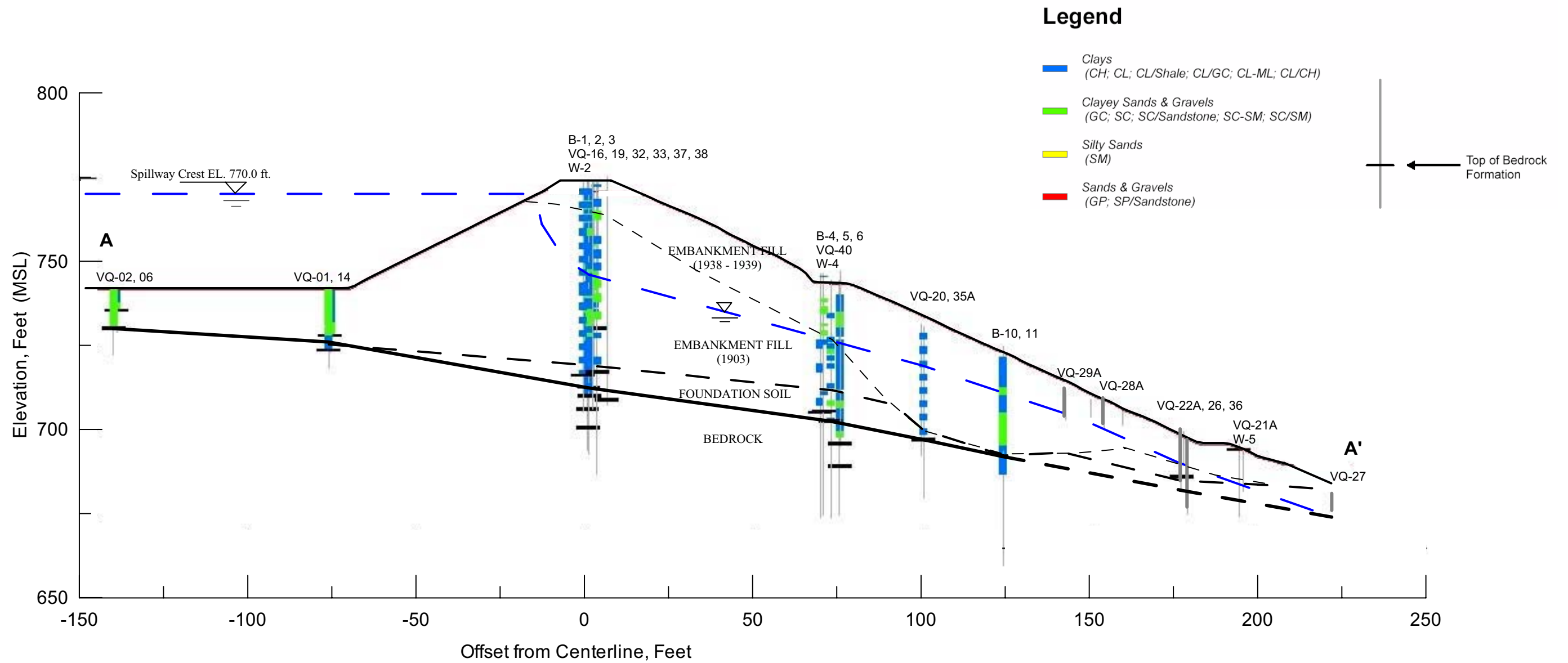
Legend

- █ Clays
(CH; CL; CL/Shale; CL/GC; CL-ML; CL/CH)
- █ Clayey Sands & Gravels
(GC; SC; SC/Sandstone; SC-SM; SC/SM)
- █ Silty Sands
(SM)
- █ Sands & Gravels
(GP; SP/Sandstone)

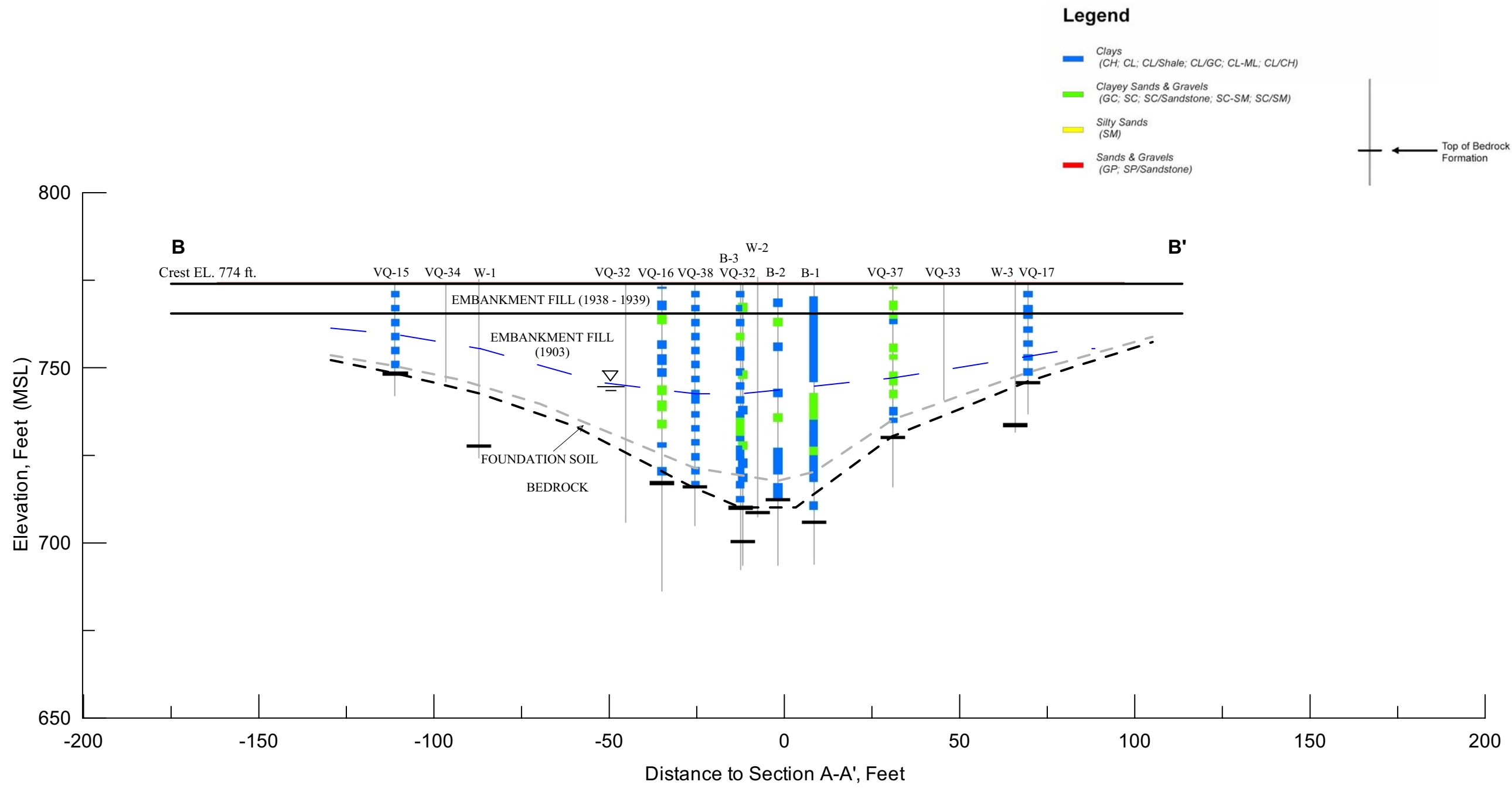


URS	Estates Dam Seismic Stability	GIS Model - Isometric View of Dam with Sample Classifications
	26814957	

**Figure
7-2**

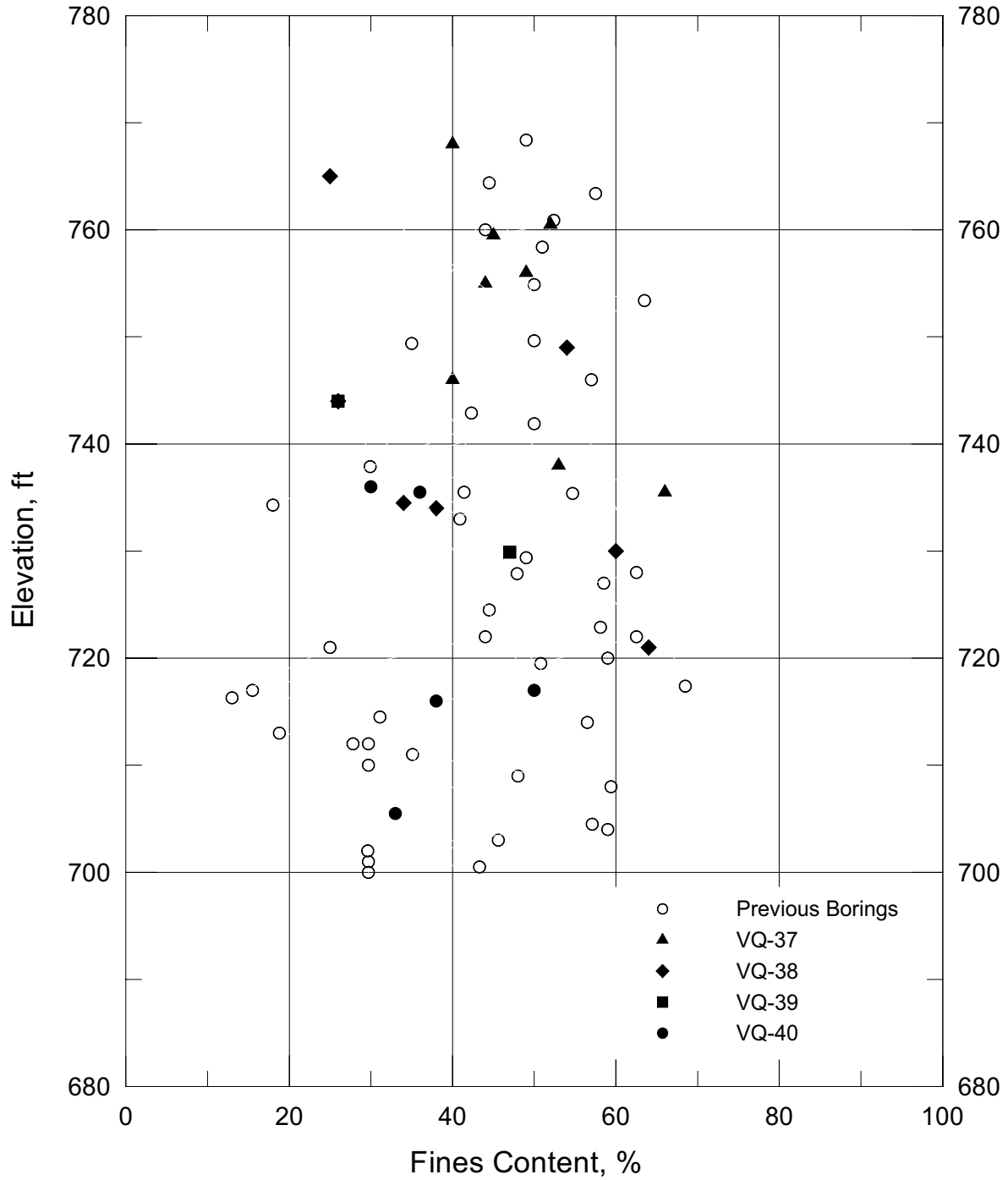


Project No. 26814957	Estates Dam Seismic Stability	Cross Section A-A'	FIGURE 7-3
URS			



Project No. 26814957	Estates Dam Seismic Stability	Cross Section B - B'	FIGURE 7-4
URS			

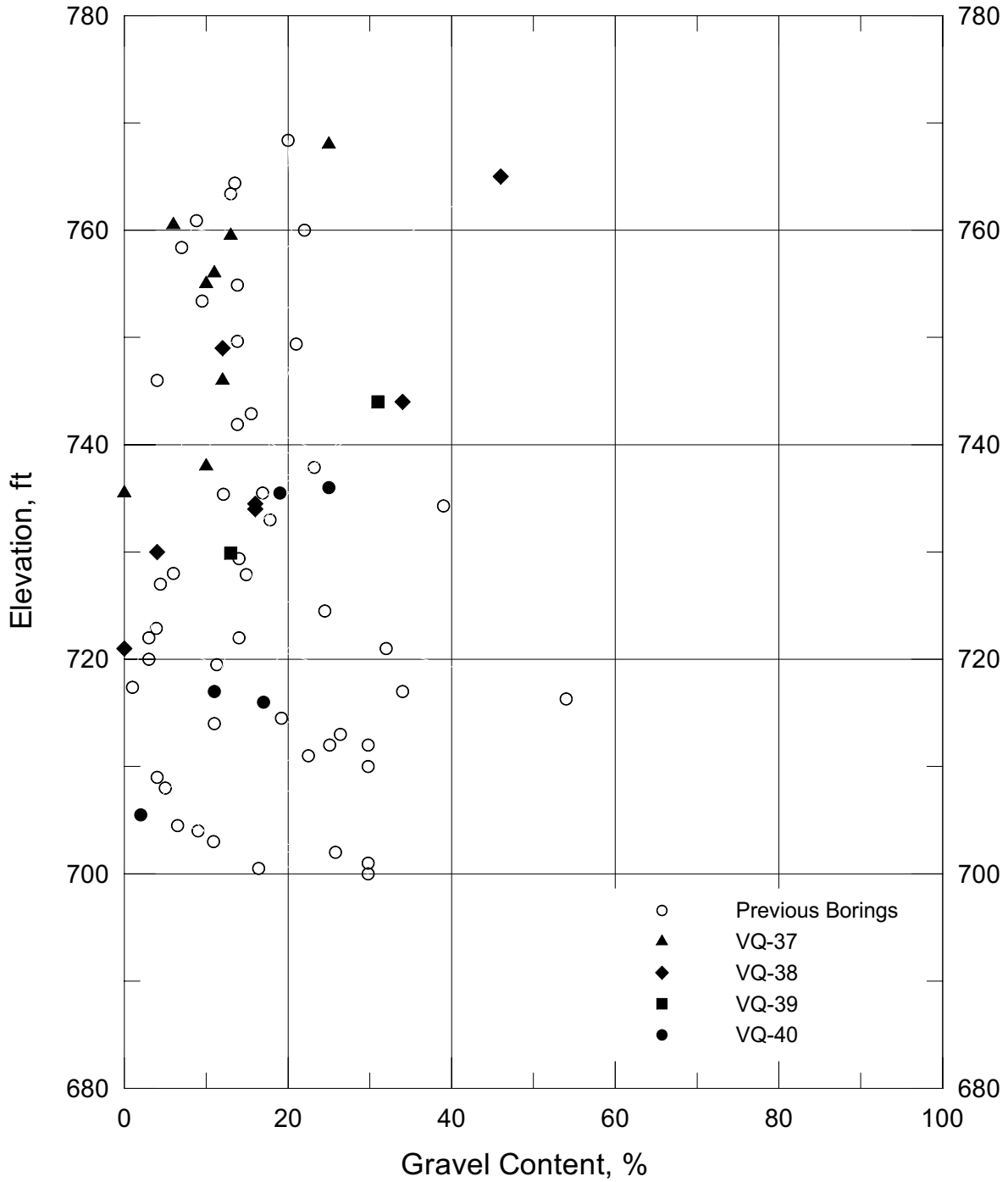
Estates Dam - Fines content



URS	Project No. 26814957	Fines Content Data From Current and Previous Investigations	Figure
	Estates Dam Seismic Stability		7-5

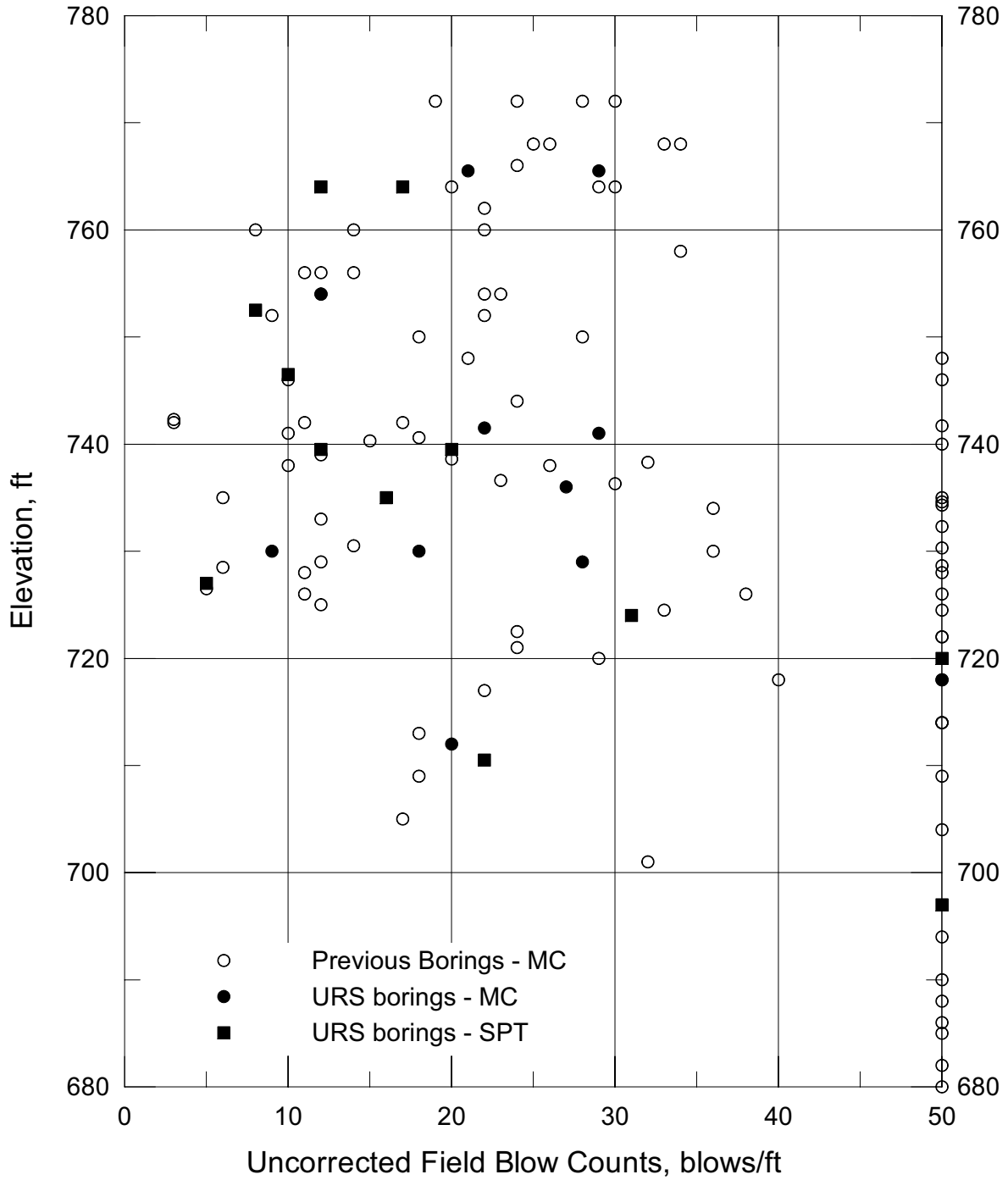
x:\x_geo\Estates dam\Task E -- Engineering Report\Figures\Figure 7-5.grf

Estates Dam - Gravel content



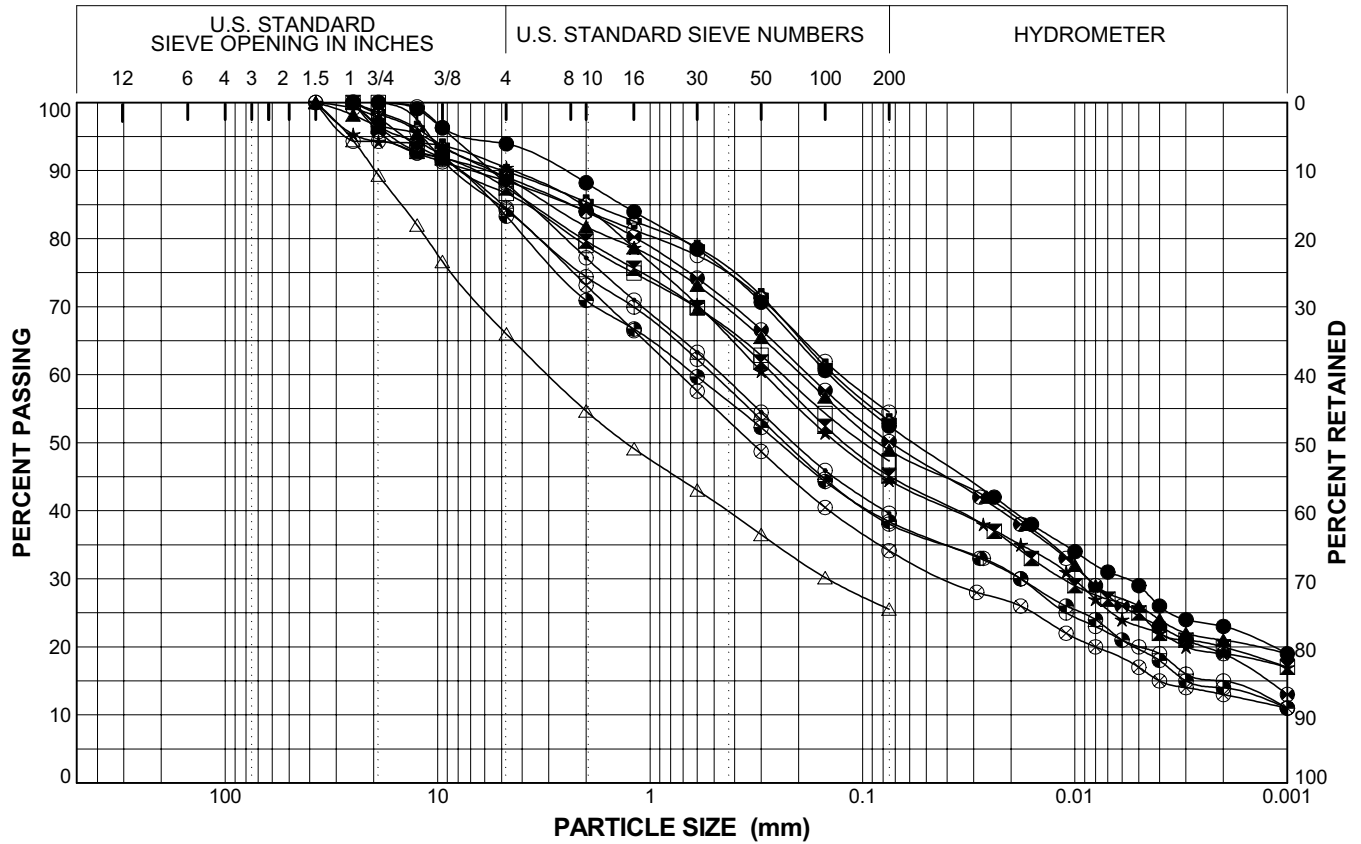
URS	Project No. 26814957	Gravel Content Data From Current and Previous Investigations	Figure
	Estates Dam Seismic Stability		7-6

Estates Dam - Blow Counts



URS	Project No. 26814957	Blow Counts Data From Current and Previous Investigations	Figure
	Estates Dam Seismic Stability		7-7

BOULDERS	COBBLES	GRAVEL		SAND			SILT OR CLAY
		coarse	fine	coarse	medium	fine	



Boring Number	Sample Number	Depth (feet)	Symbol	Classification
VQ-37	5A	13.5-14.5	●	Sandy Clay (CL)
VQ-37	5B	14.5-15.5	⊠	Clayey Sand (SC)
VQ-37	6A	17.5-18.5	▲	Clayey Sand (SC)
VQ-37	6B	18.5-19.5	★	Clayey Sand (SC)
VQ-37	9B	28-29	⊙	Clayey Sand (SC)
VQ-37	11	35-37.5	⊕	Sandy Silty Clay (CL)
VQ-38	9	24-26.5	○	Sandy Clay (CL)

Boring Number	Sample Number	Depth (feet)	Symbol	Classification
VQ-38	10	29-31.5	△	Clayey Sand with Gravel (SC)
VQ-38	13A	39-40	⊗	Clayey Sand with Gravel (SC)
VQ-38	13B	40-41	⊕	Clayey Sand with Gravel (SC)
VQ-39	8A	25-25.5	□	Clayey Sand (SC)
VQ-40	9A	29.5-30.5	⊗	Sandy Clay (CL/SC)
VQ-40	9B	30.5-32	⊕	Clayey Sand with Gravel (SC)

Report: SIEVE_12_CURVES_OAKEST; File: OAK_ESTATESDAM.GPJ; 2/17/2006 VQ-40

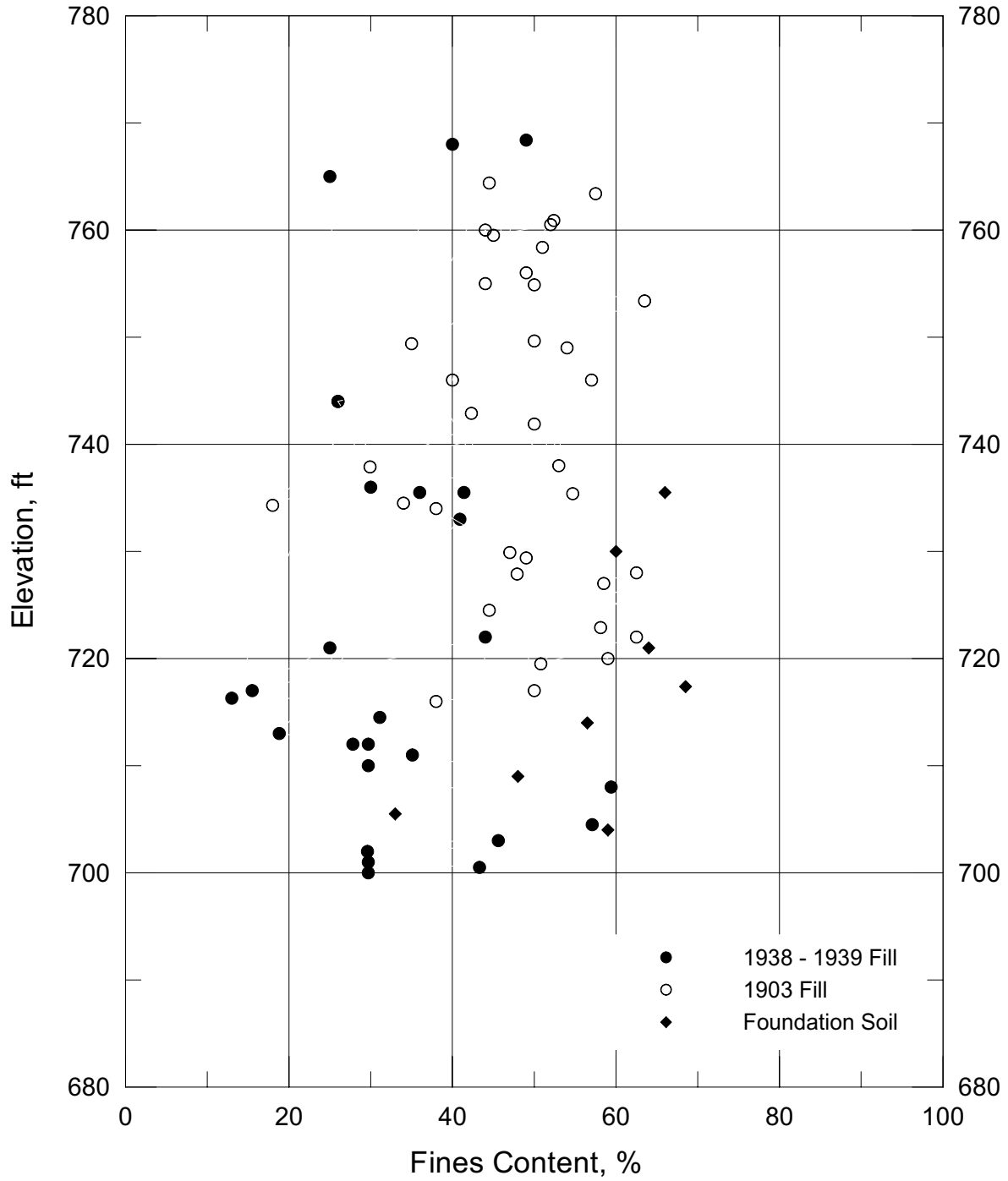
Dynamic Stability of Estates Dam
Oakland, Alameda County, California
26814957

GRADATION OF
1903 FILL



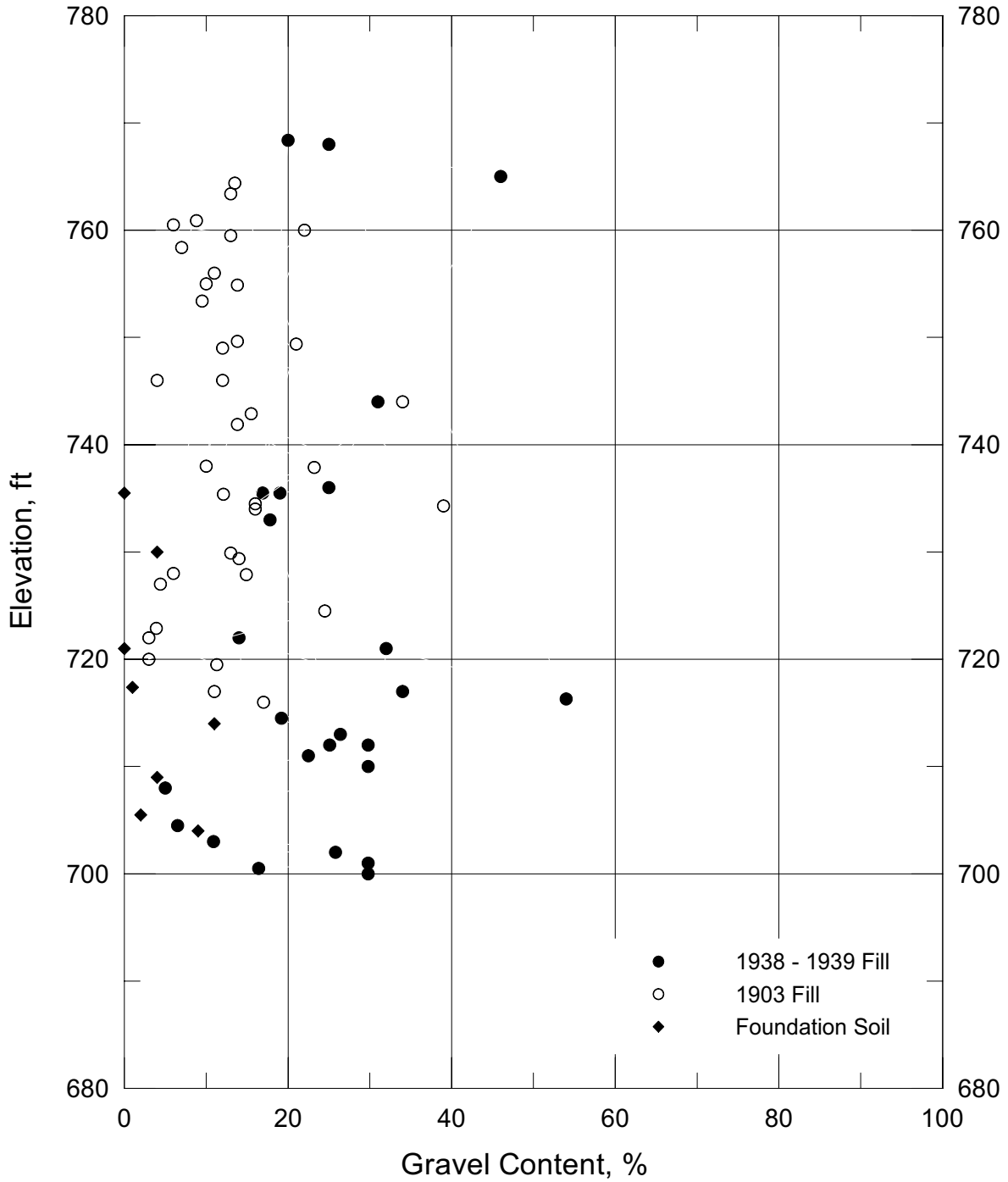
Figure 7-8

Estates Dam - Fines Content

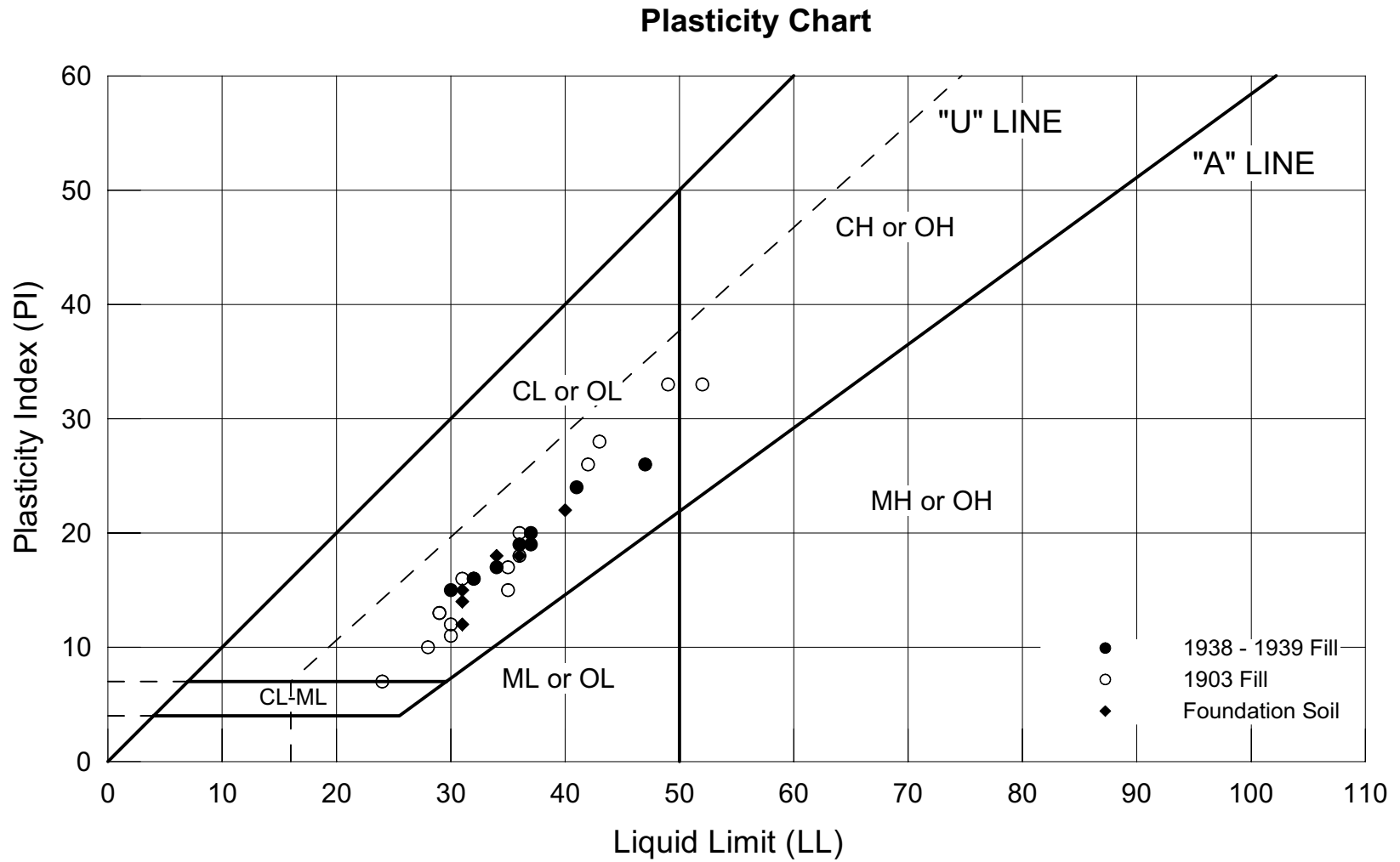


URS	Project No. 26814957	Fines Content of Embankment and Foundation Materials	Figure
	Estates Dam Seismic Stability		7-9

Estates Dam - Gravel Content

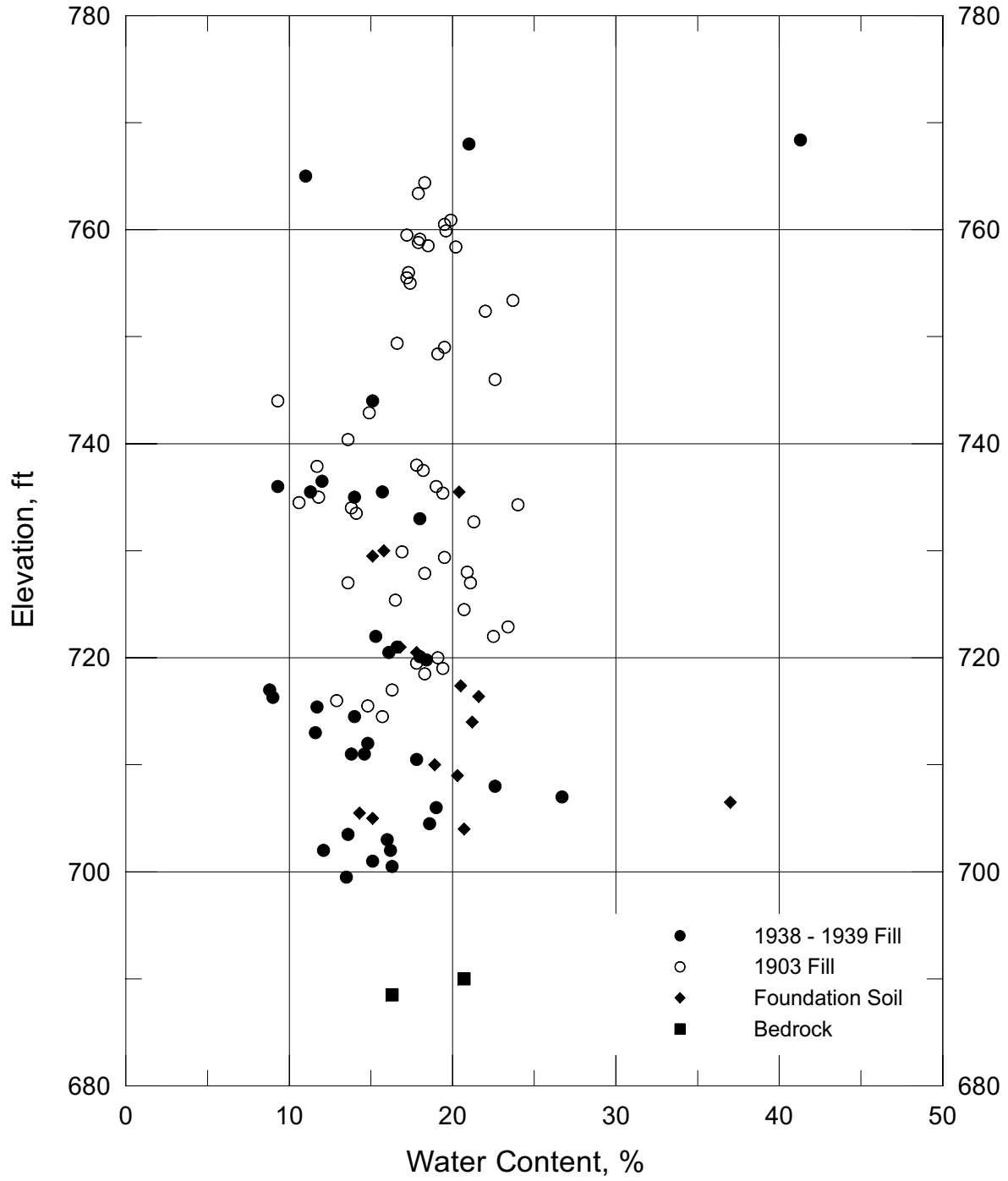


URS	Project No. 26814957	Gravel Content of Embankment and Foundation Materials	Figure
	Estates Dam Seismic Stability		7-10



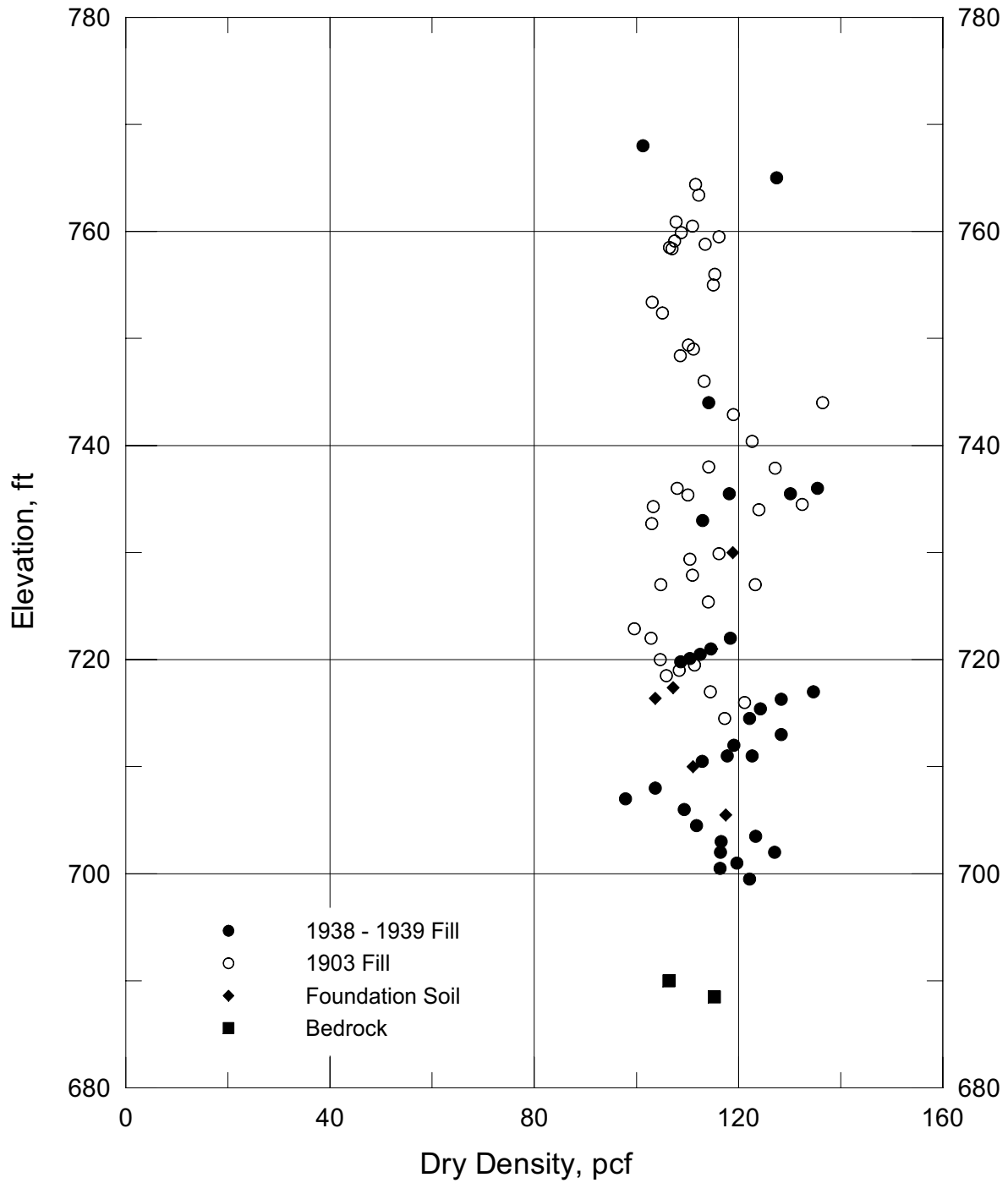
Project No. 26814957	Estates Dam Seismic Stability	Atterberg Limits of Embankment and Foundation Materials	Figure
URS			7-11

Estates Dam - Water content



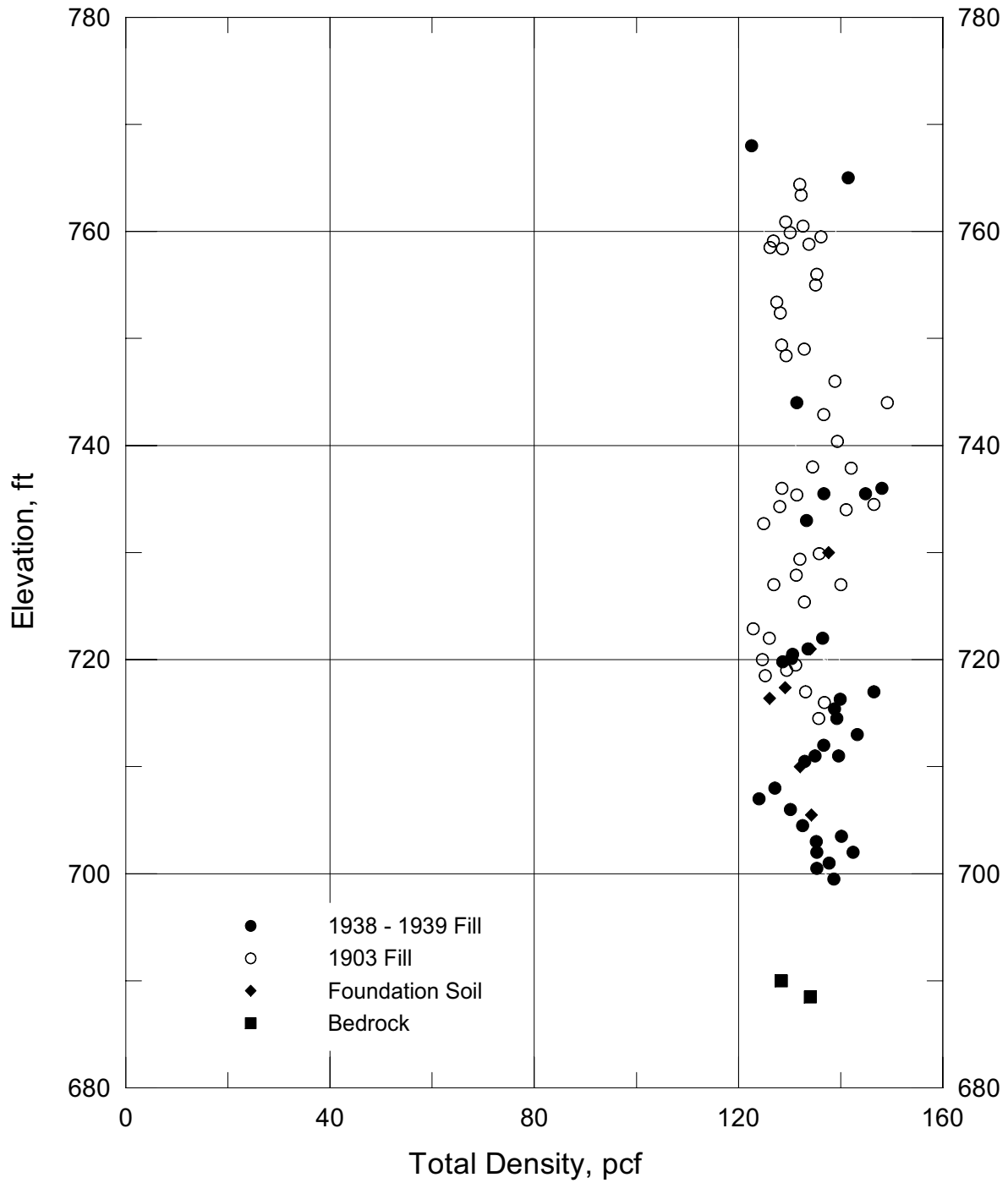
URS	Project No. 26814957	Water Content of Embankment and Foundation Materials	Figure
	Estates Dam Seismic Stability		7-12

Estates Dam - Dry Density

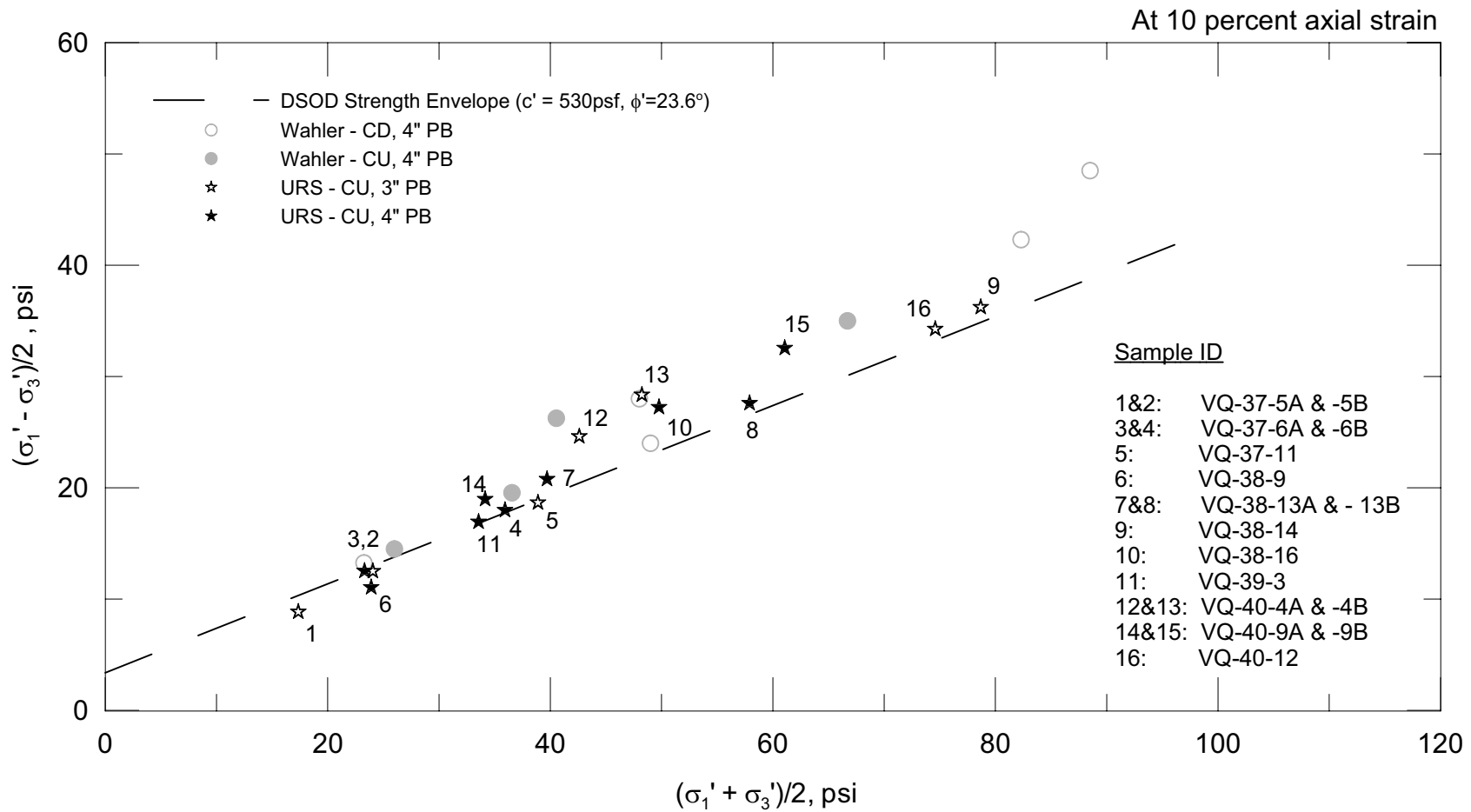


URS	Project No. 26814957	Dry Density of Embankment and Foundation Materials	Figure
	Estates Dam Seismic Stability		7-13

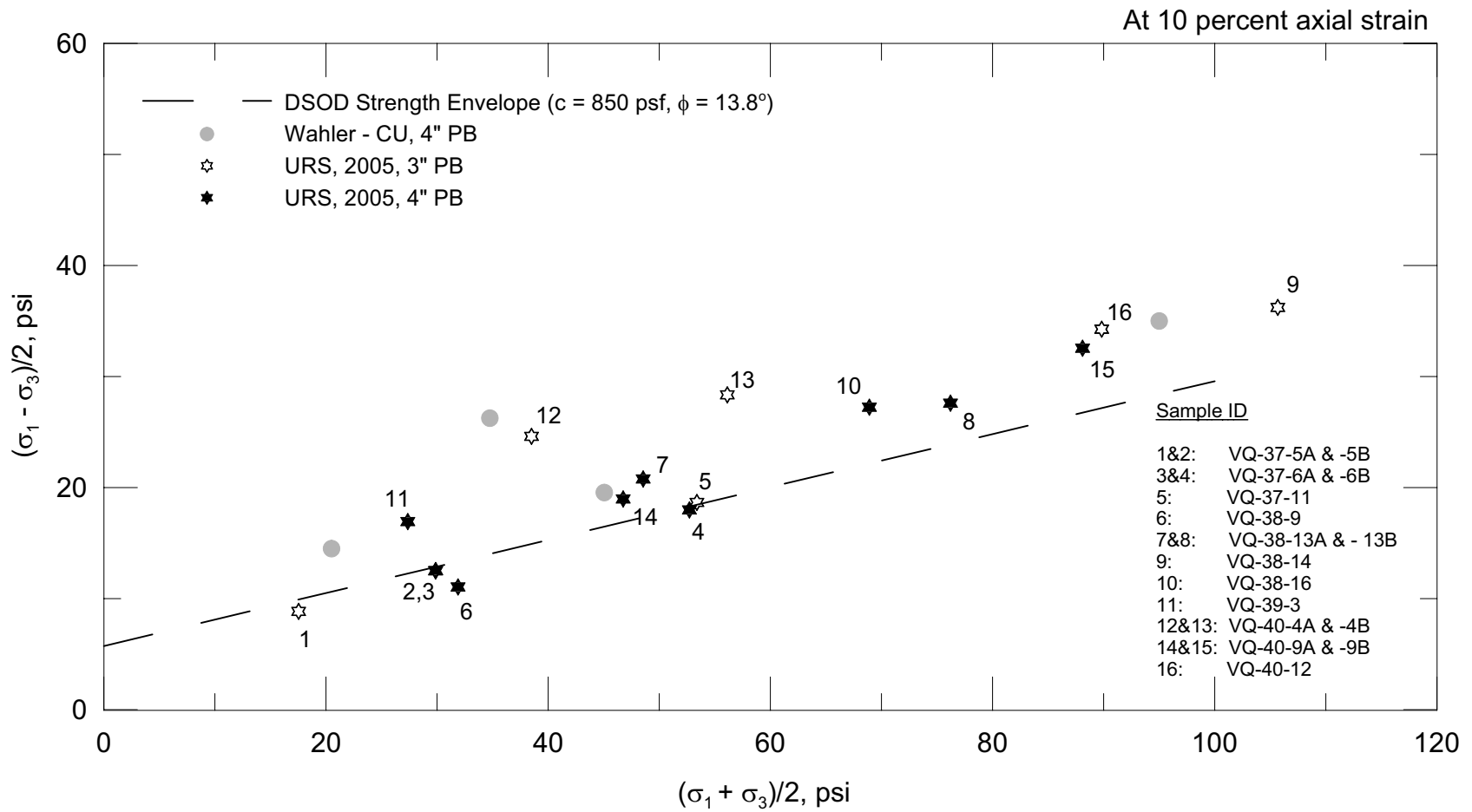
Estates Dam - Total Density



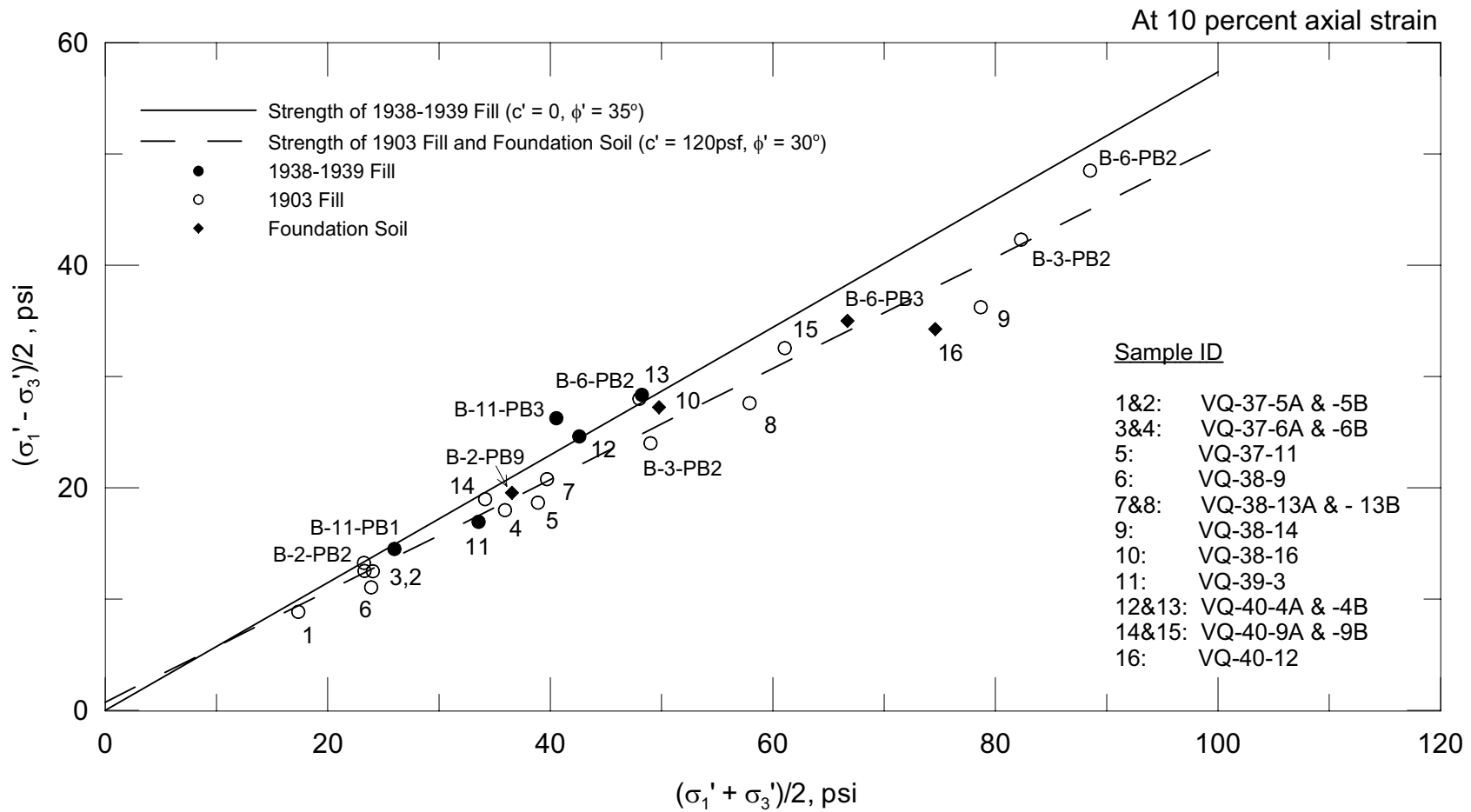
URS	Project No. 26814957	Total Density of Embankment and Foundation Materials	Figure
	Estates Dam Seismic Stability		7-14



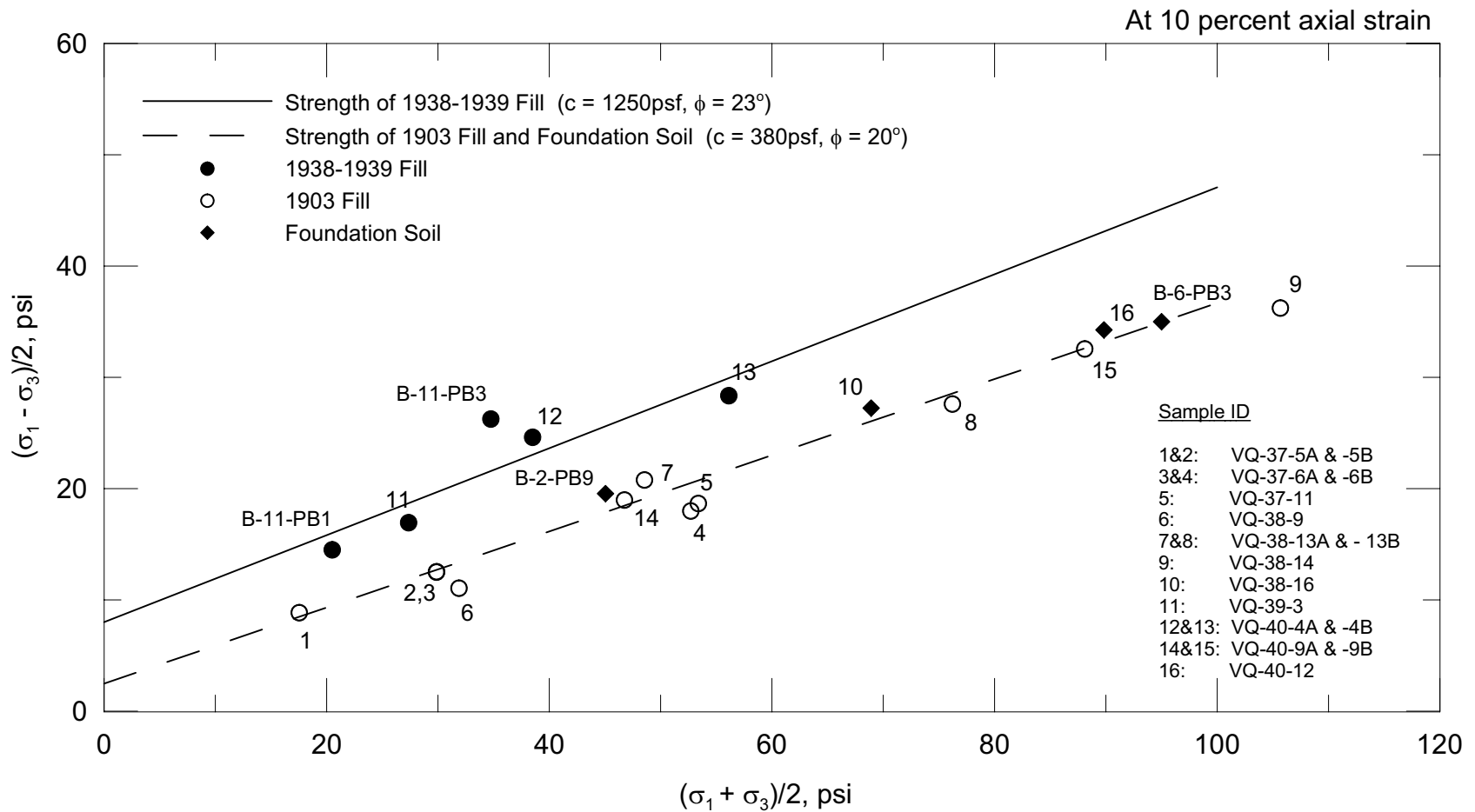
Project No. 26814957	Estates Dam Seismic Stability	Effective Stress Strength Data from Current and Previous Investigations	Figure
URS			7-15



Project No. 26814957	Estates Dam Seismic Stability	Total Stress Strength Data from Current and Previous Investigations	Figure 7-16
URS			

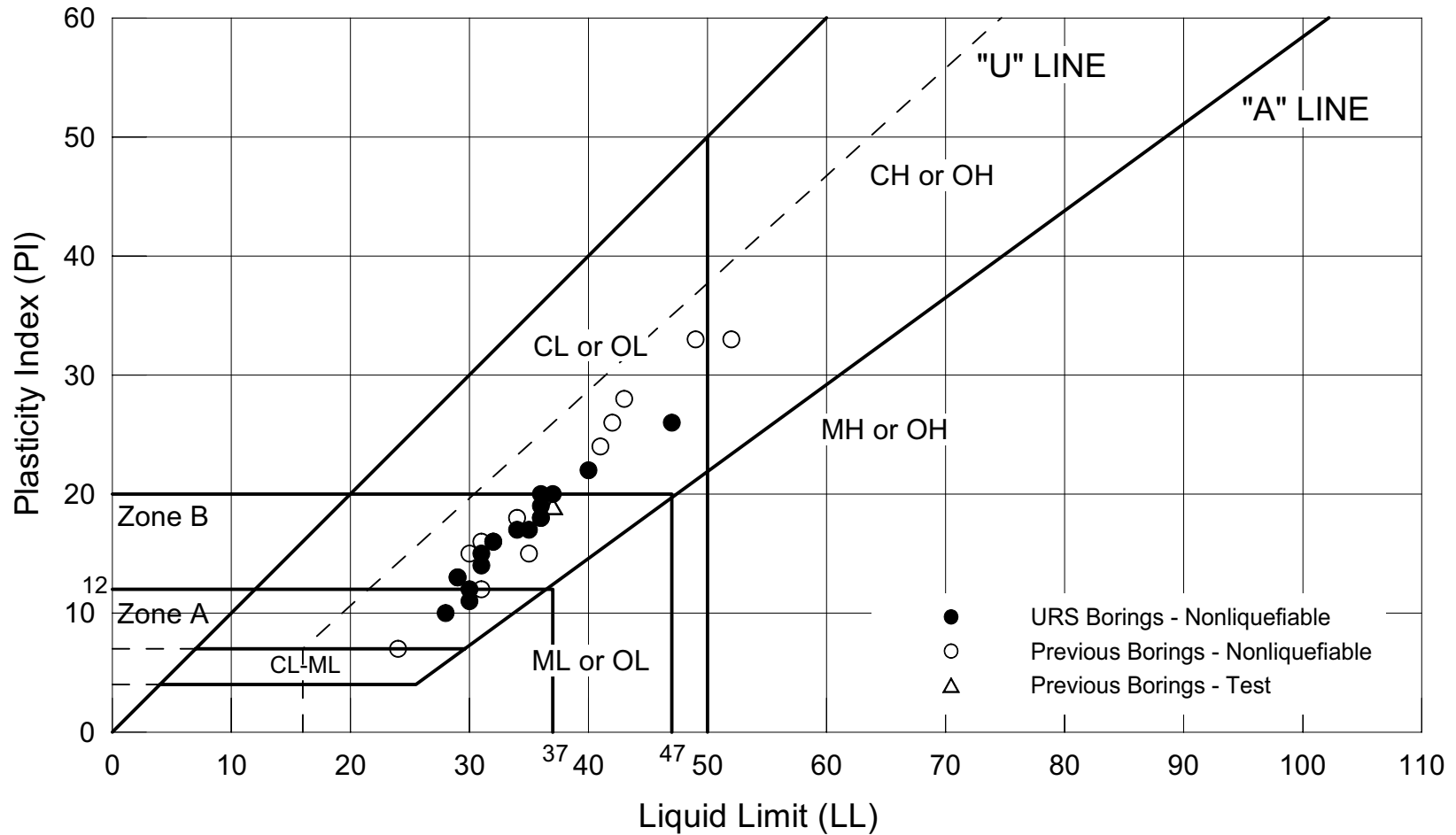


Project No. 26814957	Estates Dam Seismic Stability	Effective Stress Strength of Embankment and Foundation Materials	Figure
URS			7-17



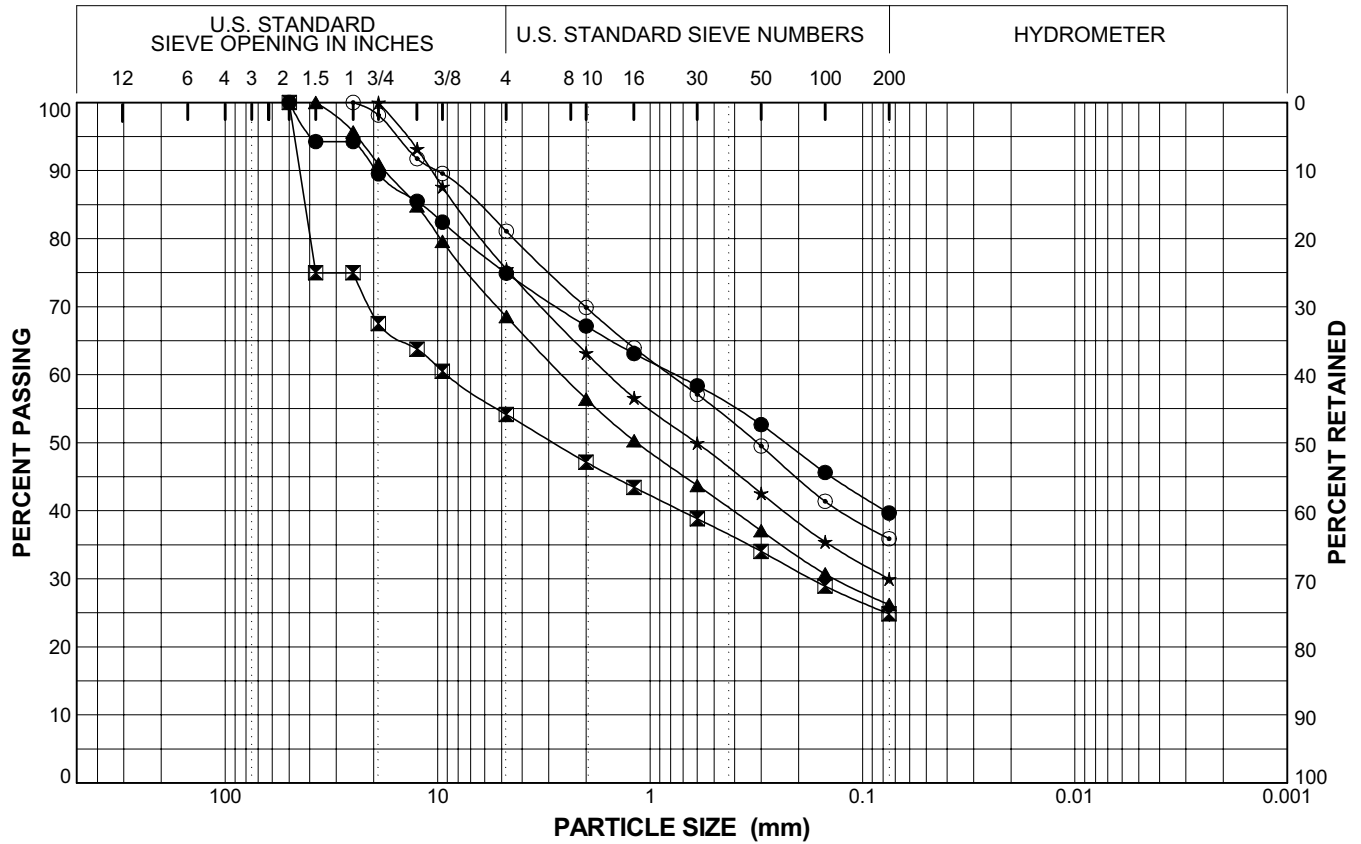
Project No. 26814957	Estates Dam Seismic Stability	Total Stress Strength of Embankment and Foundation Materials	Figure
URS			7-18

Plasticity Chart



Project No. 26814957	Estates Dam Seismic Stability	Liquefaction Susceptibility Chart for Embankment and Foundation Materials	Figure 7-19
URS			

BOULDERS	COBBLES	GRAVEL		SAND			SILT OR CLAY
		coarse	fine	coarse	medium	fine	



Boring Number	Sample Number	Depth (feet)	Symbol	Classification
VQ-37	2	5-7.5	●	Clayey Sand with Gravel (SC)
VQ-38	3B	9-10	⊠	Clayey Gravel with Sand (GC)
VQ-39	3B	11-12.5	▲	Clayey Sand with Gravel (SC)
VQ-40	4A	10.5-11.5	★	Clayey Sand with Gravel (SC)
VQ-40	4B	11.5-12.5	⊙	Clayey Sand with Gravel (SC)

Report: SIEVE_12_5_CURVES_OAKEST; File: OAK_ESTATEDAM.GPJ; 2/17/2006 VQ-40

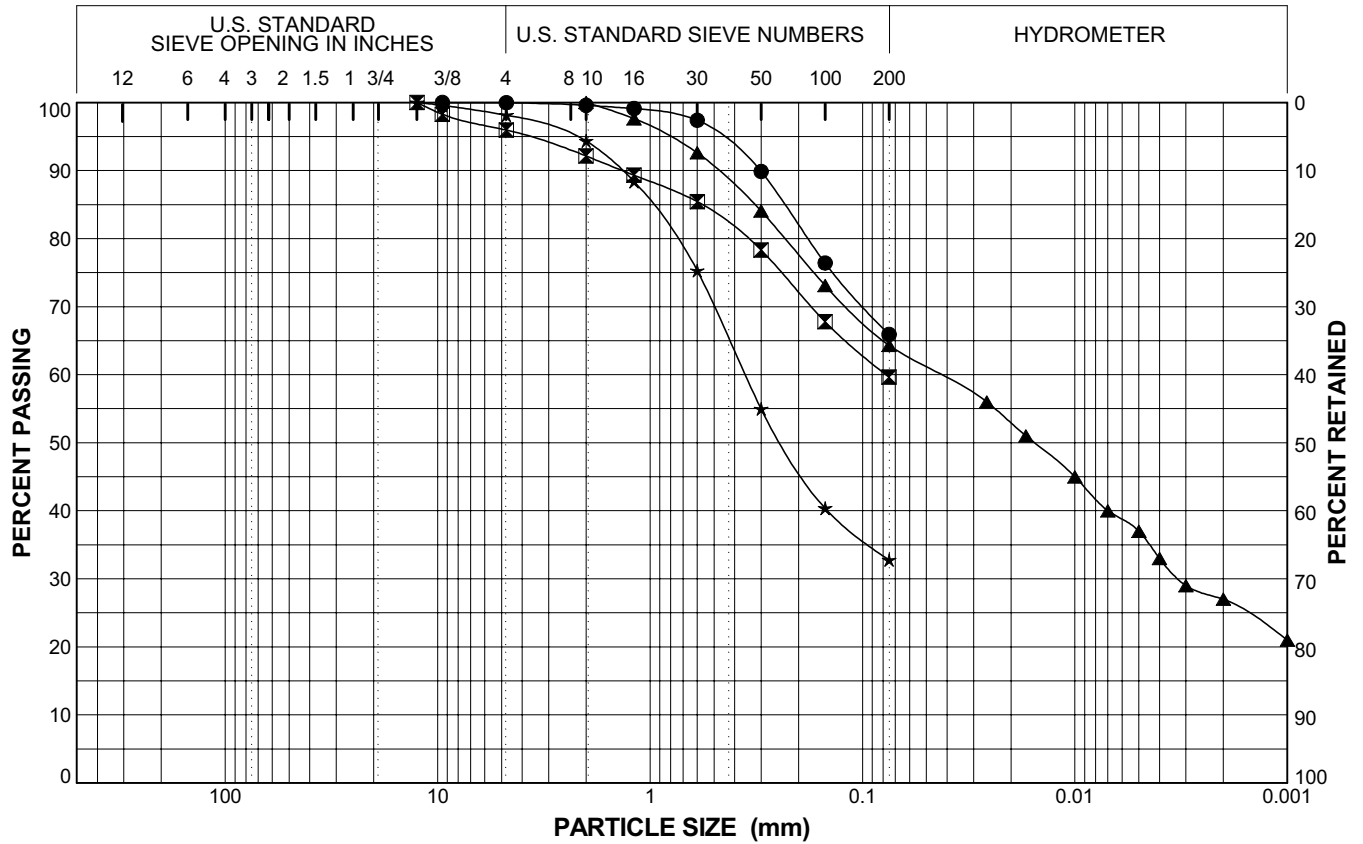
Dynamic Stability of Estates Dam
Oakland, Alameda County, California
26814957

GRADATION OF
1938-1939 FILL



Figure 7-20

BOULDERS	COBBLES	GRAVEL		SAND			SILT OR CLAY
		coarse	fine	coarse	medium	fine	



The general approach to assessing the seismic stability of the dam consisted of evaluating its dynamic response to the design earthquake motions, evaluating the potential for strength loss of the embankment and foundation materials under the earthquake shaking, estimating the deformations likely to be induced by the earthquake, and assessing the post-earthquake stability of the dam and its overall condition after the earthquake. This general approach is known as the Seed-Lee-Idriss approach (Seed, 1979).

The design earthquake was defined as the MCE on the Hayward-Rodgers Creek Fault since this earthquake is likely to generate the strongest ground motions at the site. Because the MCE on the San Andreas fault could result in strong shaking of long duration, the seismic stability of the dam was also evaluated for that earthquake. As a check of the analysis procedures, the dynamic response and deformations of the dam were also analyzed for motions representative of the 1989 Loma Prieta earthquake, for which the general performance of the dam is known.

Prior to the dynamic analyses, the dam's static stability was analyzed for comparison with the known long-term stability of the dam. The static stability was analyzed for an idealized section of the maximum cross-section of the dam. The analyses were performed using limit-equilibrium procedures and are described in Section 9.

The dynamic response, potential for strength loss, and seismic deformations of the dam were evaluated using the following two approaches:

- In the first approach, the dynamic response of the dam to the earthquake motions is analyzed initially. The earthquake-induced shear stresses calculated from that analysis are then compared with the cyclic strength of the embankment and foundation materials. From this comparison, the excess pore pressures and potential for strength loss in the materials are evaluated. The estimated strength loss in the materials is used in limit equilibrium analyses to calculate yield accelerations of potential sliding blocks within the dam. Together with the earthquake-induced accelerations calculated from the dynamic response analyses, the yield accelerations are used to calculate displacements of the blocks. Because the dam's dynamic response, potential for strength loss, and deformations are evaluated in separate analyses, this is referred to as a decoupled approach.
- In the second approach, referred to as a coupled approach, the dam's dynamic response, excess pore pressures and strength loss, and earthquake-induced deformations are calculated in a single analysis. The analytical procedure is based on nonlinear models capable of tracking the accumulation of deformations and development of excess pore pressures in the dam with time during the earthquake.

The analyses of the dam's dynamic response in the decoupled approach are discussed in Section 10. Those analyses were performed using two-dimensional finite element procedures with the computer program QUAD4M (Hudson et al. 1994). The evaluation of pore pressures, and strength loss, and the seismic stability and deformation analyses are presented in Section 11. The timing of the development of excess pore pressures and strength degradation in the embankment fill and foundation soils were evaluated first. The degraded undrained strength of the fill and foundation soils was then used in slope stability analyses to calculate yield accelerations and post-earthquake stability. Seismically induced deformations of the dam were evaluated with Newmark-type procedures using the calculated yield accelerations and the results of the dynamic response analyses.

To evaluate the sensitivity of the calculated deformations to the postulated earthquake ground motion time histories, additional acceleration time histories were developed for the Hayward fault event and used with the simplified Newmark procedure to calculate seismic displacements of the embankment. The calculated displacements were then compared to those corresponding to the two initially recommended time histories presented in Section 6. From this comparison, the sensitivity of the calculated displacements to the details of the time histories was evaluated. This sensitivity analysis is also presented in Section 11.

The non-linear dynamic analyses of the coupled approach were carried out with the two-dimensional finite difference computer code FLAC (Itasca, 2000). The methodology and results of those analyses are presented in Section 12.

In addition to the 2-dimensional (2D) analyses described above, analyses were performed to evaluate the effects of the 3-dimensional (3D) embankment geometry on the calculated slope stability factors of safety and seismic deformations. These analyses were performed using the decoupled approach. The slope stability of the dam was first evaluated using the 3D limit-equilibrium computer program CLARA (Hung, 1988). The calculated factors of safety against slope instability were compared with the 2D analysis results. The yield accelerations and post-earthquake slope stability were then calculated. The 3D dynamic response of the dam was approximated by a weighted average of the calculated response of two transverse sections of the dam. Finally, the seismically induced deformations of the dam were evaluated with Newmark-type procedures using the calculated 3D yield accelerations and the results of the weighted dynamic response analyses. The 3D analyses and results are described in Section 13.

9.1 ANALYTICAL PROCEDURES

The static stability of the dam was analyzed using the limit-equilibrium method of slices. The computer program UTEXAS3 (Wright, 1991) was used for the analyses. Spencer's method, which satisfies static equilibrium for each slice and overall equilibrium of the slide mass, was used in the UTEXAS analysis.

9.2 CROSS SECTIONS

We performed analyses on the idealized cross-section labeled A-A' in Figure 9-1 and shown in Figure 9-2. It corresponds to the maximum section of the dam and was developed based on the subsurface information shown in Figure 7-3. A modified version of this section was also analyzed to consider uncertainty in the geometry of some of the dam zones. The modified section A-A' is shown in Figure 9-3. The modification reflects uncertainty in the extent of the 1938-39 fill in the "boggy" area where the 1903 fill was over-excavated during the dam raise.

9.3 MATERIAL PROPERTIES

The analyses were performed for long-term static and pseudo-static loading conditions (with both pre-earthquake and post-earthquake strengths). For the long-term condition, drained strengths obtained from the effective-stress strength parameters were used for all materials. For pseudo-static loading, undrained strengths were used for all saturated soils while drained strengths were used for soils above the phreatic surface.

The analyses assuming no strength degradation correspond to the pre-earthquake condition and are presented in this section. The undrained strengths of the saturated embankment fills and foundation soils for the pre-earthquake condition were obtained by direct fitting of the strength envelope to the values of shear stress on the failure plane at the time of failure plotted against the normal stress on the failure plane after consolidation (i.e. the values of τ_{ff} versus σ'_{fc}). Thus, it is assumed that the undrained strength is a function of the effective normal stresses and the effective principal stress ratio (K_c) acting on the failure surface prior to seismic loading. This strength formulation was proposed by Duncan et al. (1990) and is incorporated in the UTEXAS3 program. The strength parameters used in the limit-equilibrium analyses are summarized in Tables 9-1 and 9-2.

Pseudo-static analyses were also performed to evaluate the yield accelerations of potential sliding blocks within the dam for various assumed levels of undrained strength degradation induced by the earthquake shaking. Those analyses, which correspond to pseudo-static loading with post-earthquake strength parameters and to the post-earthquake condition, are discussed in Section 11.

9.4 ANALYSIS RESULTS

The analysis results for sections A-A' and modified A-A' are presented in Figures 9-4 through 9-8. Under long-term static loading, the results for sections A-A' and modified A-A' are very similar. As shown in Figure 9-4, the computed factors of safety (FS) against slope instability for deep-seated sliding surfaces are about 2.8 and 1.4 for the upstream and downstream slopes,

respectively. For sliding surfaces passing through the crest and the upstream toe, the computed FS values are between 1.9 and 2.0.

For the pre-earthquake loading condition using undrained strengths, the computed FS values for deep-seated sliding surfaces are between 3.2 and 1.4 for the upstream and downstream slopes, respectively (Figures 9-5). For sliding surfaces passing through the crest and the upstream toe, the computed FS values are about 2.5. Under pseudo-static loading, the computed yield acceleration coefficients (K_y) for Section A-A' are equal to or greater than 0.15 for the downstream slope when pre-earthquake strengths are used (Figure 9-6). For the upstream slope, the computed pre-earthquake value of K_y for a sliding surface through the crest and the upstream toe is 0.34. For modified section A-A', the computed values of FS and K_y are slightly higher than those for Section A-A' under pre-earthquake loading (Figure 9-7). This is expected since the undrained strength of the 1938-39 fill is higher than that of the 1903 fill.

Since the analyses showed that modified section A-A' is less critical than section A-A', the latter was used in the dynamic analysis of the dam. No further analyses were performed using modified section A-A'.

**Table 9-1
UTEXAS3 Input Parameters for Static Stability Analysis - Long Term Condition**

Material	Total Unit Weight	Effective Strength Parameters	
	γ_t	c'	ϕ'
	(pcf)	(psf)	(°)
1938-39 Embankment Fill	133	0	35
1903 Embankment Fill	133	120	30
Foundation Soils	133	120	30
Bedrock	140	20,000	0

**Table 9-2
UTEXAS3 Input Parameters for Seismic Stability Analysis - Pre-Earthquake Condition**

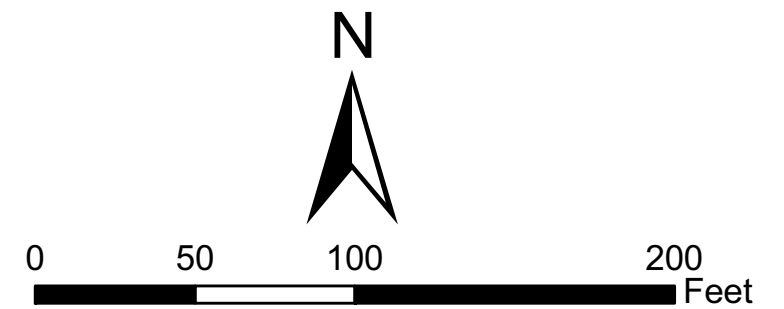
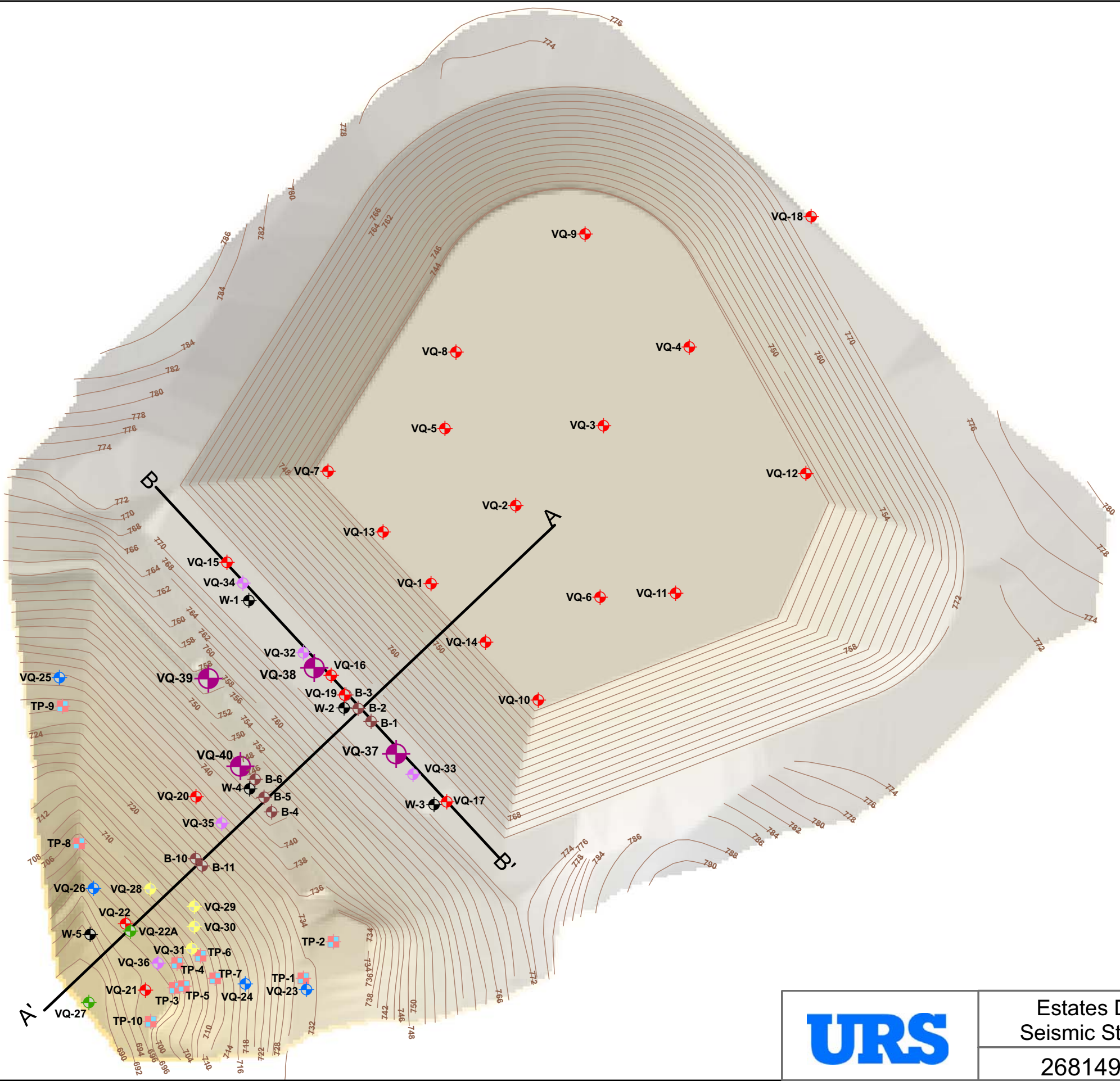
Material	Total Unit Weight	Undrained Strength Envelope ($K_c = 1$) ⁽¹⁾		Effective Strength Parameters	
	γ_t	d_R	Ψ_R	c'	ϕ'
	(pcf)	(psf)	(°)	(psf)	(°)
1938-39 Embankment Fill above phreatic surface	133	-	-	0	35
1938-39 Embankment Fill below phreatic surface	133	1547	27.7	0	35
1903 Embankment Fill above phreatic surface	133	-	-	120	30
1903 Embankment Fill below phreatic surface	133	470	24.2	120	30
Foundation Soils above phreatic surface	133	-	-	120	30
Foundation Soils below phreatic surface	133	470	24.2	120	30
Bedrock	140	-	-	20,000	0

Note:

(1) K_c = Consolidation principal stress ratio

Legend

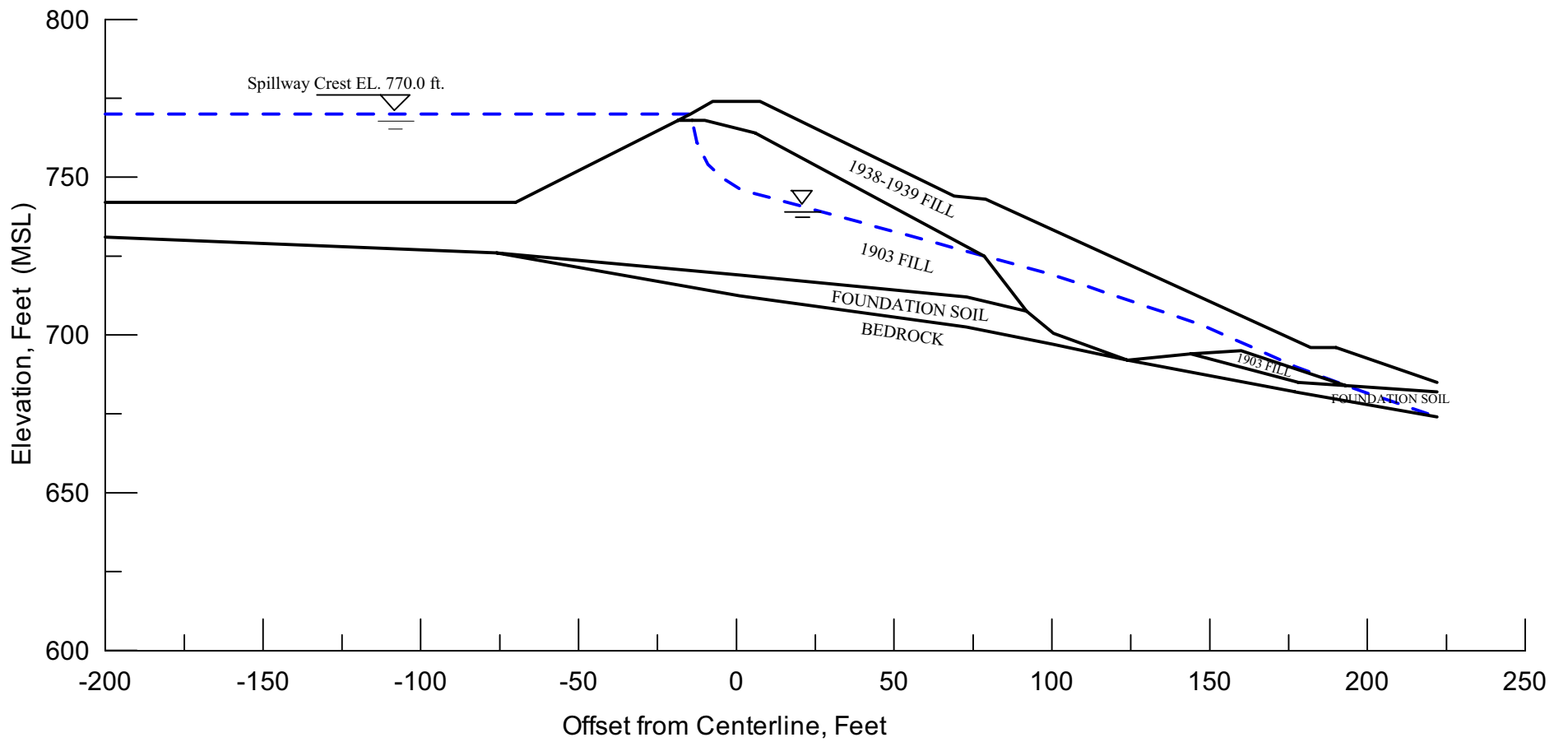
-  EBMUD; 1939 (wells)
-  EBMUD for S&W study; 1962-1965
-  S&W; 1965
-  EBMUD for S&W study; 1965 (test pits)
-  EBMUD for S&W study; 1965
-  EBMUD; 1976
-  Wahler Associates; 1978
-  EBMUD, 1999 (piezometers)
-  URS, 2005



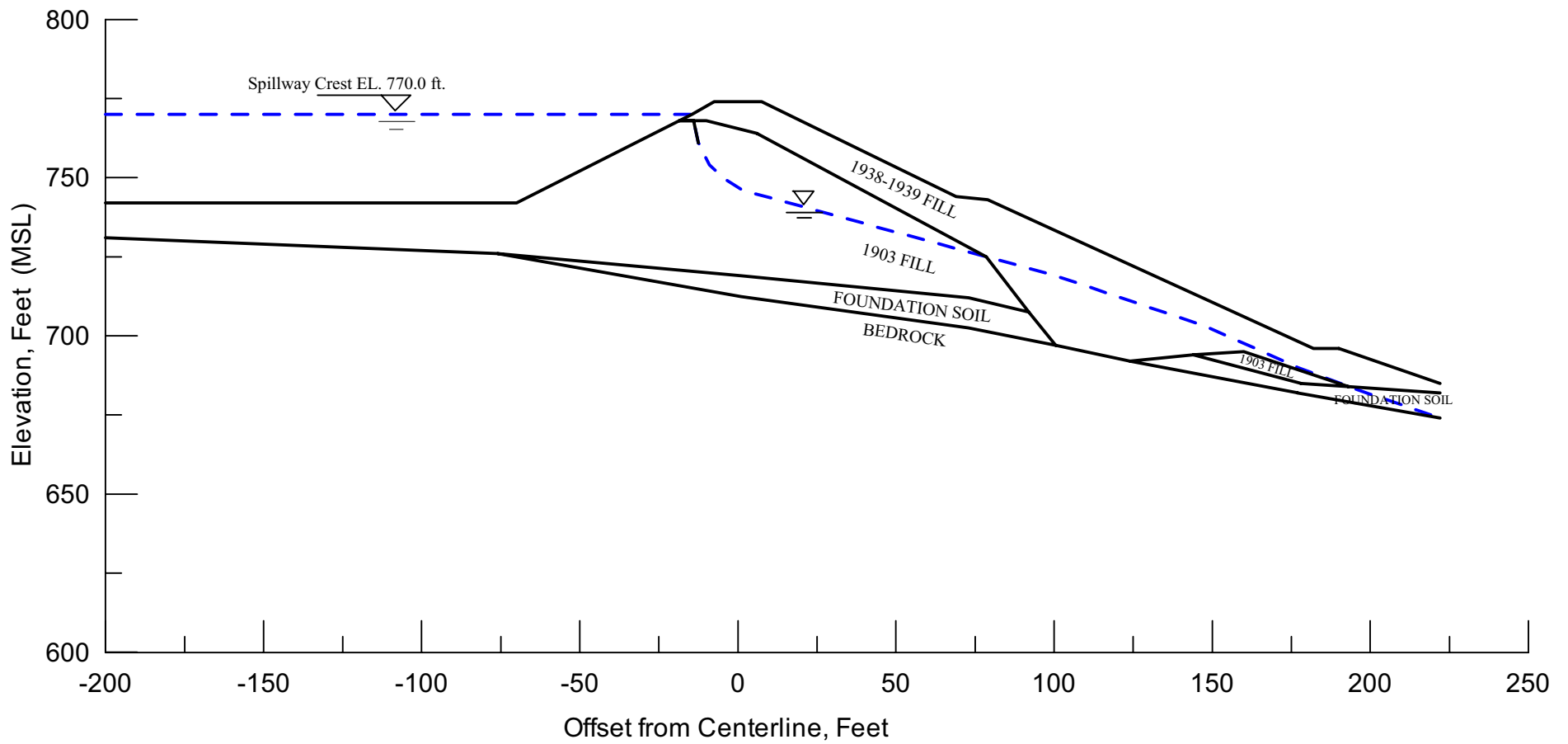
Estates Dam
Seismic Stability
26814957

Plan View of Analysis
Section A - A'

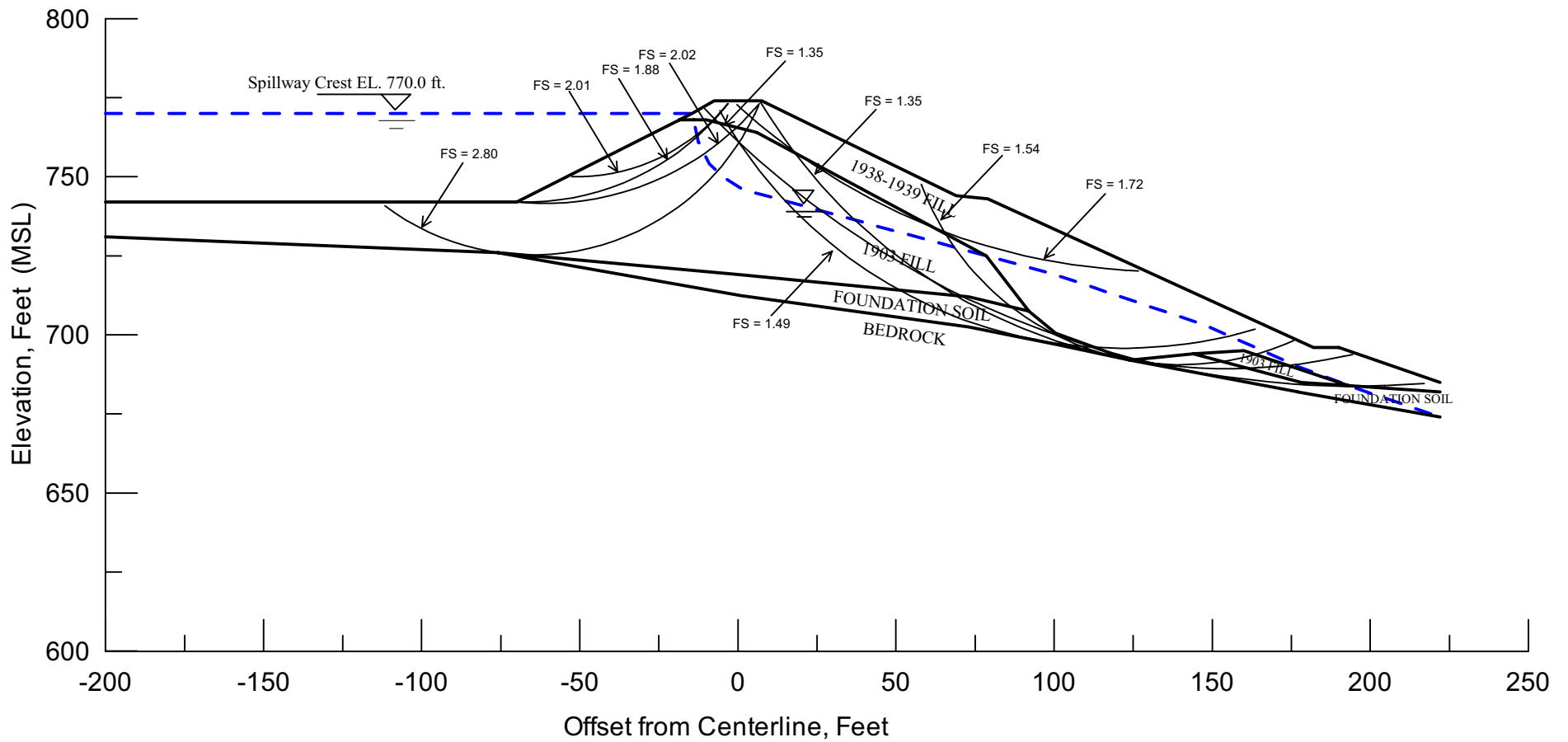
Figure
9-1



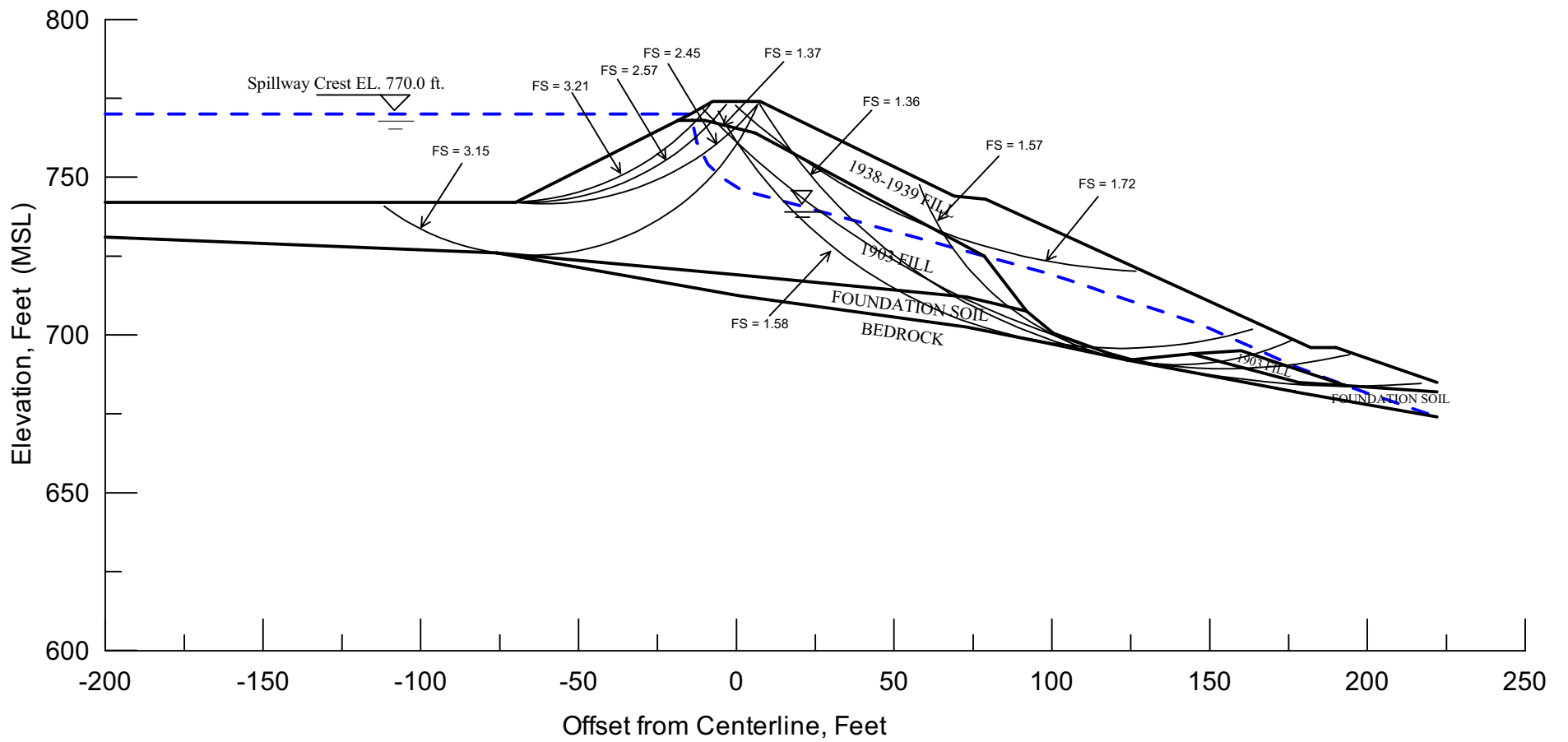
Project No. 26814957	Estates Dam Seismic Stability Analysis	Idealized Section A-A' For Slope Stability Analysis	Figure 9-2
URS			



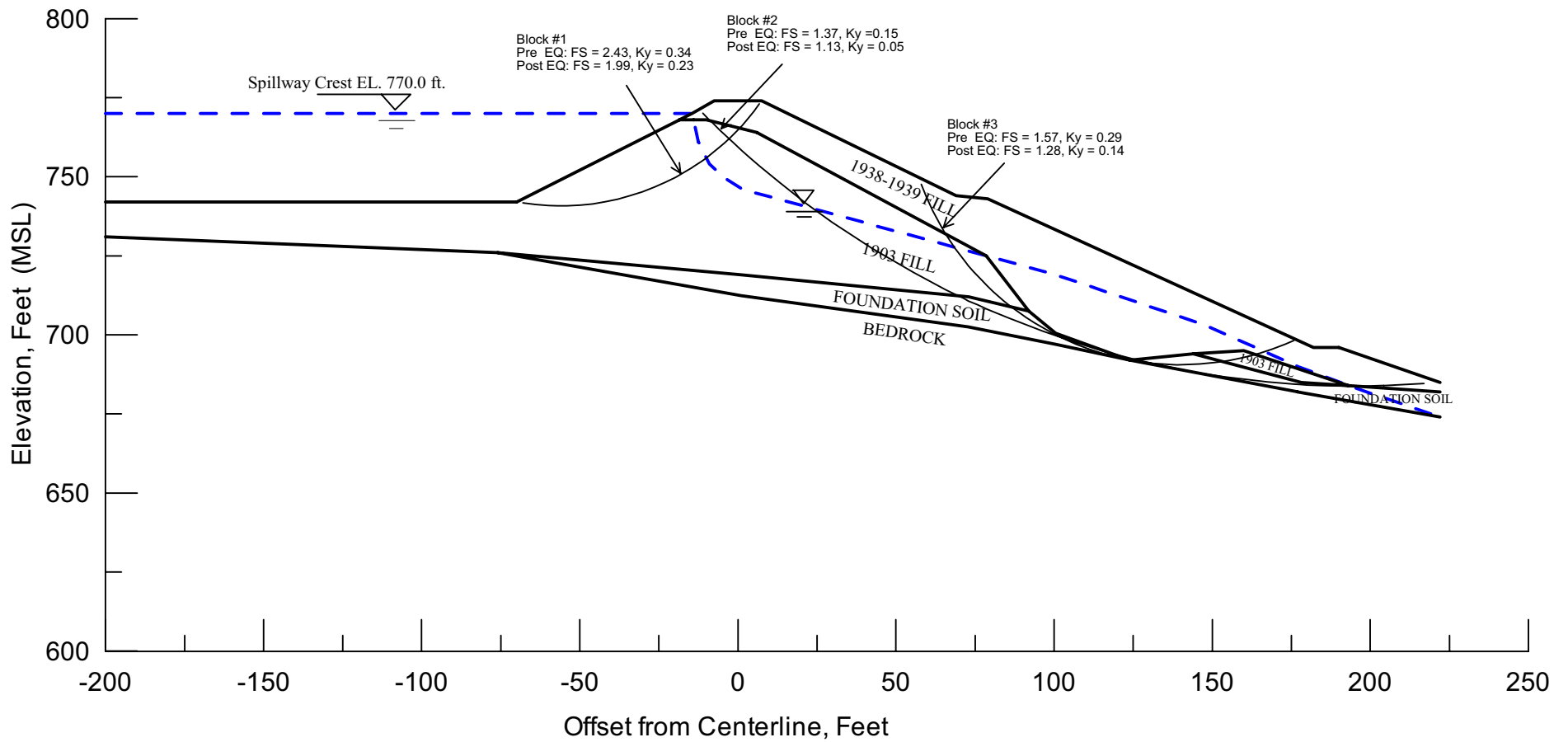
Project No. 26814957	Estates Dam Seismic Stability Analysis	Modified Section A-A' For Slope Stability Analysis	Figure
URS			9-3



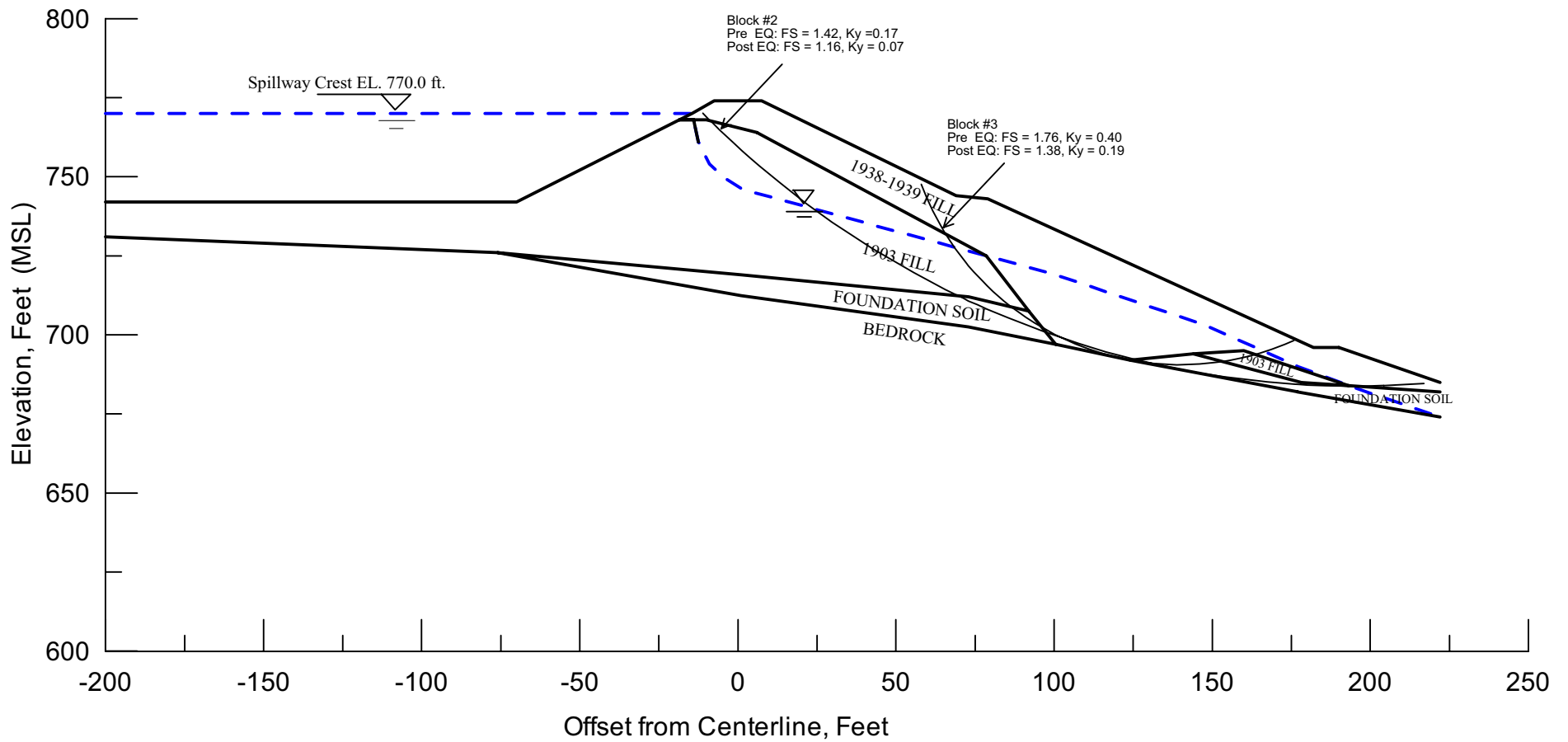
Project No. 26814957	Estates Dam Seismic Stability Analysis	Slope Stability Analysis Long-Term Condition	Figure 9-4
URS			



Project No. 26814957	Estates Dam Seismic Stability Analysis	Slope Stability Analysis Pre-Earthquake Condition	Figure
URS			9-5



Project No. 26814957	Estates Dam Seismic Stability Analysis	Slope Stability Analysis Selected Critical Sliding Blocks Section A-A'	Figure
URS			9-6



Project No. 26814957	Estates Dam Seismic Stability Analysis	Slope Stability Analysis Selected Critical Sliding Blocks Modified Section A-A'	Figure 9-7
URS			

10.1 METHODOLOGY

Two-dimensional dynamic response analyses were performed to estimate the stresses and accelerations induced by the design earthquake within the dam. The results of the analyses were used to evaluate the potential for strength loss in the embankment and foundation soils. The results were also used to evaluate the earthquake-induced average mass accelerations of selected potential sliding blocks within the dam. Together with the yield accelerations obtained from the limit equilibrium analyses, the average mass accelerations were used to calculate seismic displacements of the sliding blocks using a Newmark-type deformation analysis.

The computer program QUAD4M was used for the dynamic response analyses. QUAD4M (Hudson et al. 1994) is a dynamic, time-domain, equivalent-linear, two-dimensional, finite element program. The dynamic stress-strain behavior of the materials is assumed to be viscoelastic. The elastic modulus and viscous damping of the materials are calculated iteratively until they are compatible with the computed shear strains.

The dynamic response analyses were performed on idealized section A-A', which corresponds to the maximum section of the dam. This section was judged to be the most representative for assessing the seismic deformations of the dam. It was also shown to be more critical than the modified section in the pseudo-static analyses. The section was discretized using the finite element mesh shown in Figure 10-1. A transmitting boundary was specified along the base of the model to simulate the unbounded extent of the foundation bedrock beneath the dam. The mesh was extended in the upstream and downstream directions to minimize the effects of side boundary reflections on the dam response, and "horizontal roller" supports were specified for the side boundaries to allow free movement in the horizontal direction. The calculated site response near the boundaries was compared with the free-field response computed with computer program SHAKE (Schnabel et al, 1972), to confirm that the boundary effects are small.

The analyses were performed for the Hayward-Rodgers Creek and San Andreas fault MCEs using the time histories developed to represent those earthquakes. The acceleration, velocity, and displacement time histories for those earthquakes are presented in Figures 6-12, 6-13 and 6-15. The acceleration time histories were input so that they would represent bedrock outcrop motions in the upstream-downstream direction.

The response of the dam was also analyzed for the estimated motions during the 1989 Loma Prieta earthquake. Based on the ground motion records obtained during that earthquake, the motions recorded at the Piedmont Junior High School Station, which is located approximately 1.4 km from the dam site, were assumed to be reasonably representative of the motions that occurred at the dam site during the earthquake. The time history used in the analyses to represent the earthquake motions is shown in Figure 10-2. The calculated performance was compared against the known performance of the dam during that earthquake as a check of the analysis procedures and models.

10.2 DYNAMIC MATERIAL PROPERTIES

Table 10-1 summarizes the material properties used in the QUAD4M analyses. These parameters include total unit weight (γ), maximum shear modulus (G_{\max}), Poisson's ratio (ν), and the modulus reduction (G/G_{\max}) and damping ratio (λ) relationships with shear strain. The

maximum shear moduli of the materials were obtained from their shear wave velocities. The shear wave velocity for the 1903 fill was expressed as a function of the mean effective stress as shown in Table 10-1. This expression was derived from the measured shear wave velocities at the dam. The mean effective stresses were obtained from a static stress analysis of the dam performed using the computer program FLAC. The FLAC analyses are discussed in Section 12.

10.2.1 Shear Wave Velocities

Figure 10-3 shows the seismic wave velocities measured in the 1980 Wahler investigations, along with the stratigraphy at the locations of borings B-1, 2 and 3. Down-hole geophysical surveys were performed in borings VQ-38 and 40 drilled for this investigation. The measured seismic wave velocities are shown in Figures 10-4 and 10-5. The figures also show the values of Poisson's ratio calculated from the measured shear and compression velocities (V_s and V_p) using the following equation:

$$\nu = (3 \cdot K - 2 \cdot G) / (6 \cdot K + 2 \cdot G),$$

where: G = shear modulus, and K = bulk modulus. The shear and bulk moduli are obtained from:

$$G = \gamma \cdot V_s^2 / g$$

$$K = \gamma \cdot V_p^2 / g - 2 \cdot G$$

These figures show that the shear wave velocity of the 1938-39 fill is between 700 and 1,000 feet per second (fps), while the shear wave velocity for the 1903 fill increases gradually with depth from about 700 fps to about 1,100 fps. In the foundation soils, the shear wave velocity ranges between 900 and 1,400 fps. The seismic surveys also indicate that the shear wave velocity of the rock immediately below the dam ranges between about 1,500 and 3,500 fps. A representative average value of 2,000 fps was assigned to the bedrock. Similarly, average shear wave velocities of 870 and 1,200 fps were assigned to the 1938-39 fill and the foundation soils, respectively.

10.2.2 Modulus Reduction and Damping Relationships

The average modulus reduction relationship for sands proposed by Seed and Idriss (1970) was used to represent the variation in normalized shear modulus (G/G_{max}) with effective shear strain. This relationship was selected based on the characteristics of the materials and on past experience with similar materials.

The lower bound damping curve for sands (Seed and Idriss, 1970) was selected for the embankment and foundation soils. In our experience, this relationship is suitable for many compacted, silty and clayey sand materials. The rock was assigned a constant shear modulus ($G/G_{max} = 1$) and a constant damping ratio of 0.5 percent.

A simple average of the curves for sand and clay by Seed and Idriss (1970) was used by Wahler Associates in their dynamic response analyses of the dam.

10.3 ANALYSIS RESULTS

The results of the QUAD4M analyses are presented in terms of: a) time histories of shear stress at the elements shown in Figure 10-6, b) acceleration outputs for the nodal points shown in Figure 10-7, and c) time histories of average mass acceleration for the sliding blocks shown in

Figure 10-8. In addition, peak horizontal shear stresses were output throughout the model. Those shear stresses were used to calculate the earthquake-induced cyclic stress ratio (CSR) in the embankment and foundation materials. CSR is defined as the ratio of the average cyclic shear stress to the initial effective overburden stress as follows.

$$CSR = \tau_{ave} / \sigma_{vo}' = 0.65 \cdot \tau_{peak} / \sigma_{vo}'$$

where: τ_{ave} = average cyclic shear stress

τ_{peak} = peak shear stress

σ_{vo}' = effective overburden stress.

These stress ratios were compared with the cyclic strength of the embankment and foundation soils to evaluate the potential for strength loss of those materials, as will be discussed in Section 11.

The dynamic response analysis results are presented in Figures 10-9 through 10-18. The results of the analyses for the Loma Prieta earthquake are presented first, followed by the results for the Hayward and San Andreas events.

10.3.1 1989 Loma Prieta Earthquake

The analysis results for the 1989 Loma Prieta Earthquake are presented in Figures 10-9 and 10-10. Figure 10-9 shows the calculated peak accelerations at the selected points within the dam during the earthquake. The calculated peak acceleration at the crest of the dam is approximately 0.18g. Figure 10-10 shows the time histories of average mass acceleration for the sliding blocks shown in Figure 10-8.

10.3.2 Hayward-Rogers Creek Fault MCE

Two time histories were initially developed to represent the design ground motions for the Hayward–Rogers Creek fault MCE (Section 6.4) and were used in the dynamic response analyses. The analysis results for those two time-histories are presented in Figures 10-11 through 10-16.

Figures 10-11 and 15 show the calculated peak accelerations within the embankment and foundation. Figure 10-12 shows acceleration time histories at nodal points below the reservoir (see Figure 10-7 for locations), and illustrates how the ground motions propagate upward through the foundation.

Figures 10-14 and 10-16 shows shear stress time histories within elements below the crest (see Figure 10-6 for locations). The calculated shear stresses generally correspond to a few cycles of high amplitude shear stress. Near the center and base of the dam, the amplitude of the stresses exceeds the static undrained strength of the materials, which is a limitation of equivalent-linear methods of dynamic response analysis. Figure 10-13 shows the time histories of average mass acceleration for the selected sliding blocks shown in Figure 10-8.

10.3.3 San Andreas Fault MCE

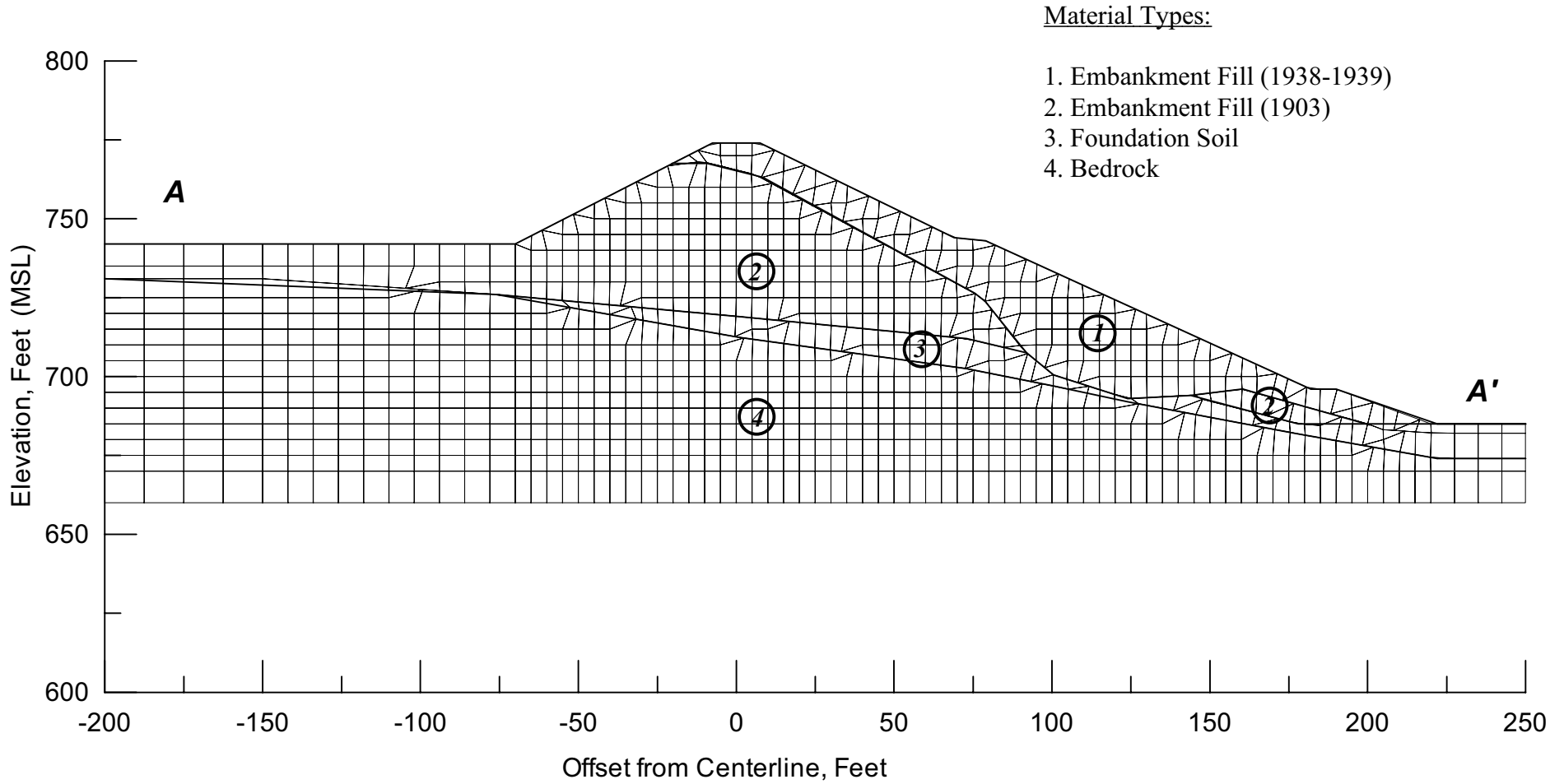
The analysis results for the San Andreas Fault MCE are illustrated in Figures 10-17 and 10-18. As shown in these figures, this earthquake induces a dynamic response of the dam lower than that calculated for the Hayward Fault MCE. The calculated dam accelerations and shear stresses for the San Andreas event are significantly lower than those calculated for the Hayward event. Thus, the analyses indicate that the San Andreas Fault MCE is a less critical event than the Hayward Fault MCE regarding the seismic stability of the dam. The time histories of average mass acceleration for the selected sliding blocks are shown in Section 11.

Table 10-1
Material Parameters for Dynamic Response Analysis

Material	γ_t (pcf)	V_s (fps)	Poisson's Ratio ⁽¹⁾	Modulus Reduction	Damping
1938-39 Embankment Fill	133	870	0.35, 0.45	Sands, Ave ⁽³⁾	Sands, L/B ⁽³⁾
1903 Embankment Fill	133	$600 \bullet (\sigma_m')^{0.38}$, but not less than 700 ⁽²⁾	0.40, 0.45	Sands, Ave	Sands, L/B
Foundation Soils	133	1,100	0.48	Sands, Ave	Sands, L/B
Bedrock	140	2,000	0.45	-	-

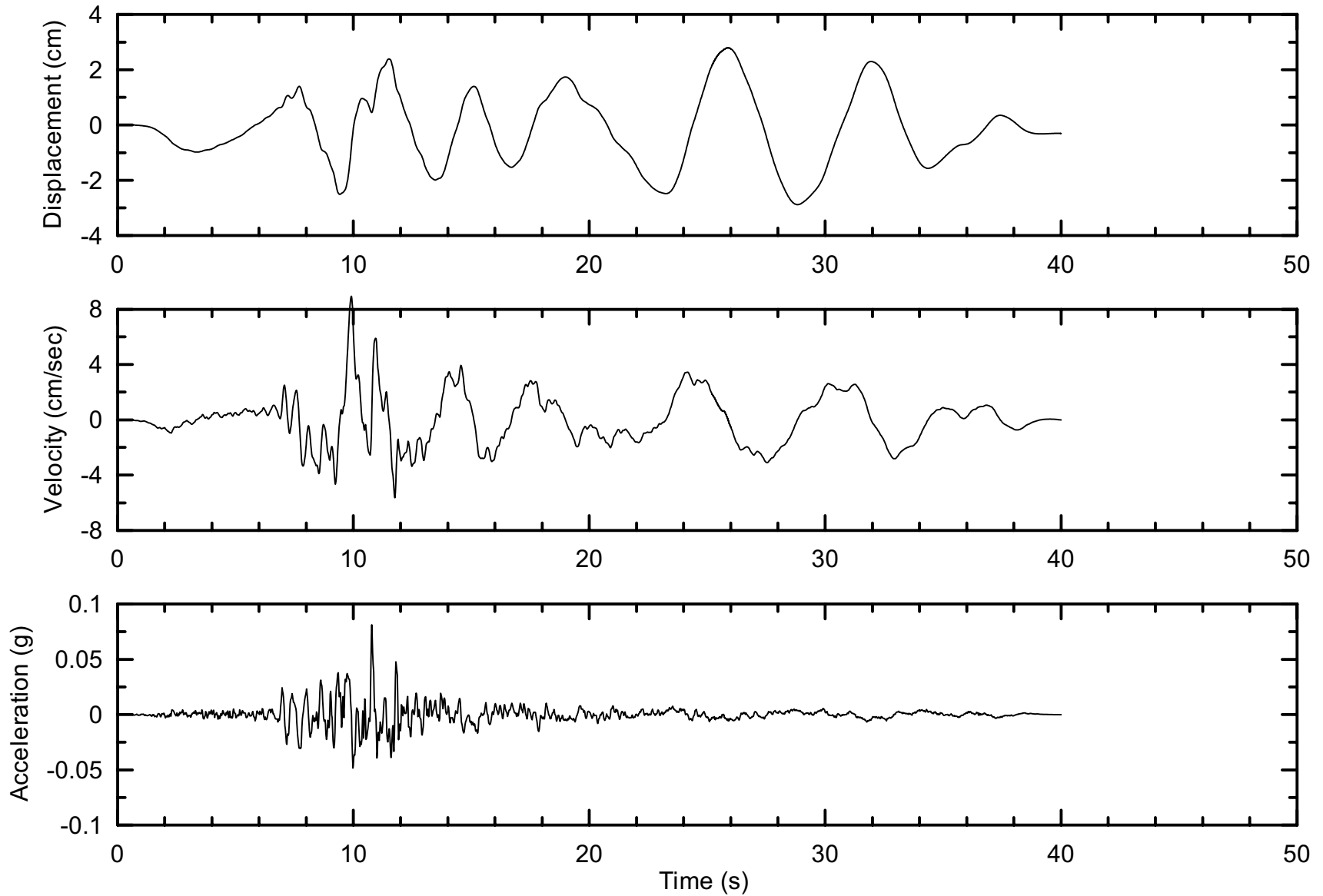
Note:

1. Dual values correspond to materials above and below the phreatic line, where applicable.
2. Mean effective stress, σ_m' , in ksf.
3. Seed and Idriss, 1970



Project No. 26814957	Estates Dam Seismic Stability Analysis	Finite Element Mesh for Cross-Section A-A' QUAD4M Analysis	Figure
URS			10-1

1989 Loma Prieta, CA Earthquake Time History
 Recorded at Piedmont Jr. High School Ground, 045 degree component



Project No.
26814957

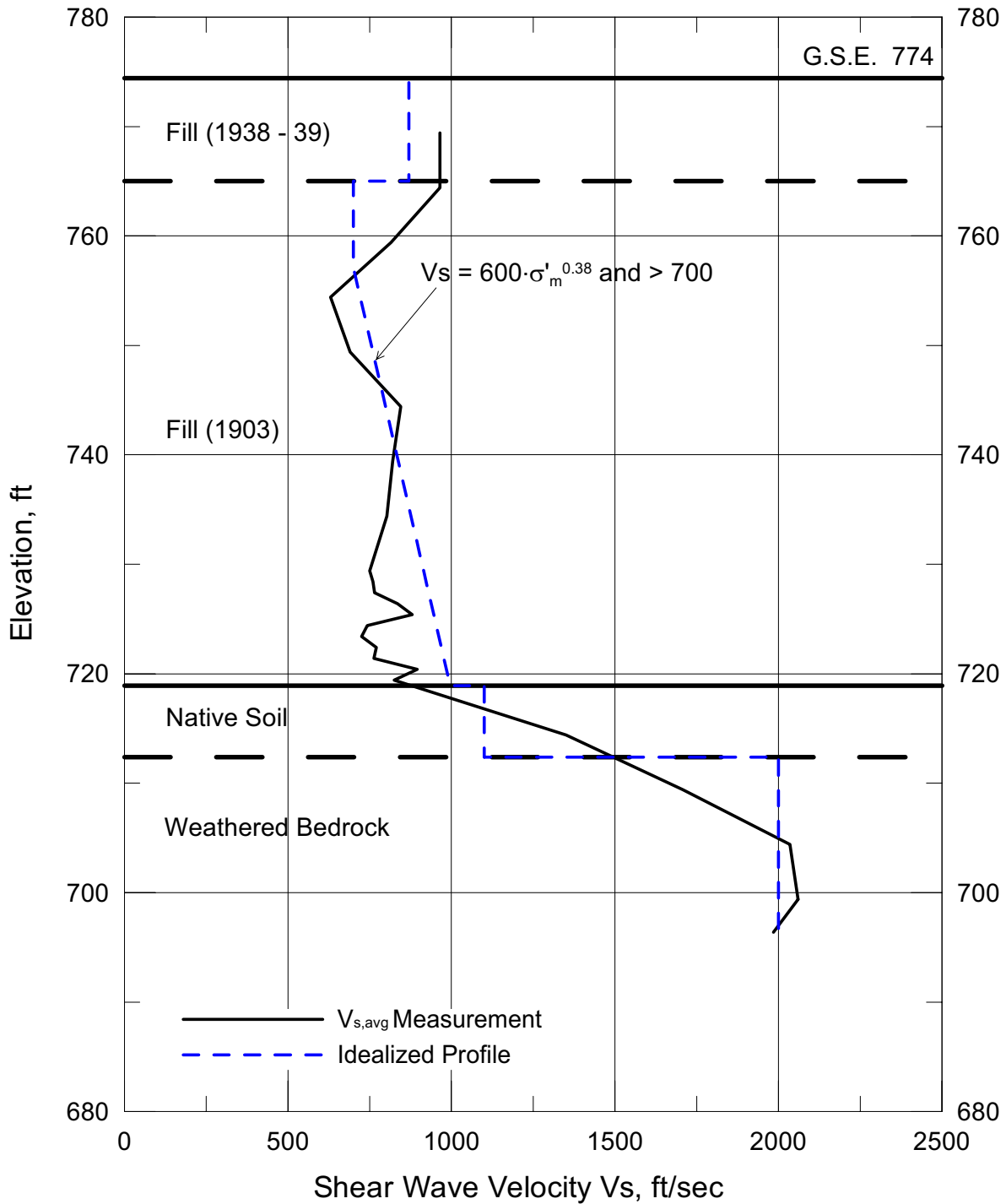
Estates Dam
Seismic Stability

Recorded Time History
1989 Loma Prieta, CA Earthquake
at Piedmont Jr. High School Station,
Horizontal Component, 045 deg.

Figure

10-2

URS

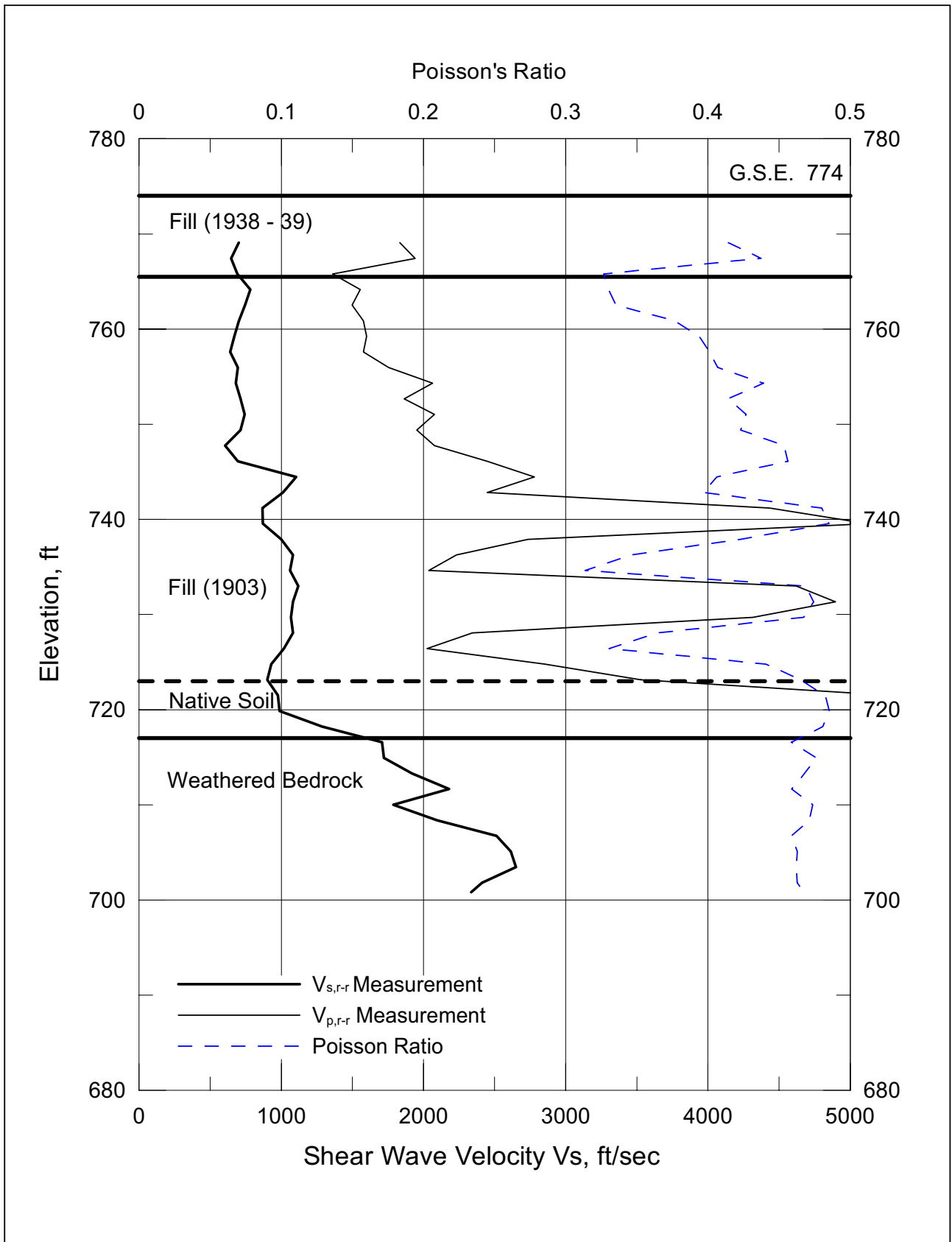


Project No. 26814957

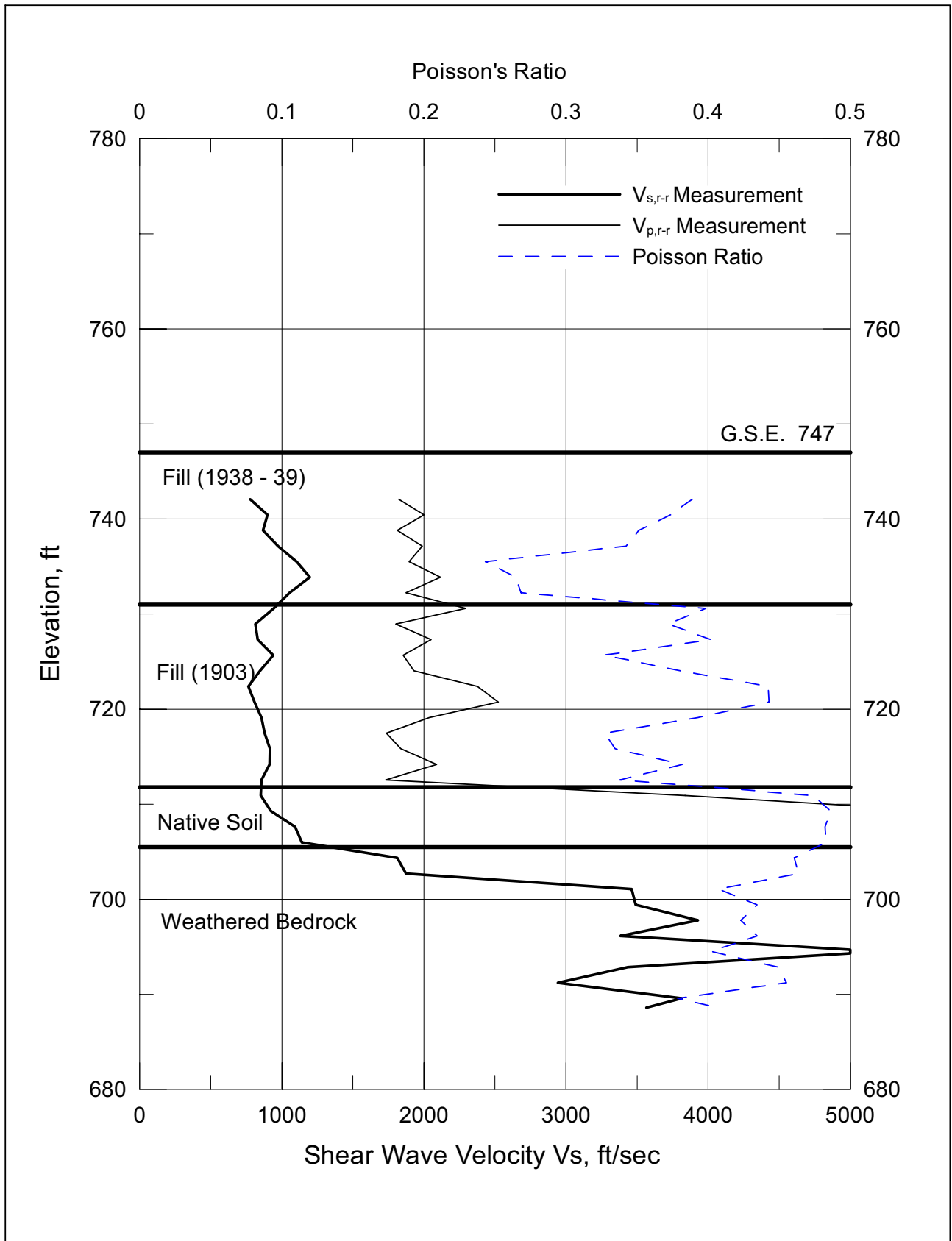
Estates Dam
Seismic Stability

**Seismic Wave Velocity Profile and
Stratigraphy from Borings B-1, 2, and 3**

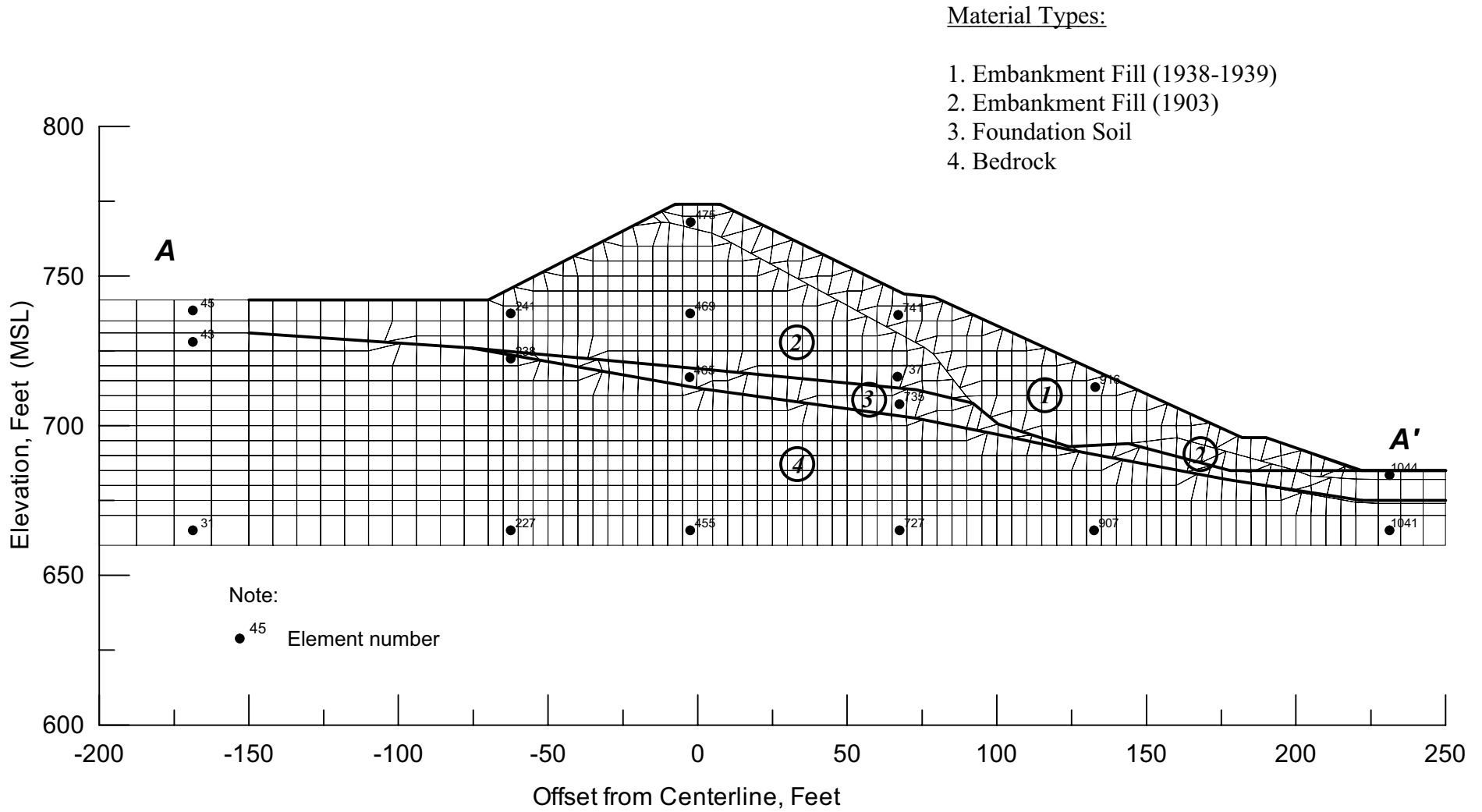
Figure
10-3



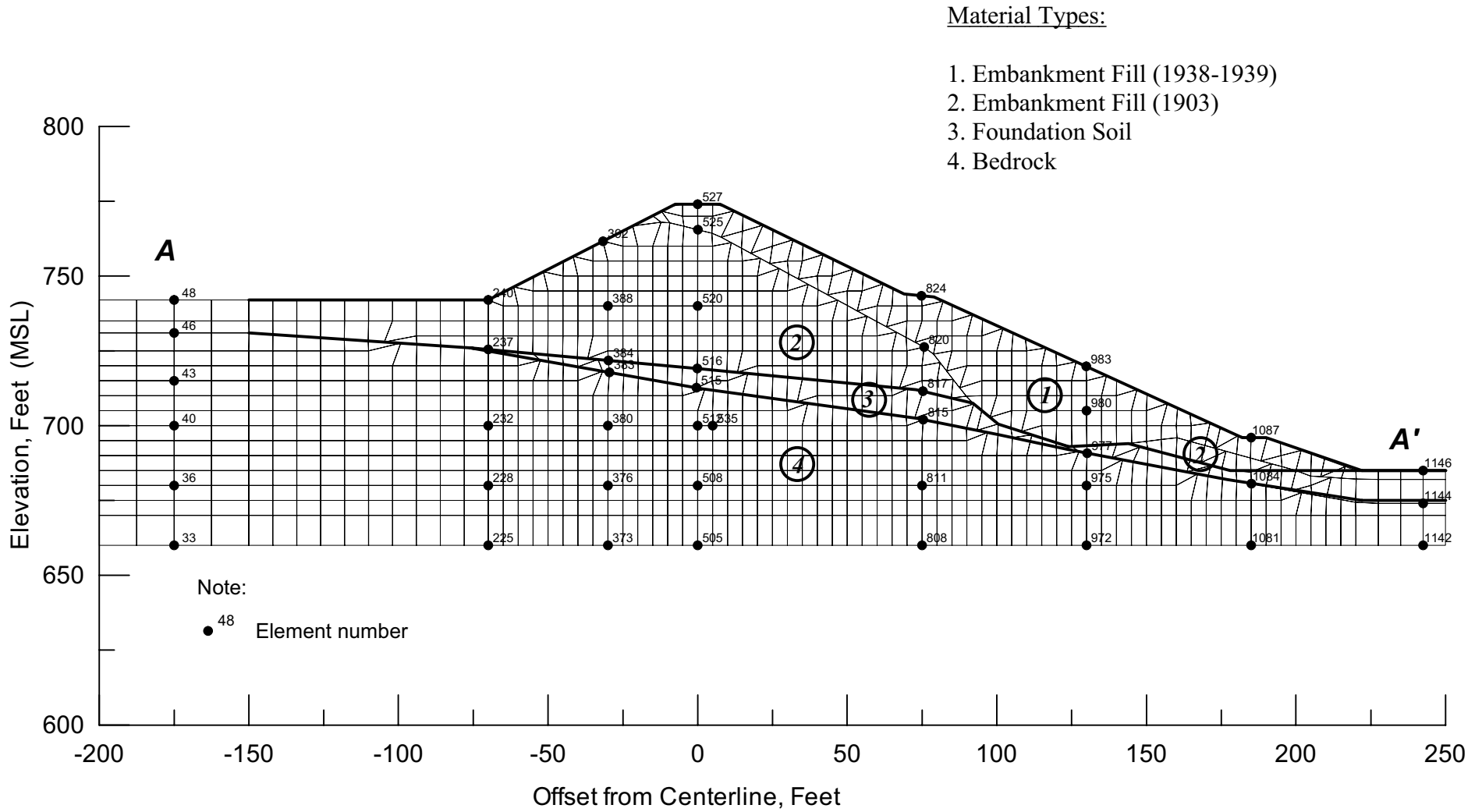
URS	Project No. 26814957	Seismic Wave Velocity Profile and Stratigraphy from Boring VQ-38	Figure
	Estates Dam Seismic Stability		10-4



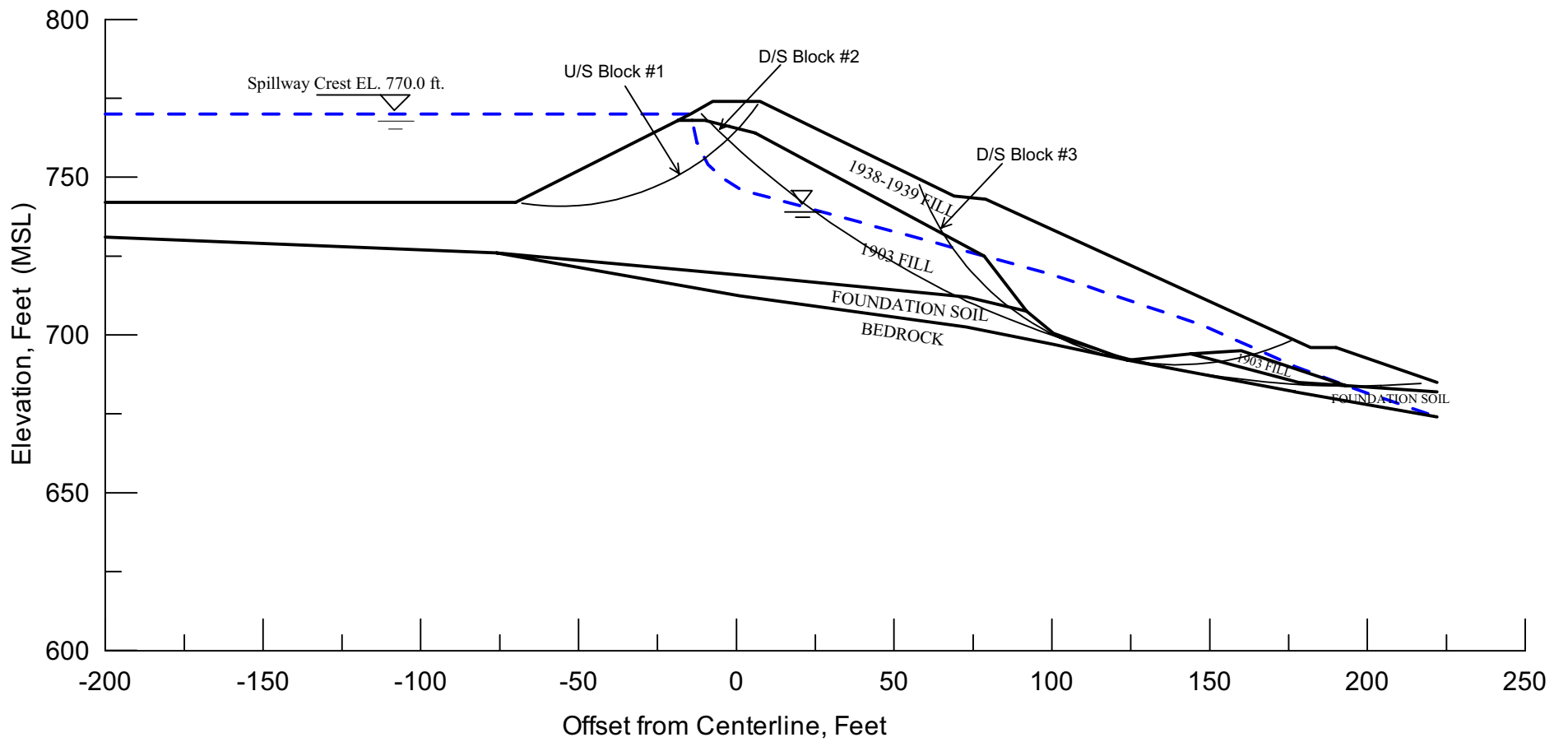
URS	Project No. 26814957	Seismic Wave Velocity Profile and Stratigraphy from Boring VQ-40	Figure
	Estates Dam Seismic Stability		10-5



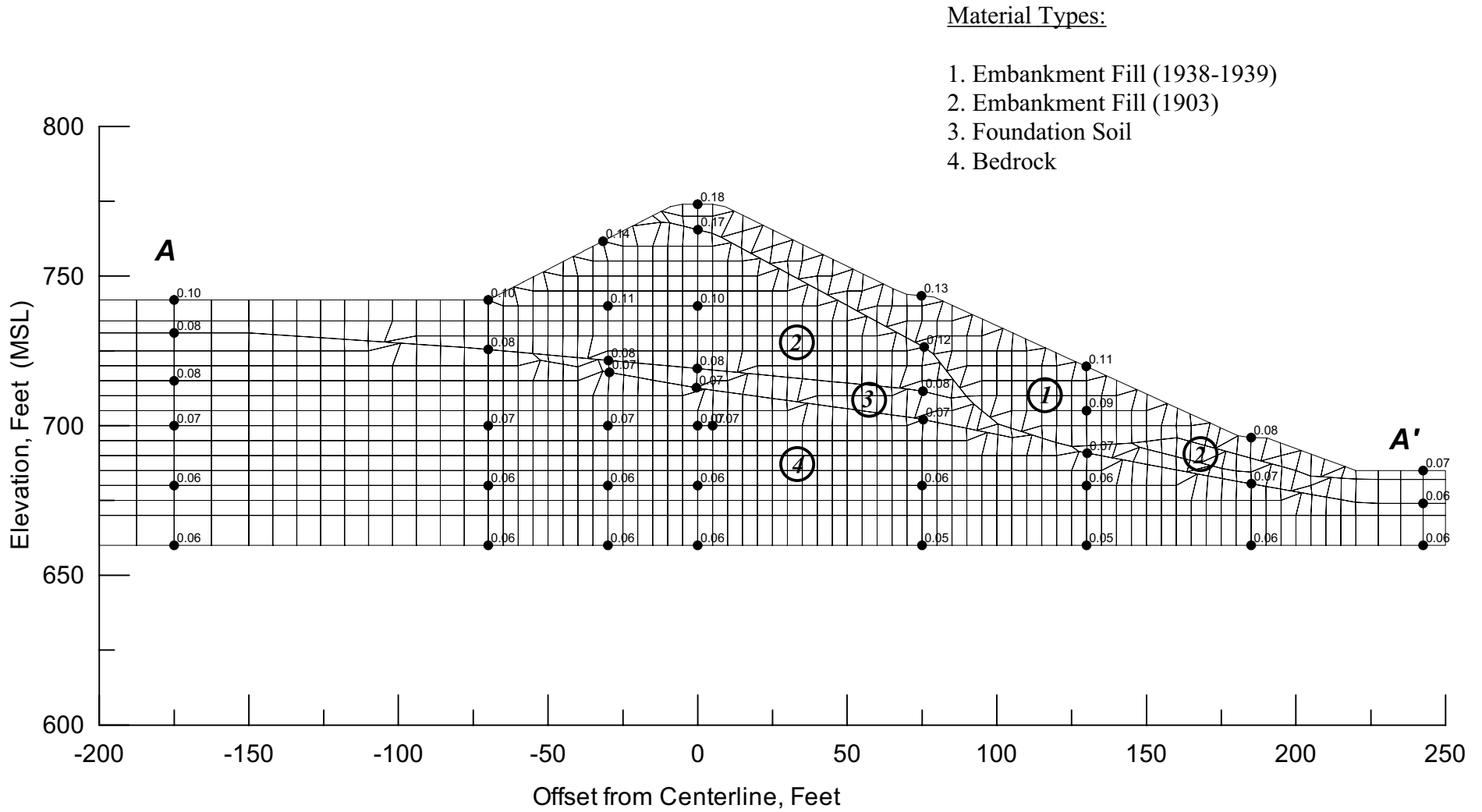
Project No. 26814957	Estates Dam Seismic Stability Analysis	Selected Element Locations For Stress Time-history Plots QUAD4M Analysis	Figure
URS			10-6



Project No. 26814957	Estates Dam Seismic Stability Analysis	Selected Nodal Points For Acceleration Outputs QUAD4M Analysis	Figure
URS			10-7

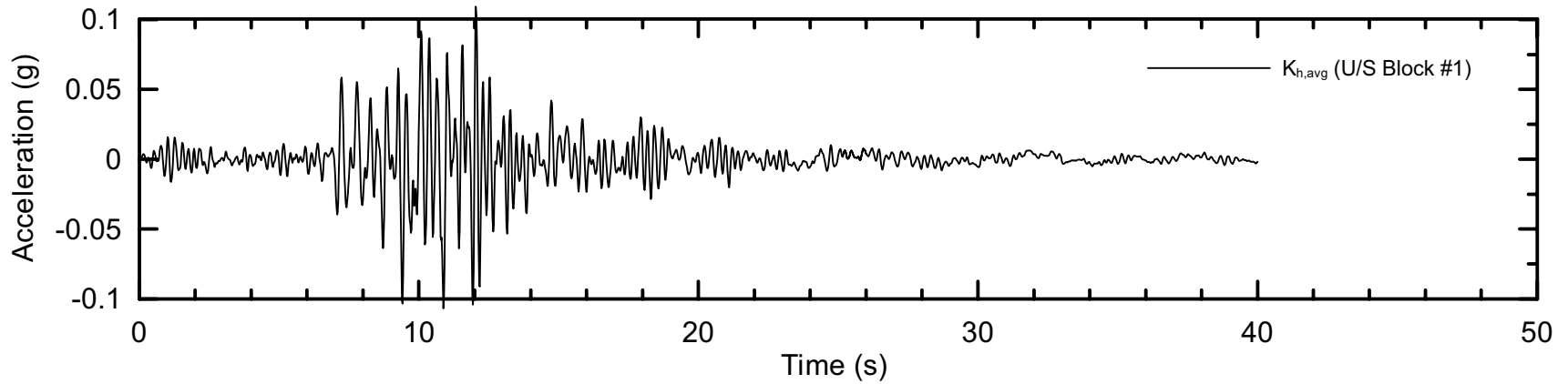
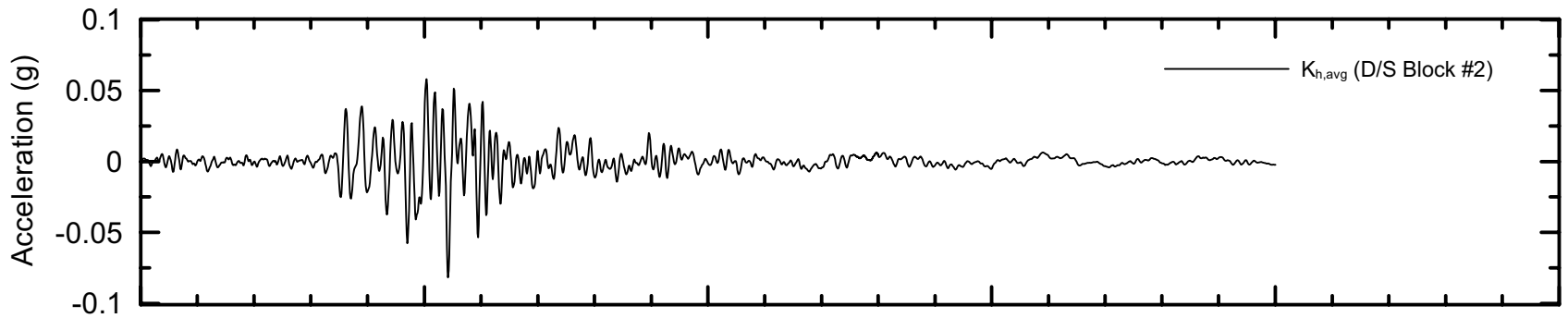
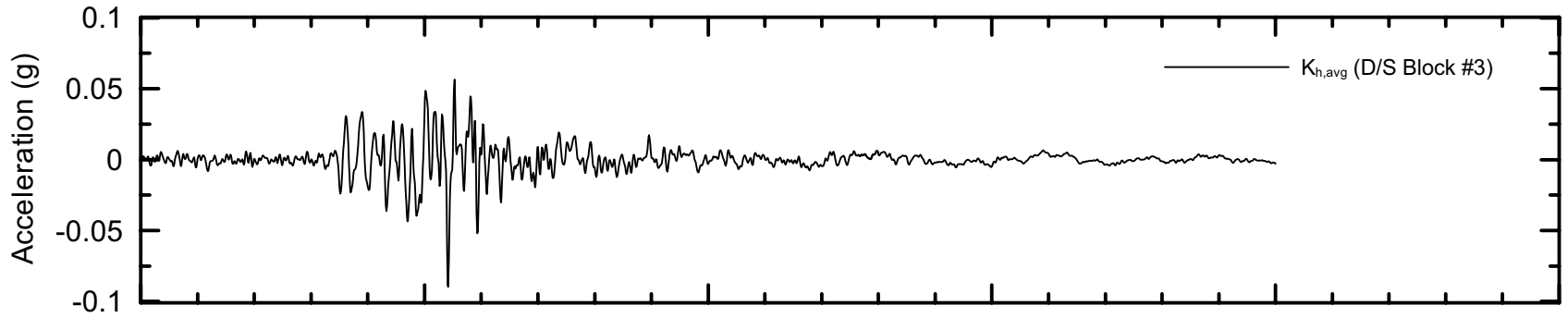


Project No. 26814957	Estates Dam Seismic Stability Analysis	Sliding Blocks for Newmark Deformation Analyses Cross Section A-A'	Figure
URS			10-8

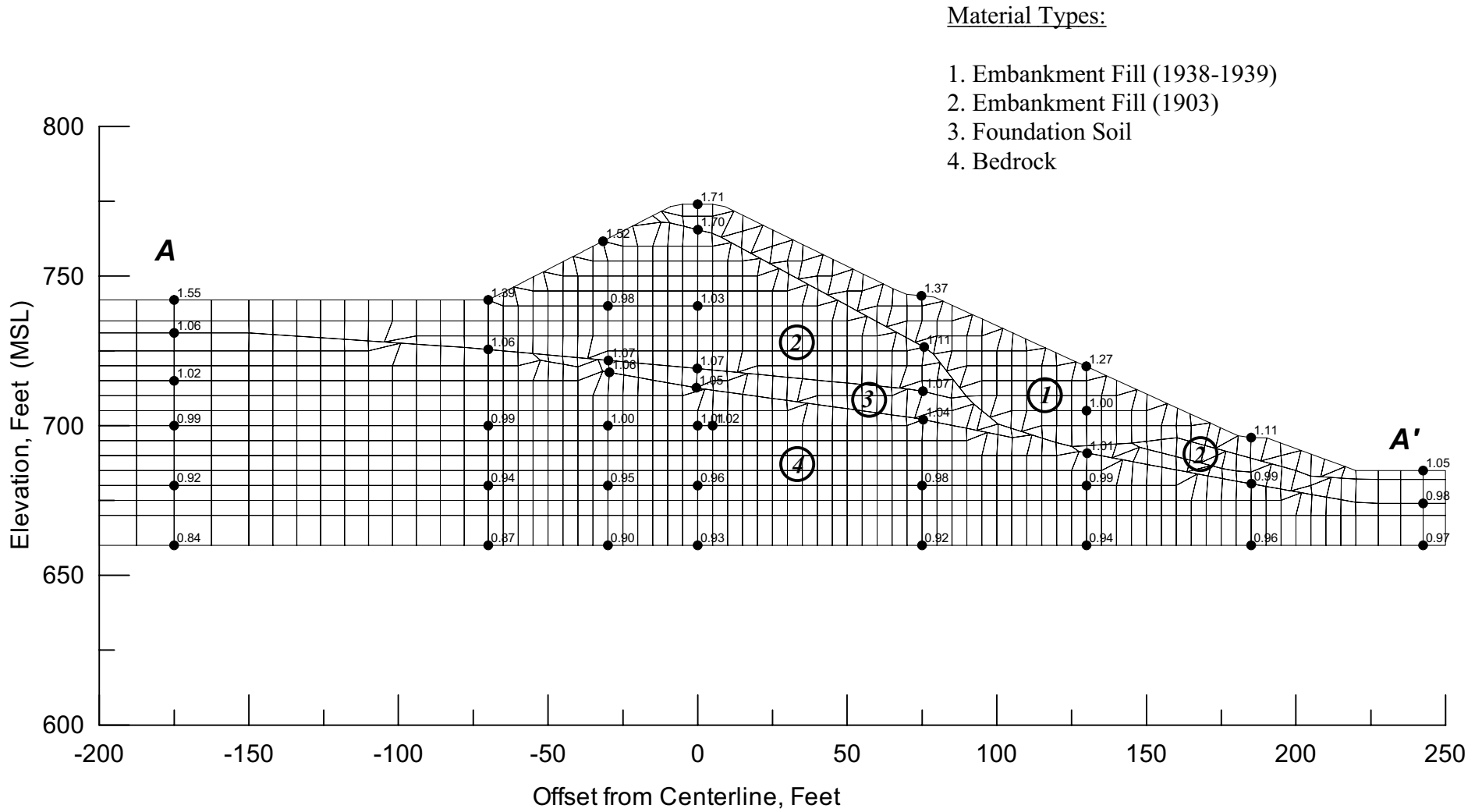


Note:
Horizontal acceleration in g's.

Project No. 26814957	Estates Dam Seismic Stability Analysis	Peak Horizontal Acceleration QUAD4M Analysis 1989 Loma Prieta Earthquake	Figure 10-9
URS			

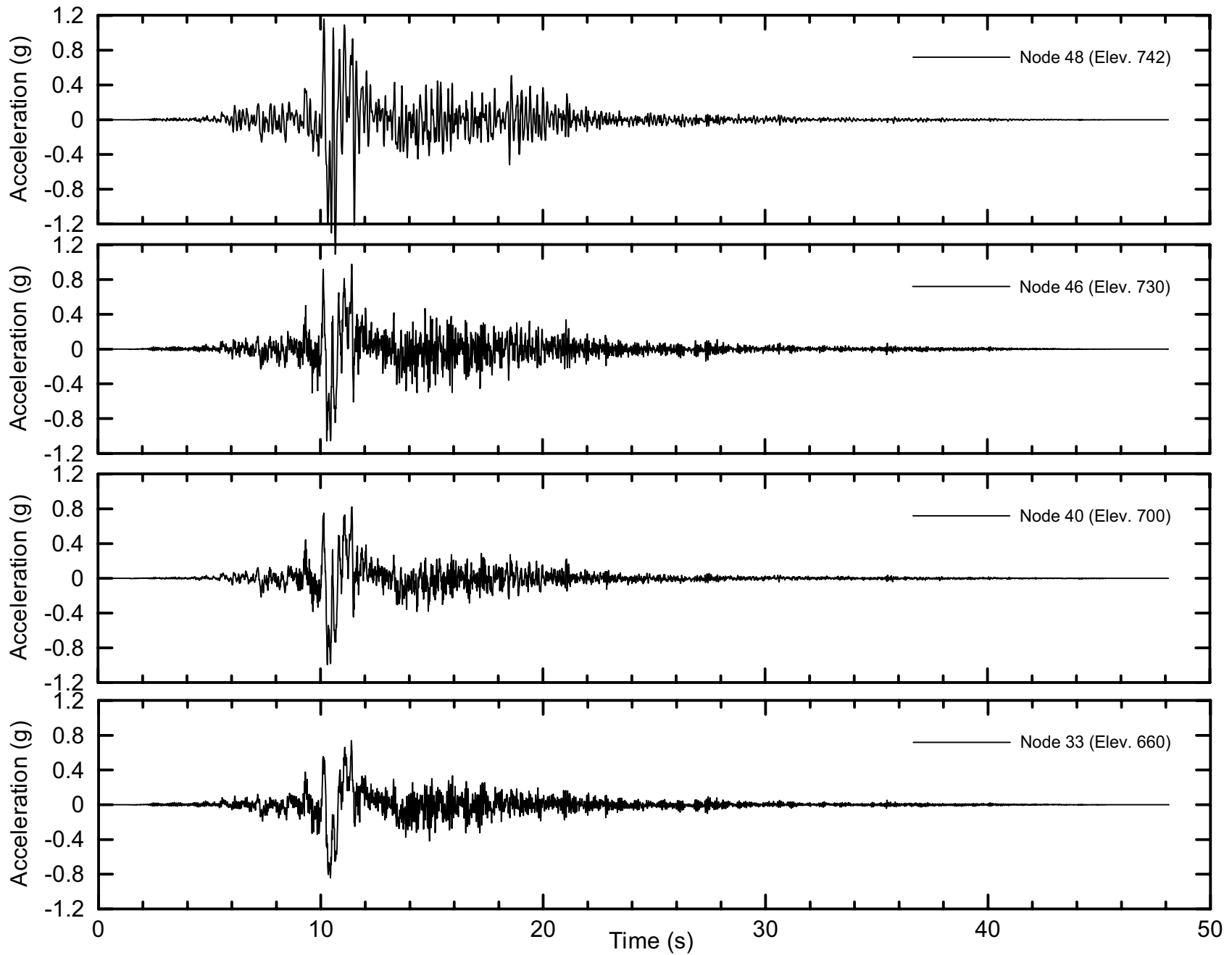


Project No. 26814957	Estates Dam Seismic Stability Analysis	Average Mass Acceleration QUAD4M Analysis 1989 Loma Prieta Earthquake	Figure 10-10
URS			

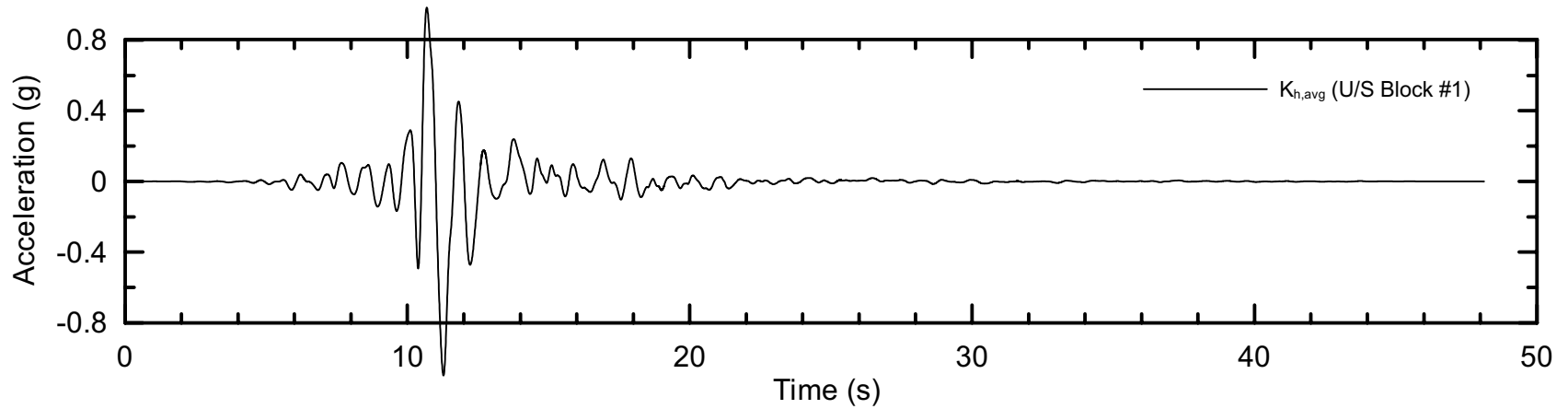
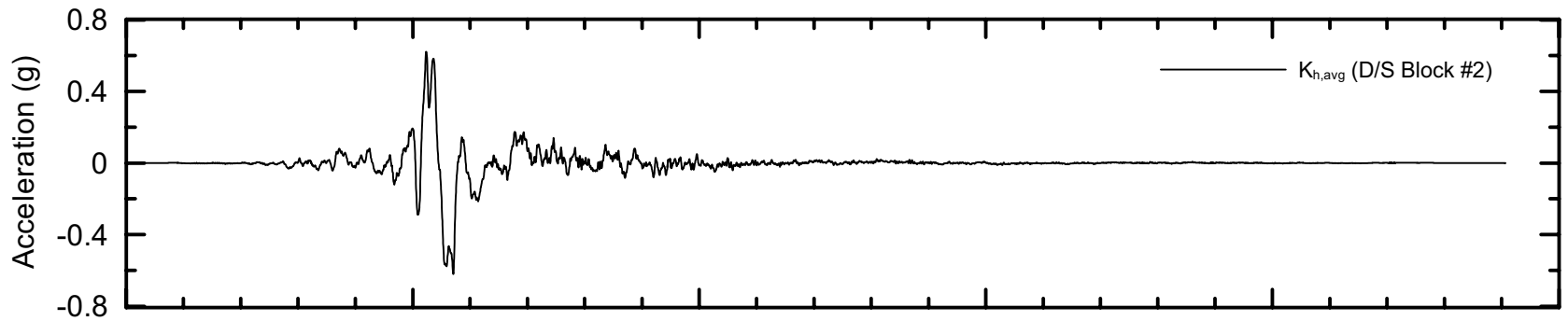
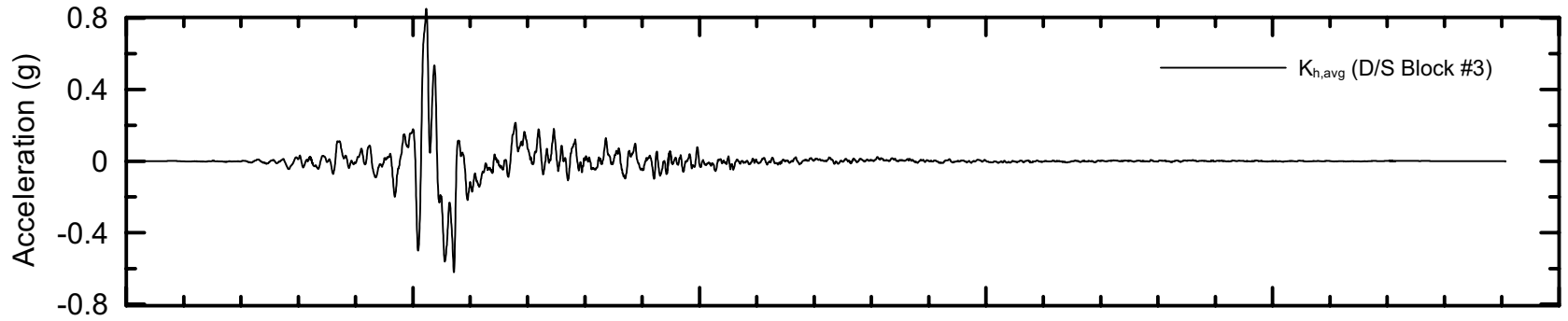


Note:
Horizontal acceleration in g's.

Project No. 26814957	Estates Dam Seismic Stability Analysis	Peak Horizontal Acceleration QUAD4M Analysis Cross-Section A-A' Hayward Fault Event TH #1	Figure 10-11
URS			



Project No. 26814957	Estates Dam Seismic Stability Analysis	Acceleration Time History 175 FT Offset Upstream QUAD4M Analysis Hayward Fault Event TH #1	Figure 10-12
URS			



Project No.
26814957

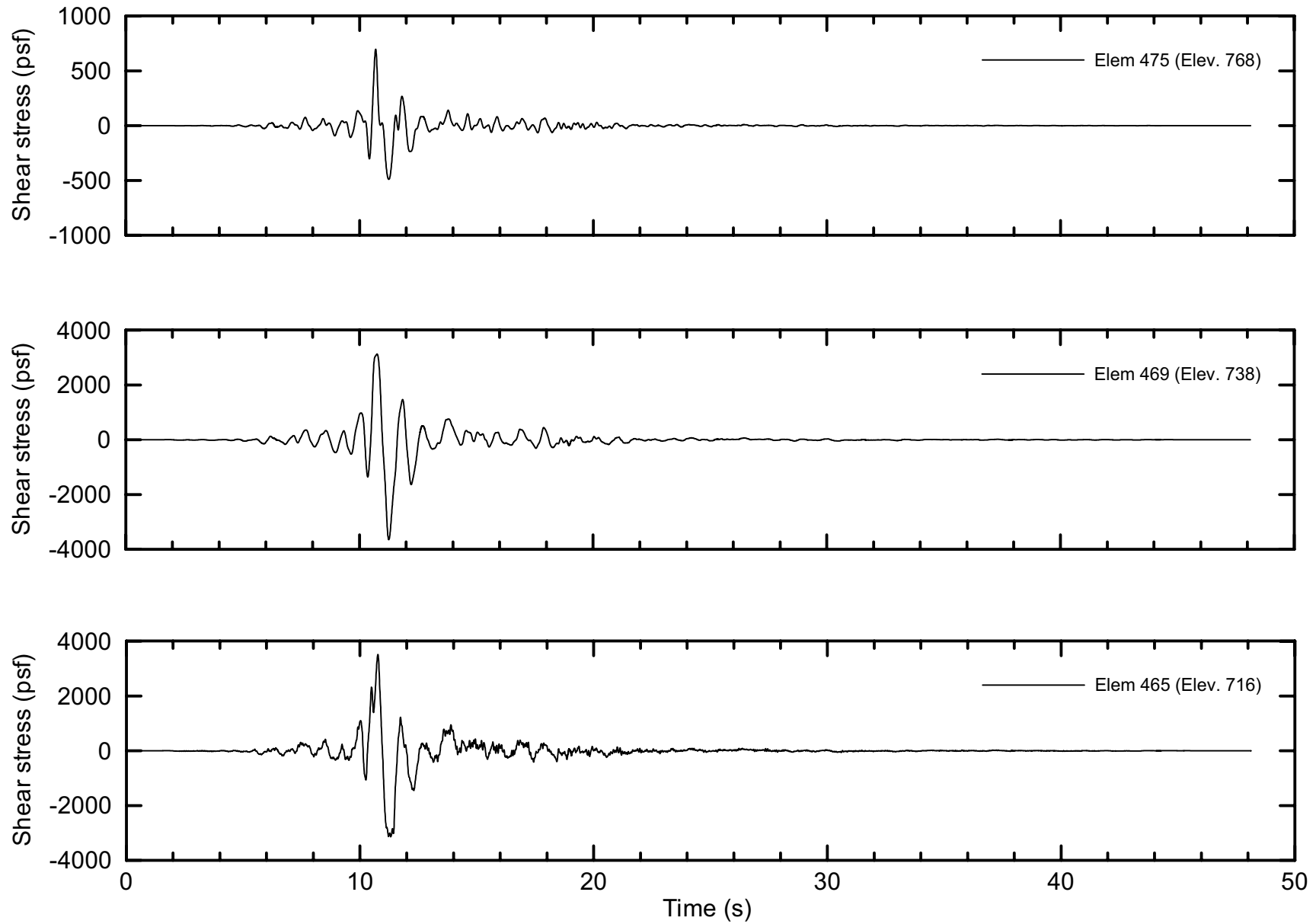
Estates Dam
Seismic Stability Analysis

Average Mass Acceleration
QUAD4M Analysis
Hayward Fault MCE TH #1

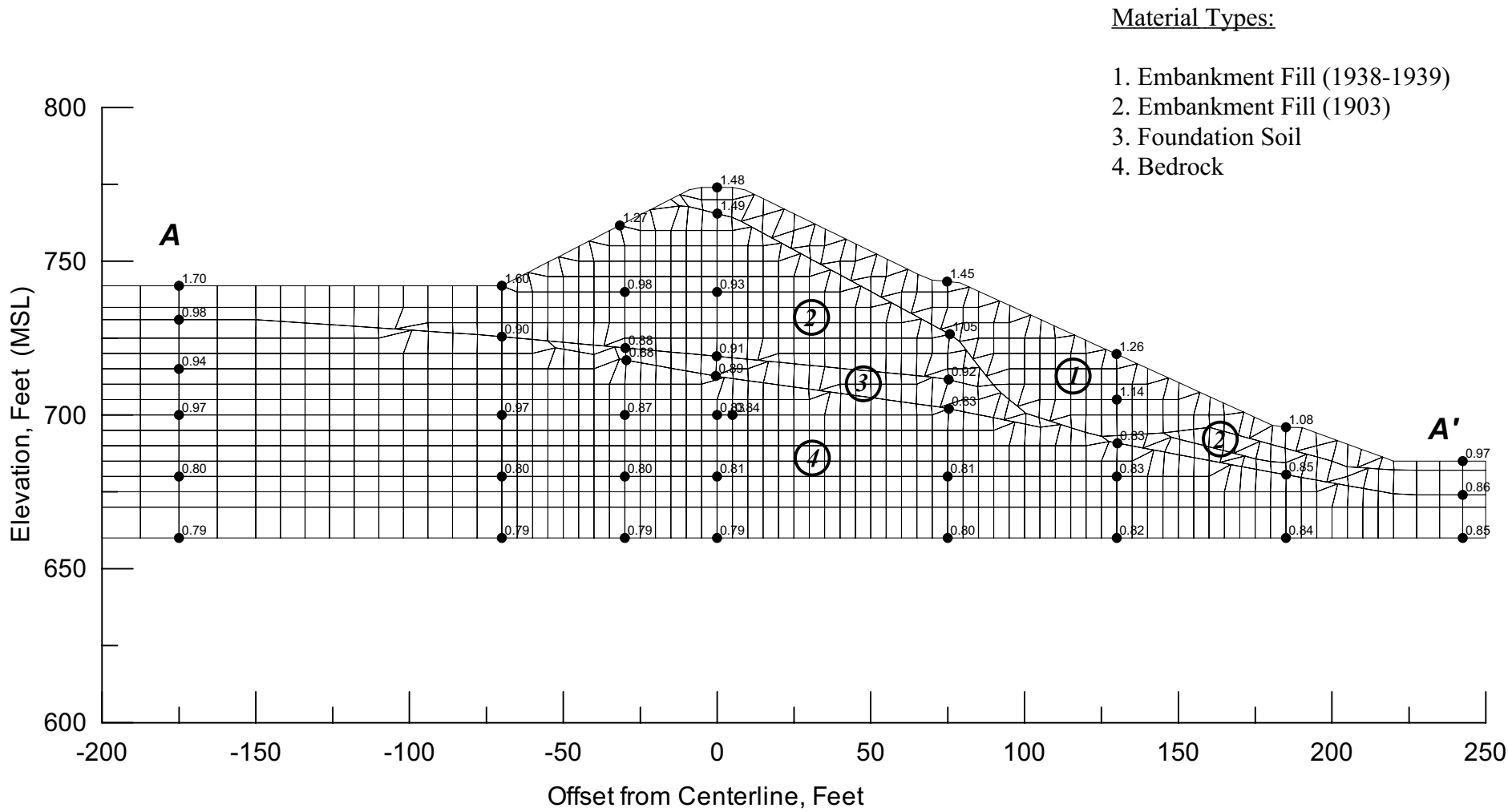
Figure

10-13

URS

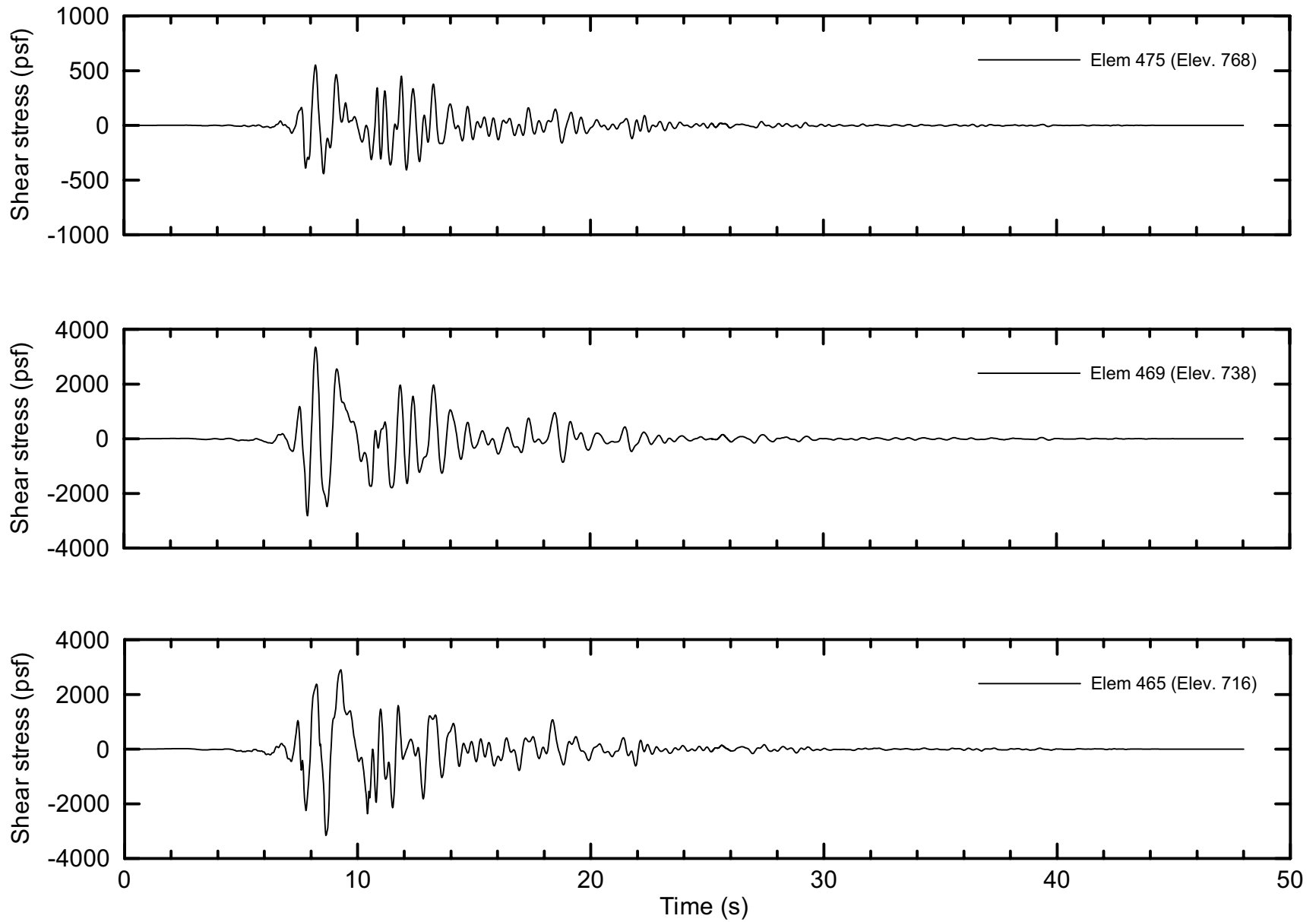


Project No. 26814957	Estates Dam Seismic Stability Analysis	Shear Stress Time History Beneath Crest Elements 465, 469, and 475 Hayward Fault MCE TH #1	Figure 10-14
URS			



Note:
Horizontal acceleration in g's.

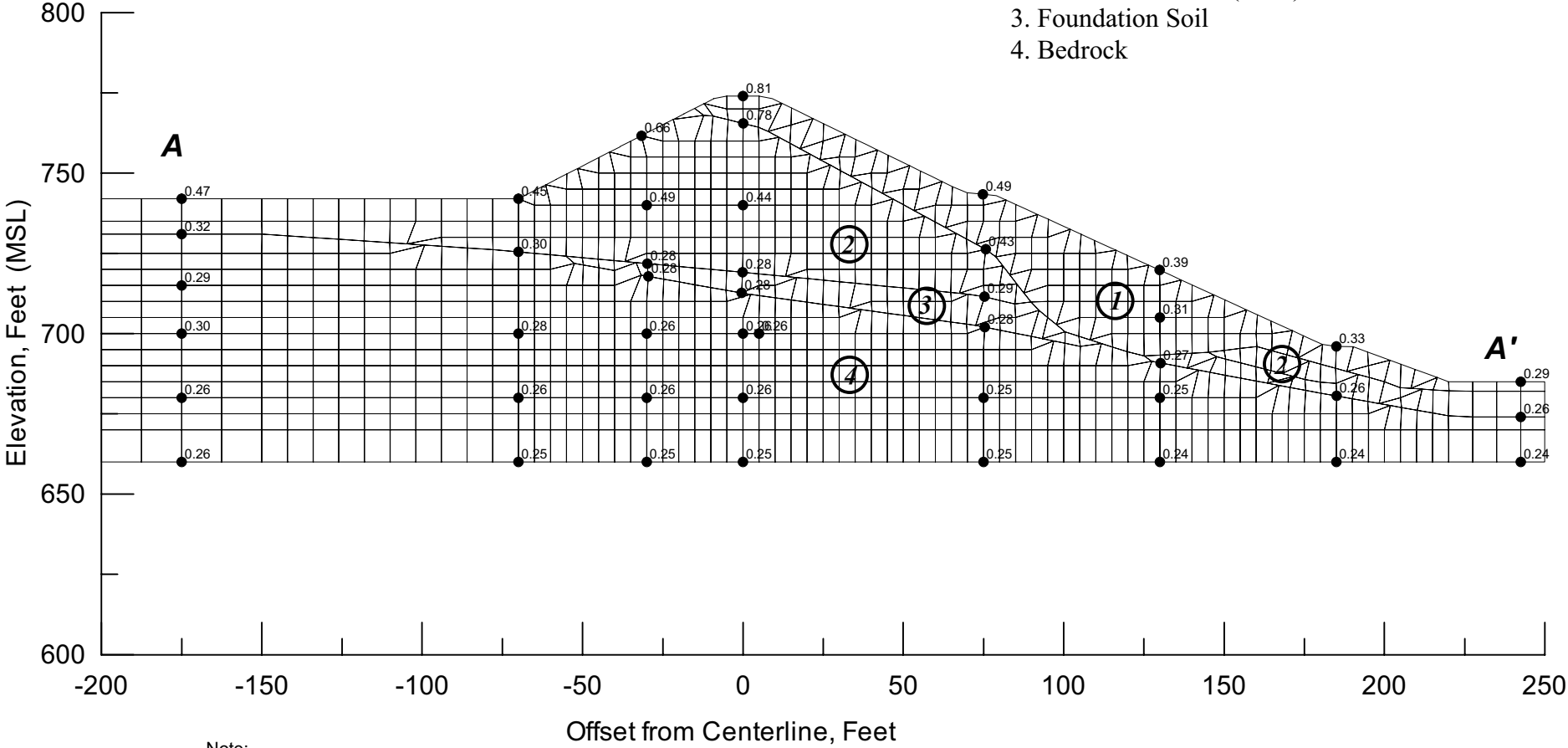
Project No. 26814957	Estates Dam Seismic Stability Analysis	Peak Horizontal Acceleration QUAD4M Analysis Cross-Section A-A' Hayward Fault Event TH #2	Figure 10-15
URS			



Project No. 26814957	Estates Dam Seismic Stability Analysis	Shear Stress Time History Beneath Crest Elements 465, 469, and 475 Hayward Fault MCE TH #2	Figure 10-16
URS			

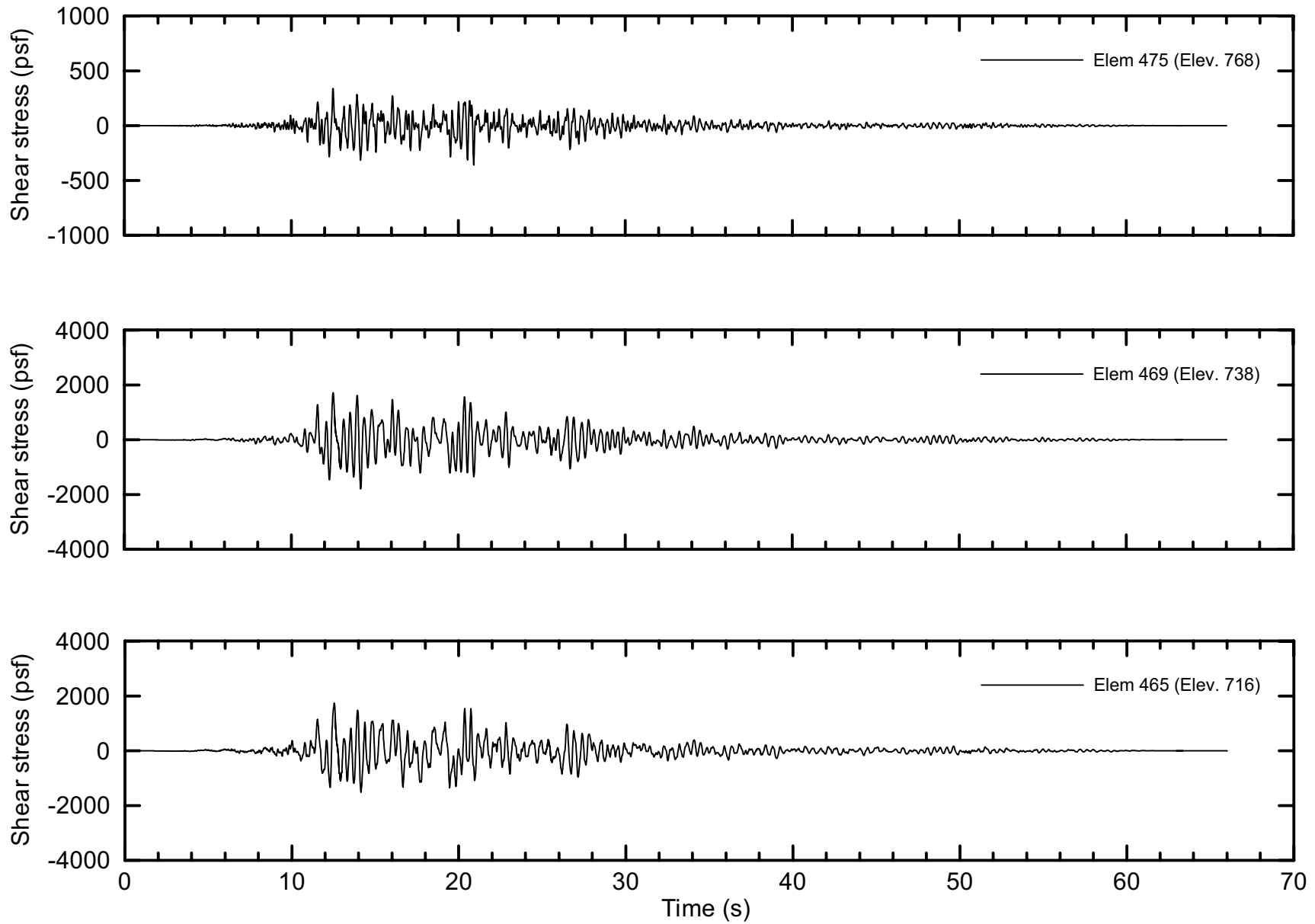
Material Types:

- 1. Embankment Fill (1938-1939)
- 2. Embankment Fill (1903)
- 3. Foundation Soil
- 4. Bedrock



Note:
Horizontal acceleration in g's.

Project No. 26814957	Estates Dam Seismic Stability Analysis	Peak Horizontal Acceleration QUAD4M Analysis San Andreas Fault MCE	Figure 10-17
URS			



Project No. 26814957	Estates Dam Seismic Stability Analysis	Shear Stress Time History Beneath Crest Elements 465, 469, and 475 San Andreas Fault MCE	Figure 10-18
URS			

11.1 APPROACH

As described in Section 8, the approach to the seismic stability analysis of the dam consisted of using the results of the dynamic response analyses presented in Section 10 to evaluate the potential for cyclic strength degradation of the embankment and foundation soils. The slope stability factors of safety and yield accelerations of potential sliding blocks were then evaluated using limit-equilibrium analyses and shear strengths appropriate for the materials subject to cyclic strength degradation. Together with the average mass accelerations of the sliding blocks obtained from the dynamic response analyses, the yield accelerations were used to calculate seismic displacements of the sliding blocks using a Newmark-type deformation analysis.

Analyses were also performed to evaluate the sensitivity of the calculated seismic deformations to the details of the input acceleration time histories. For these analyses, additional time histories to those presented in Section 6 were developed to represent the design earthquake motions. The simplified Newmark method was used for the sensitivity analyses.

11.2 EVALUATION OF POTENTIAL STRENGTH LOSS IN EMBANKMENT AND FOUNDATION SOILS

11.2.1 Evaluation Procedures

The potential for strain and strength loss of the embankment and foundation soils was evaluated by comparing the earthquake-induced cyclic stress ratio with the cyclic strength of the materials. The cyclic strength of the materials was expressed in terms of the cyclic stress ratio required to develop a cyclic shear strain, γ , of 3.75%, which approximately corresponds to a cyclic axial strain, ϵ , of 2.5% under undrained conditions and is commonly assumed to correspond to an excess pore pressure ratio, r_u , of 100%. Thus, this cyclic strength ratio (CSR) is adopted as the cyclic resistance ratio (CRR) of the materials.

The CRR was estimated based on the results of the cyclic triaxial strength tests performed by Wahler (1980), considering the measured undrained strength of the materials. For a magnitude 7.5 earthquake, or about 30 cycles of loading in clayey soils (Boulanger and Idriss, 2004), the cyclic resistance ratio of the 1903 fill and the foundation soil was estimated to be $CRR_{7.5} = 0.28$, for conditions of zero static shear stress ratio ($\alpha=0$) and effective overburden stress, (σ_v'), equal to 1 tsf. Similarly, the $CRR_{7.5}$ for the 1938-39 fill was estimated to be 0.56. The estimated cyclic resistance curve for the materials for 1 to 100 cycles of loading is illustrated in Figure 11-1.

The factor of safety against development of shear strains of 3.75% was calculated as:

$$FS_{3.75} = CRR/CSR$$

where: CSR = earthquake-induced cyclic stress ratio and CRR is given by:

$$CRR = K_{\sigma} \cdot K_{\alpha} \cdot MSF \cdot CRR_{7.5}$$

where: $CRR_{7.5}$ = cyclic resistance ratio defined as the cyclic stress ratio required to produce a shear strain of 3.75% in thirty cycles of loading

MSF = magnitude scaling factor

K_σ = correction factor for effective overburden stress

K_α = correction factor for initial static shear stress ratio

The magnitude-scaling factor was obtained from the following expression (Boulanger and Idriss, 2004):

$$MSF = 1.12 \exp(-M/4) + 0.828 ; MSF \leq 1.13$$

where M is the moment magnitude of the earthquake. The overburden correction factors were obtained from the following expressions, which were derived from the results of the available strength tests:

$$K_\sigma = (\sigma_v')^{-0.2} ; K_\sigma \leq 1.2; \text{ for the 1903 fill and foundation soil, and}$$

$$K_\sigma = (\sigma_v')^{-0.4} ; K_\sigma \leq 1.3; \text{ for the 1938-39 fill.}$$

where σ_v' = effective vertical stress in tsf. The available cyclic strength data was insufficient to fully define the shear stress correction factor, but suggested that this factor is similar to that evaluated by URS (2005) for the fill and foundation soils of Chabot Dam. Accordingly, this factor was obtained from the following expression:

$$K_\alpha = 1 + 3.29\alpha - 6.61\alpha^2 - 3.84\alpha^3 ; \alpha \leq 0.35$$

where: α = initial static shear stress ratio.

In the Wahler investigations (1980), twelve post-cyclic consolidated undrained triaxial tests were performed on Pitcher-barrel samples. The post-cyclic strength data from these tests is shown on Figure 11-2. Although pore pressures were not measured during the cyclic loading, the available measurements suggest that a maximum residual excess pore pressure ratio (r_u) of about 95% developed during the cyclic tests. Because no pore pressures were measured during the cyclic tests, the excess pore pressures during shaking were estimated based on the results of cyclic tests with pore pressure measurements on similar materials (WCC, 1989), which yielded the following expression:

$$r_u = 1/FS_{3.75} ; r_u \leq 0.95$$

The data shown in Figure 11-2 suggest that the potential reduction in strength of the materials due to the residual excess pore pressures could be as much as 40 percent. This value is consistent with published information for similar materials (Thiers and Seed, 1969; Lee and Focht, 1976; Idriss, 1985; Mejia, 1989). Based on this information, the post-cyclic strength of the embankment fill and foundation soils was estimated from the following expression:

$$(\tau_{\max}) / (\tau_{\max})_{\text{static}} = (1 - r_u)^{0.16} ; (\tau_{\max}) / (\tau_{\max})_{\text{static}} \geq 0.6$$

where:

(τ_{\max}) = Post-cyclic undrained shear strength

$(\tau_{\max})_{\text{static}}$ = Static undrained shear strength

The above formulation of cyclic behavior and strength was used in the non-linear analyses as discussed in Section 12. The values of static stress ratio, vertical effective stress, and cyclic shear stress were calculated using the computer program FLAC.

11.2.2 Potential for Strength Loss

For the seismic stability analyses under the post-earthquake condition, the undrained strengths of the saturated embankment fills and foundation soils were reduced by 20 percent to account for seismically induced strength degradation. This assumption was based on the results of the post-cyclic, undrained triaxial compression tests from the Wahler investigations (1980) and our experience with similar materials. The actual strength reduction of the materials depends on the input seismic motion and the dynamic response of the dam. In the non-linear analyses performed for this study (Section 12), the strength reduction of the materials was directly evaluated using the procedure discussed above. The results from the non-linear analyses support the assumption of a 20 percent reduction for the Newmark-type deformation analysis.

11.3 POST-EARTHQUAKE SLOPE STABILITY

Limit equilibrium methods were used to check the post-earthquake stability of the dam. The analyses were performed assuming a 20 percent reduction of the undrained strength of the embankment fill and foundation soils as discussed above. No strength reduction was applied to the unsaturated fills or foundation soils. The strength parameters for the post-earthquake condition are summarized in Table 11-1.

The calculated post-earthquake factors of safety for the selected sliding blocks are shown in Figure 11-3. A minimum factor of safety of about 1.1 was calculated for a deep-seated downstream block. These results indicate that while the safety margin is relatively small, the dam can be expected to remain stable after the design earthquake.

11.4 DEFORMATION ANALYSES

11.4.1 Methodology

The seismic deformations of the dam were estimated with the Newmark sliding block method of analysis. The method is based on the assumption of rigid-perfectly plastic stress-strain behavior on a potential failure surface. Displacements of the sliding block are calculated by integrating twice with time the difference between the earthquake-induced average acceleration of the slide mass and its yield acceleration.

The results of the QUAD4M analyses were used to evaluate the earthquake-induced average mass accelerations of potential sliding blocks within the dam. Together with the yield accelerations obtained from the limit equilibrium analyses, the average mass accelerations were used to calculate seismic displacements of the sliding blocks. Double integration of the difference between the average mass and yield accelerations was performed with the computer program TNMN.

11.4.2 Yield Acceleration Evaluation

The yield accelerations, K_y , used in the analyses were calculated from pseudo-static limit-equilibrium analyses. The calculated K_y values for the selected sliding blocks are tabulated in Table 11-2 for various levels of strength degradation in the embankment and foundation materials. The K_y for the pre-earthquake condition corresponds to the yield acceleration of the

sliding blocks prior to seismic strength degradation of the materials. The K_y for the post-cyclic condition assumes that the saturated embankment fills and foundation soils have undergone strength loss.

Together with the results of the FLAC analyses presented in Section 12, the calculated dynamic response (e.g. acceleration and shear stress time histories) within the dam were used to estimate the timing of strength reduction of the materials during the earthquake shaking. The yield acceleration coefficients (see Table 11-2) and the timing of strength reduction were then used to develop time histories of yield acceleration for each potential sliding block. Those time histories are shown in Figures 11-4 through 11-9, together with the time histories of earthquake-induced average mass acceleration.

For Hayward fault MCE time history No. 1 (Figures 11-4 through 11-6), little strength reduction is assumed during the first 10.8 seconds of shaking and the yield acceleration for that period corresponds to that for pre-earthquake conditions. Between about 10.8 and 12.2 seconds, the yield acceleration corresponds to a 10% strength reduction. A yield acceleration corresponding to 20% strength reduction is used after about 12.2 seconds. Similarly, for Hayward fault MCE time history No. 2 (Figures 11-7 through 11-9), little strength reduction is expected during the first 8.5 seconds of shaking and the yield acceleration for that period corresponds to that for pre-earthquake conditions. Between about 8.5 and 9.5 seconds, the yield acceleration corresponds to a 10% strength reduction. A yield acceleration corresponding to 20% strength reduction is used after about 9.5 seconds.

11.4.3 Analysis Results

The Newmark-type deformation analyses results are presented in Figures 11-4 through 11-9. The calculated displacements are summarized in Table 11-3. These calculated displacements correspond to horizontal translation of the center of mass of each sliding block. The corresponding vertical displacements can be obtained from the rotation of the block necessary to accommodate the horizontal displacements.

For the Loma Prieta earthquake, because the dynamic response of the dam is small (Figure 10-9), little strength degradation is expected during the earthquake and the peak mass acceleration for each block (Figure 10-10) is less than the corresponding yield acceleration (Table 11-2). Thus, the calculated deformations are nil, and it may be concluded that the calculated dynamic response and seismic deformations from the Newmark-type analyses are in good agreement with the known performance of the dam during that earthquake.

The displacements calculated for Hayward fault MCE time history No. 1 are shown in Figures 11-4 through 11-6. Horizontal displacements of 3 to 5 feet are calculated for the deep-seated downstream block No.2. Based on the geometry of the block, such displacements would correspond to downward vertical displacements of the crest of 2 to 4 feet. Smaller horizontal displacements (2 to 4 feet) are calculated for upstream block No. 1. Much smaller horizontal displacements (1 to 2 feet) are calculated for downstream block No. 3.

The displacements calculated for Hayward fault MCE time history No. 2 are shown in Figures 11-7 through 11-9. Horizontal displacements of 4 to 11 feet are calculated for the deep-seated downstream block No.2. Based on the geometry of the block, such displacements would correspond to downward vertical displacements of the crest of 3 to 8 feet. Somewhat smaller

horizontal displacements (4 to 6 feet) are calculated for upstream block No. 1. Smaller horizontal displacements (2 to 4 feet) are calculated for downstream block No. 3.

As discussed in Section 6-4, both Hayward fault MCE time histories No. 1 and No.2 are spectrally matched to the same target spectrum (Figure 6-14). However, the Newmark-type analyses for the two time histories show a wide range of calculated displacements. Thus, these results indicate that the dam deformations for the Hayward fault event are sensitive to the details of the ground motion time histories used.

Since the seismic response of the dam for the San Andreas event (see Figures 10-17 and 10-18) is smaller than that for the Hayward fault event, the dam deformations for the San Andreas event are expected to be lower than those for the Hayward event.

11.5 SENSITIVITY OF CALCULATED DEFORMATIONS TO GROUND MOTION TIME HISTORIES

11.5.1 Additional Ground Motion Time Histories

To evaluate the sensitivity of the calculated seismic deformations to the details of the ground motion time histories, additional ground motion time histories were developed. Two additional spectrum-compatible acceleration time histories were developed for the Hayward fault MCE, using the same criteria and procedures presented in Section 6.4. The additional time histories (Nos.3 and 4) were based on the 040-degree component of the LGPC Station record of the 1989 Loma Prieta, California earthquake, and the 090-degree component of the Izmit Station record of the 1999 Kocaeli, Turkey earthquake. The recorded time histories were modified so that their spectra after modification closely match the recommended spectrum for the MCE. The acceleration, velocity and displacement time histories of the modified motions and the corresponding 5%-damped acceleration response spectra are plotted in Figures 11-10 through 11-13.

In addition, two recorded motions (without modification) were used for the sensitivity study. They are the 344-degree component of the Tabas Station record of the M 7.4 1978 Tabas, Iran earthquake and the 000-degree component of the LGPC Station record of the M 7 1989 Loma Prieta, California earthquake. The acceleration, velocity and displacement time histories of these records and the corresponding 5%-damped acceleration response spectra are plotted in Figures 11-14 through 11-17.

11.5.2 Simplified Newmark Analysis

The sensitivity of calculated seismic deformations to the input acceleration time histories was evaluated using the simplified Newmark method. In a simplified Newmark analysis, the earthquake ground motion (bedrock motion) is used directly as the average mass acceleration of the sliding block. Together with the yield accelerations, this acceleration is used to calculate seismic displacements of the block. Thus, a dynamic response analysis is not performed in the simplified Newmark analysis. The sensitivity analyses were performed for downstream sliding block No.2 because this is the critical sliding block.

The results of the simplified Newmark analyses for block No. 2 are presented in Figures 11-18 through 11-25. The yield acceleration was assumed to be a constant of 0.05g, which corresponds

to the K_y value for the block under the post-earthquake condition. The calculated horizontal displacements are summarized in Table 11-4.

In general, the horizontal deformations calculated using the simplified Newmark method are similar to those calculated using the Newmark-type deformation analysis (Table 11-4). Thus, the simplified method may be viewed as a reasonable tool to evaluate the sensitivity of the calculated seismic deformations to the details of the ground motion time histories.

As shown in Table 11-4, the range of horizontal deformations for block No. 2 for the Hayward fault MCE using the simplified Newmark method is between 2 and 12 feet. The analyses indicate that the range of calculated deformations using the additional time histories (Nos. 3 and 4) is similar to that calculated for time histories Nos. 1 and 2. In addition, the calculated deformations using recorded time histories are within the range calculated using spectrally matched time histories. The results suggest that a representative average of the calculated deformations is about 7 feet. Thus, such horizontal deformation may be considered to represent the average deformation response of block No. 2 calculated with the simplified Newmark method for the design earthquake.

Table 11-1
UTEXAS3 Input Parameters for Seismic Stability Analysis – Post-Earthquake Condition

Material	Total Unit Weight	Undrained Strength Envelope ($K_c = 1$) ⁽¹⁾		Effective Strength Parameters	
	γ_t	d_R	Ψ_R	c'	ϕ'
	(pcf)	(psf)	(°)	(psf)	(°)
1938-39 Embankment Fill above phreatic surface	133	-	-	0	35
1938-39 Embankment Fill below phreatic surface	133	1238	22.8	0	29.3
1903 Embankment Fill above phreatic surface	133	-	-	120	30
1903 Embankment Fill below phreatic surface	133	376	19.8	96	24.8
Foundation Soils above phreatic surface	133	-	-	120	30
Foundation Soils below phreatic surface	133	376	19.8	96	24.8
Bedrock	140	-	-	20,000	0

Note:

(1) K_c = Consolidation principal stress ratio

Table 11-2
Yield Acceleration Coefficients of Selected Sliding Blocks

Sliding Block ⁽¹⁾	Pre-Earthquake Condition ⁽²⁾	Assumed Reduction in Post-cyclic Strength of Saturated Embankment Fills and Foundation Soils	
		10% ⁽³⁾	20%
U/S #1	0.34	0.28	0.23
D/S #2	0.15	0.10	0.05
D/S #3	0.29	0.22	0.14

Note:

- (1) See Figure 10-8 for location and geometry of sliding blocks.
- (2) This condition applies to earthquake shaking period before strength degradation occurs.
- (3) The yield acceleration coefficient, K_y , for 10% strength reduction was estimated by interpolation from the K_y values for pre-earthquake and post-cyclic earthquake conditions with 20% strength reduction.

**Table 11-3
Calculated Horizontal Displacement in Newmark-type Analyses**

Earthquake	Sliding Block ⁽¹⁾	Max. Strength Reduction ⁽²⁾	Displacement, ft	
			Standard Polarity	Reverse Polarity
Hayward fault MCE TH #1	U/S 1	20%	2.4	4.3
	D/S 2	20%	3.1	5.2
	D/S 3	20%	0.8	1.5
Hayward fault MCE TH #2	U/S 1	20%	3.5	6.3
	D/S 2	20%	4.0	11.2
	D/S 3	20%	2.2	3.6

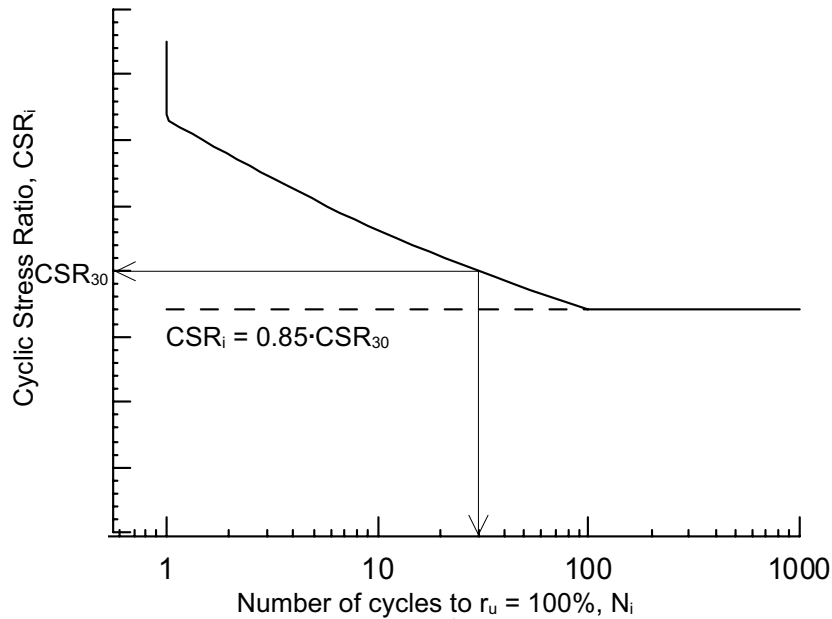
Note:

1. See Figure 10-8 for location and geometry of sliding blocks.
2. See Figures 11-4 through 11-9 for the assumed timing of strength reduction during the earthquake.

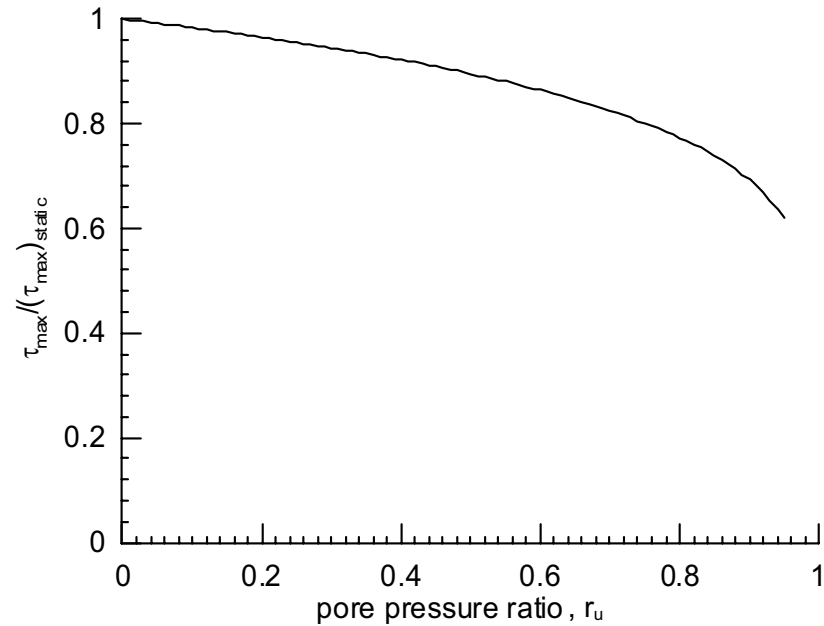
**Table 11-4
Calculated Horizontal Displacements in Newmark-type and Simplified Newmark Analyses**

Earthquake	Time History	Spectrum-Compatible	Ground Motion Polarity	Newmark Type (QUAD4M)	Simplified Newmark
Hayward fault MCE	#1	Yes	Standard	3	2
			Reverse	5	2
	#2	Yes	Standard	4	5
			Reverse	11	11
	#3	Yes	Standard	-	9
			Reverse	-	12
	#4	Yes	Standard	-	7
			Reverse	-	8
San Andreas fault MCE	#1	Yes	Standard	-	2
			Reverse	-	2
1978 Tabas, Iran	Tabas Station	No	Standard	-	4
			Reverse	-	4
1989 Loma Prieta, California	LGPC	No	Standard	-	7
			Reverse	-	7
	Piedmont Jr. High	No	Standard	0	0
			Reverse	0	0

Cyclic Strength
 $CSR_{30} = 0.28, 0.56$



Strength Degradation



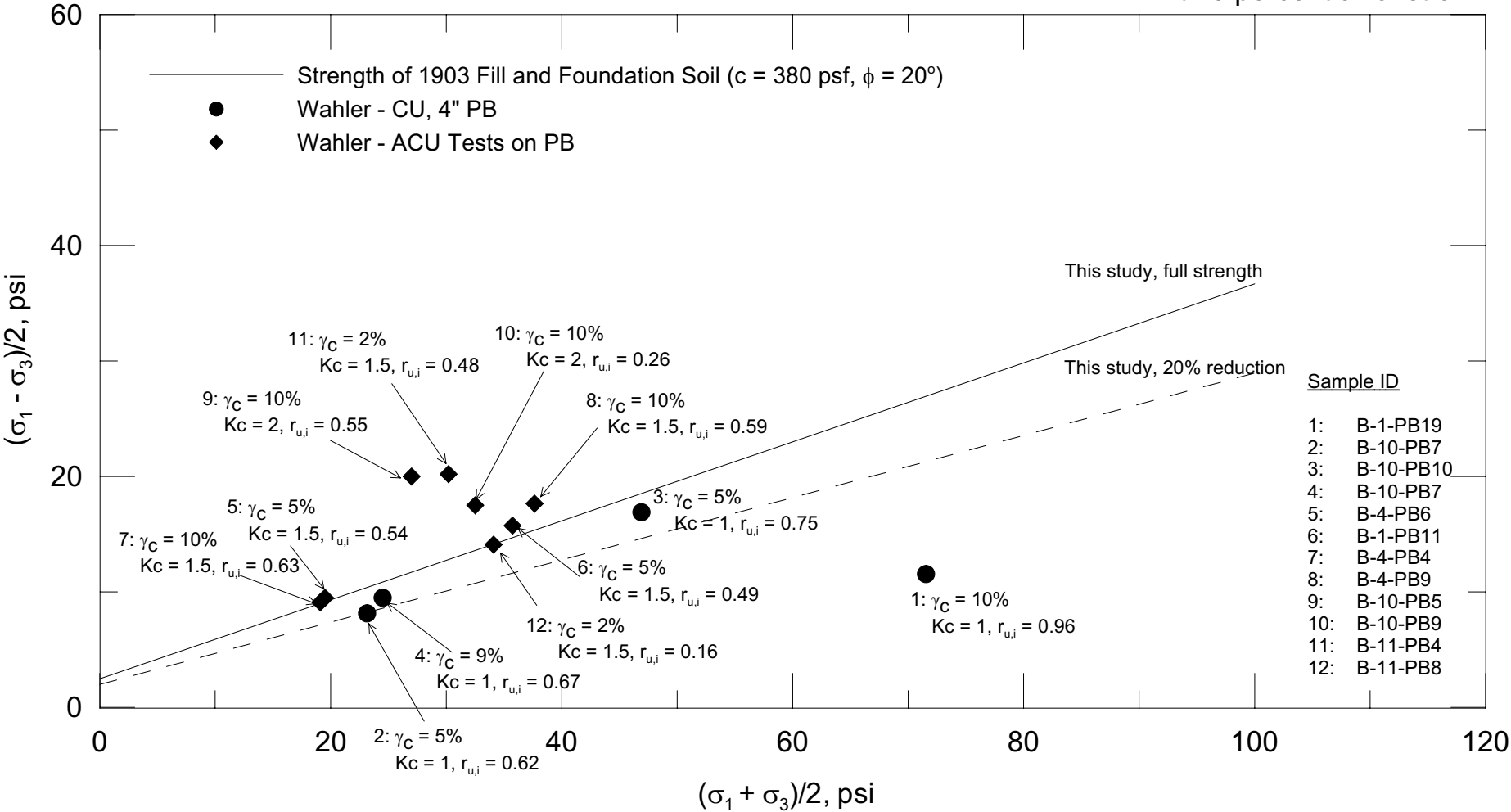
$$N_i = 30 \left(\frac{CSR_{30}}{CSR_i} \right)^{7.41} \quad 1 \leq N_i \leq 100$$

where $CSR_{30} = 0.28$ (1903 Fill and Foudation Soil)
 or
 0.56 (1938-39 Fill)

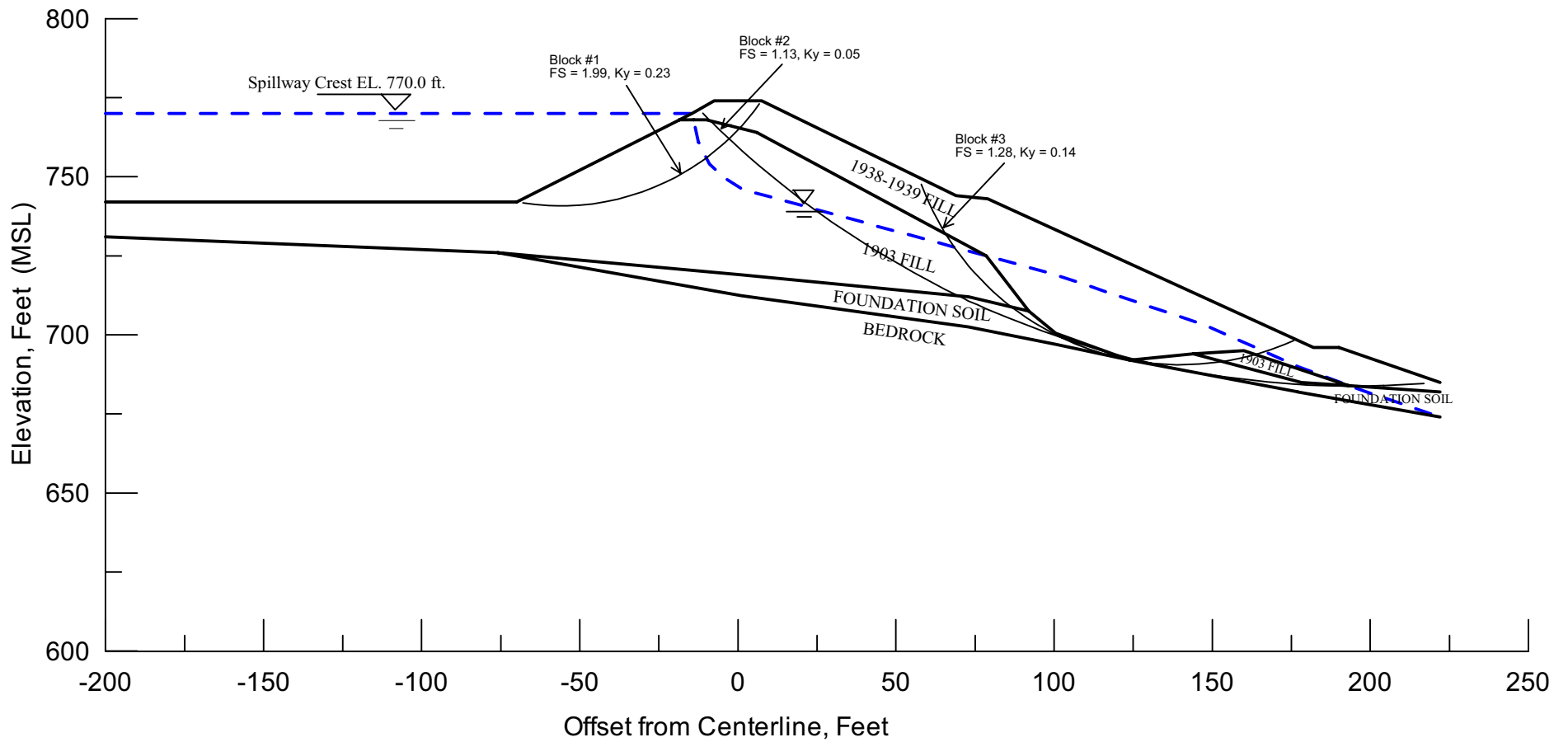
$$\frac{\tau_{\max}}{(\tau_{\max})_{\text{static}}} = (1 - r_u)^{0.16}$$

Project No. 26814957	Estates Dam Seismic Stability Analysis	Cyclic Strength and Undrained Strength Degradation of Saturated Embankment Fills and Foundation Soils	Figure
URS			11-1

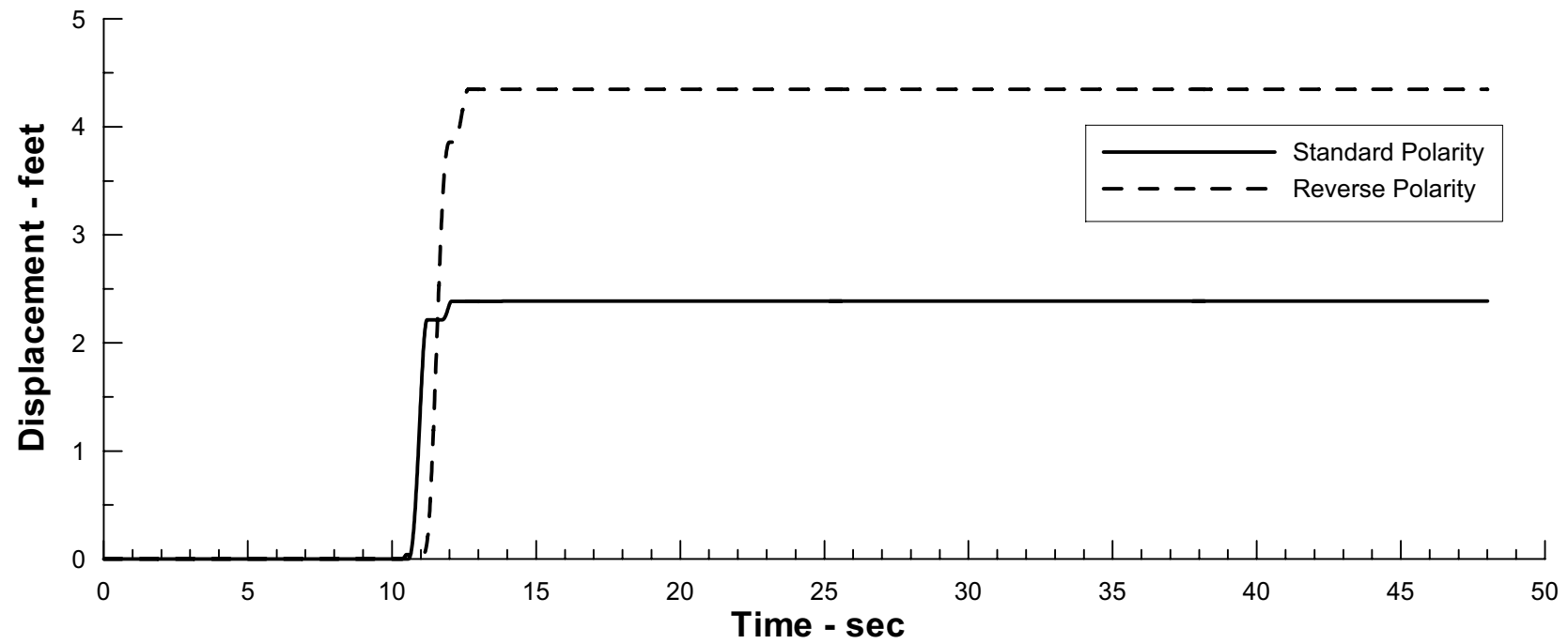
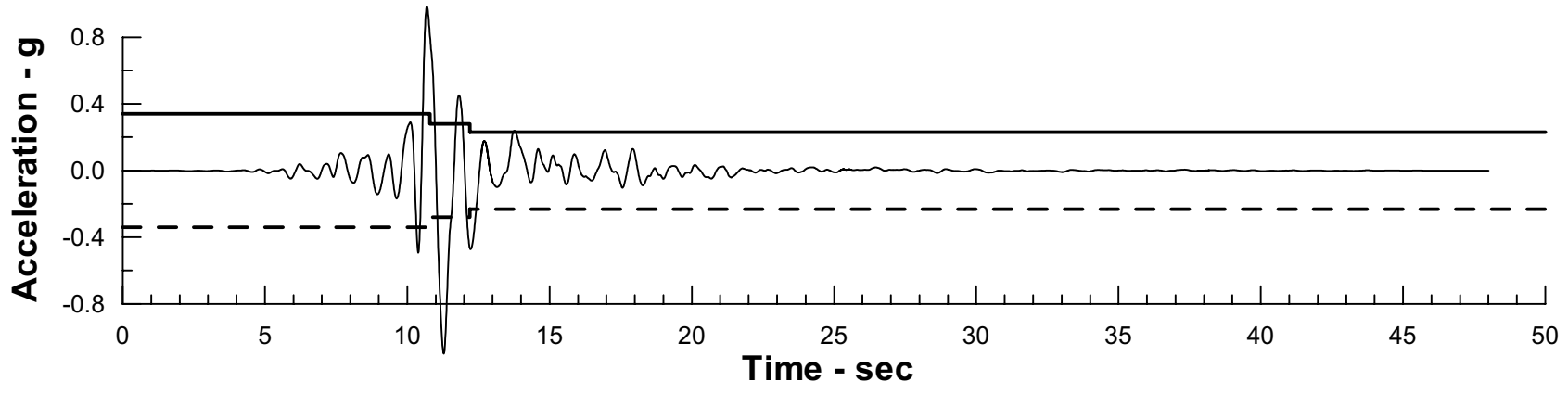
At 10 percent axial strain



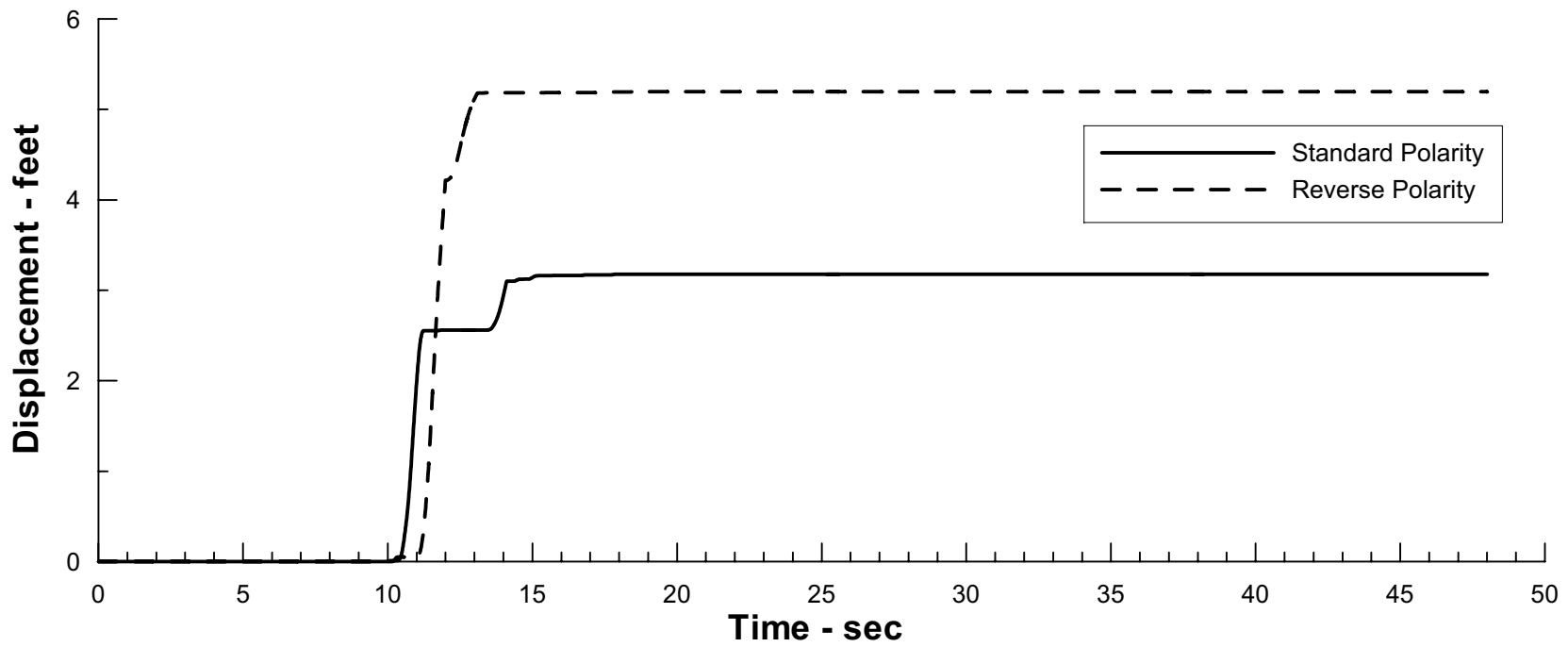
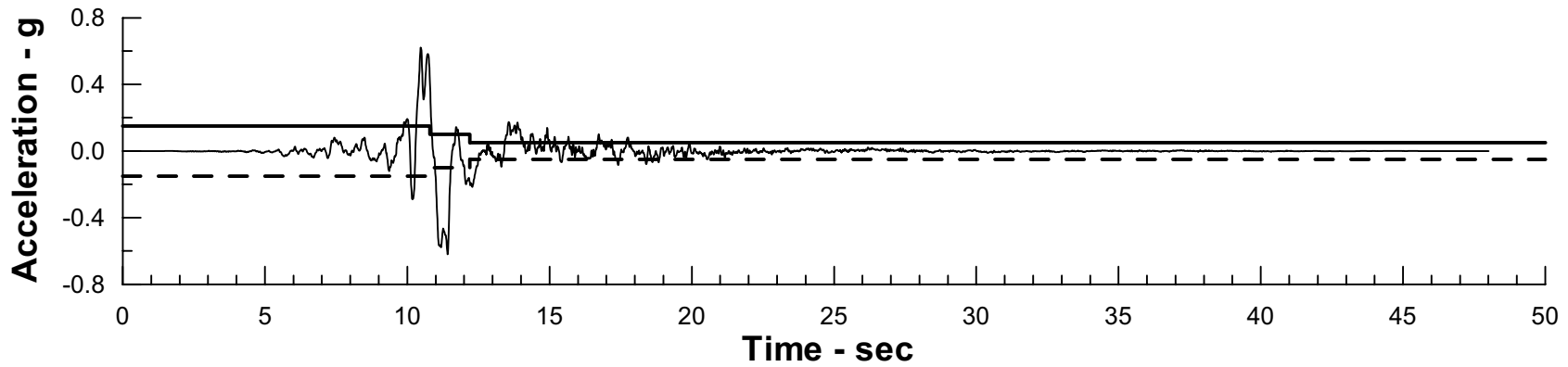
Project No. 26814957	Estates Dam Seismic Stability Analysis	Total Stress Strength Data from Post-Cyclic Consolidated Undrained Triaxial Tests	Figure
URS			11-2



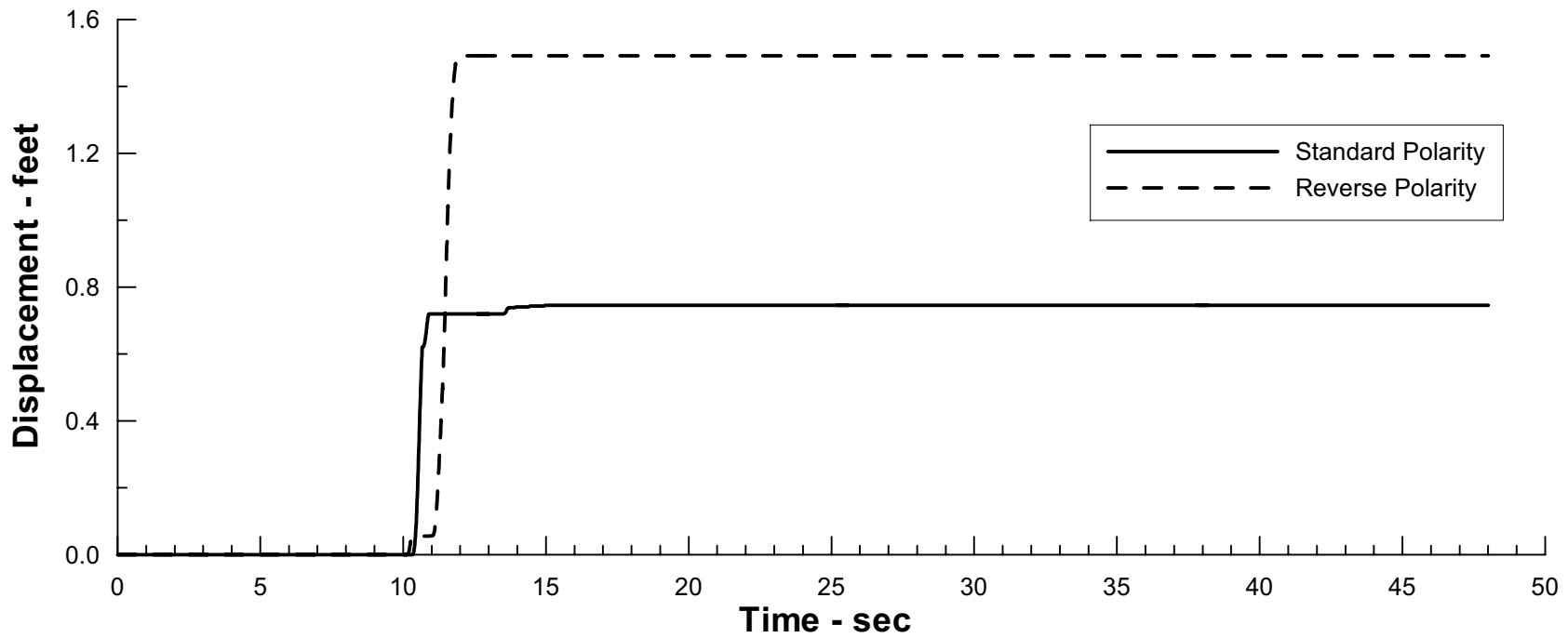
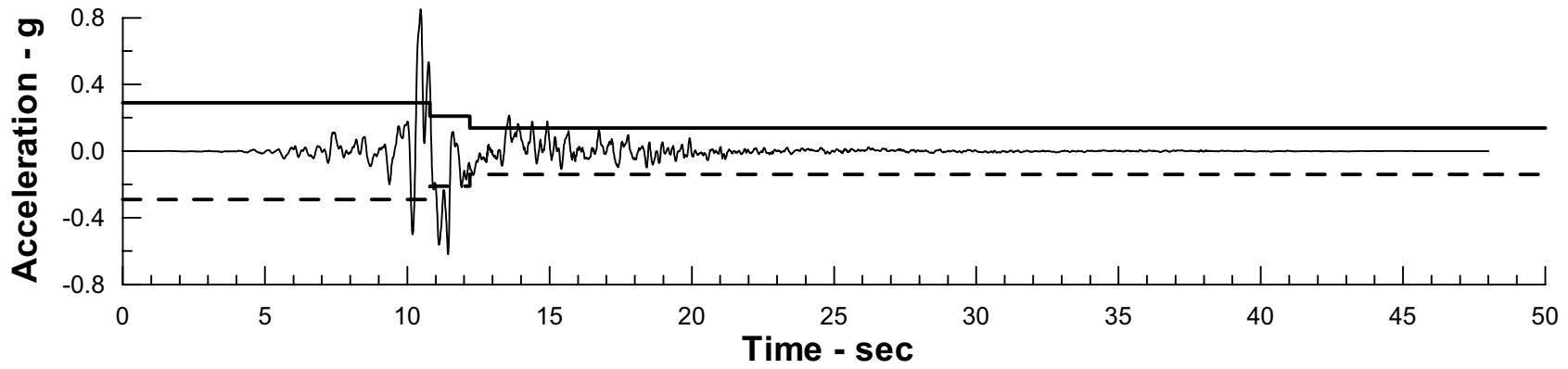
Project No. 26814957	Estates Dam Seismic Stability Analysis	Slope Stability Analysis Selected Critical Sliding Blocks Post-Earthquake Conditions	Figure
URS			11-3



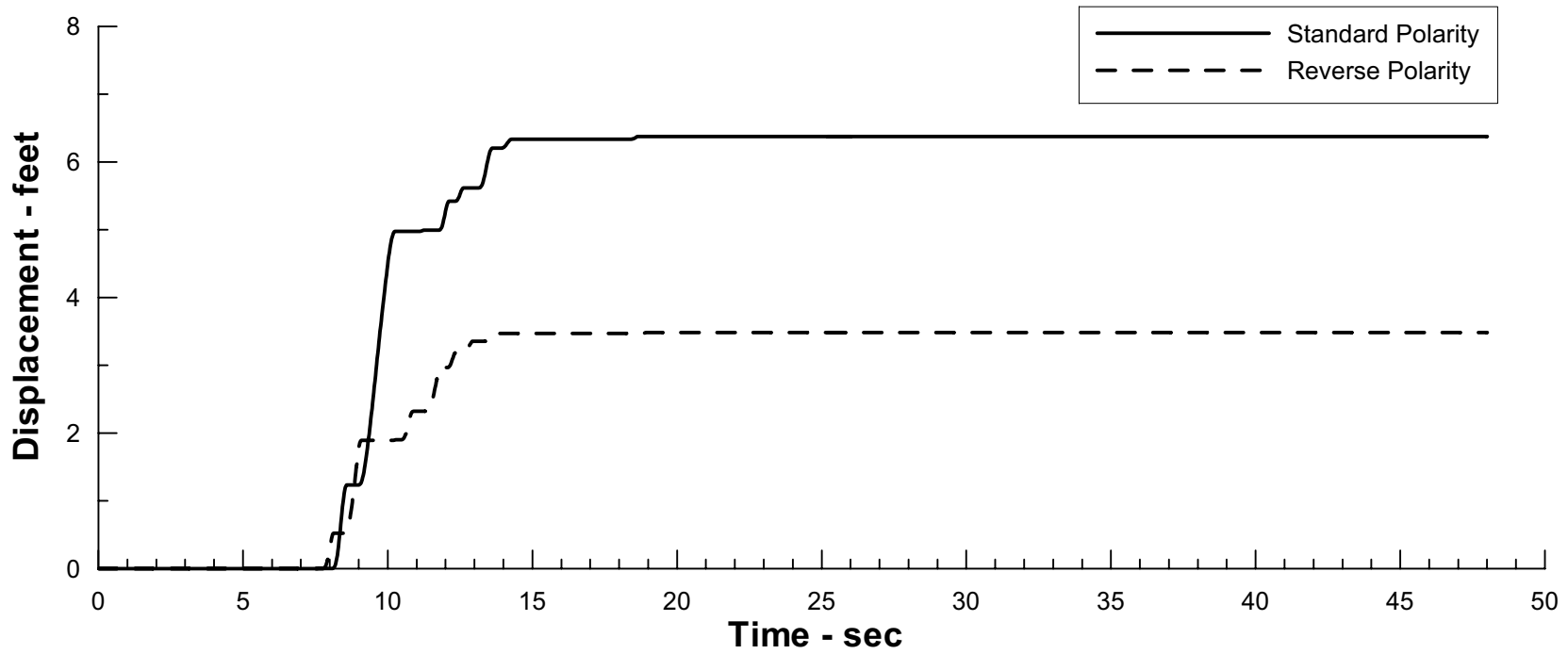
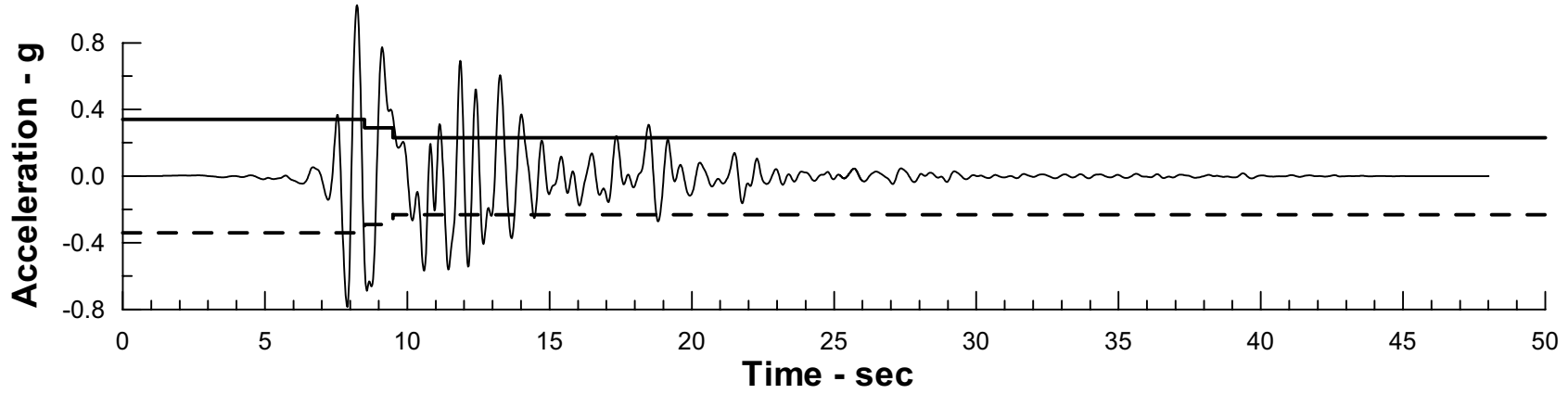
Project No. 26814957	Estates Dam Seismic Stability Analysis	Newmark Deformation Analysis Calculated Displacement U/S Block #1 Hayward Fault MCE TH #1	Figure 11-4
URS			



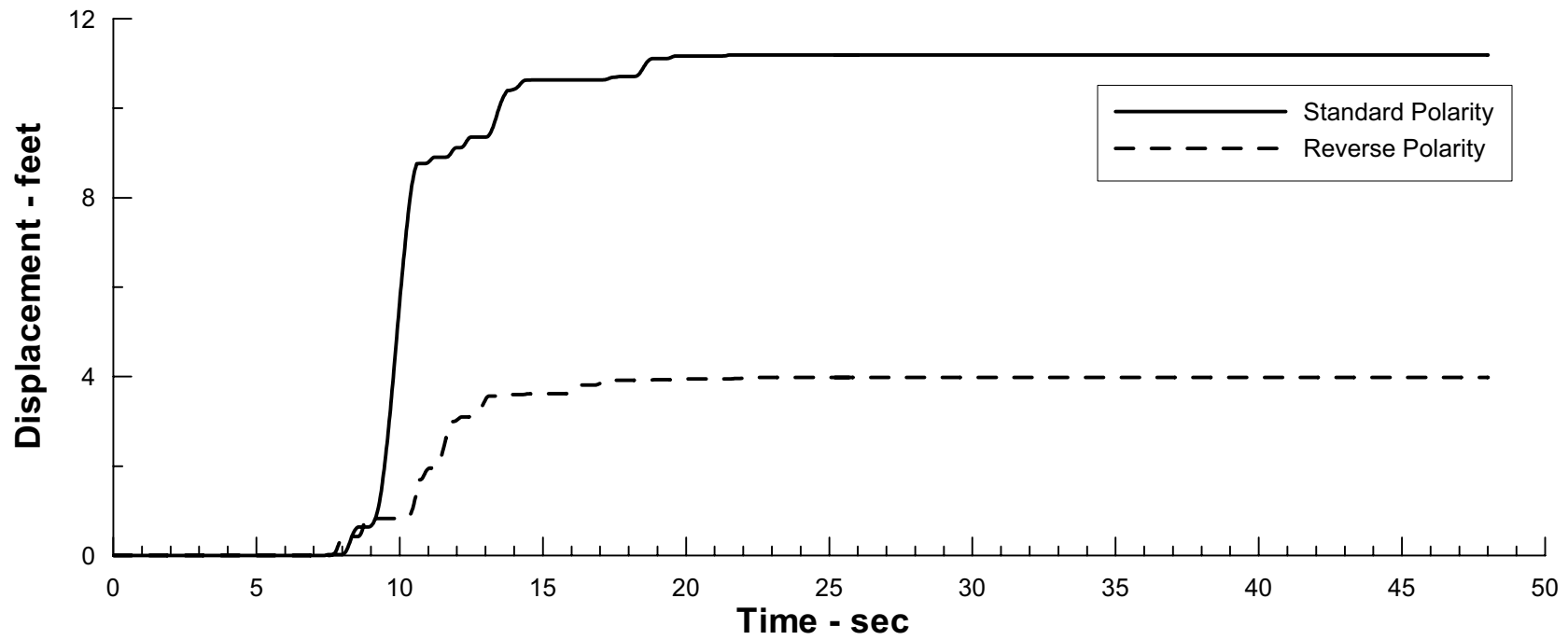
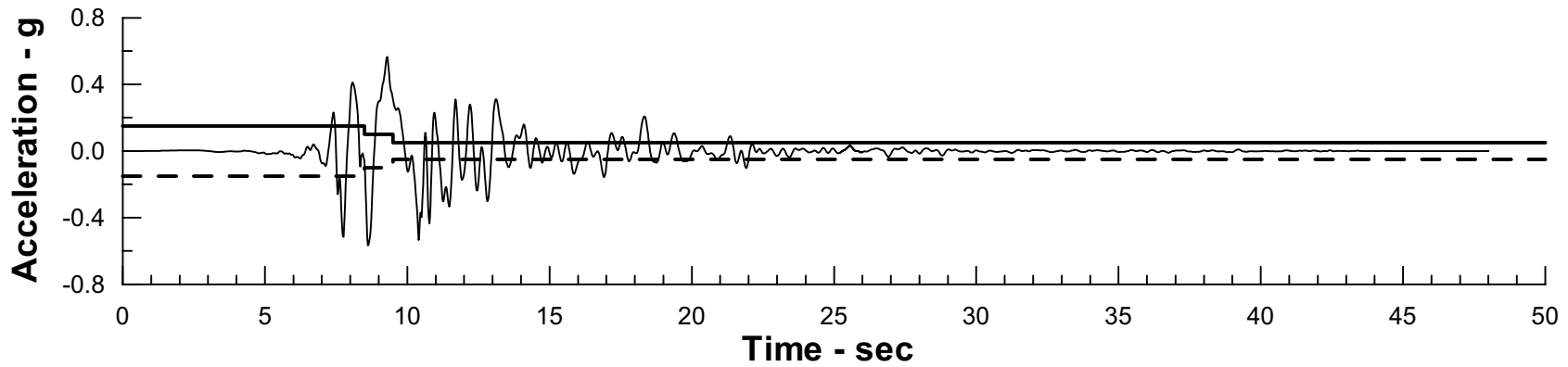
Project No. 26814957	Estates Dam Seismic Stability Analysis	Newmark Deformation Analysis Calculated Displacement D/S Block #2 Hayward Fault MCE TH #1	Figure 11-5
URS			



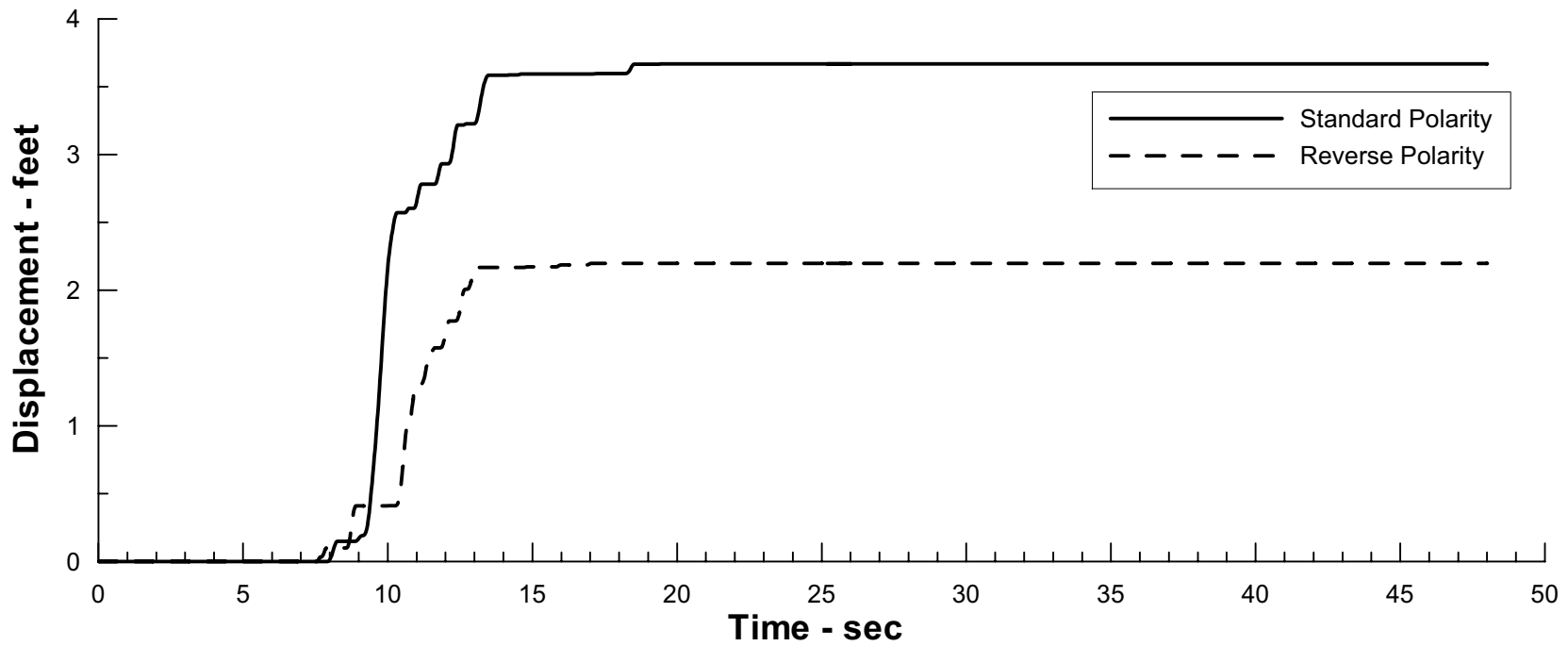
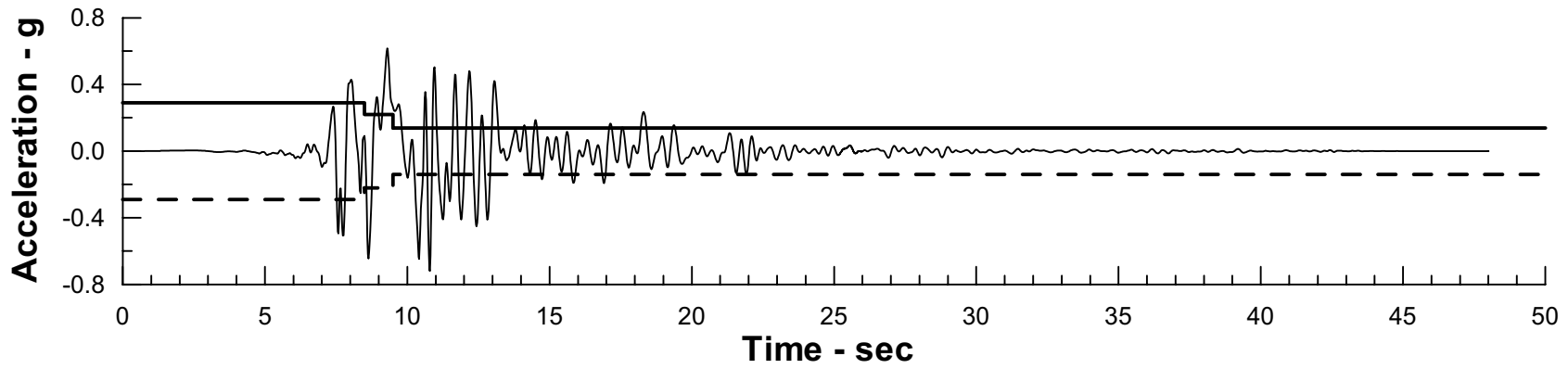
Project No. 26814957	Estates Dam Seismic Stability Analysis	Newmark Deformation Analysis Calculated Displacement D/S Block #3 Hayward Fault MCE TH #1	Figure
URS			11-6



Project No. 26814957	Estates Dam Seismic Stability Analysis	Newmark Deformation Analysis Calculated Displacement U/S Block #1 Hayward Fault MCE TH #2	Figure
URS			11-7

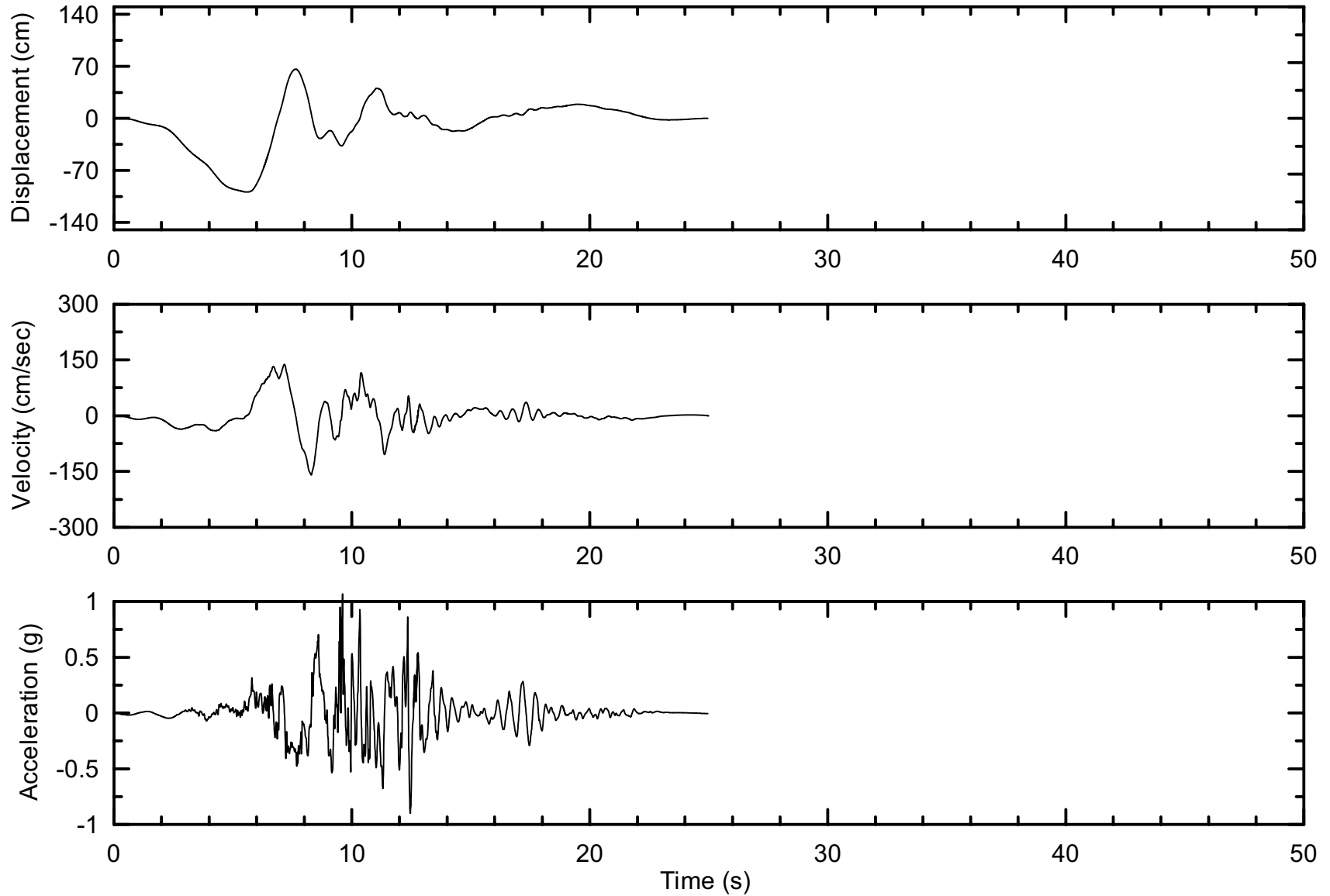


Project No. 26814957	Estates Dam Seismic Stability Analysis	Newmark Deformation Analysis Calculated Displacement D/S Block #2 Hayward Fault Event TH #2	Figure
URS			11-8

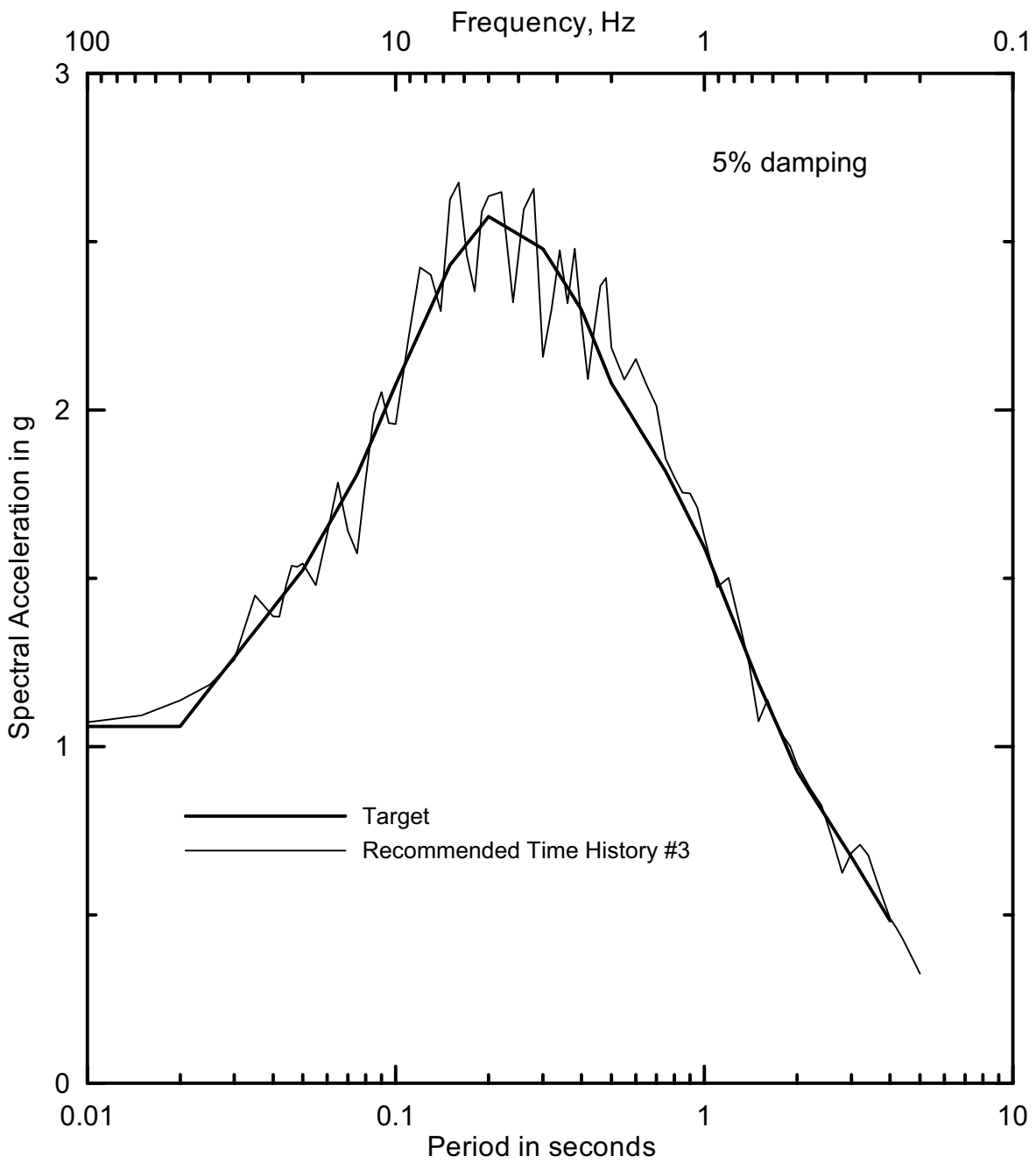


Project No. 26814957	Estates Dam Seismic Stability Analysis	Newmark Deformation Analysis Calculated Displacement D/S Block #3 Hayward Fault Event TH #2	Figure
URS			11-9

Hayward - Rodgers Creek Fault Event - Recommended Time History # 3
 (Modified from 1989 Loma Prieta, CA Earthquake - UCSC - LGPC Station,
 Horizontal Component, 040 deg.)

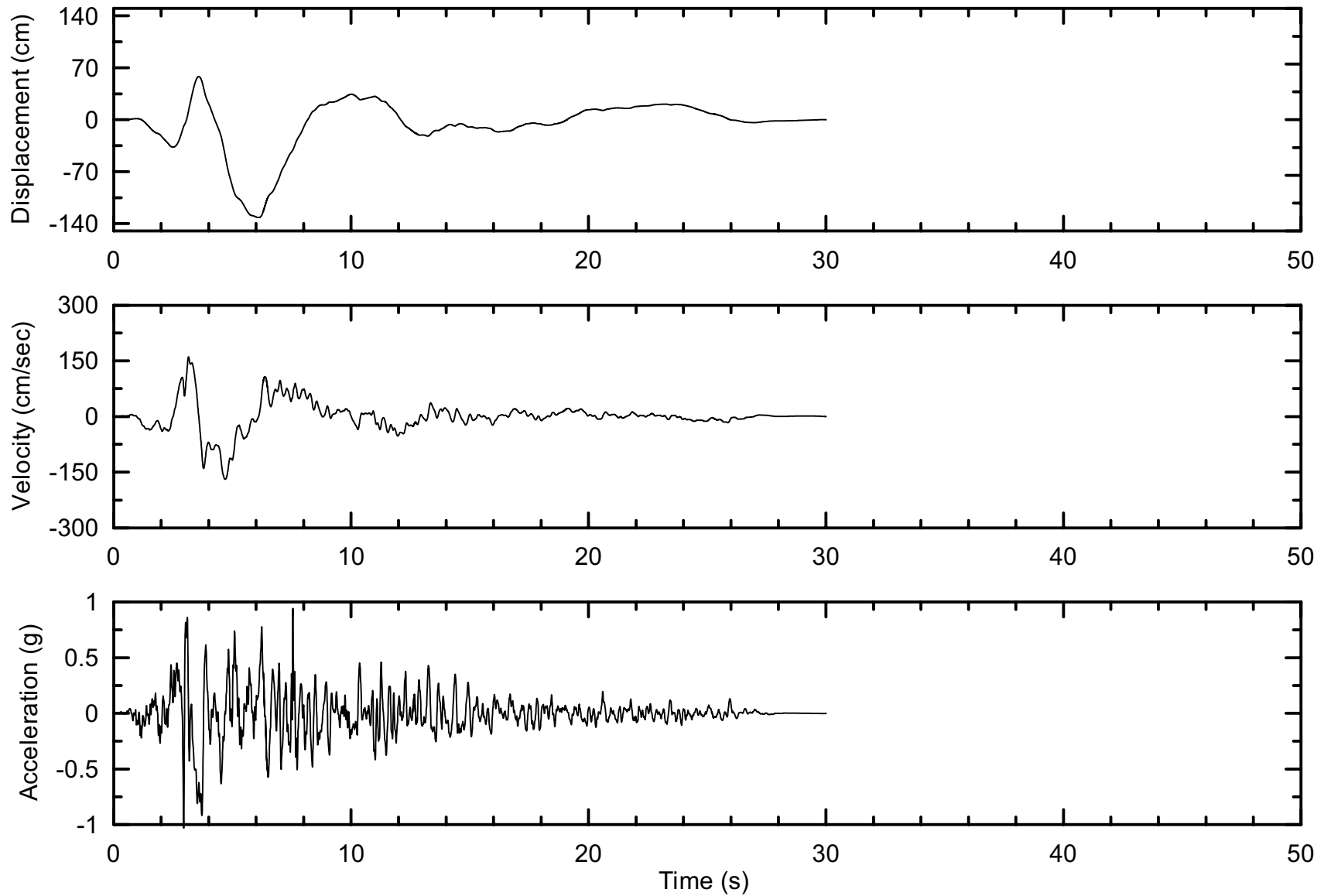


Project No. 26814957	Estates Dam Seismic Stability	Hayward - Rodgers Creek Fault MCE Recommended Time History #3	Figure 11-10
URS			

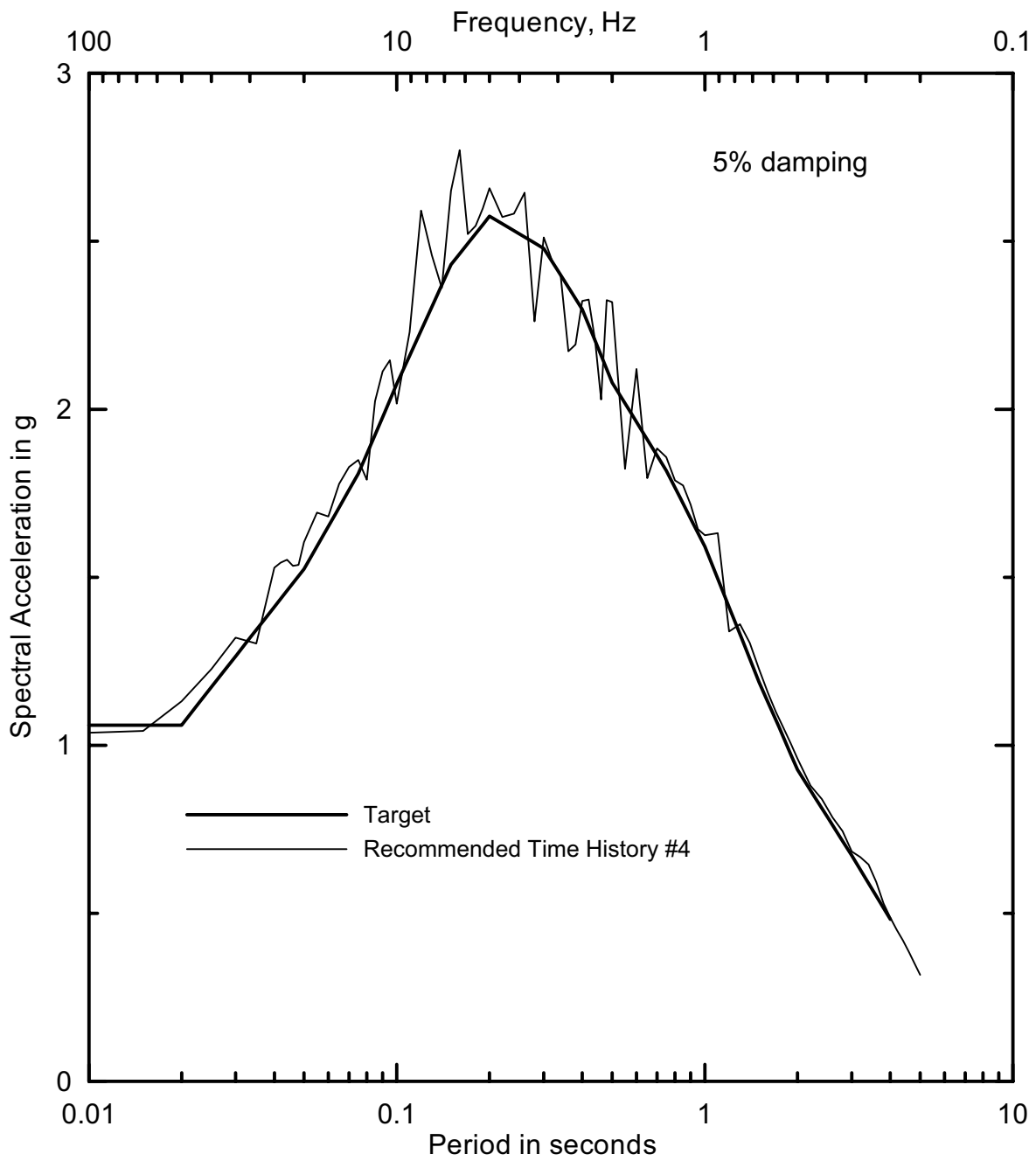


Project No. 26814957	Estates Dam Seismic Stability	Comparison of Acceleration Response Spectra for Hayward - Rodgers Creek Fault MCE Time History #3	Figure
URS			11-11

Hayward - Rodgers Creek Fault Event - Recommended Time History # 4
 (Modified from 1999 Kocaeli, Turkey Earthquake - Izmit Station,
 Horizontal Component, 090 deg.)

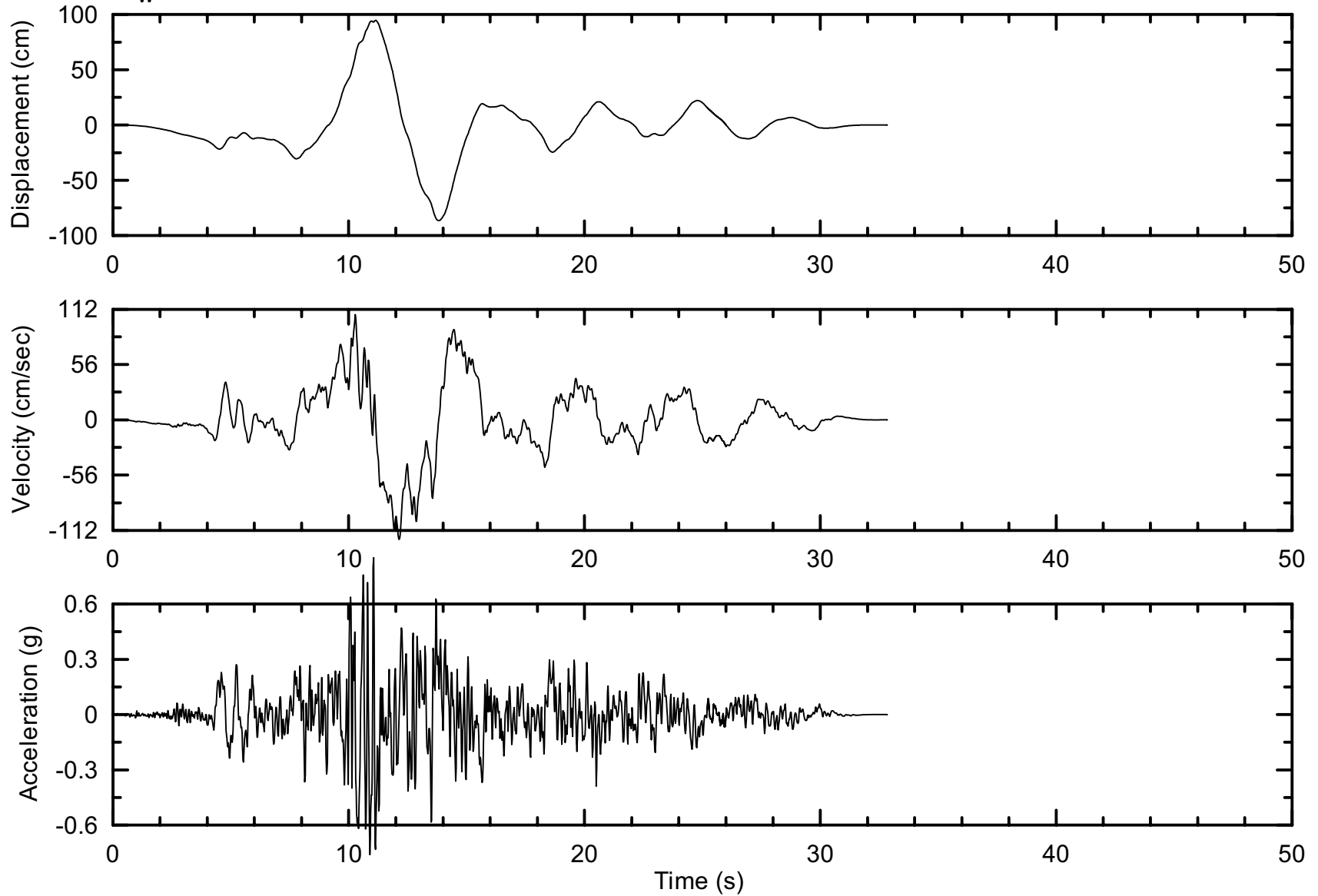


Project No. 26814957	Estates Dam Seismic Stability	Hayward - Rodgers Creek Fault MCE Recommended Time History #4	Figure 11-12
URS			

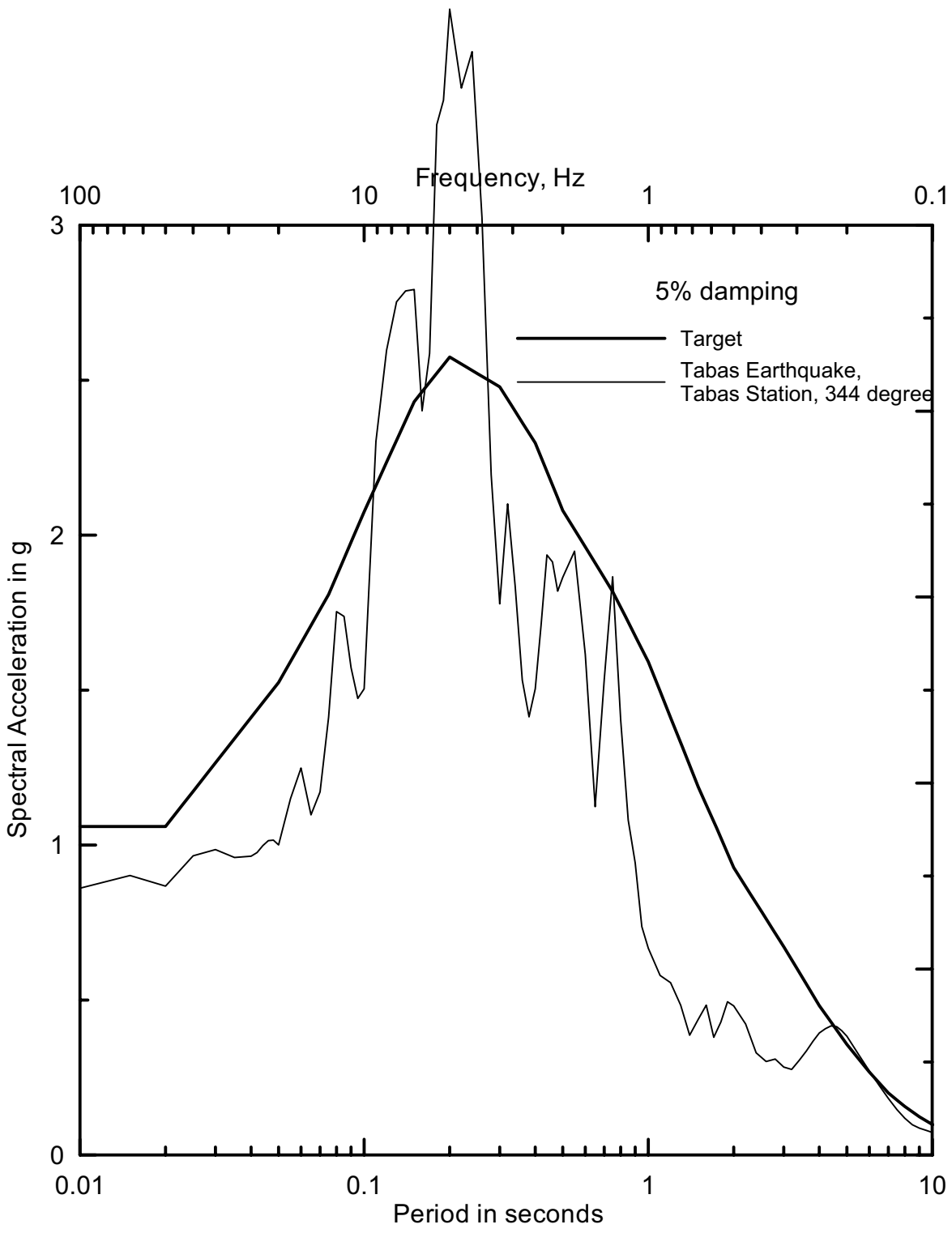


Project No. 26814957	Estates Dam Seismic Stability	Comparison of Acceleration Response Spectra for Hayward - Rodgers Creek Fault MCE Time History #4	Figure
URS			11-13

1978 Tabas, Iran Earthquake Time History
 at Tabas Station,
 $M_w = 7.4$, $R = 3$ km

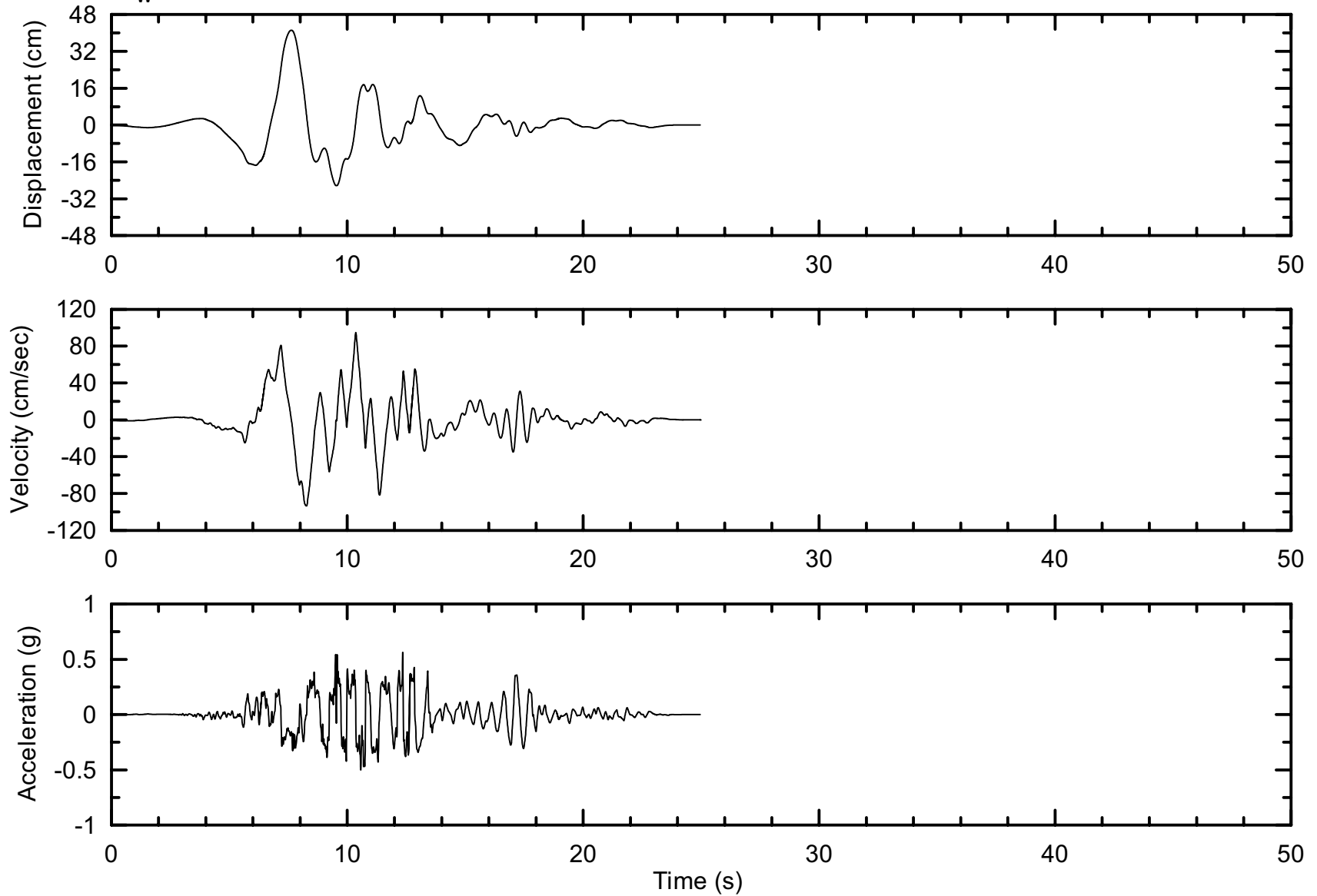


Project No. 26814957	Estates Dam Seismic Stability	Recorded Time History 1978 Tabas, Iran Earthquake at Tabas Station, Horizontal Component, 344 deg.	Figure 11-14
URS			

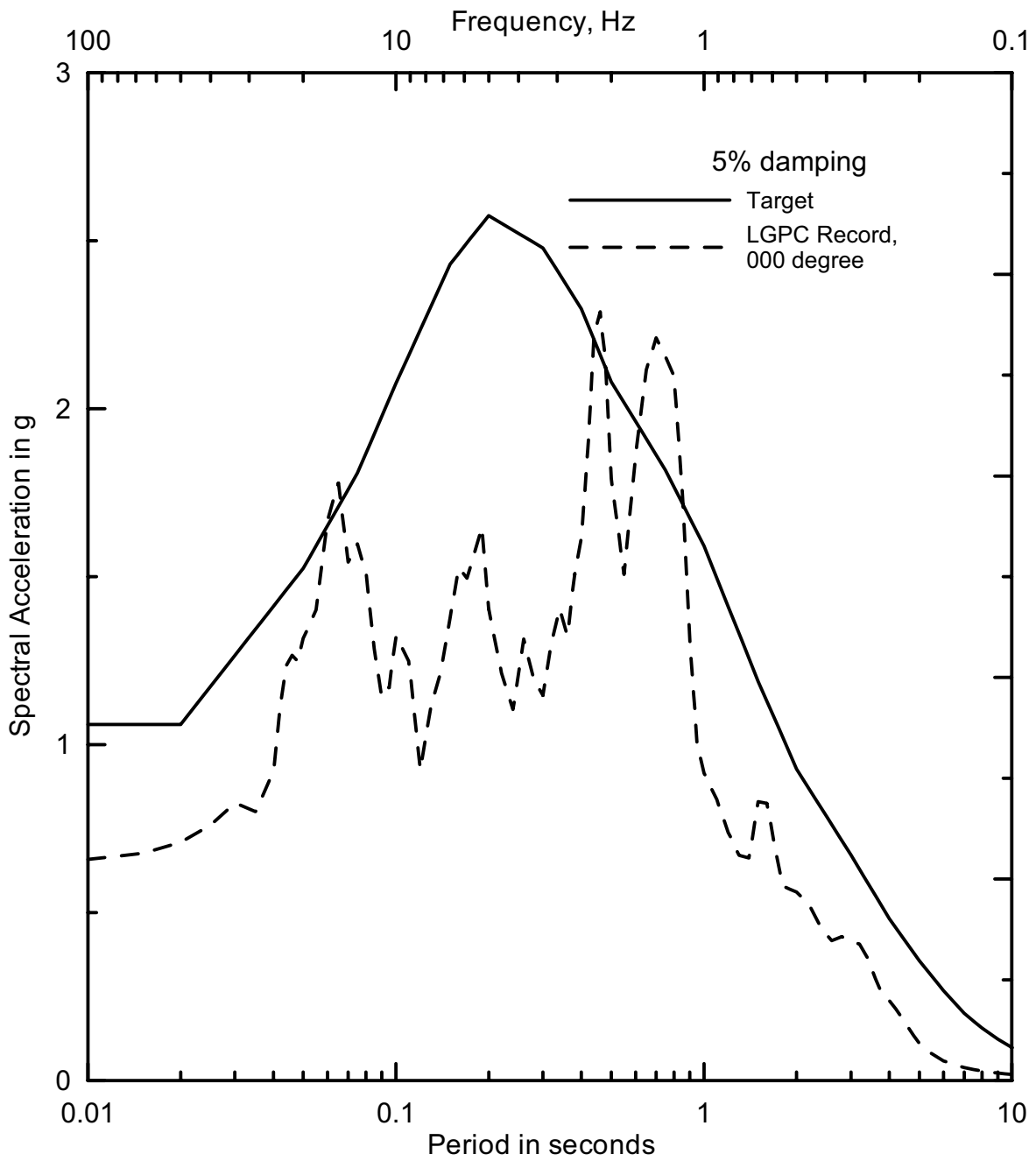


Project No. 26814957	Estates Dam Seismic Stability	1978 Tabas, Iran Earthquake at Tabas Station, Horizontal Component, 344 Degree	Figure 11-15
URS			

1989 Loma Prieta, CA Earthquake Time History
 Recorded at UCSC - LGPC Station, 000 degree
 $M_w = 7.0$, $R = 6.1$ km

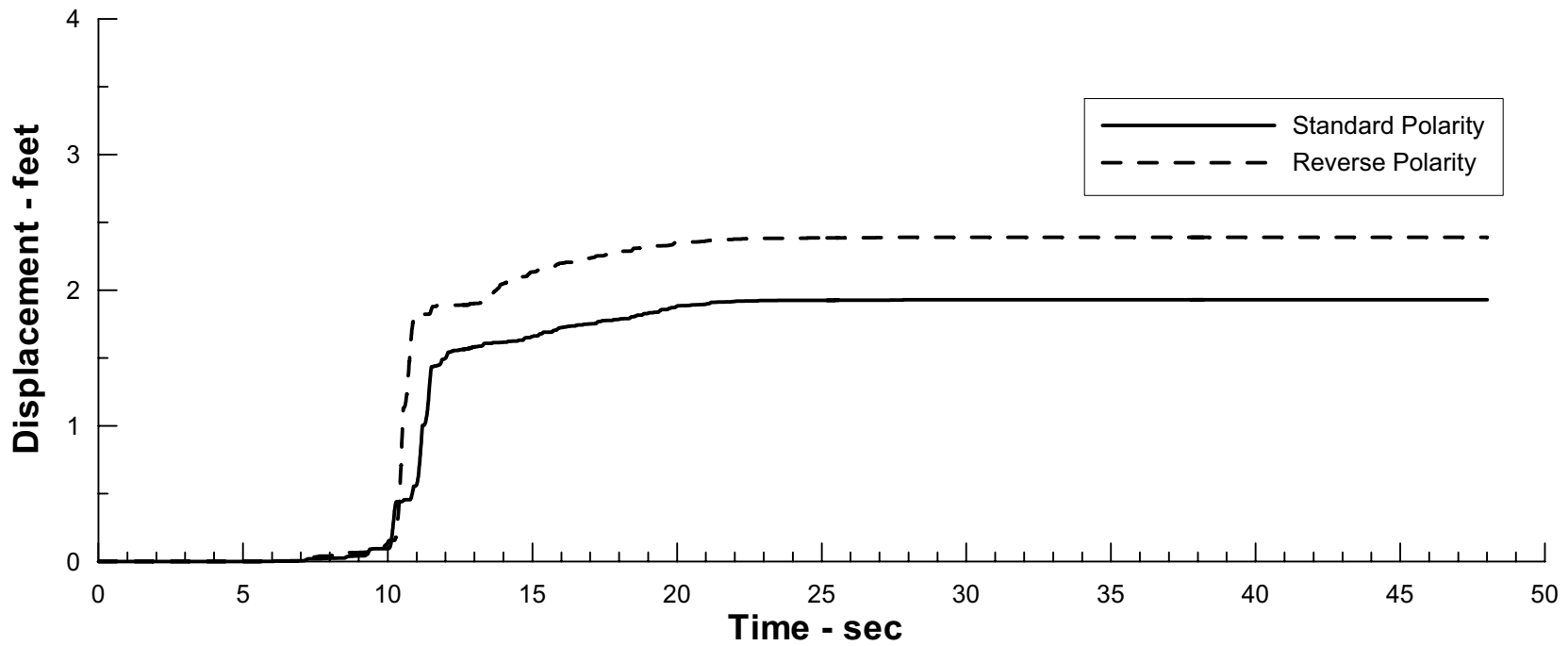
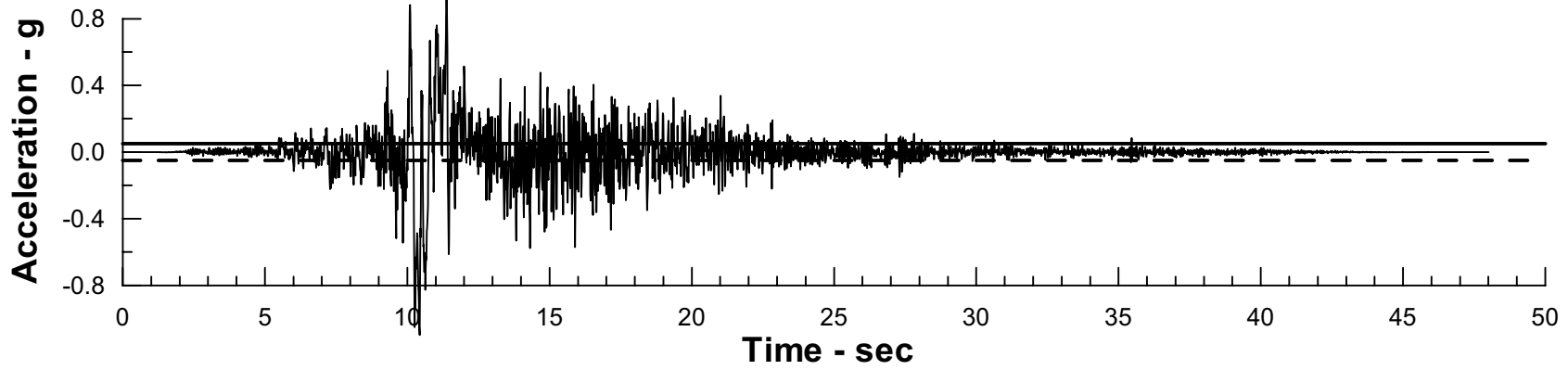


Project No. 26814957	Estates Dam Seismic Stability Analysis	Recorded Time History 1989 Loma Prieta, CA Earthquake at UCSC - LGPC Station, Horizontal Component, 000 deg.	Figure 11-16
URS			

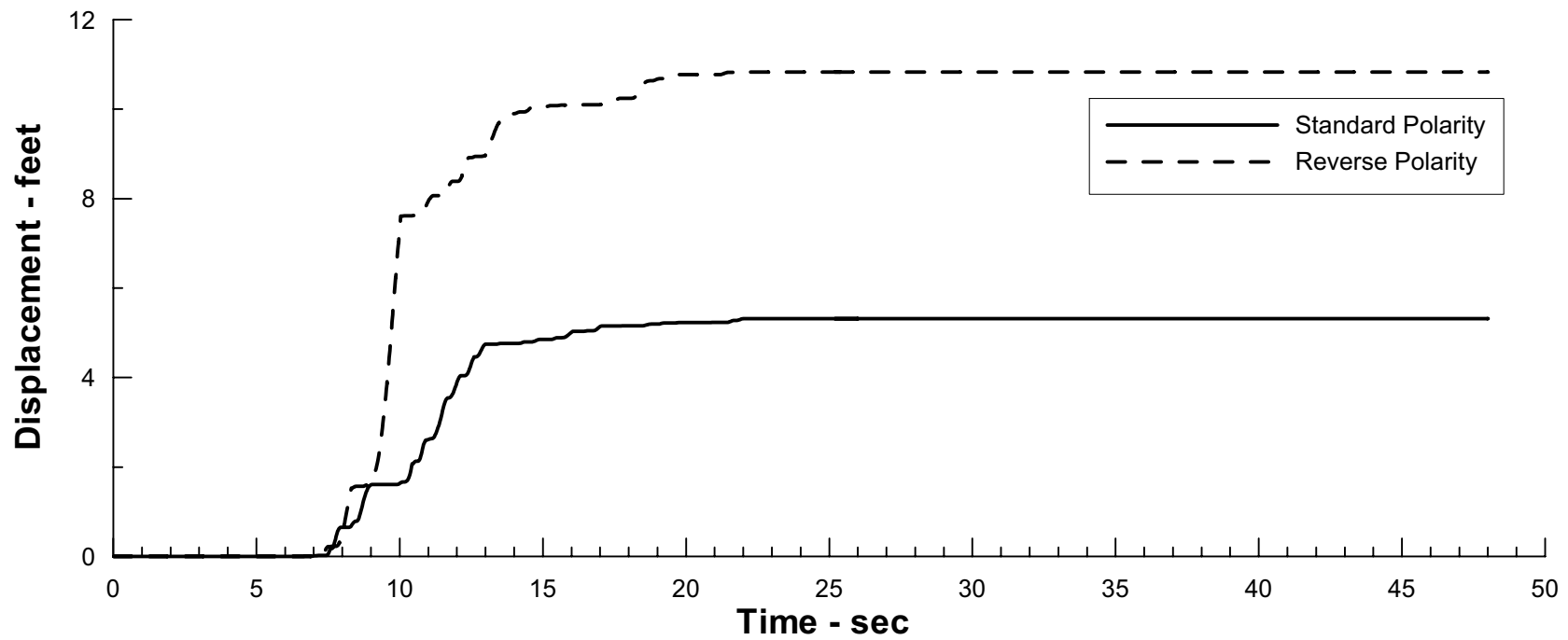
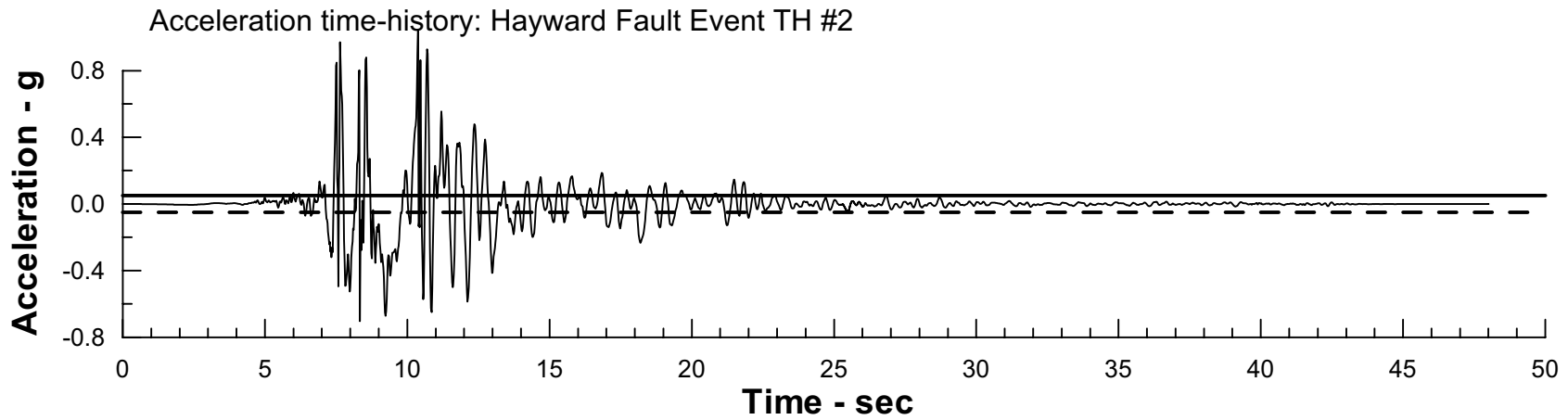


Project No. 26814957	Estates Dam Seismic Stability	1989 Loma Prieta, CA Earthquake at UCSC - LGPC Station, Horizontal 000 deg Component	Figure 11-17
URS			

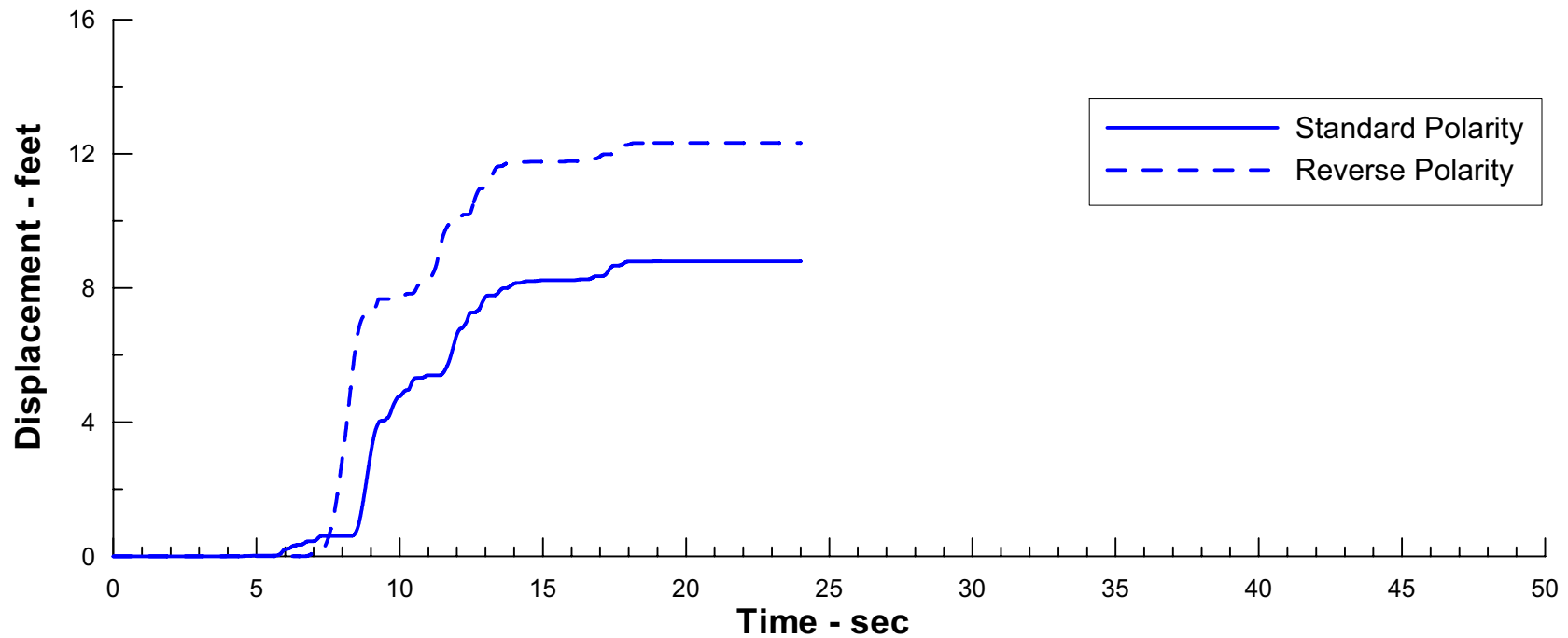
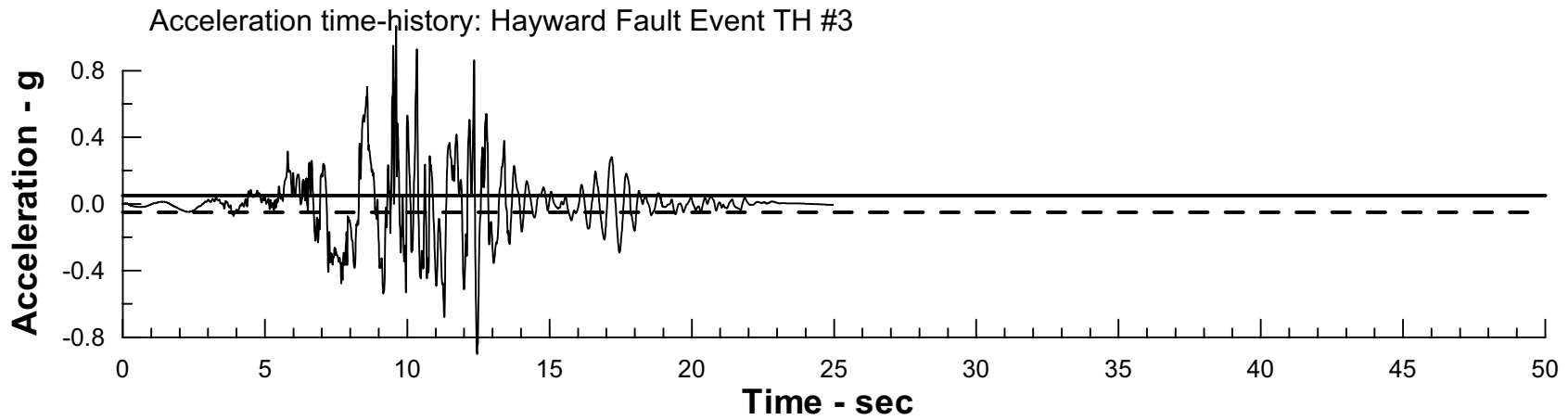
Acceleration time-history: Hayward Fault Event TH #1



Project No. 26814957	Estates Dam Seismic Stability Analysis	Simplified Newmark Analysis Calculated Displacement Assumed $K_y = 0.05$ Hayward Fault MCE TH #1	Figure
URS			11-18

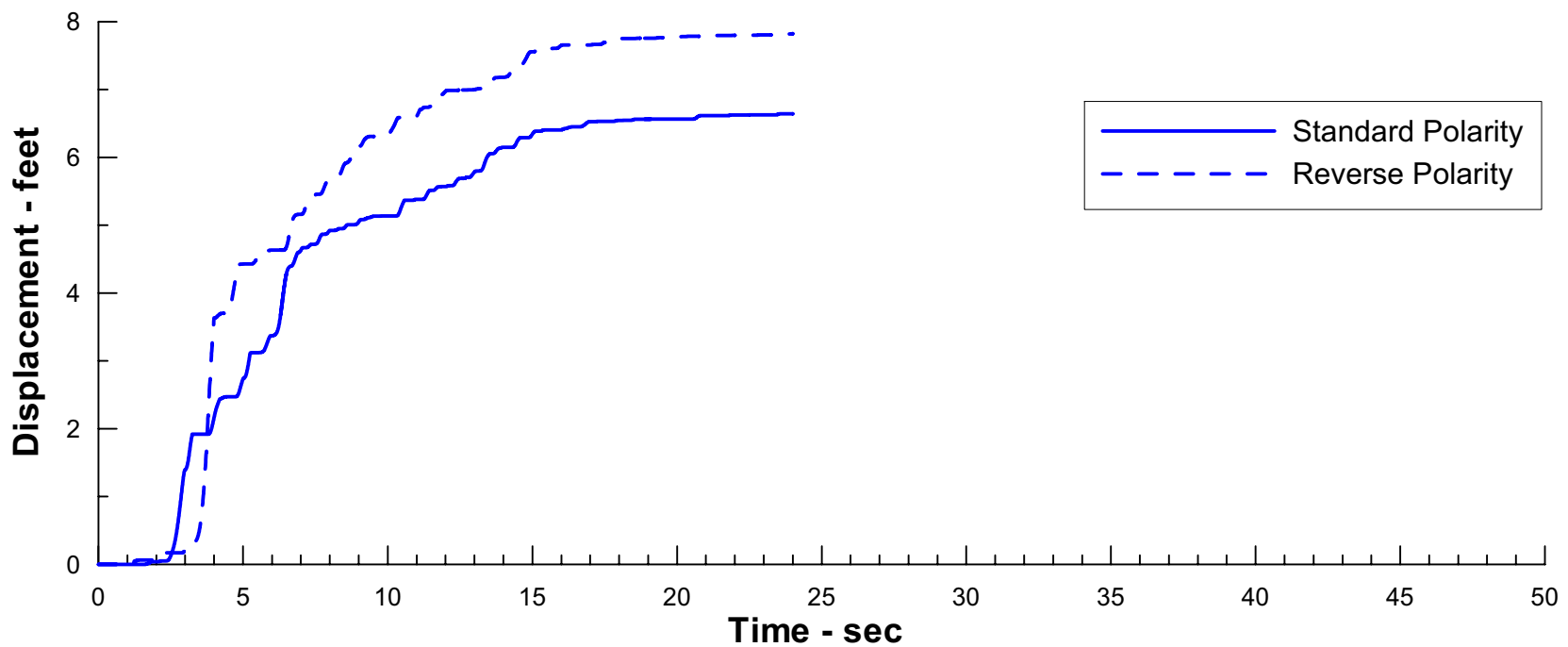
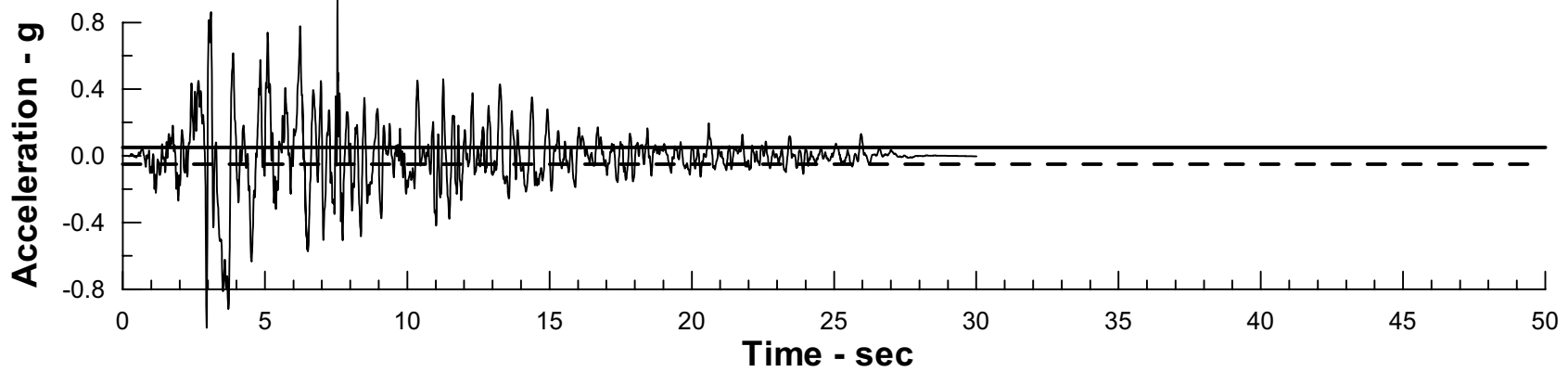


Project No. 26814957	Estates Dam Seismic Stability Analysis	Simplified Newmark Analysis Calculated Displacement Assumed $K_y = 0.05$ Hayward Fault MCE TH #2	Figure
URS			11-19



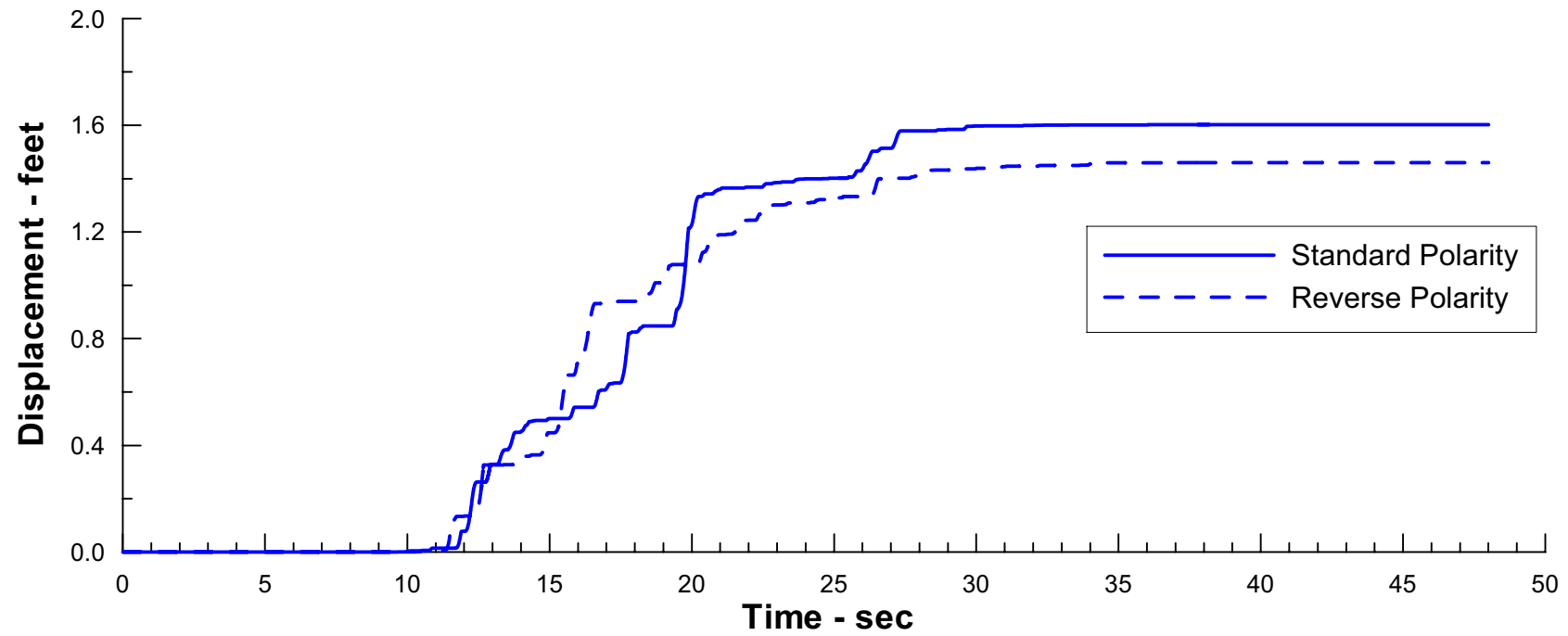
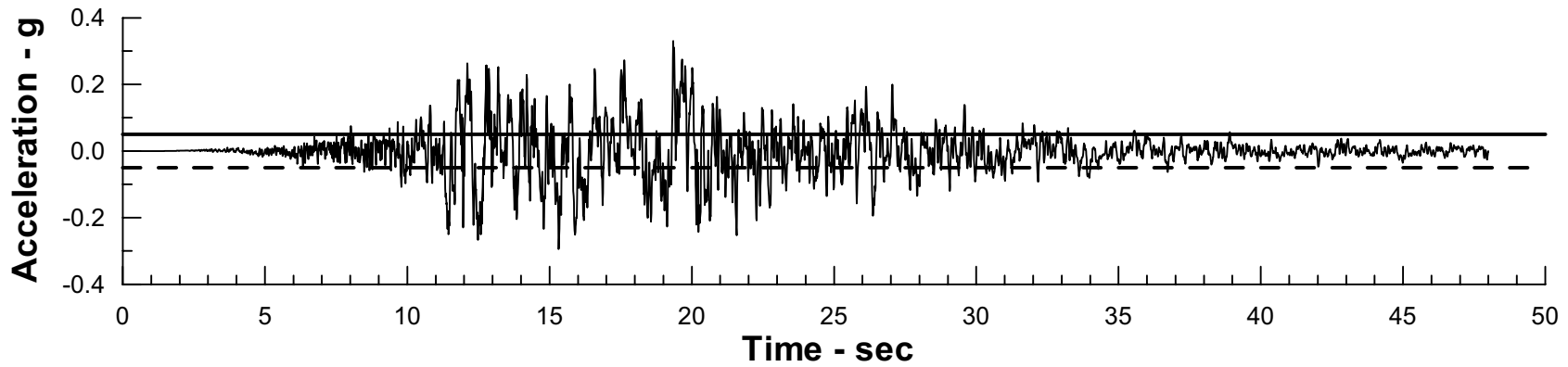
Project No. 26814957	Estates Dam Seismic Stability Analysis	Simplified Newmark Analysis Calculated Displacement Assumed $K_y = 0.05$ Hayward Fault MCE TH #3	Figure
URS			11-20

Acceleration time-history: Hayward Fault Event TH #4

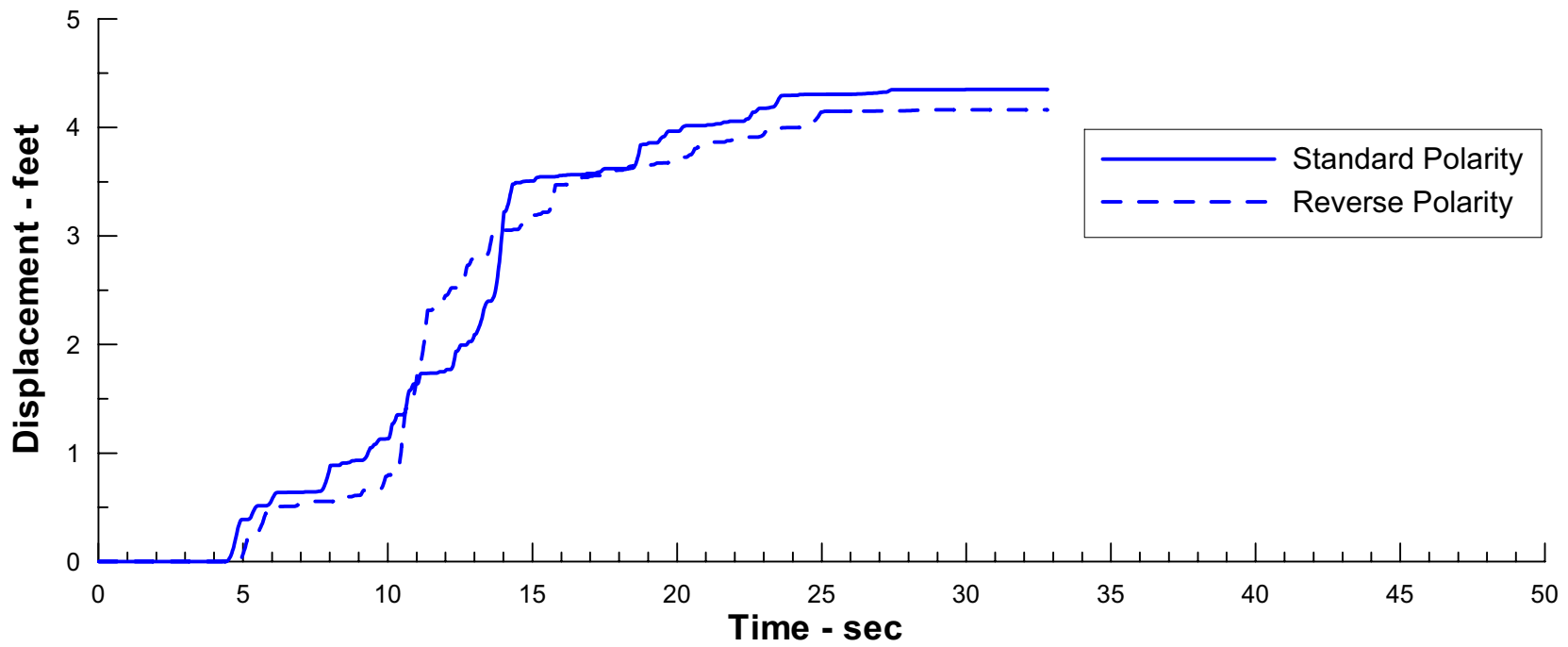
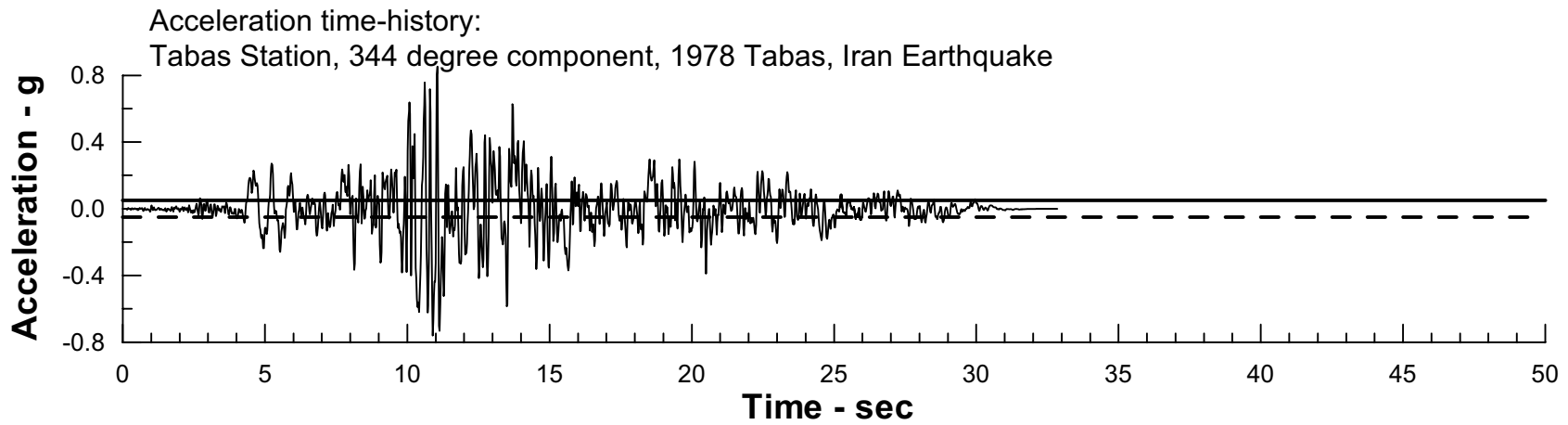


Project No. 26814957	Estates Dam Stability and Deformation Analysis	Simplified Newmark Analysis Calculated Displacement Assumed $K_y = 0.05$ Hayward Fault MCE TH #4	Figure 11-21
URS			

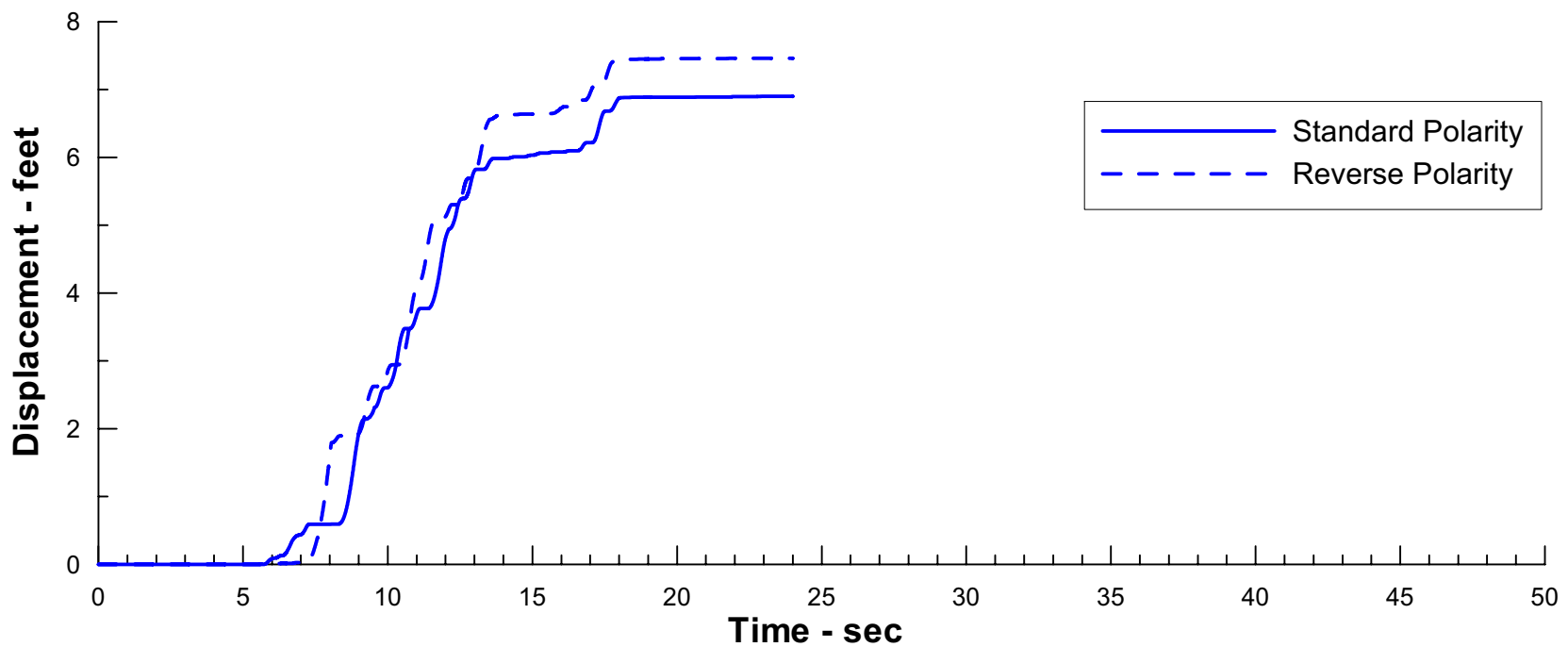
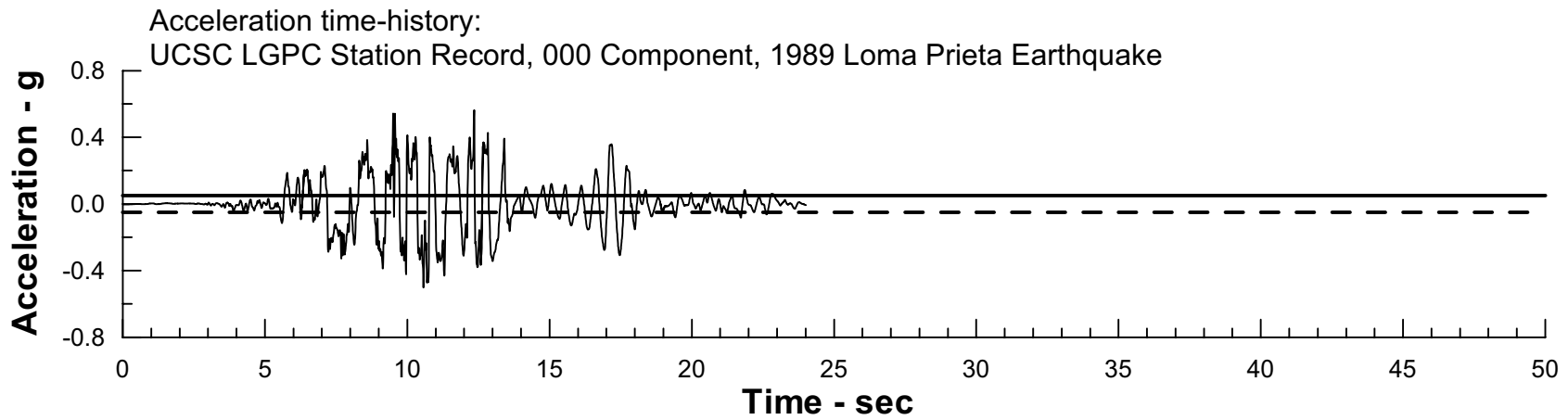
Acceleration time-history: San Andreas Fault MCE



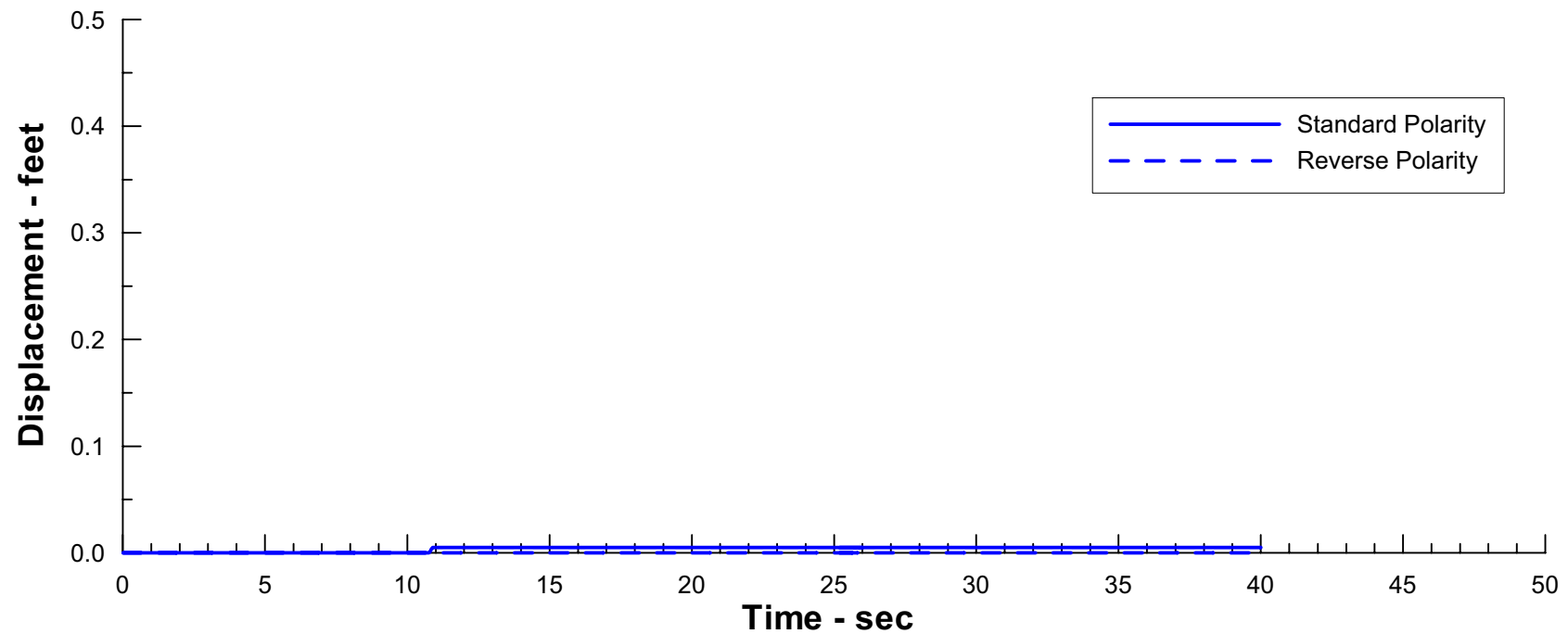
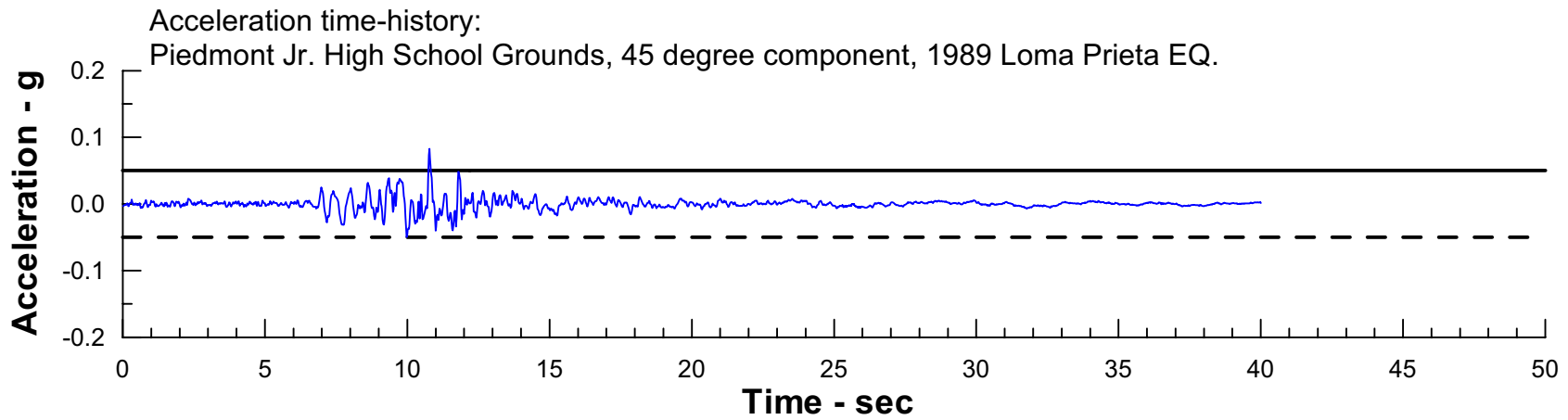
Project No. 26814957	Estates Dam Seismic Stability Analysis	Simplified Newmark Analysis Calculated Displacement Assumed $K_y = 0.05$ San Andreas Fault MCE	Figure 11-22
URS			



Project No. 26814957	Estates Dam Seismic Stability Analysis	Simplified Newmark Analysis Calculated Displacement Assumed $K_y = 0.05$ Tabas Earthquake, Tabas 344	Figure 11-23
URS			



Project No. 26814957	Estates Dam Stability and Deformation Analysis	Simplified Newmark Analysis Calculated Displacement Assumed $K_y = 0.05$ Loma Prieta EQ, LGPC 000	Figure 11-24
URS			



Project No. 26814957	Estates Dam Seismic Stability Analysis	Simplified Newmark Analysis Calculated Displacement Assumed $K_y = 0.05$ Loma Prieta Earthquake	Figure
URS			11-25

12.1 METHODOLOGY

The dynamic response and seismic deformations of the dam were directly calculated from fully nonlinear analyses with the computer program FLAC, Version 4.0 (Itasca, 2000). In these analyses, the calculation of seismic deformations is coupled with the calculation of dynamic response. Thus, the seismic deformations, excess pore water pressures, and cyclic degradation are calculated directly from the dynamic response analyses of the dam. To establish the state of stress in the dam prior to the earthquake, a staged dam construction analysis and a static stress analysis with full reservoir were performed with FLAC. The resulting state of stress in the dam served as the initial state for the dynamic analysis. The initial state of stress calculated with FLAC was also used to develop the input for the dynamic response analyses with QUAD4M (see Section 11).

The FLAC analyses were performed for section A-A'. The section was discretized using the mesh shown on Figure 12-1. A compliant boundary was specified along the base of the model to simulate the unbounded extent of the foundation bedrock beneath the dam. The earthquake motions are input as a stress time history at this boundary. Analyses were performed for both standard and reverse polarities of each ground motion time history.

The analyses were performed using the Mohr-Coulomb elasto-plastic constitutive model in the FLAC code. Two types of analyses were performed. In the first type of analyses the cyclic strength degradation in the embankment and foundation soils is implemented to replicate the amount and timing of degradation used in the Newmark-type deformation analyses. The second type of analyses use a cyclic degradation model developed by URS to directly predict the generation of excess pore pressures and the associated strength reduction in saturated soils during the earthquake shaking. The first type of analysis may be thought of as a total stress analysis whereas the second may be thought of as an effective stress analysis.

12.2 MATERIAL PROPERTIES

The material properties for the static stress analysis are summarized in Table 12-1. These parameters were selected based on the results of laboratory tests for the dam and foundation materials and on published data for similar soils.

The FLAC dynamic analyses were conducted with the same material characterization used for the limit-equilibrium and QUAD4M dynamic response analyses, but adapted to the specific input requirements of FLAC. The material properties for dynamic analysis are listed in Table 12-2. The effective stress analyses were performed by coupling the constitutive models with the pore pressure generation scheme shown in Figure 12-2. In this scheme, which is based on the cyclic stress approach proposed by Seed (1979), pore pressures are continuously updated for each element in response to shear stress cycles, and the effective stresses decrease with increasing pore pressure.

The models for cyclic strength and undrained strength degradation of the saturated embankment and foundation soils are illustrated in Figure 12-3. The strength degradation of the materials is expressed through the ratio of post-cyclic strength to pre-cyclic (i.e. static) strength as a function of excess pore pressure ratio (see Section 11.2.1). As discussed in Section 11, the selected CSR₃₀ values are 0.56 for the 1938-1939 fill and 0.28 for the 1903 fill and foundation soils.

12.3 ANALYSIS RESULTS

Slope stability analyses were performed using the FLAC code to check that the geotechnical characterization modeled with the FLAC input parameters is consistent with that used for the decoupled analyses discussed in Section 11. The results of the FLAC stability analyses are shown in Figures 12-4 through 12-7. As shown in Figures 12-4 and 12-5, the FLAC analyses result in calculated factors of safety of 2.24 and 1.36 in the upstream and downstream directions, respectively, for the pre-earthquake condition. These values are in very good agreement with those calculated from the limit equilibrium analyses (2.43 and 1.37, as shown in Figure 9-6). As shown in Figures 12-6 and 12-7, under post-earthquake conditions, the FLAC calculated factors of safety for the upstream and downstream slopes are 1.97 and 1.12, respectively. These values are in excellent agreement with those calculated from the limit equilibrium analyses (1.99 and 1.13, as shown in Figure 11-3).

Dynamic analyses were performed for the 1989 Loma Prieta earthquake and the Hayward fault and San Andreas fault MCEs. The results of the analyses for the Loma Prieta earthquake are discussed first, followed by the results for the Hayward and San Andreas fault MCE's.

12.3.1 1989 Loma Prieta Earthquake

For the 1989 Loma Prieta earthquake, analyses were performed with the cyclic degradation model, which automatically tracks pore pressure generation and accompanying strength degradation of the saturated soils. As in the case of the Newmark-type deformation analyses, the FLAC dynamic analysis for the 1989 Loma Prieta earthquake calculated very small permanent deformations (< 0.1 inch). In addition, the models predict nil cyclic strength degradation within the dam. Thus, the results for the Loma Prieta event are in good agreement with the known performance of the dam.

12.3.2 Hayward-Rogers Creek Fault MCE

Two types of FLAC analyses were performed for Hayward fault MCE's: one with assumed strength degradation, and the other with the cyclic degradation model that automatically tracks pore pressure generation and strength reduction.

The FLAC analyses with assumed strength degradation were performed for Hayward fault MCE time histories No. 1 and 2. The analysis results are shown in Figures 12-8 through 12-16. For time history No. 1, the calculated horizontal displacement of the downstream slope and the vertical displacement at the crest are about 6 and 2 feet, respectively. Larger displacements, 10 feet horizontal and 5 feet vertical, were calculated for time history No. 2. From these figures, it may be seen that, by the end of the strong shaking, a sharp gradient in displacement has developed just above the bedrock beneath the downstream slope, indicating a concentrated shear zone along this surface. The majority of the downstream embankment above this sliding surface is displaced in the downstream direction, resembling a rigid sliding block. The calculated horizontal displacements of the downstream slope and vertical displacements of the crest are summarized in Tables 12-3 and 12-4.

The FLAC analyses with the cyclic degradation model were performed for all four Hayward fault MCE time histories. The calculated downstream slope horizontal displacements and vertical displacements at the crest are summarized in Tables 12-3 and 12-4. The results for Hayward fault

MCE time history No. 1 (reverse polarity) are presented in Figures 12-17 through 12-25. As shown in Figures 12-17 and 12-18, the calculated downstream slope horizontal displacement and the vertical displacement at the crest are on the order of 5 and 2 feet, respectively. These displacements are similar to the values calculated in the FLAC analyses with assumed degradation. Figure 12-19 shows the deformed mesh after shaking. As shown in Figures 12-20 and 12-21, the displacement time histories indicate that most of the displacement occurs during the period between 10.4 and 11.5 seconds, after which relatively little additional displacement is accumulated. Figure 12-22 shows the calculated excess pore pressure ratio at the end of earthquake shaking. Figure 12-23 shows the corresponding strength reduction ratio defined as the ratio between the post-cyclic undrained strength and the initial undrained strength. The time histories of strength reduction ratio at selected locations (see Figure 12-24) within the dam and foundation are shown in Figure 12-25. It may be seen from these figures that the foundation soils beneath the dam and near the downstream toe experience moderate strength degradation of 15 percent or less. Only minor degradation (a few percent) is expected in the 1903 fill beneath the crest and no strength degradation is predicted within the 1938-39 fill. The results also indicate that the calculated strength degradation occurs mainly in the downstream embankment and foundation soils between 10.0 and 11.8 seconds. This is in very good agreement with the assumed window of 10.8 to 12.2 seconds for strength degradation used in the Newmark analyses.

As summarized in Tables 12-3 and 12-4, the FLAC analyses result in 5 to 12 feet of horizontal displacement in the downstream embankment and about 2 to 6 feet of vertical displacement at the crest for the Hayward fault MCE event. In general, the horizontal deformations calculated with FLAC are similar those calculated using the decoupled analysis methods described in Section 11. The calculated deformations with FLAC using the cyclic degradation model are, however, viewed as providing a greater degree of refinement than those calculated with the decoupled methods, and are viewed as offering a greater level of reliability.

The results suggest that a representative average of the calculated horizontal deformations of the downstream slope is about 8 feet. Likewise, a representative average of the calculated vertical displacement of the crest is about 5 to 6 feet. Thus, such deformations may be considered to represent the average deformation response of the dam calculated with FLAC for the design earthquake.

12.3.3 San Andreas Fault MCE

The San Andreas fault MCE event was analyzed with FLAC using the cyclic degradation model. The calculated horizontal displacements are on the order of one foot in the downstream direction, and about one-half foot in the upstream direction. The calculated vertical displacements at the crest are less than one foot. While some excess pore pressure (about 30 percent or higher) is generated in the upstream embankment, little strength degradation is calculated in the dam beneath the crest and downstream slope. Since the calculated displacements, summarized in Tables 12-3 and 12-4, are significantly smaller than those for the Hayward fault event, it is clear the San Andreas event is less critical.

Table 12-1
Material Properties for Static Stress Analysis

Property	Symbol	1938-39 Embankment Fill	1903 Embankment Fill	Foundation Soils	Bedrock
Modulus Number	K	320	320	320	-
Modulus Number	K_b	240	240	240	-
Modulus Exponent	m	0.4	0.4	0.4	-
Modulus Exponent	n	0.5	0.5	0.5	-
Elastic Bulk Modulus	B, psf	$K_b * Pa(\sigma_3' / Pa)^m$	$K_b * Pa(\sigma_3' / Pa)^m$	$K_b * Pa(\sigma_3' / Pa)^m$	-
Youngs Modulus	E, psf	$K * Pa(\sigma_3' / Pa)^n$	$K * Pa(\sigma_3' / Pa)^n$	$K * Pa(\sigma_3' / Pa)^n$	-
Poisson's Ratio	ν	$0.5 - E/(6*B)$	$0.5 - E/(6*B)$	$0.5 - E/(6*B)$	0.45
Elastic Shear Modulus	G, psf	$E/(2+2\nu)$	$E/(2+2\nu)$	$E/(2+2\nu)$	1.74E+07
Cohesion	c', psf	0	120	120	20,000
Friction Angle	$\phi', degree$	35	30	30	0

Table 12-2
Material Properties for Dynamic Analysis

Property	Symbol	Units	1938-39 Embankment Fill	1903 Embankment Fill	Foundation Soils	Bedrock
Poisson's Ratio ⁽¹⁾	ν	-	0.35, 0.45	0.40, 0.45	0.48	0.45
Shear wave velocity ⁽²⁾	V_s	fps	870	$600 * (\sigma_m')^{0.38}$ and > 700 ⁽²⁾	1,100	2,000
Maxim Shear Modulus	G_{max}	psf	$\rho * V_s^2$	$\rho * V_s^2$	$\rho * V_s^2$	$\rho * V_s^2$
Shear Modulus	G	psf	$0.7 * G_{max}$	$0.7 * G_{max}$	$0.7 * G_{max}$	$0.7 * G_{max}$
Rayleigh Damping	ϵ_{min}	-	3%	3%	3%	0.5%
Rayleigh Damping Center Frequency	f_{min}	Hz	3	3	3	3
Hysteretic Damping	-	-	see note 3	see note 3	see note 3	see note 3
Cohesion	c	psf	0, 580	120, 280	120, 280	20,000
Friction Angle	ϕ	degree	35, 30.5	30, 27	30, 27	0
Cyclic Resistance ⁽⁴⁾	CSR_{30}	0.56	0.28	0.28	-	

Notes:

- (1). Dual values correspond to unsaturated and saturated conditions, where applicable.
- (2). $\sigma_m' = (\sigma_1' + \sigma_2' + \sigma_3')/3$, in ksf
- (3). Hysteretic damping is automatically generated and added to the Rayleigh damping in FLAC analyses when materials yield.
- (4). Cyclic resistance ratio only applies to saturated soils.

**Table 12-3
Calculated Downstream Slope Horizontal Displacements (in feet)**

Earthquake	Time History	Ground Motion Polarity	Newmark Type (QUAD4M)	Simplified Newmark	FLAC with Assumed Strength Degradation	FLAC with Calculated Strength Degradation
Hayward fault MCE	#1	Standard	3	2	6	7
		Reverse	5	2	6	5
	#2	Standard	4	5	7	6
		Reverse	11	11	10	12
	#3	Standard	-	9	-	7
		Reverse	-	12	-	9
	#4	Standard	-	7	-	8
		Reverse	-	8	-	11
San Andreas fault MCE	#1	Standard	-	2	-	1
		Reverse	-	2	-	1
1989 Loma Prieta, California	Piedmont Jr. High	Standard	-	0	-	0
		Reverse	-	0	-	0

**Table 12-4
Calculated Crest Vertical Displacements (in feet)**

Earthquake	Time History	Ground Motion Polarity	FLAC with Assumed Strength Degradation	FLAC with Calculated Strength Degradation
Hayward fault MCE	#1	Standard	5	6
		Reverse	2	2
	#2	Standard	4	5
		Reverse	5	6
	#3	Standard	-	5
		Reverse	-	5
	#4	Standard	-	6
		Reverse	-	6
San Andreas fault MCE	#1	Standard	-	<1
		Reverse	-	<1

JOB TITLE : Estates Dam Dynamic Analysis

(*10^-2)

FLAC (Version 4.00)

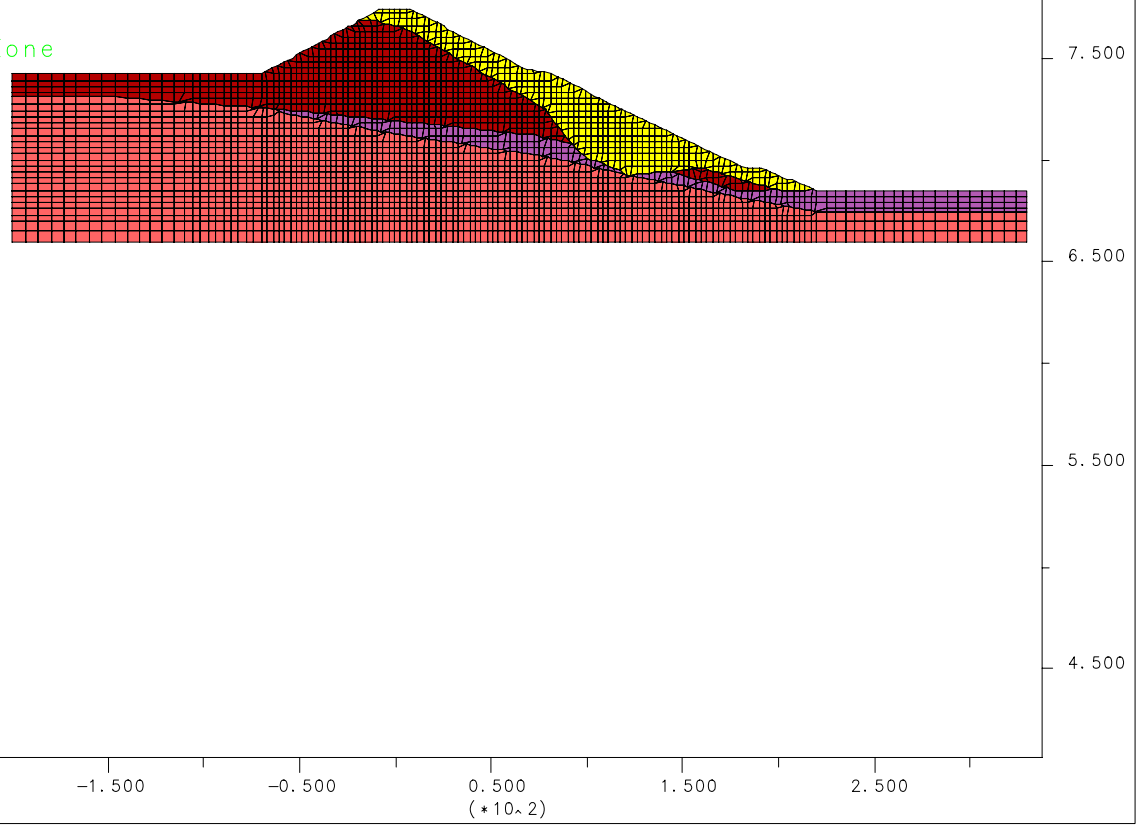
LEGEND

17-Nov-05 15:34
step 29948
-2.109E+02 <x< 3.375E+02
4.063E+02 <y< 9.547E+02

Foundation and Embankment Zone

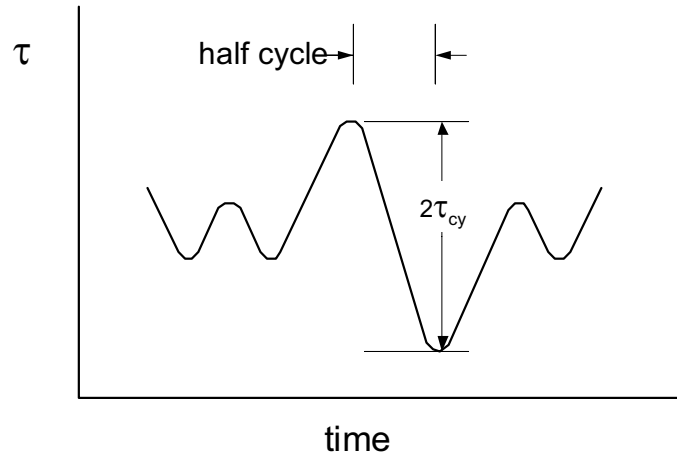
- Bedrock
- 1903_Fill
- Foundation_Soil
- 1938_Fill

Grid plot

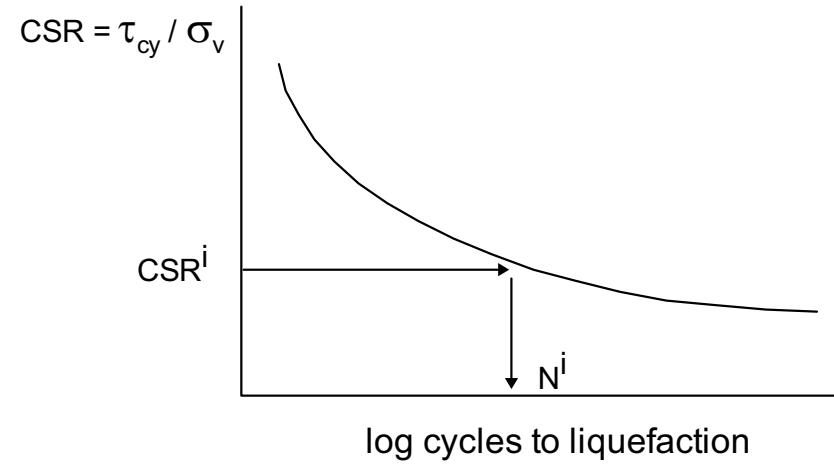


Project No. 26814957	Estates Dam Seismic Stability Analysis	Finite Difference Mesh for Cross-Section A-A'	Figure
URS		FLAC Analysis	12-1

Shear Stress Time History



Cyclic Strength

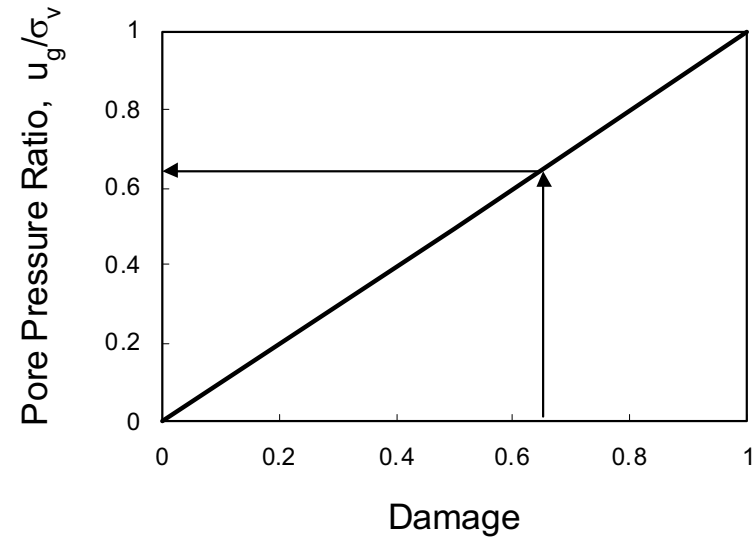


Damage Increment

$$\Delta D^i = 0.5 / N_L^i$$

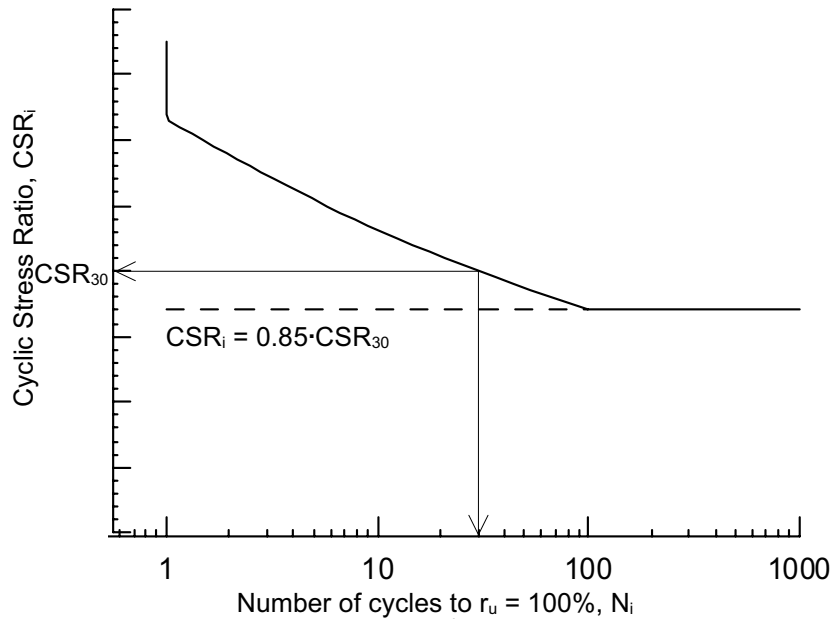
Cumulative Damage

$$D = \sum \Delta D^i$$

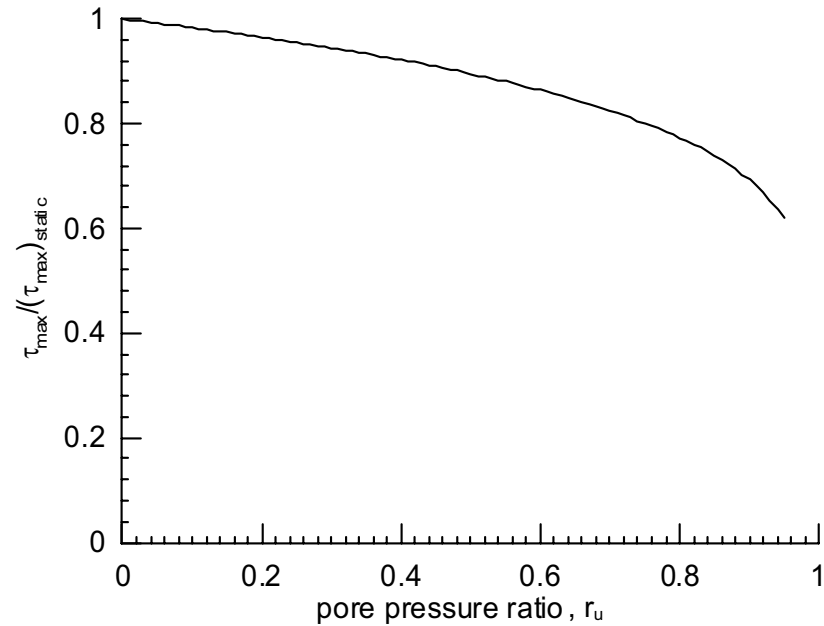


Project No. 26814536	Chabot Dam Seismic Stability Analysis	FLAC Analysis Pore Pressure Generation Model	Figure 12-2
URS			

Cyclic Strength
 $CSR_{30} = 0.28, 0.56$



Strength Degradation



$$N_i = 30 \left(\frac{CSR_{30}}{CSR_i} \right)^{7.41} \quad 1 \leq N_i \leq 100$$

where $CSR_{30} = 0.28$ (1903 Fill and Foundation Soil)
 or
 0.56 (1938-39 Fill)

$$\frac{\tau_{\max}}{(\tau_{\max})_{\text{static}}} = (1 - r_u)^{0.16}$$

Project No. 26814957	Estates Dam Seismic Stability Analysis	Cyclic Strength and Undrained Strength Degradation of Saturated Embankment Fills and Foundation Soils	Figure
URS			12-3

FLAC (Version 4.00)

LEGEND

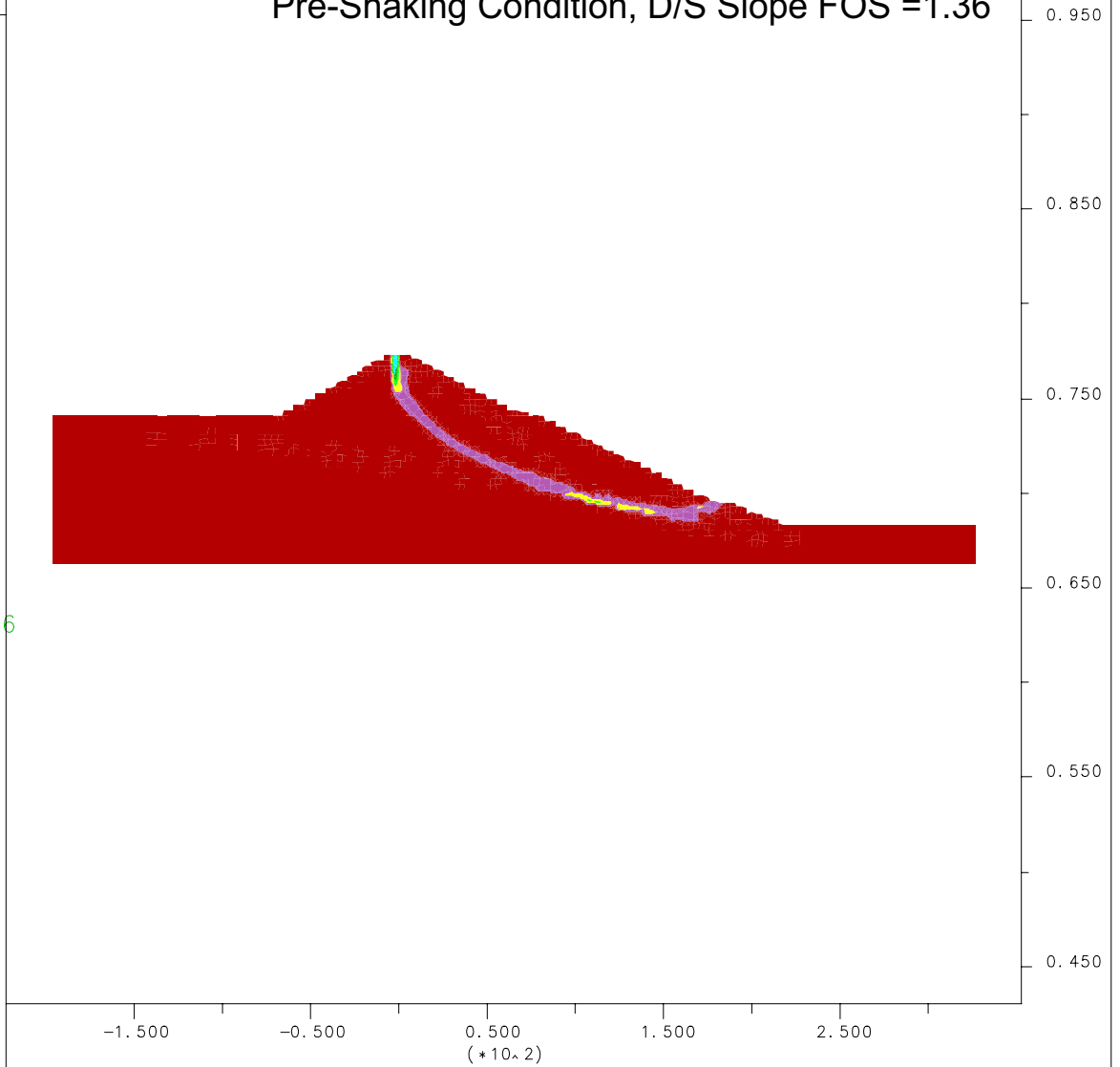
10-Nov-05 10:08
 step 50689
 -2.229E+02 <x< 3.532E+02
 4.298E+02 <y< 1.006E+03

Max. shear strain-rate



Contour interval = 5.00E-06

Pre-Shaking Condition, D/S Slope FOS = 1.36



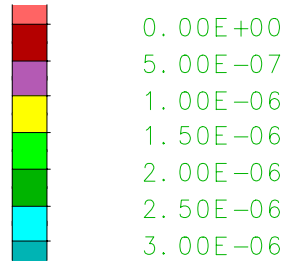
Project No. 26814957	Estates Dam Seismic Stability Analysis	FLAC Static Analysis Downstream Slope Pre-Earthquake Stability	Figure 12-4
URS			

FLAC (Version 4.00)

LEGEND

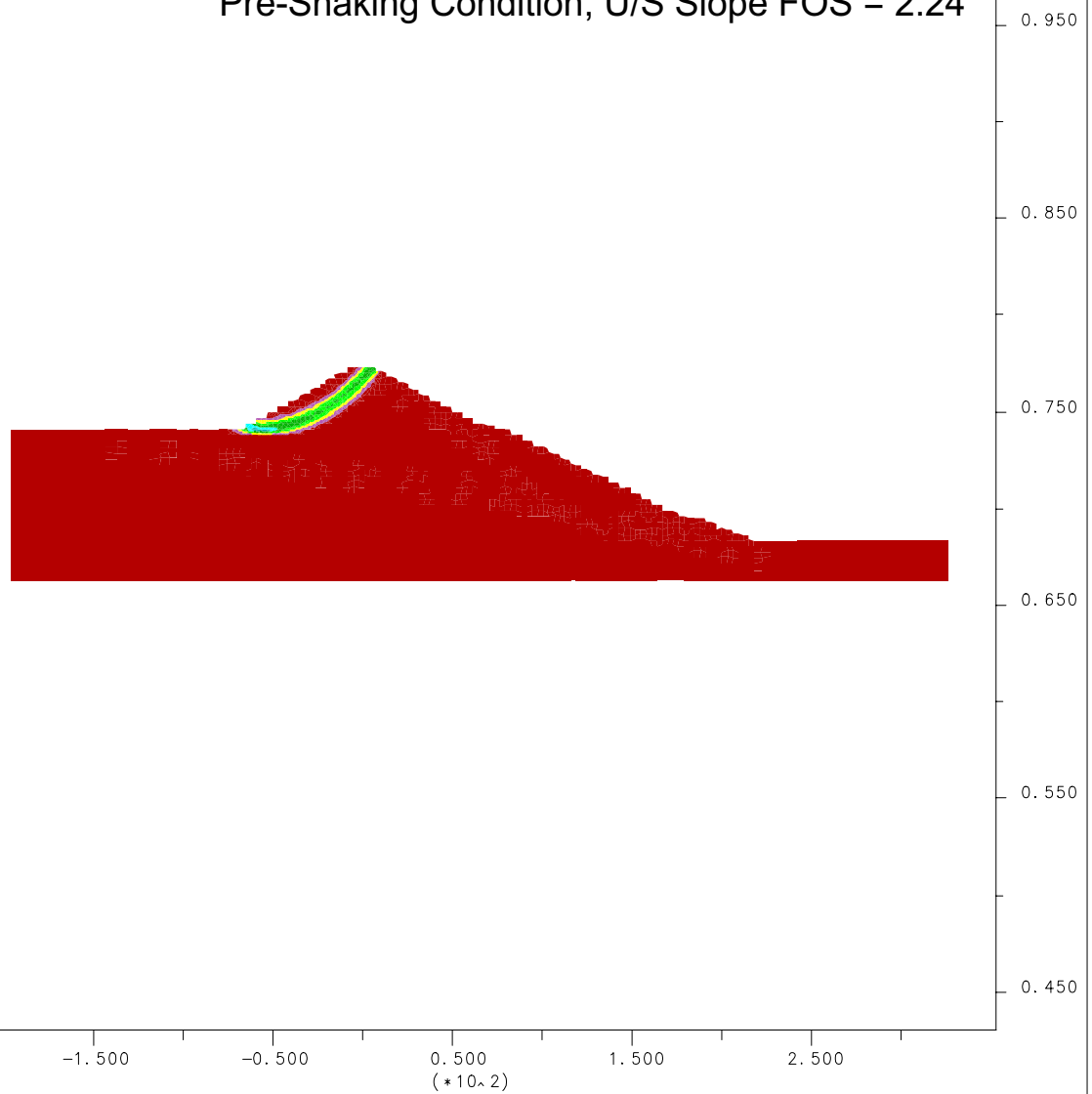
10-Nov-05 10:26
 step 64709
 -2.229E+02 <x< 3.532E+02
 4.298E+02 <y< 1.006E+03

Max. shear strain-rate



Contour interval = 5.00E-07

Pre-Shaking Condition, U/S Slope FOS = 2.24



Project No.
26814957

Estates Dam
Seismic Stability Analysis



FLAC Static Analysis
Upstream Slope
Pre-Earthquake Stability

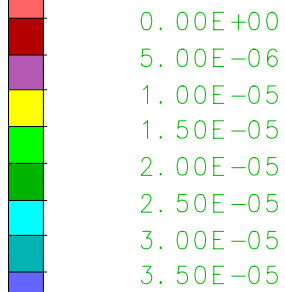
Figure
12-5

FLAC (Version 4.00)

LEGEND

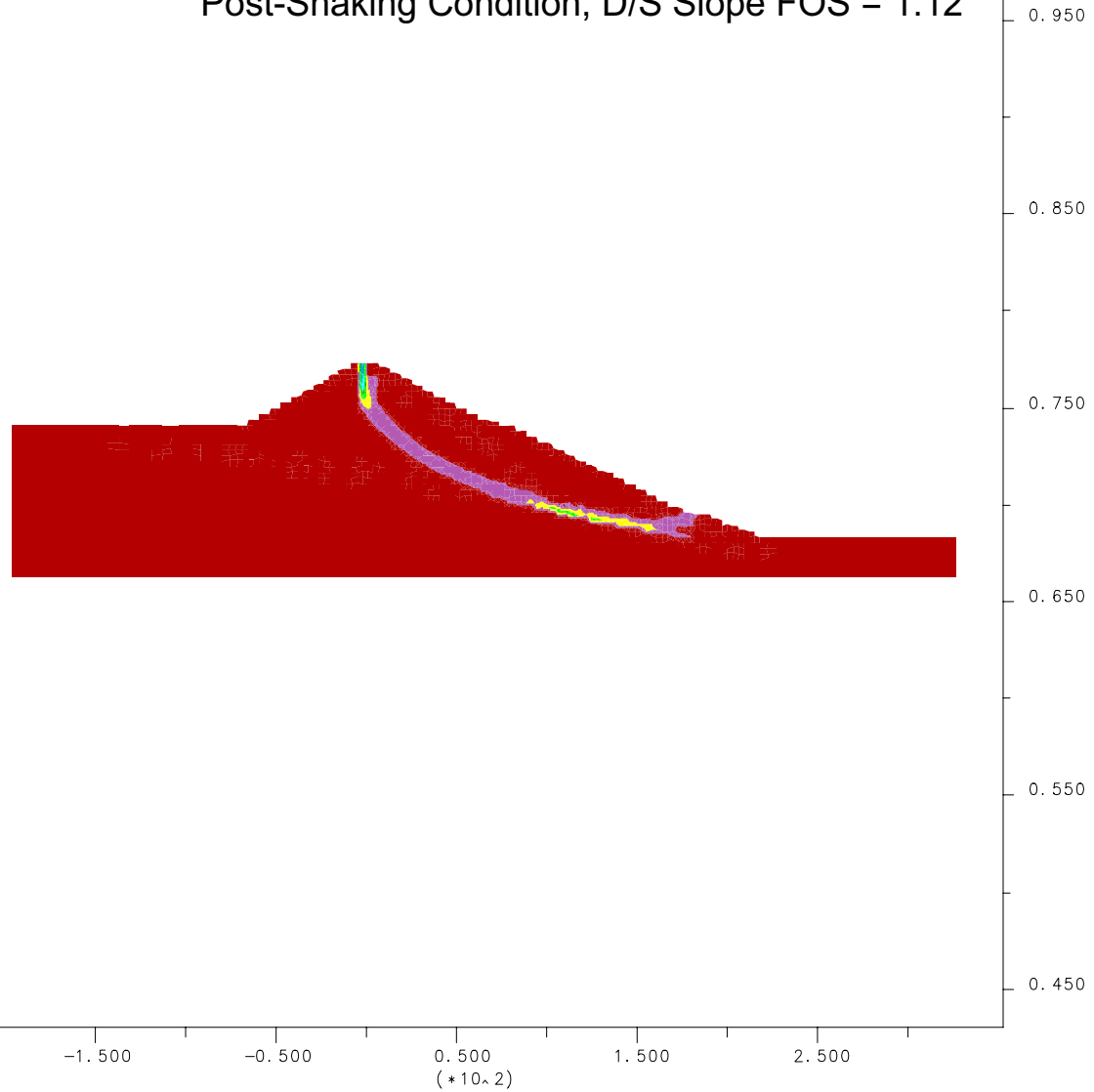
10-Nov-05 14:23
 step 51988
 -2.229E+02 <x< 3.532E+02
 4.298E+02 <y< 1.006E+03

Max. shear strain-rate



Contour interval = 5.00E-06

Post-Shaking Condition, D/S Slope FOS = 1.12



Project No.
26814957

Estates Dam
Seismic Stability Analysis



FLAC Static Analysis
Downstream Slope
Post-Earthquake Stability

Figure
12-6

FLAC (Version 4.00)

LEGEND

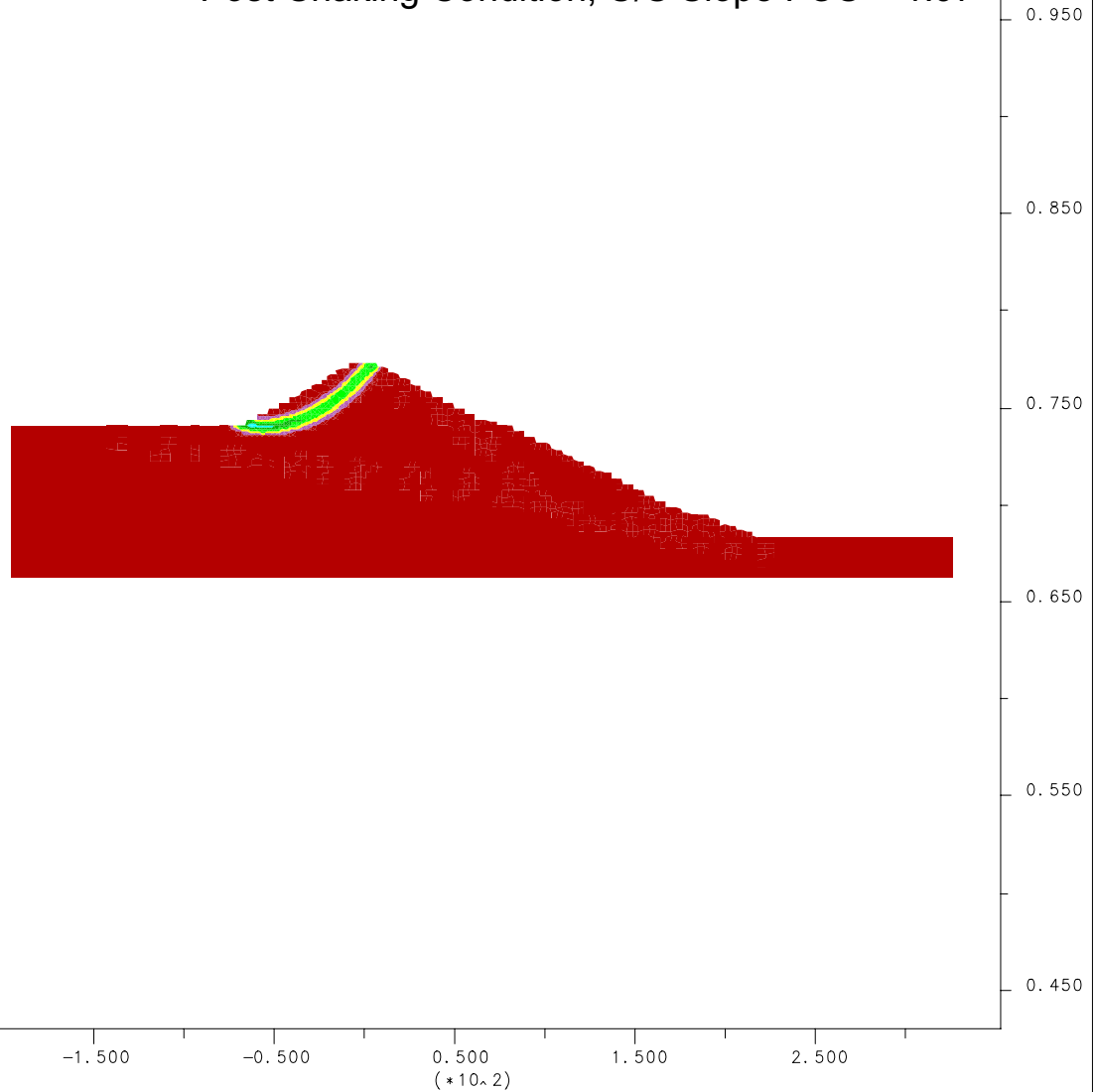
10-Nov-05 14:47
 step 49988
 -2.229E+02 <x< 3.532E+02
 4.298E+02 <y< 1.006E+03

Max. shear strain-rate

- 0.00E+00
- 2.50E-06
- 5.00E-06
- 7.50E-06
- 1.00E-05
- 1.25E-05

Contour interval = 2.50E-06

Post-Shaking Condition, U/S Slope FOS = 1.97



Project No.
26814957

Estates Dam
Seismic Stability Analysis



FLAC Static Analysis
Upstream Slope
Post-Earthquake Stability

Figure
12-7

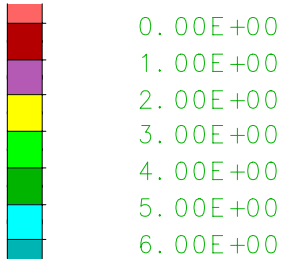
JOB TITLE : Estates Dam Dynamic Analysis with Assumed Degradation, Hayward MCE TH #1 (*10.2)

FLAC (Version 4.00)

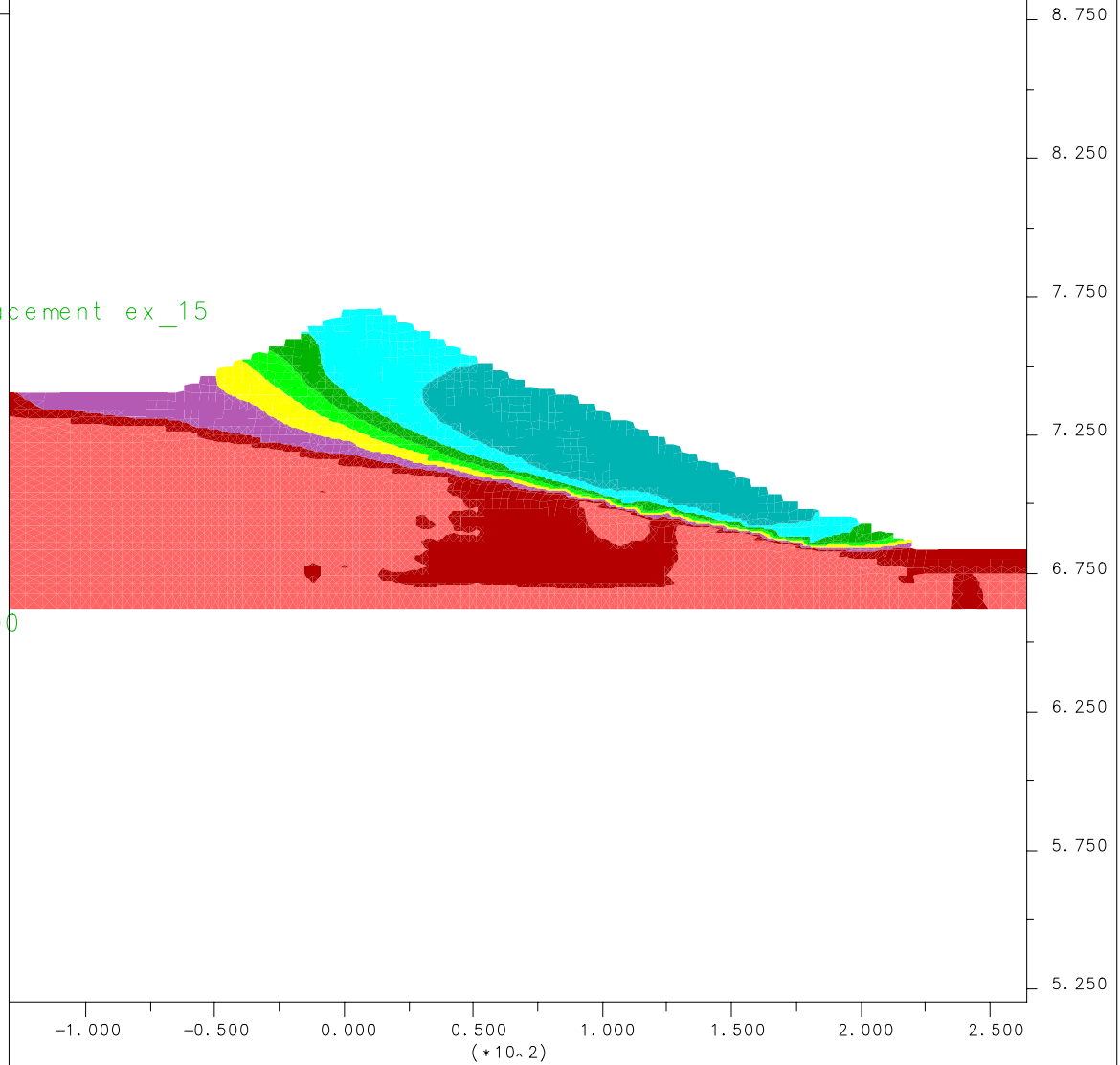
LEGEND

22-Nov-05 10:26
 step 6691791
 -1.296E+02 <x< 2.641E+02
 5.198E+02 <y< 9.135E+02

Relative Horizontal Displacement ex_15



Contour interval = 1.00E+00



Project No. 26814957	Estates Dam Seismic Stability Analysis	FLAC Dynamic Analysis with Assumed Strength Degradation Permanent Horizontal Displacement Hayward MCE TH #1	Figure 12-8
URS			

JOB TITLE : Estates Dam Dynamic Analysis with Assumed Degradation, MCE #1

(*10^-2)

FLAC (Version 4.00)

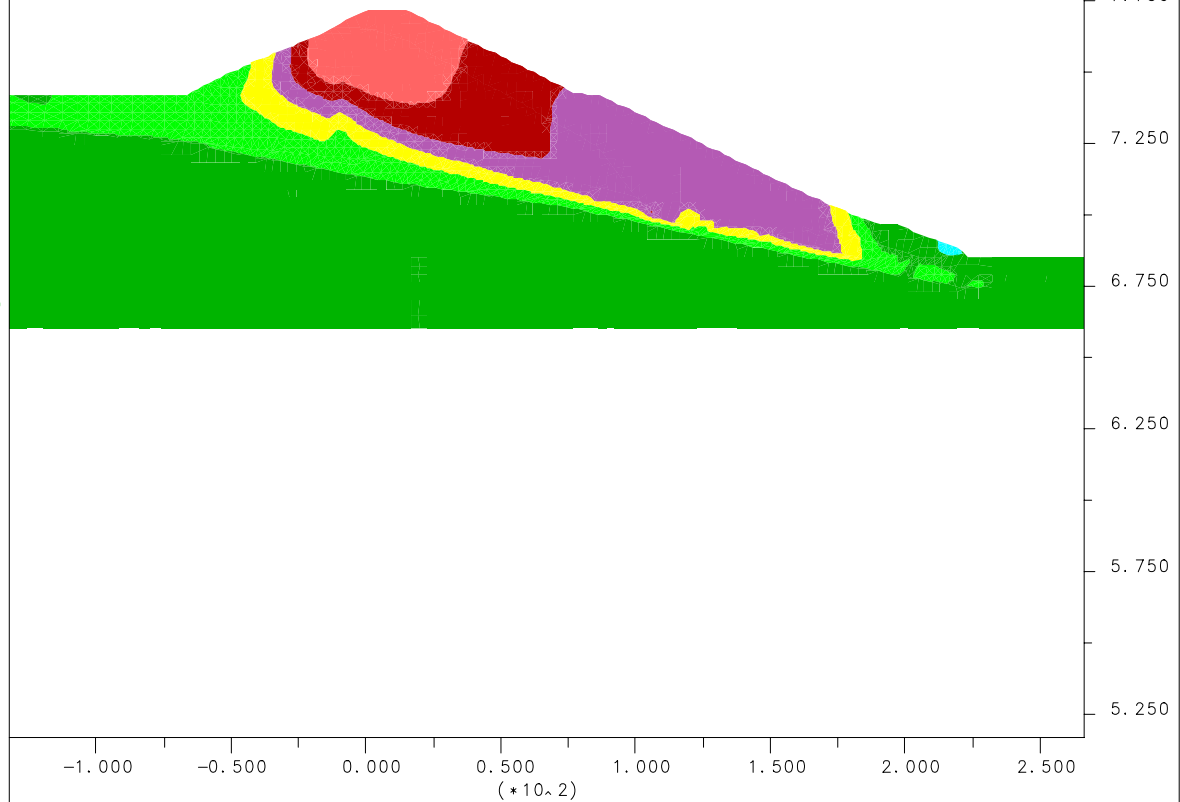
LEGEND

9-Nov-05 11:21
 step 6691791
 -1.321E+02 <x< 2.663E+02
 5.166E+02 <y< 9.150E+02

Vertical Displacement, ft



Contour interval = 5.00E-01



Project No. 26814957	Estates Dam Seismic Stability Analysis	FLAC Dynamic Analysis with Assumed Strength Degradation Permanent Vertical Displacement Hayward MCE TH #1	Figure 12-9
URS			

FLAC (Version 4.00)

LEGEND

18-Nov-05 4:01
 step 4352489
 -2.055E+02 <x< 3.355E+02
 4.465E+02 <y< 9.875E+02

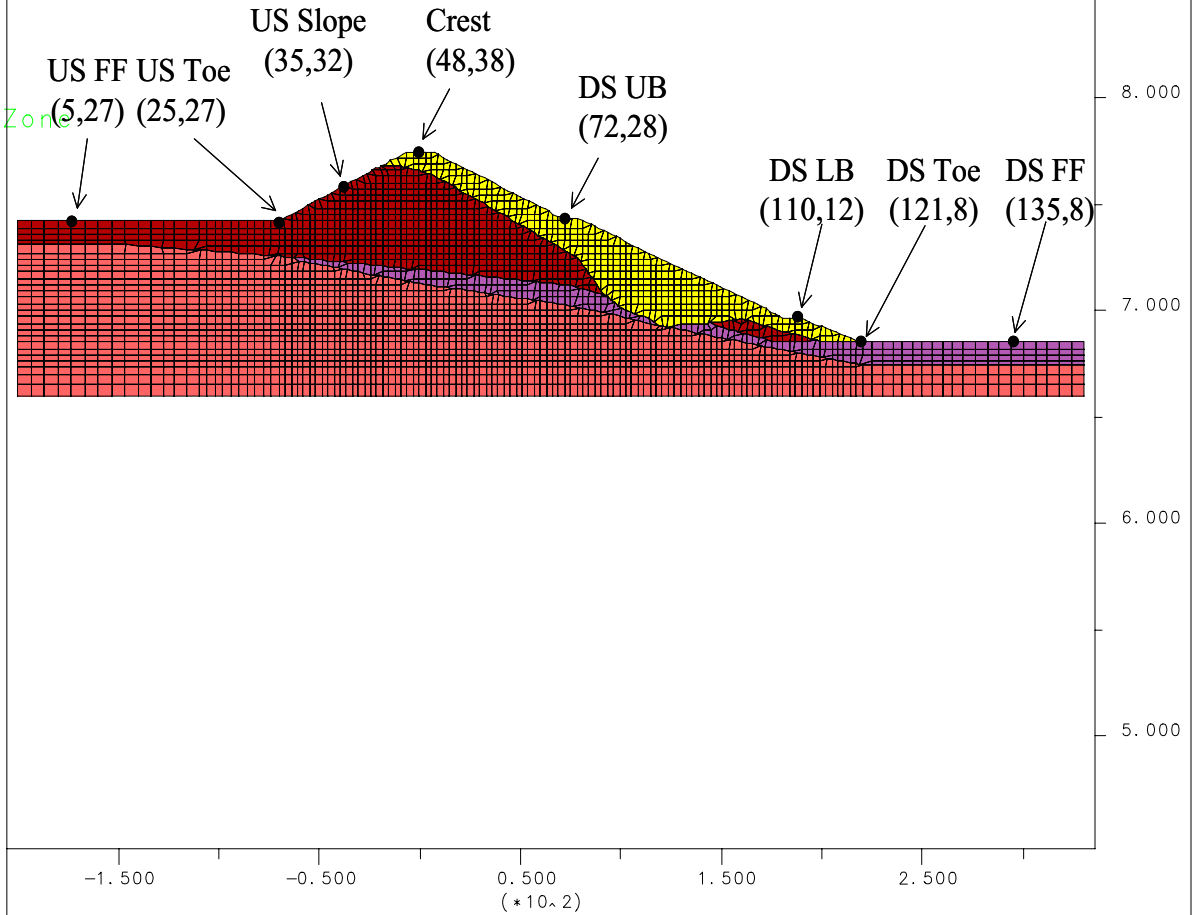
Foundation and Embankment Zone

- Bedrock
- 1903_Fill
- Foundation_Soil
- 1938_Fill

Grid plot



Locations of Displacement Time History



Project No.
26814957

Estates Dam
Seismic Stability Analysis

FLAC Dynamic Analysis
Locations of Displacement
Time History

Figure
12-10



FLAC (Version 4.00)

LEGEND

9-Nov-05 11:21
step 6691791

HISTORY PLOT

Y-axis :

usff_xdisp (FISH)

us_toe_xdisp (FISH)

us_slope_xdisp (FISH)

crest_xdisp (FISH)

ds_ub_xdisp (FISH)

ds_lb_xdisp (FISH)

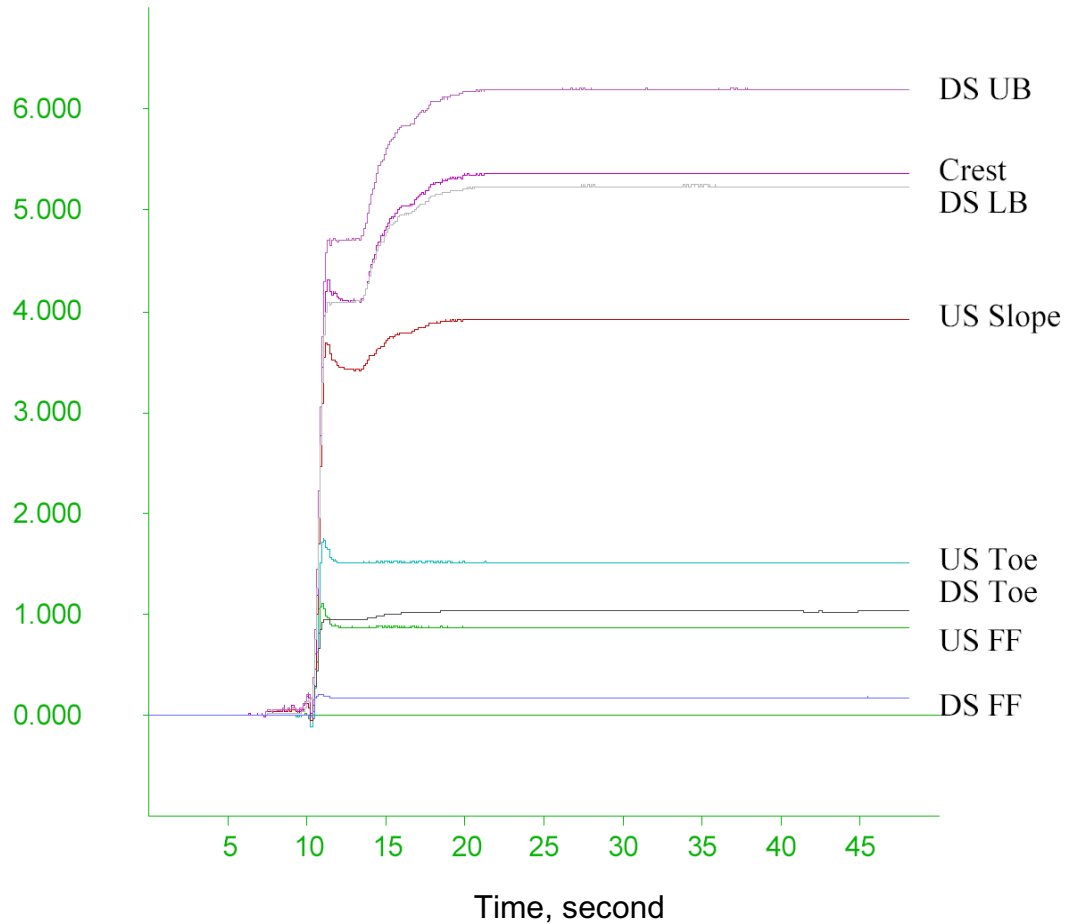
ds_toe_xdisp (FISH)

ds_ff_xdisp (FISH)

X-axis :

Dynamic time

Horizontal Displacement, ft



Project No.
26814957

Estates Dam
Seismic Stability Analysis



FLAC Dynamic Analysis
with Assumed Strength Degradation
Horizontal Displacement Time Histories
Hayward MCE TH #1

Figure
12-11

FLAC (Version 4.00)

LEGEND

9-Nov-05 11:21
step 6691791

HISTORY PLOT

Y-axis :

Y displacement(5, 27)

Y displacement(25, 27)

Y displacement(35, 32)

Y displacement(48, 38)

Y displacement(72, 28)

Y displacement(110, 12)

Y displacement(110, 12)

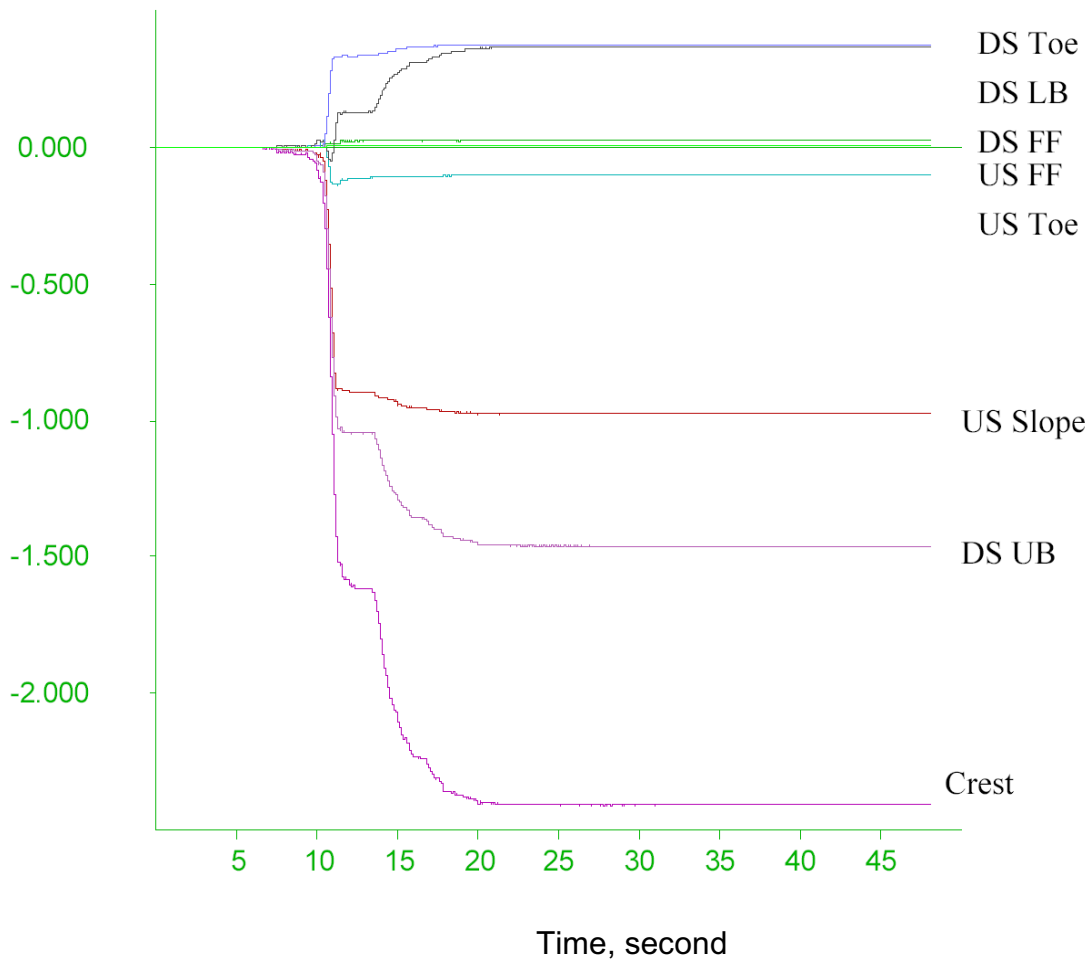
Y displacement(121, 8)

Y displacement(135, 8)

X-axis :

Dynamic time

Vertical Displacement, ft



Project No.
26814957

Estates Dam
Seismic Stability Analysis



FLAC Dynamic Analysis
with Assumed Strength Degradation
Vertical Displacement Time Histories
Hayward MCE TH #1

Figure
12-12

JOB TITLE : Estates Dam Dynamic Analysis with Assumed Degradation, Hayward MCE TH #2 (*10.2)

FLAC (Version 4.00)

LEGEND

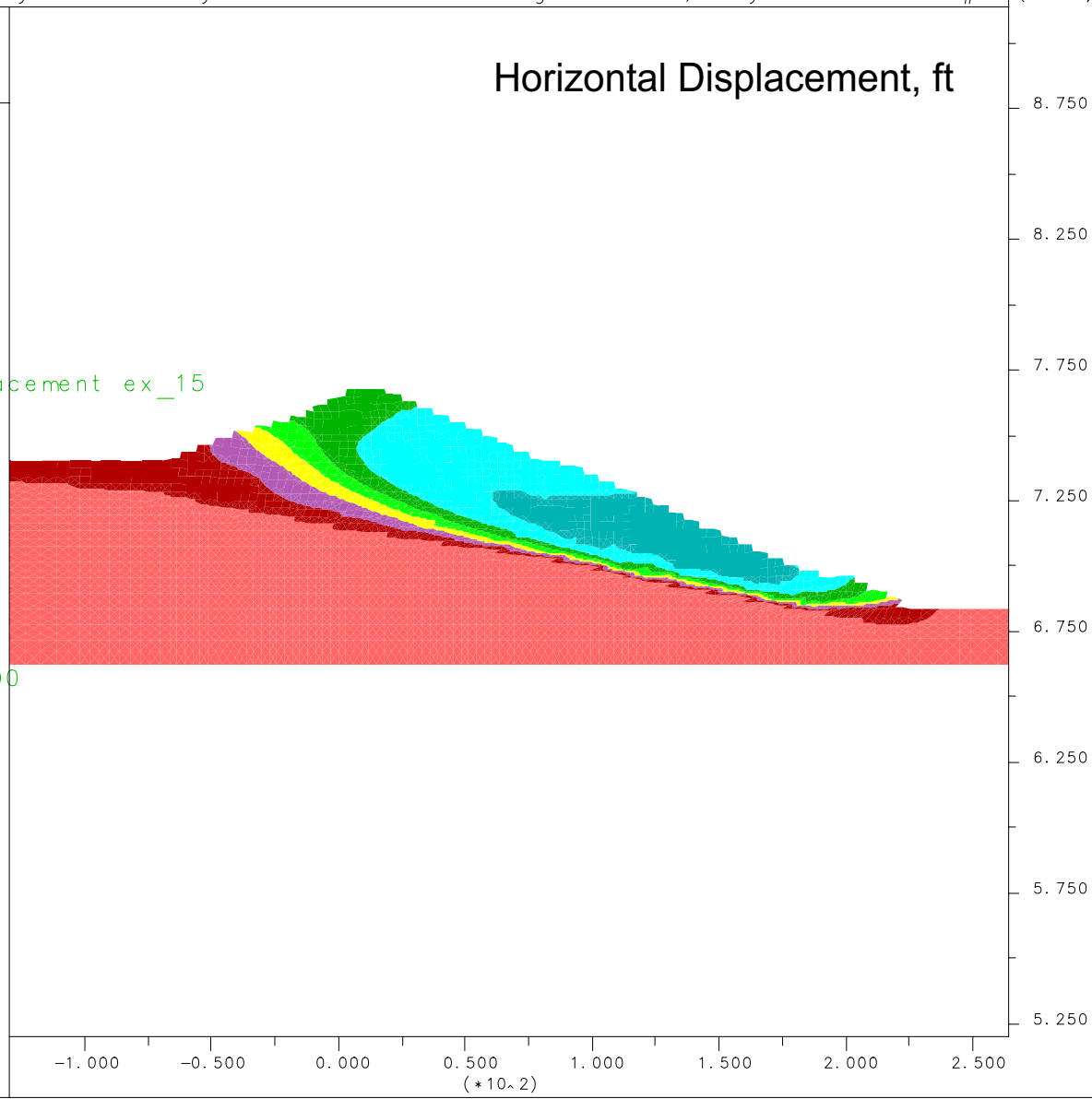
22-Nov-05 10:42
 step 12182338
 -1.296E+02 <x< 2.641E+02
 5.198E+02 <y< 9.135E+02

Relative Horizontal Displacement ex_15

- 0.00E+00
- 2.00E+00
- 4.00E+00
- 6.00E+00
- 8.00E+00
- 1.00E+01
- 1.20E+01

Contour interval = 2.00E+00

Horizontal Displacement, ft



Project No.
26814957

Estates Dam
Seismic Stability Analysis



FLAC Dynamic Analysis
with Assumed Strength Degradation
Permanent Horizontal Displacement
Hayward MCE TH #2

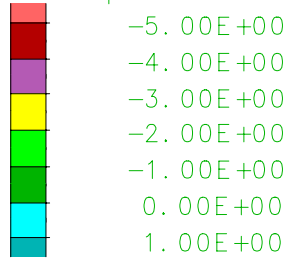
Figure
12-13

FLAC (Version 4.00)

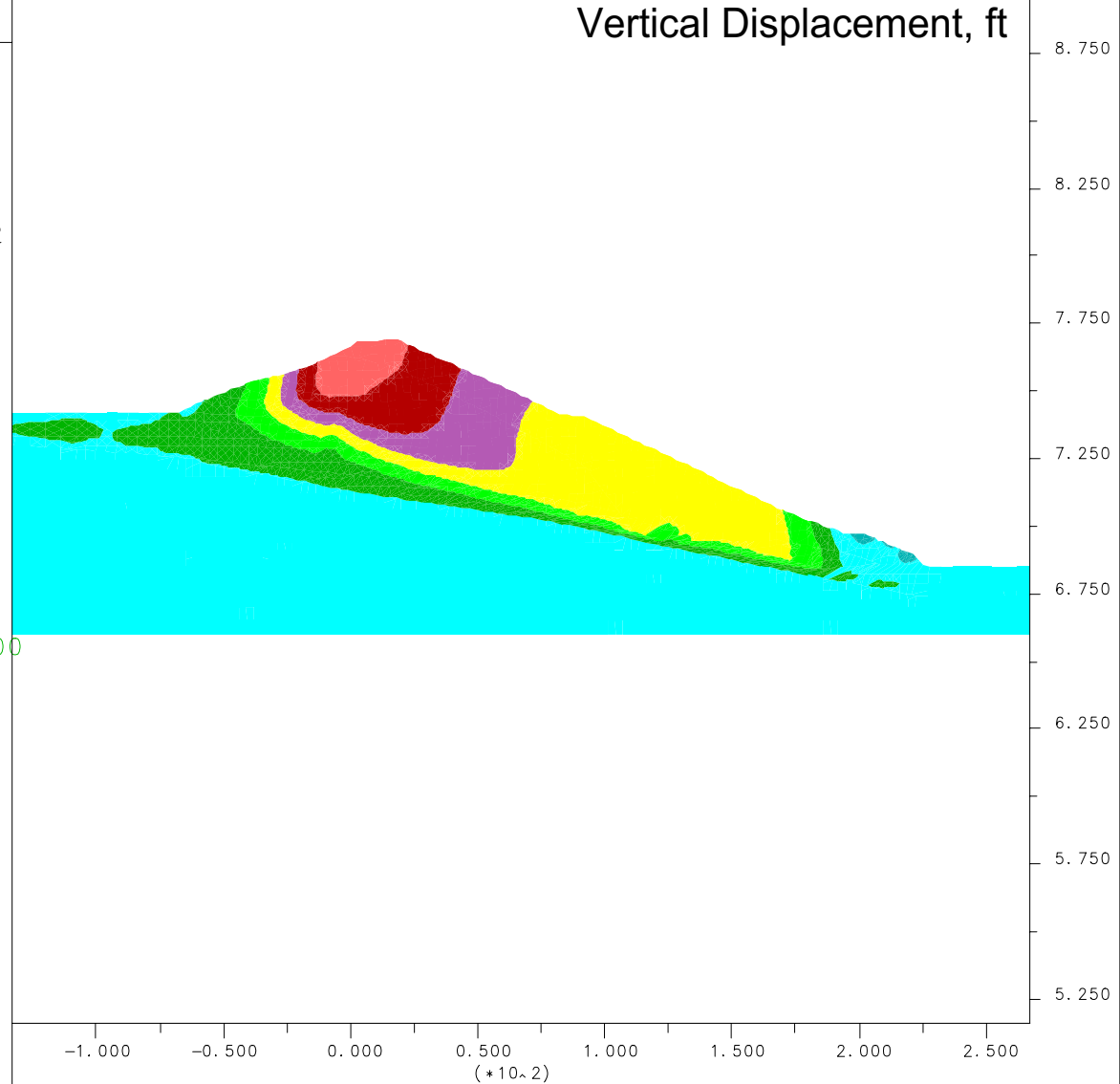
LEGEND

13-Nov-05 18:24
 step 12182338
 -1.330E+02 <x< 2.671E+02
 5.158E+02 <y< 9.159E+02

Y-displacement contours



Contour interval= 1.00E+00



Project No. 26814957	Estates Dam Seismic Stability Analysis	FLAC Dynamic Analysis with Assumed Strength Degradation Permanent Vertical Displacement Hayward MCE TH #2	Figure 12-14
URS			

FLAC (Version 4.00)

LEGEND

13-Nov-05 18:24
step 12182338

HISTORY PLOT

Y-axis :

usff_xdisp (FISH)

us_toe_xdisp (FISH)

us_slope_xdisp (FISH)

crest_xdisp (FISH)

ds_ub_xdisp (FISH)

ds_lb_xdisp (FISH)

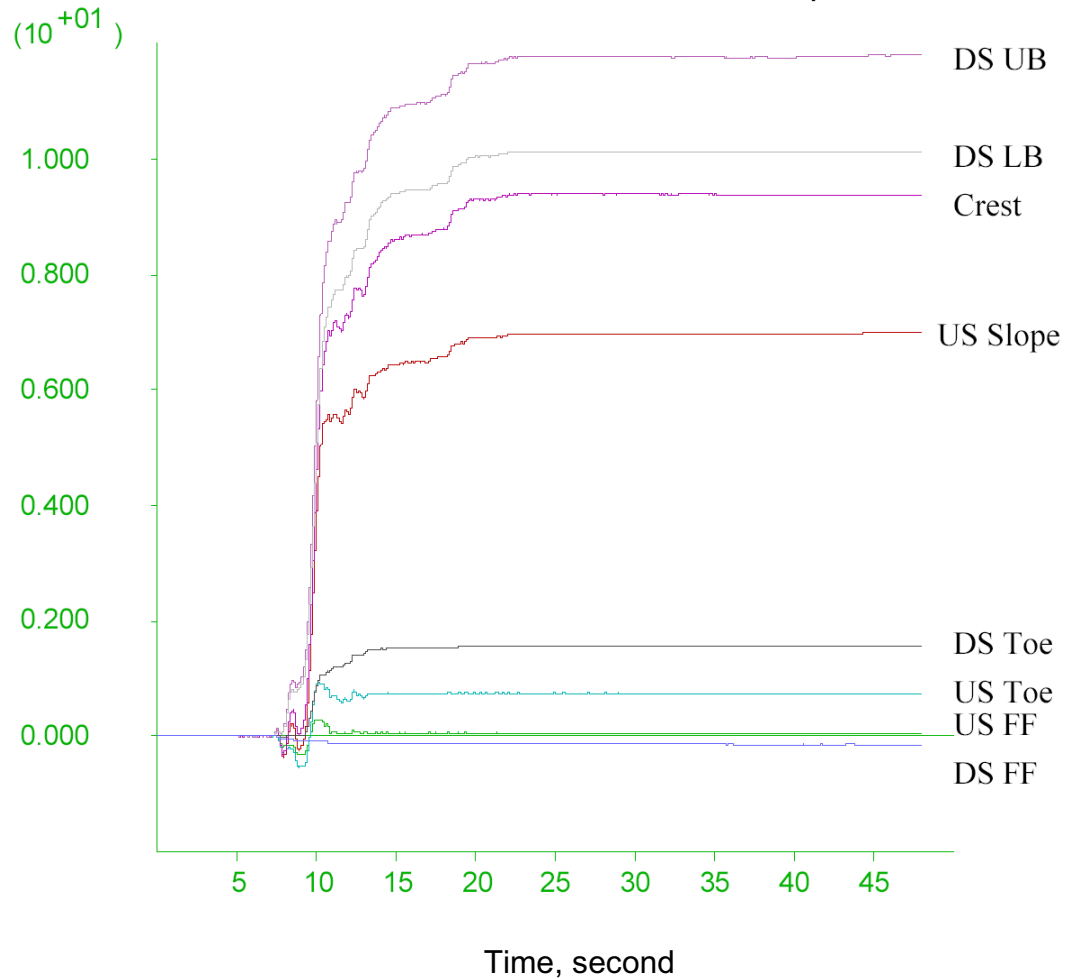
ds_toe_xdisp (FISH)

ds_ff_xdisp (FISH)

X-axis :

Dynamic time

MCE #2, Horizontal Displacements, ft



Project No.
26814957

Estates Dam
Seismic Stability Analysis



FLAC Dynamic Analysis
with Assumed Strength Degradation
Horizontal Displacement Time Histories
Hayward MCE TH #2

Figure
12-15

FLAC (Version 4.00)

LEGEND

13-Nov-05 18:24
step 12182338

HISTORY PLOT

Y-axis :

Y displacement(5, 27)

Y displacement(25, 27)

Y displacement(35, 32)

Y displacement(48, 38)

Y displacement(72, 28)

Y displacement(110, 12)

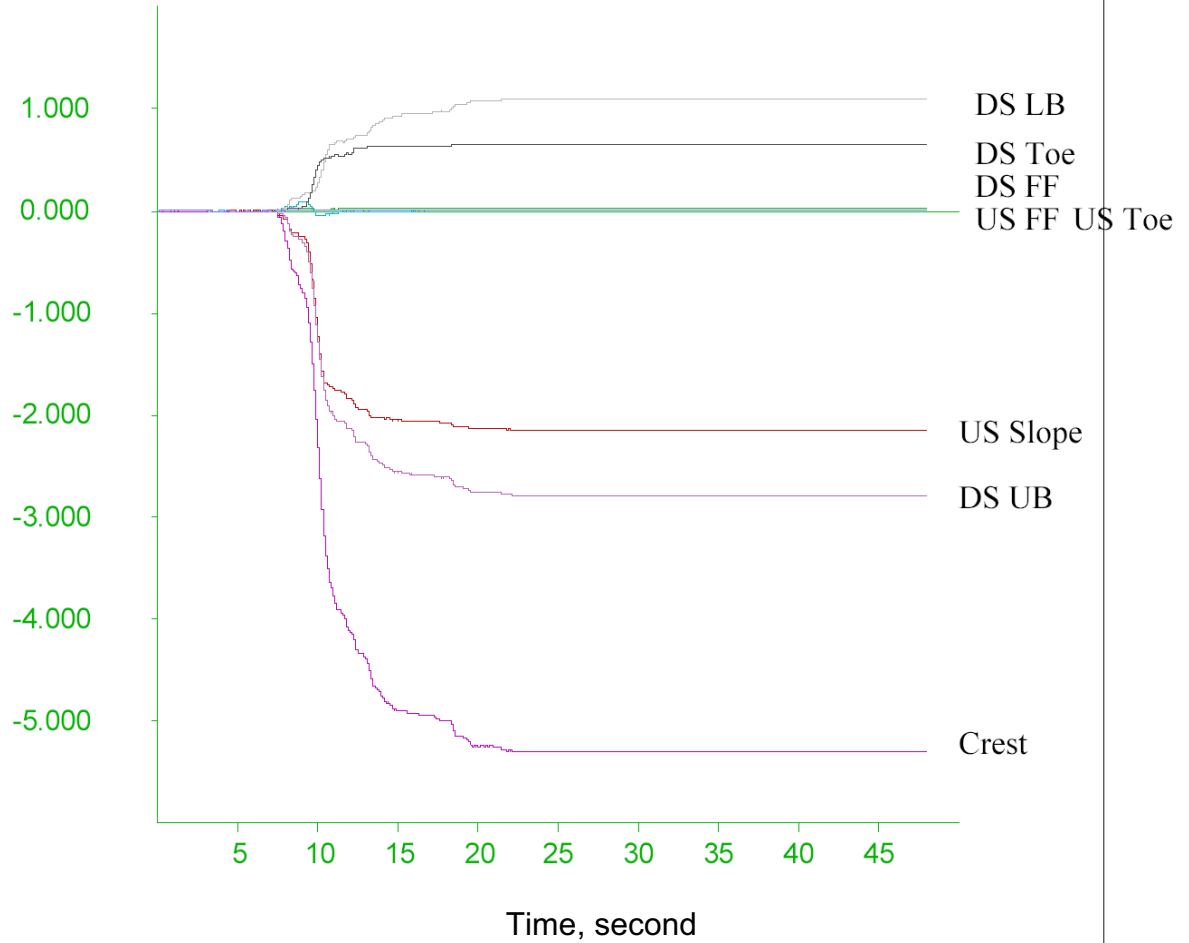
Y displacement(121, 8)

Y displacement(135, 8)

X-axis :

Dynamic time

MCE TH #2, Vertical Displacements (ft)



Project No.
26814957

Estates Dam
Seismic Stability Analysis



FLAC Dynamic Analysis
with Assumed Strength Degradation
Vertical Displacement Time Histories
Hayward MCE TH #2

Figure
12-16

FLAC (Version 4.00)

LEGEND

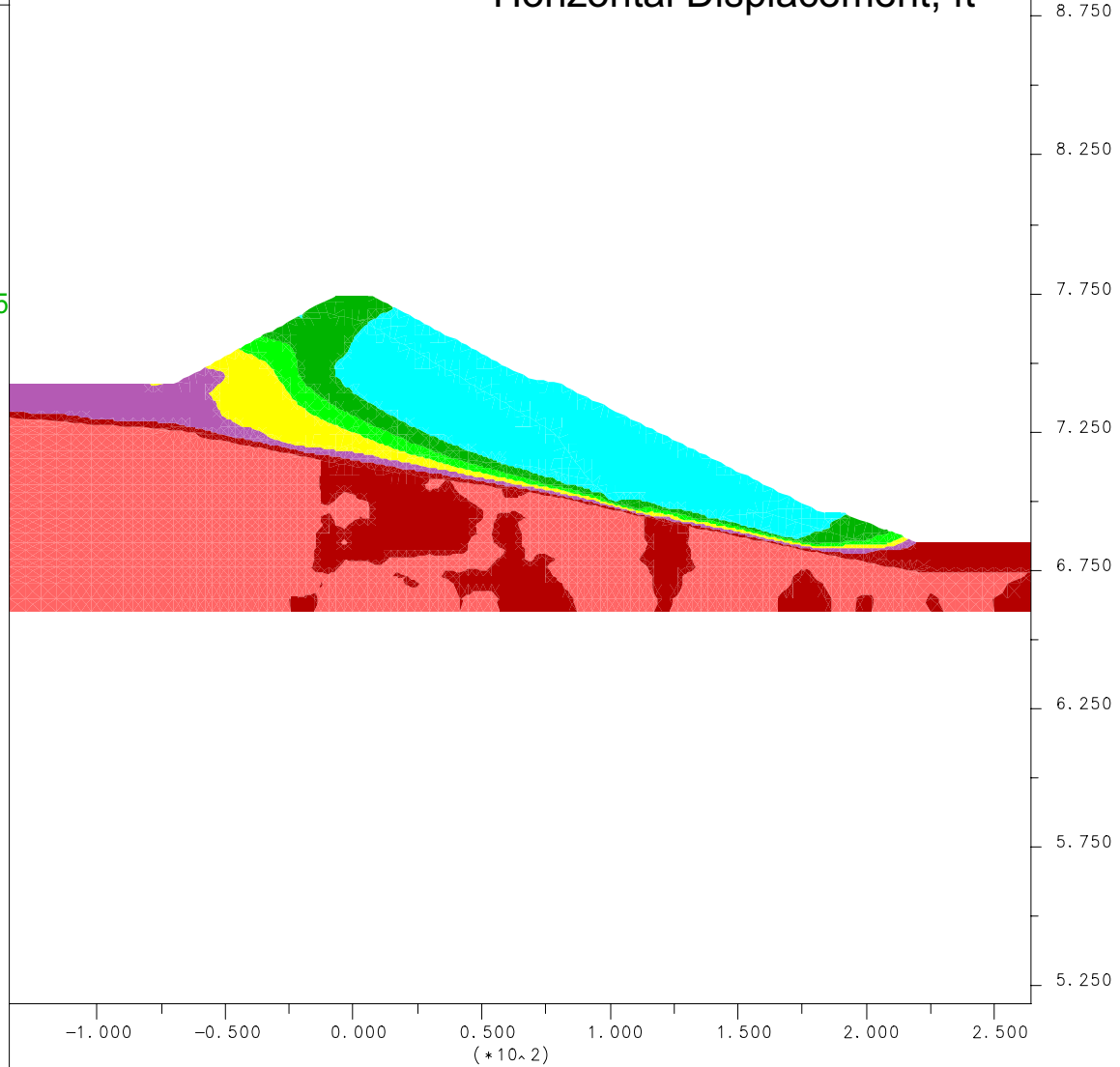
22-Nov-05 10:49
 step 4352489
 -1.341E+02 <x< 2.641E+02
 5.179E+02 <y< 9.161E+02

Relative Horizontal Displacement ex_15



Contour interval= 1.00E+00

Horizontal Displacement, ft



Project No.
26814957

Estates Dam
Seismic Stability Analysis



FLAC Dynamic Analysis
with Cyclic Degradation Model
Permanent Horizontal Displacement
Hayward MCE TH #1

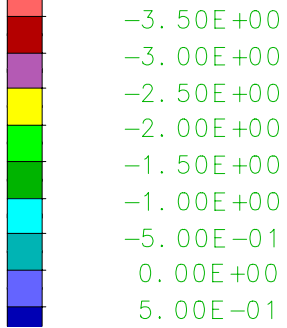
Figure
12-17

FLAC (Version 4.00)

LEGEND

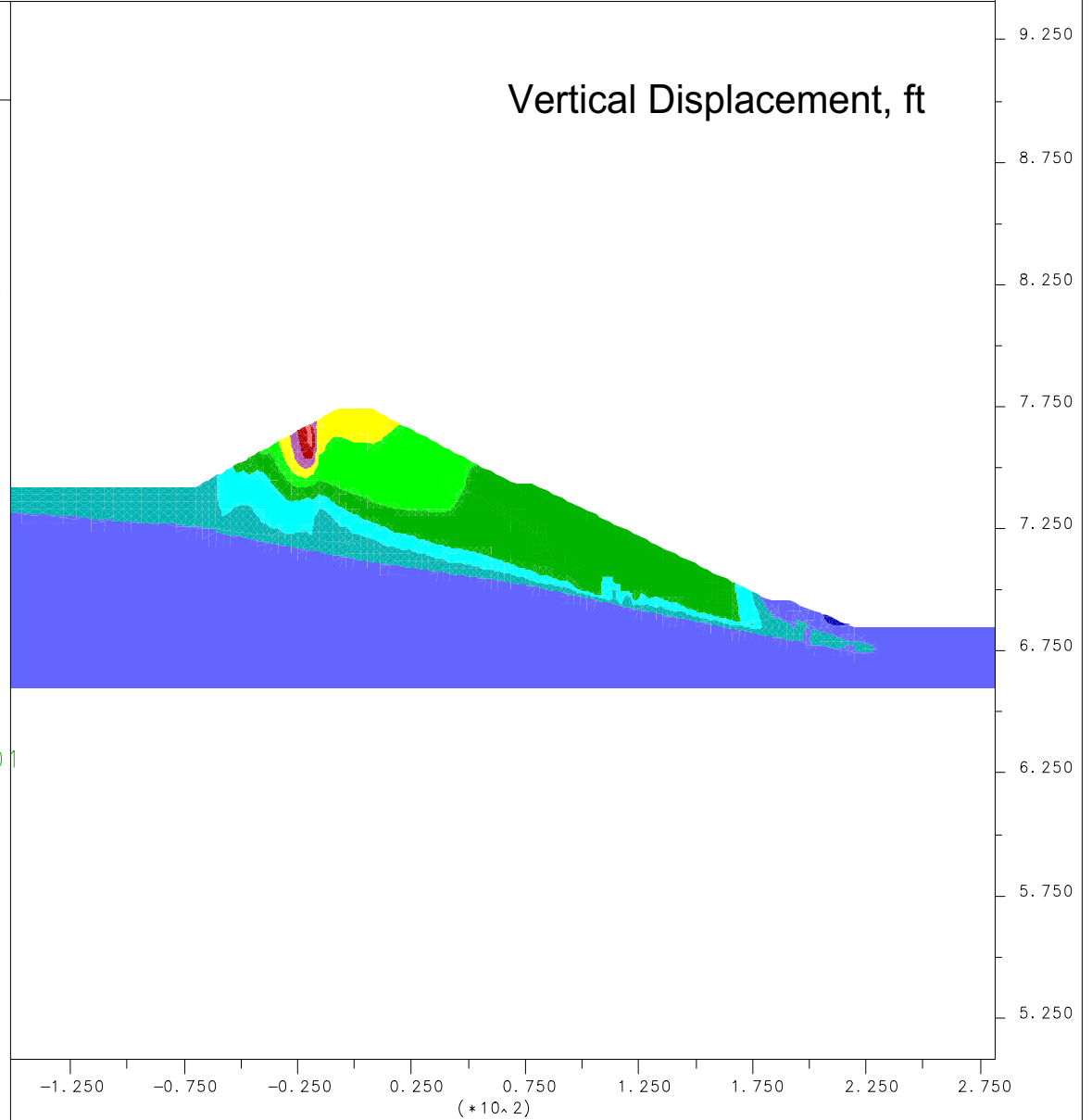
18-Nov-05 4:01
 step 4352489
 -1.512E+02 <x< 2.816E+02
 5.076E+02 <y< 9.404E+02

Y-displacement contours



Contour interval = 5.00E-01

Vertical Displacement, ft



Project No. 26814957	Estates Dam Seismic Stability Analysis	FLAC Dynamic Analysis with Cyclic Degradation Model Permanent Vertical Displacement Hayward MCE TH #1	Figure 12-18
URS			

FLAC (Version 4.00)

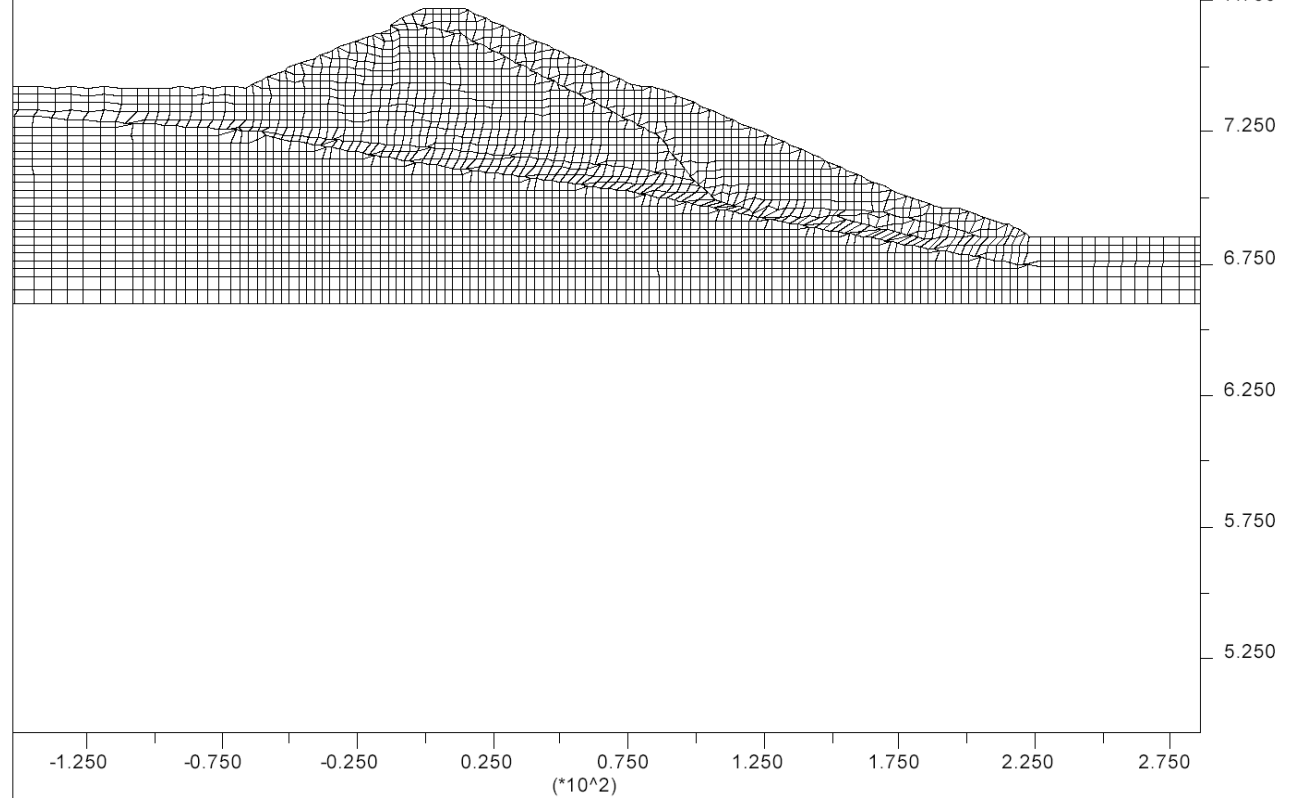
LEGEND

18-Nov-05 4:01
 step 4352489
 -1.522E+02 <x< 2.861E+02
 4.967E+02 <y< 9.350E+02

Exaggerated Grid Distortion

Magnification = 1.000E+00
 Max Disp = 8.166E+00

Deformed Mesh



Project No.
26814957

Estates Dam
Seismic Stability Analysis



FLAC Dynamic Analysis
with Cyclic Degradation Model
Deformed Mesh
Hayward MCE TH #1

Figure
12-19

FLAC (Version 4.00)

LEGEND

18-Nov-05 4:01
step 4352489

HISTORY PLOT

Y-axis :

usff_xdisp (FISH)

us_toe_xdisp (FISH)

us_slope_xdisp (FISH)

crest_xdisp (FISH)

ds_ub_xdisp (FISH)

ds_lb_xdisp (FISH)

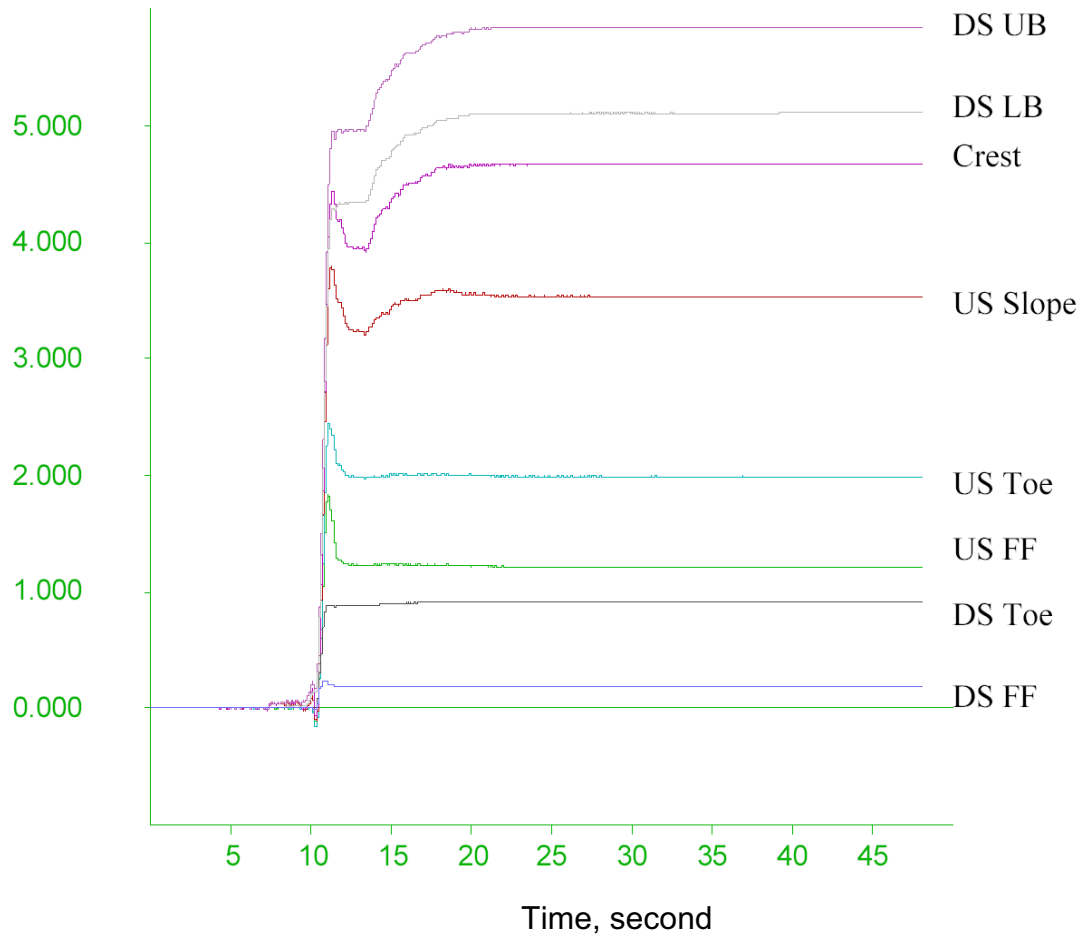
ds_toe_xdisp (FISH)

ds_ff_xdisp (FISH)

X-axis :

Dynamic time

Horizontal Displacement (ft)



Project No.
26814957

Estates Dam
Seismic Stability Analysis



FLAC Dynamic Analysis
with Cyclic Degradation Model
Horizontal Displacement Time Histories
Hayward MCE TH #1

Figure
12-20

FLAC (Version 4.00)

LEGEND

18-Nov-05 4:01
step 4352489

HISTORY PLOT

Y-axis :

Y displacement(5, 27)

Y displacement(25, 27)

Y displacement(35, 32)

Y displacement(48, 38)

Y displacement(72, 28)

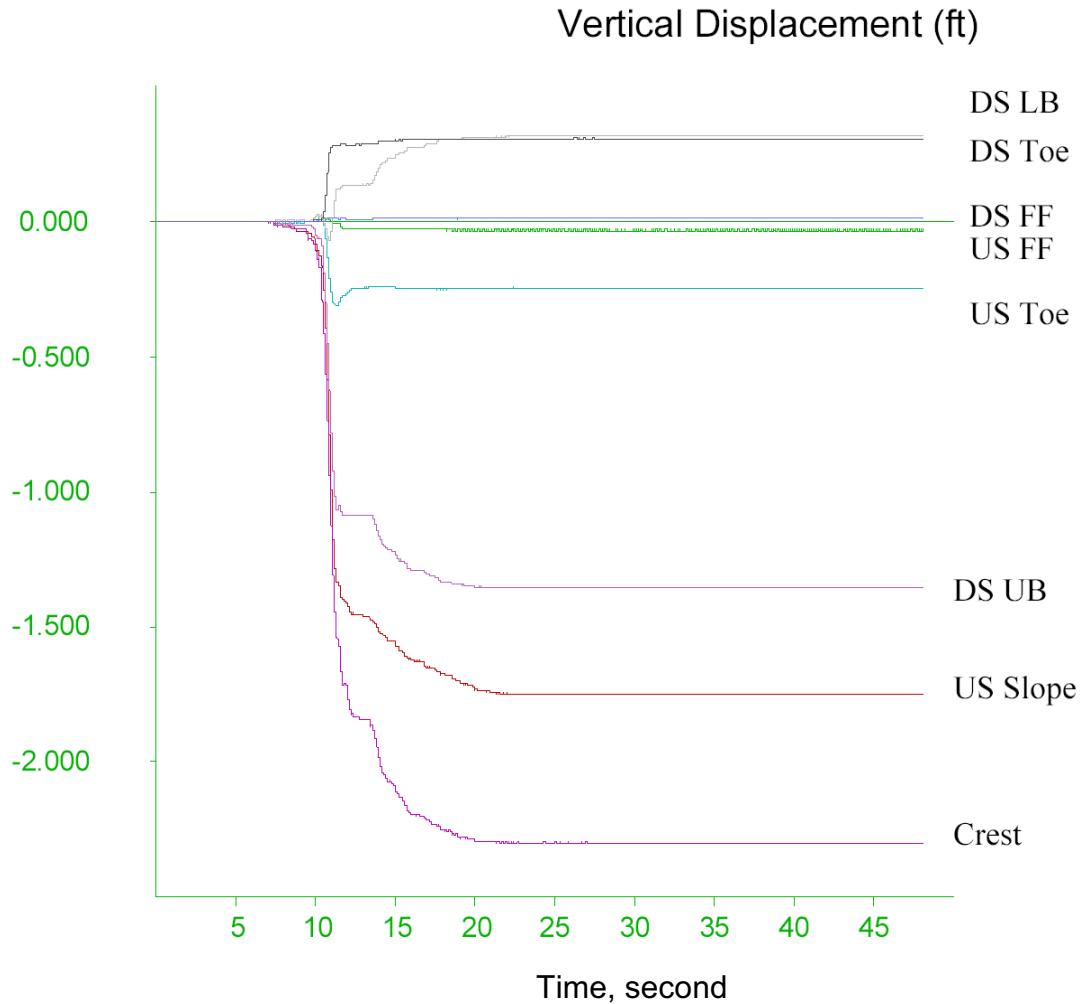
Y displacement(110, 12)

Y displacement(121, 8)

Y displacement(135, 8)

X-axis :

Dynamic time



Project No.
26814957

Estates Dam
Seismic Stability Analysis



FLAC Dynamic Analysis
with Cyclic Degradation Model
Vertical Displacement Time Histories
Hayward MCE TH #1

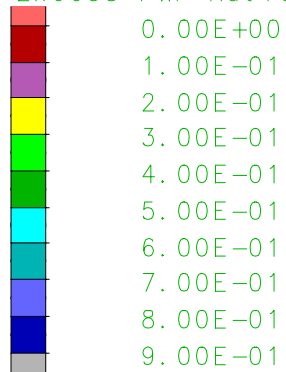
Figure
12-21

FLAC (Version 4.00)

LEGEND

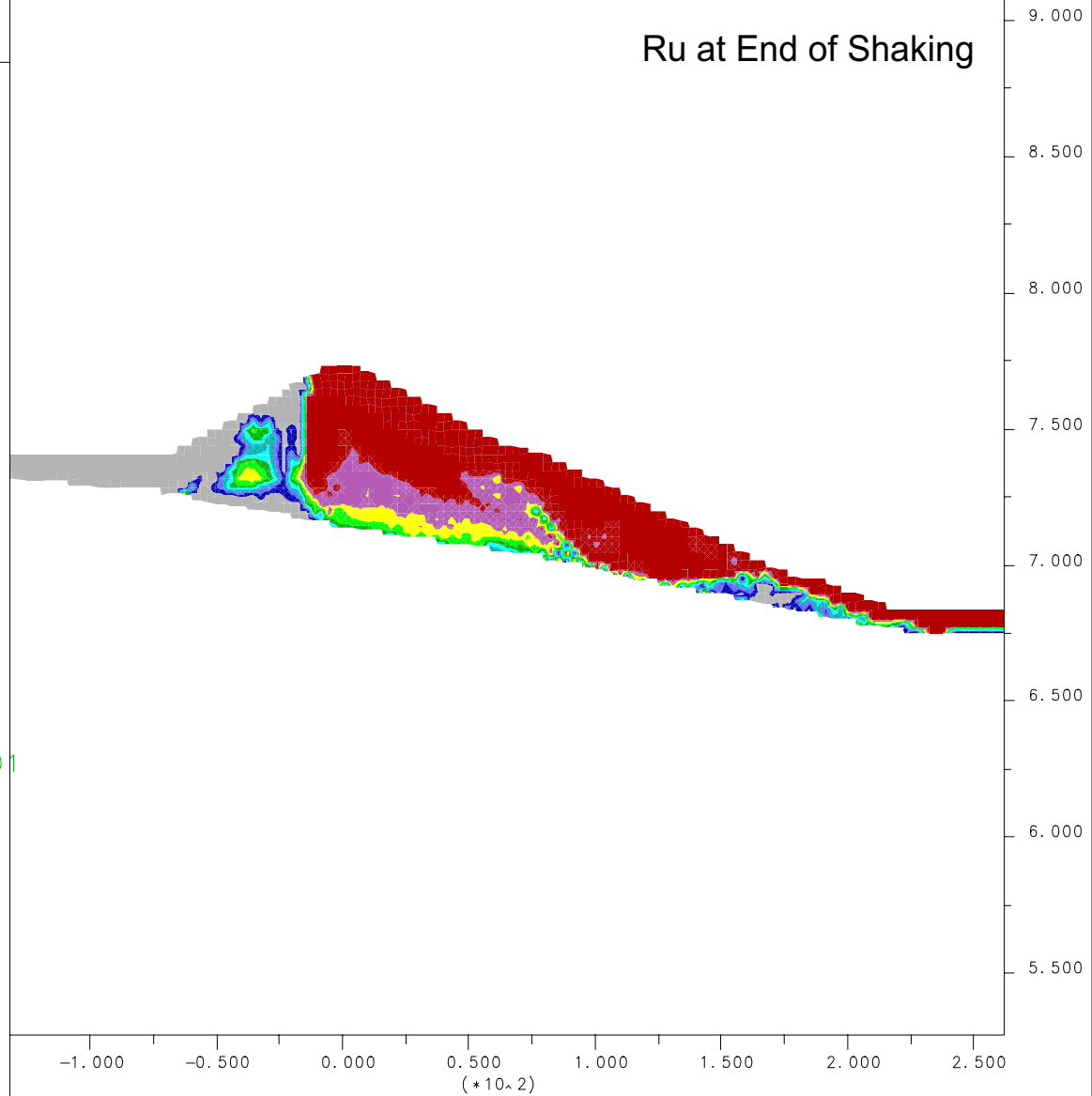
18-Nov-05 4:01
 step 4352489
 -1.316E+02 <x< 2.619E+02
 5.273E+02 <y< 9.207E+02

Excess PWP Ratio Ru



Contour interval = 1.00E-01

Ru at End of Shaking



Project No.
26814957

Estates Dam
Seismic Stability Analysis



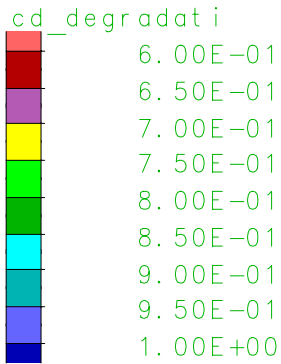
FLAC Dynamic Analysis
with Cyclic Degradation Model
Excess Pore Pressure Ratio Contour
Hayward MCE TH #1

Figure
12-22

FLAC (Version 4.00)

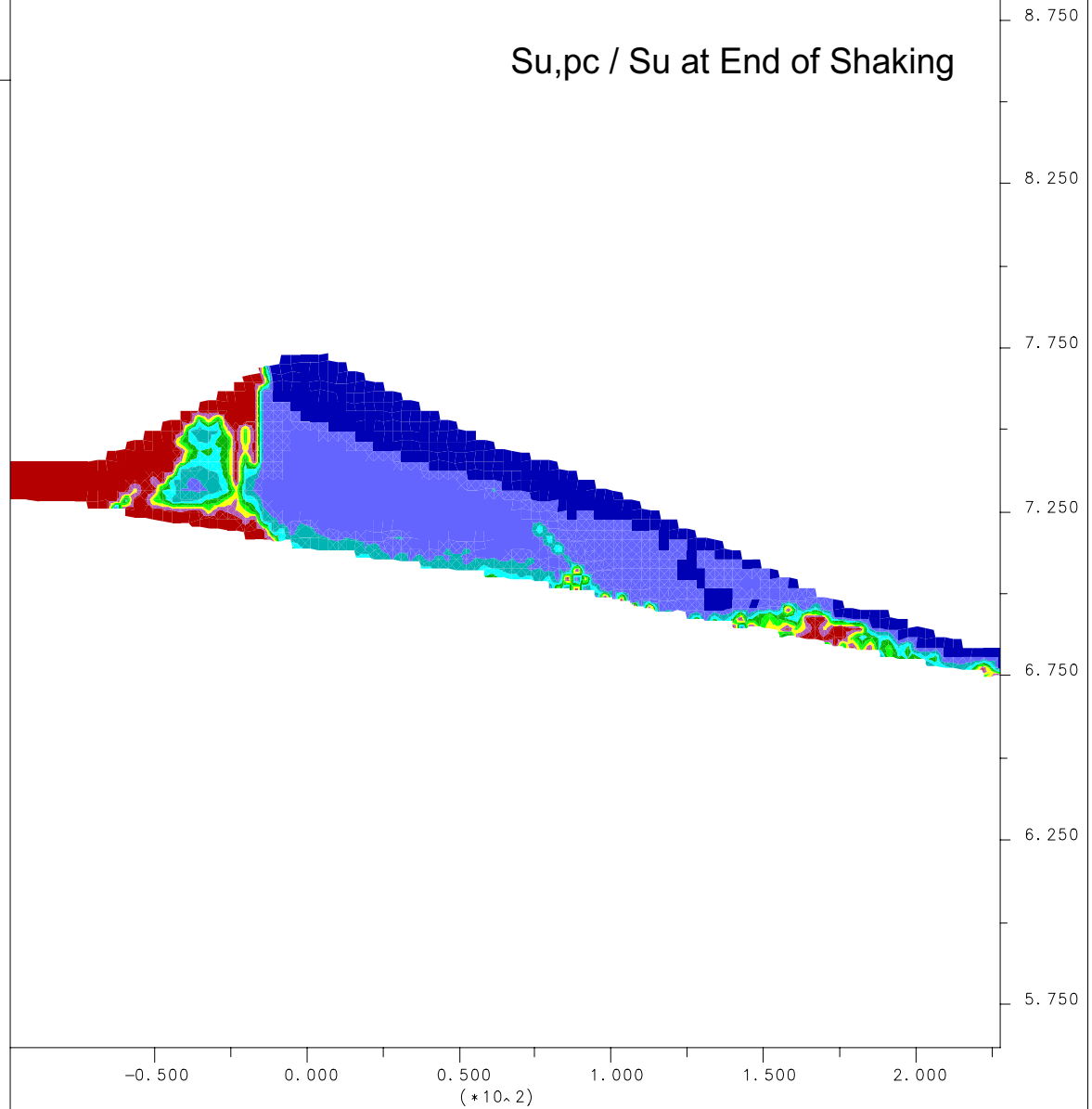
LEGEND

18-Nov-05 4:01
 step 4352489
 -9.741E+01 <x< 2.277E+02
 5.614E+02 <y< 8.866E+02



Contour interval= 5.00E-02

Su,pc / Su at End of Shaking



Project No.
26814957

Estates Dam
Seismic Stability Analysis



FLAC Dynamic Analysis
with Cyclic Degradation Model
Cyclic Degradation Contour
Hayward MCE TH #1

Figure
12-23

FLAC (Version 4.00)

LEGEND

15-Nov-05 6:49
 step 4325897
 -1.373E+02 <x< 2.554E+02
 5.362E+02 <y< 9.288E+02

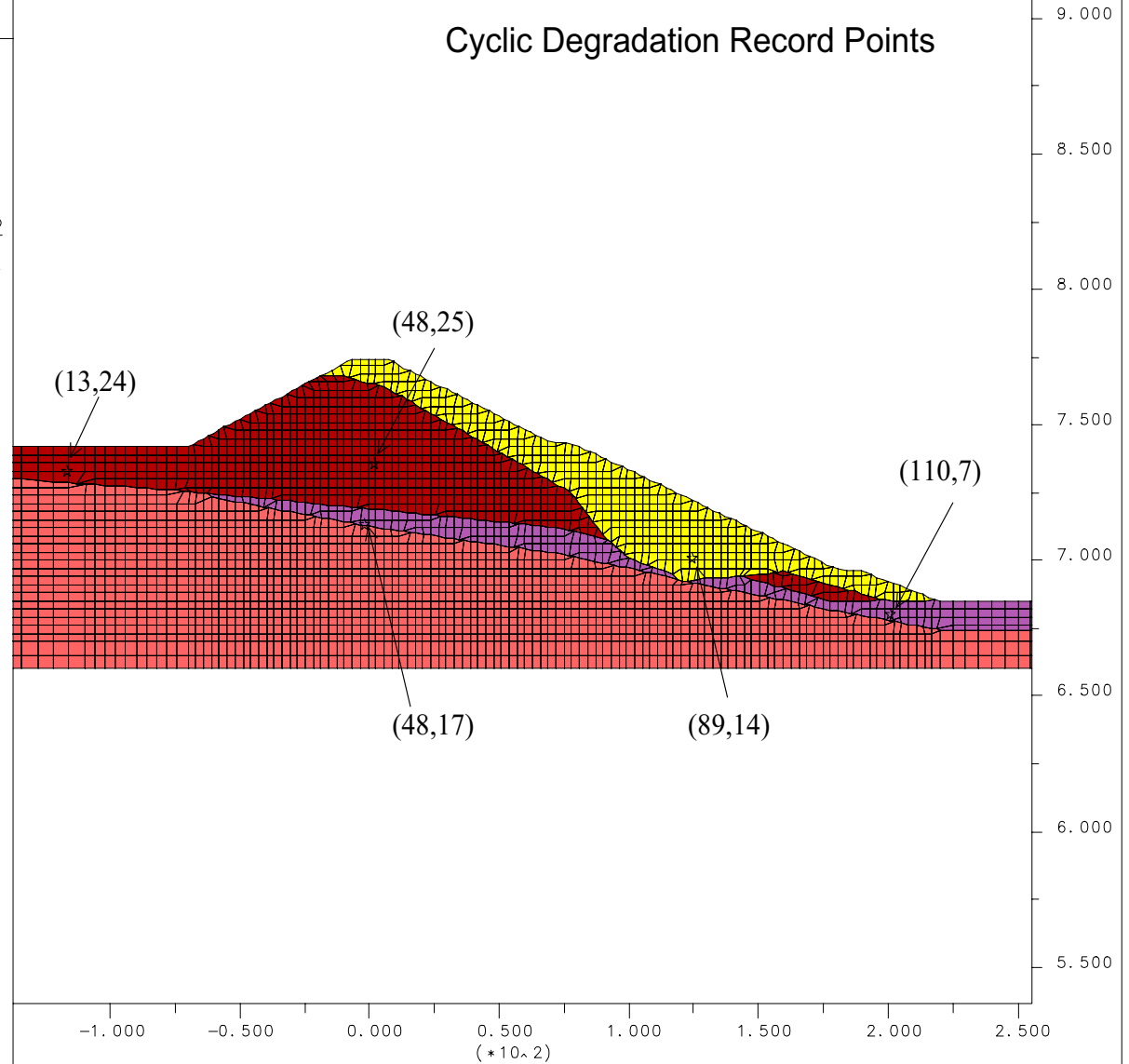
User-defined Groups

- Bedrock
- 1903_Fill
- Foundation_Soil
- 1938_Fill

Grid plot



Cyclic Degradation Record Points



Project No.
26814957

Estates Dam
Seismic Stability Analysis



FLAC Dynamic Analysis
with Cyclic Degradation Model
Locations of Cyclic Degradation TH

Figure
12-24

FLAC (Version 4.00)

LEGEND

18-Nov-05 4:01
step 4352489

HISTORY PLOT

Y-axis :

cd_degradati (13, 24) UDP

cd_degradati (48, 25) UDP

cd_degradati (48, 17) UDP

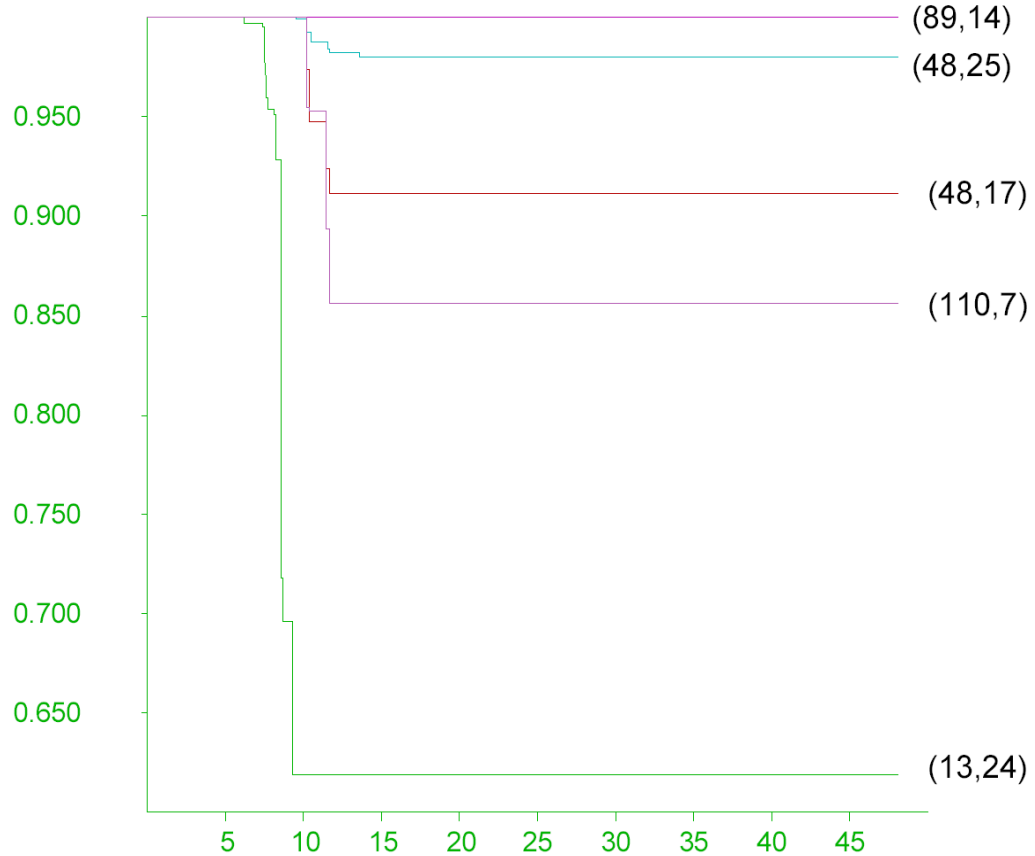
cd_degradati (89, 14) UDP

cd_degradati (110, 7) UDP

X-axis :

Dynamic time

Undrained Strength Degradation



Project No.
26814957

Estates Dam
Seismic Stability Analysis



FLAC Dynamic Analysis
with Cyclic Degradation Model
Cyclic Degradation Time Histories
Hayward MCE TH #1

Figure
12-25

As described in Section 3, the dam is located at the head of a ravine. As shown in Figure 13-1, the dam geometry is that of a relatively narrow wedge confined by the abutments on both sides. This geometry may have significant three-dimensional (3-D) effects on the overall stability and seismic performance of the dam. This section presents the analyses performed to assess such 3-D stability effects.

13.1 APPROACH

A 3-D model of the dam and foundation was first developed based on the available geotechnical and piezometric data. Static and pseudo-static slope stability analyses were subsequently performed using the 3-D model and 3-D limit equilibrium analysis procedures. From these 3-D slope stability analyses, the critical 3-D downstream sliding block was identified and its yield acceleration coefficients under pre- and post-earthquake conditions were calculated. The corresponding mass acceleration time history of the critical 3-D block for the design earthquake was estimated by combining the mass accelerations calculated from 2-D dynamic response analyses on two transverse sections of the dam. The estimated average mass acceleration time history for the 3-D block was then used, together with the corresponding yield acceleration coefficients, in Newmark-type analyses to calculate the seismic horizontal displacement of the block.

13.2 THREE DIMENSIONAL SLOPE STABILITY ANALYSIS

The 3-D slope stability analyses were performed using the computer code CLARA (Hung, 1988). CLARA uses limit equilibrium procedures to calculate the factor of safety against instability of a 3-D sliding mass. It is designed primarily for 3-D slope stability analyses, but can also be used in two-dimensional (2-D) mode to perform 2-D stability analyses. The shear strength parameters used for the CLARA analyses are the same as those used in the stability analyses with FLAC (see Section 12).

Based on the available geotechnical and piezometric data, nine transverse cross sections were developed along the length of the dam to define its 3-D geometry. These nine sections, which include section A-A' used for the 2-D stability analyses (see Section 9), were idealized and input to CLARA. From these data the program interpolated the various zone boundaries to create a 3-D model of the embankment and foundation as shown in Figure 13-2. Examples of the dam cross sections interpolated by CLARA are shown in Figures 13-3 and 13-4. The cross section shown in Figure 13-3 is cut 4 feet to the right of the section A-A'. The section shown in Figure 13-4 is cut parallel to and 5 feet downstream of the axis of the dam.

In addition to the 3-D model described above, a 2-D model was independently developed with CLARA to represent section A-A' used in the 2-D stability analyses described in Sections 9 through 12. As a check of the CLARA input strength parameters, the slope stability of the 2-D model was analyzed with CLARA and the results were compared with those obtained from the 2-D analyses with UTEXAS. The factors of safety computed with CLARA for downstream block No.2 under static, pre- and post-earthquake conditions are summarized in Table 13-1. The CLARA-calculated factors of safety are very similar to the values calculated with UTEXAS (see Figures 9-5 and 11-3).

The factors of safety for block No. 2 were also calculated with CLARA in 2-D mode using the 3-D embankment and foundation model. This analysis neglects the 3-D effects on stability and provides a check of the 3-D model geometry for the maximum section. The computed factors of safety under static, pre- and post-earthquake conditions are summarized in Table 13-1, and are very similar to those calculated with UTEXAS and with the CLARA 2-D model.

The yield acceleration coefficients for downstream block No. 2 were also calculated with CLARA in 2-D mode. The values of K_y under pre- and post-earthquake conditions are 0.11 and 0.03, respectively (Table 13-1). These values are slightly lower than those computed with UTEXAS.

Upon completion of the above checks, the 3-D model was analyzed in 3-D mode. A search for the critical 3-D sliding block was performed by varying the location and shape of an ellipsoidal sliding surface until the minimum factor of safety was found. The calculated 3-D factors of safety are summarized in Table 13-1. Under the same loading conditions, the 3-D factors of safety are systematically higher than the 2-D factors of safety. This difference in the calculated factor of safety is expected because of the restraining effects imposed by the limited extent of the 3-D failure surface. The critical 3-D sliding block was found to be slightly shallower than block No.2 in the 2-D analyses. The shape of the critical 3-D sliding block under post-earthquake conditions is illustrated in Figures 13-5 through 13-9.

As shown in Table 13-1, the values of yield acceleration coefficient (K_y) also increase substantially when 3-D stability effects are considered. The minimum K_y value under post-earthquake conditions, which has a large effect on the calculated seismic displacement, shows the largest increase from 0.03 to 0.13.

13.3 DYNAMIC RESPONSE ANALYSIS

To estimate the time history of average mass acceleration for the critical 3-D sliding block, an additional 2-D section (Section C-C') was constructed and analyzed with QUAD4M. Section C-C' is located 55 feet to the right of section A-A' and is shown in Figure 13-6. Its location with respect to section A-A' is shown in Figures 13-1 and 13-7 through 13-9.

The intersection of the slip surface of the critical 3-D sliding block on sections A-A' and C-C' was used to define corresponding 2-D sliding blocks on those sections for dynamic response analysis using QUAD4M, as shown in Figures 13-10 and 13-11. The QUAD4M analyses were performed for Hayward fault MCE time histories Nos. 1 and 2. The methodology and material properties used for these analyses are described in Section 10.

The computed average mass acceleration time histories for the 2-D sliding blocks are shown in Figures 13-12 and 13-13. The computed time histories for sections A-A' and C-C' are generally similar in amplitude and in-phase. Thus, it seems reasonable to use a weighted-average to estimate the overall 3-D average mass acceleration from these individual 2-D time histories. The weighted average mass acceleration time histories for the critical 3-D sliding block are shown in Figures 13-14 and 13-15.

13.4 DEFORMATION ANALYSIS RESULTS

The horizontal seismic displacements of the critical 3-D sliding block were estimated by double-integrating the difference between the average mass acceleration and the yield acceleration, K_y , in a Newmark-type analysis. The K_y values of the 3-D sliding block for pre-earthquake and post-earthquake conditions with 10 and 20 percent strength reduction are 0.22, 0.17 and 0.13, respectively. The timings of strength reduction used in constructing the time histories of yield acceleration are the same as those presented in Section 11. The results of the Newmark-type analyses for the 3-D sliding block are shown in Figures 13-14 and 13-15. The 3-D results are compared with the 2-D results in Table 13-2.

From these analyses, it is concluded that the 3-D geometry of the dam has a significant effect on the calculated seismic deformations for the design earthquake. In general, the calculated horizontal seismic displacements considering 3-D effects are between one-half ($1/2$) and four-fifths ($4/5$) of those calculated assuming 2-D conditions. The results shown in Table 13-2 suggest that a reasonable average for the ratio between horizontal seismic displacements calculated considering 3-D effects and assuming 2-D conditions is about two-thirds ($2/3$).

**Table 13-1
Calculated Factors of Safety and Yield Acceleration Coefficients**

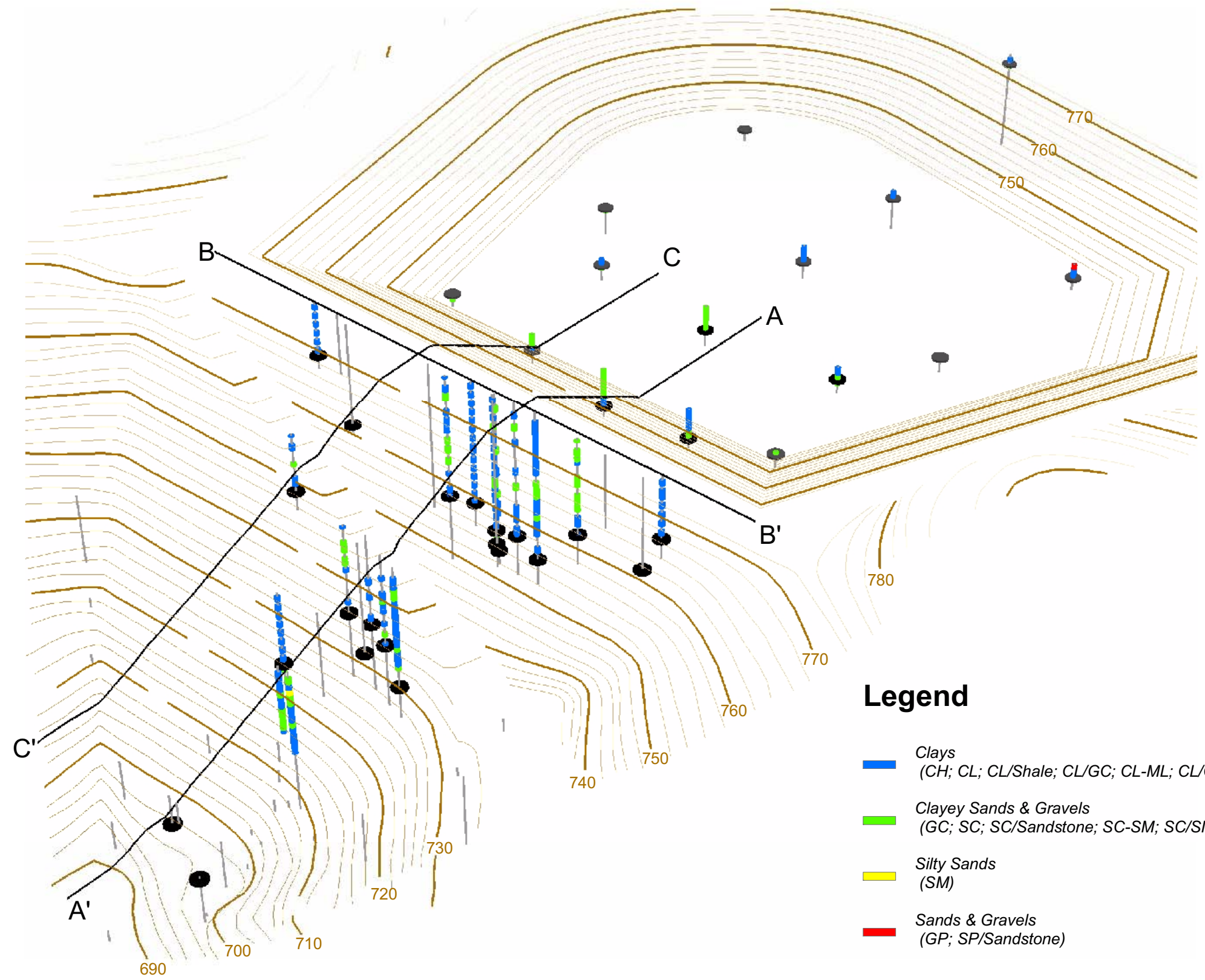
Loading Condition	UTEXAS 2-D Model	CLARA 2-D Model	CLARA 2-D Mode 3-D Model	CLARA 3-D Mode 3-D Model
Long term static	1.35	1.32	1.31	1.53
Pre-earthquake	1.37 / 0.15	1.32	1.32 / 0.11	1.67 / 0.22
Post-earthquake	1.13 / 0.05	1.10	1.09 / 0.03	1.44 / 0.13

Note:

(1) Dual values are factor of safety and yield acceleration coefficient, respectively.

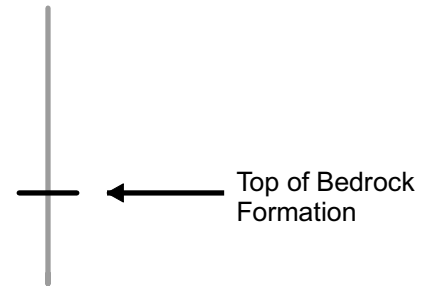
**Table 13-2
Calculated Downstream Horizontal Displacements (in feet)**

Earthquake	Time History	Ground Motion Polarity	Newmark Type 2-D Analysis	Newmark Type 3-D Analysis
Hayward fault MCE	#1	Standard	3	2
		Reverse	5	4
	#2	Standard	4	2
		Reverse	11	6

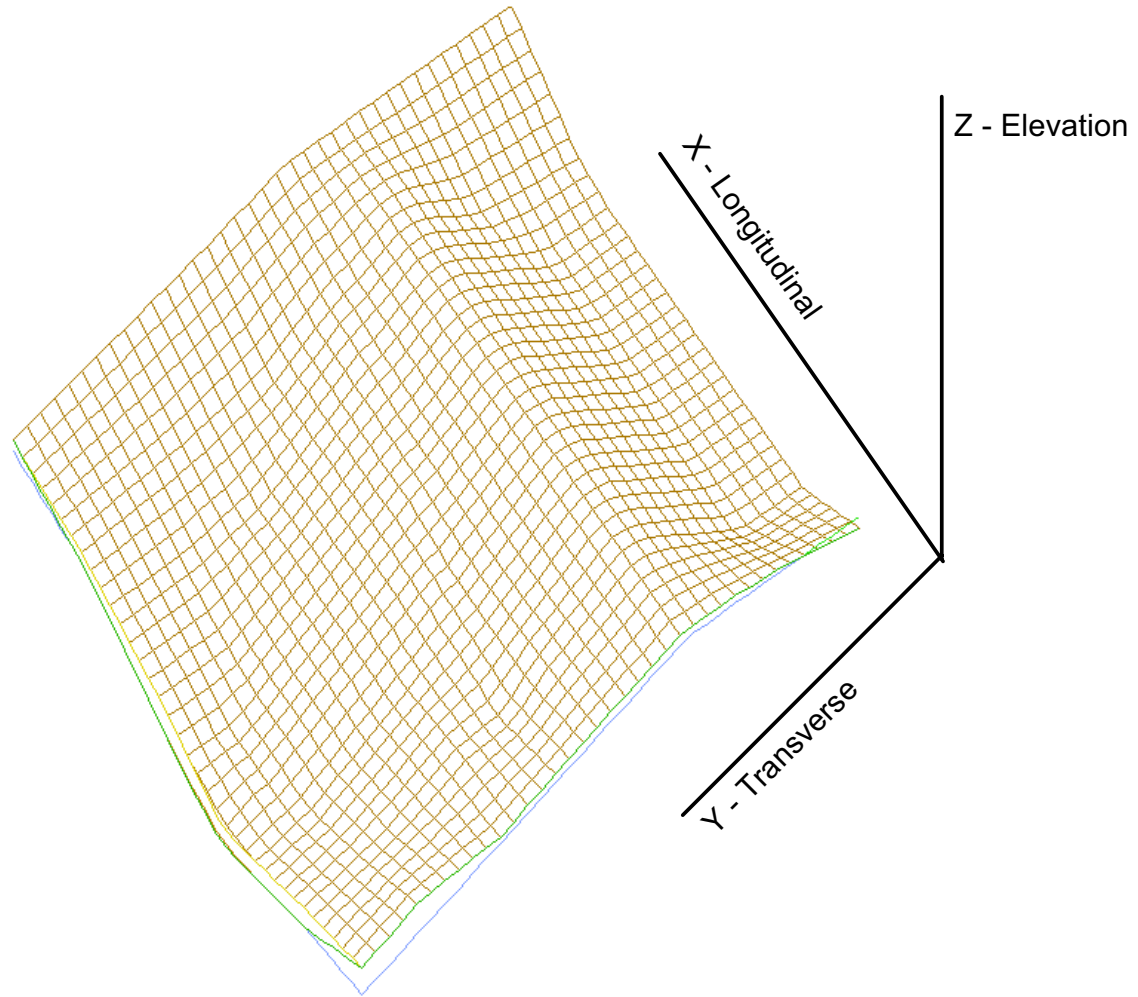


Legend

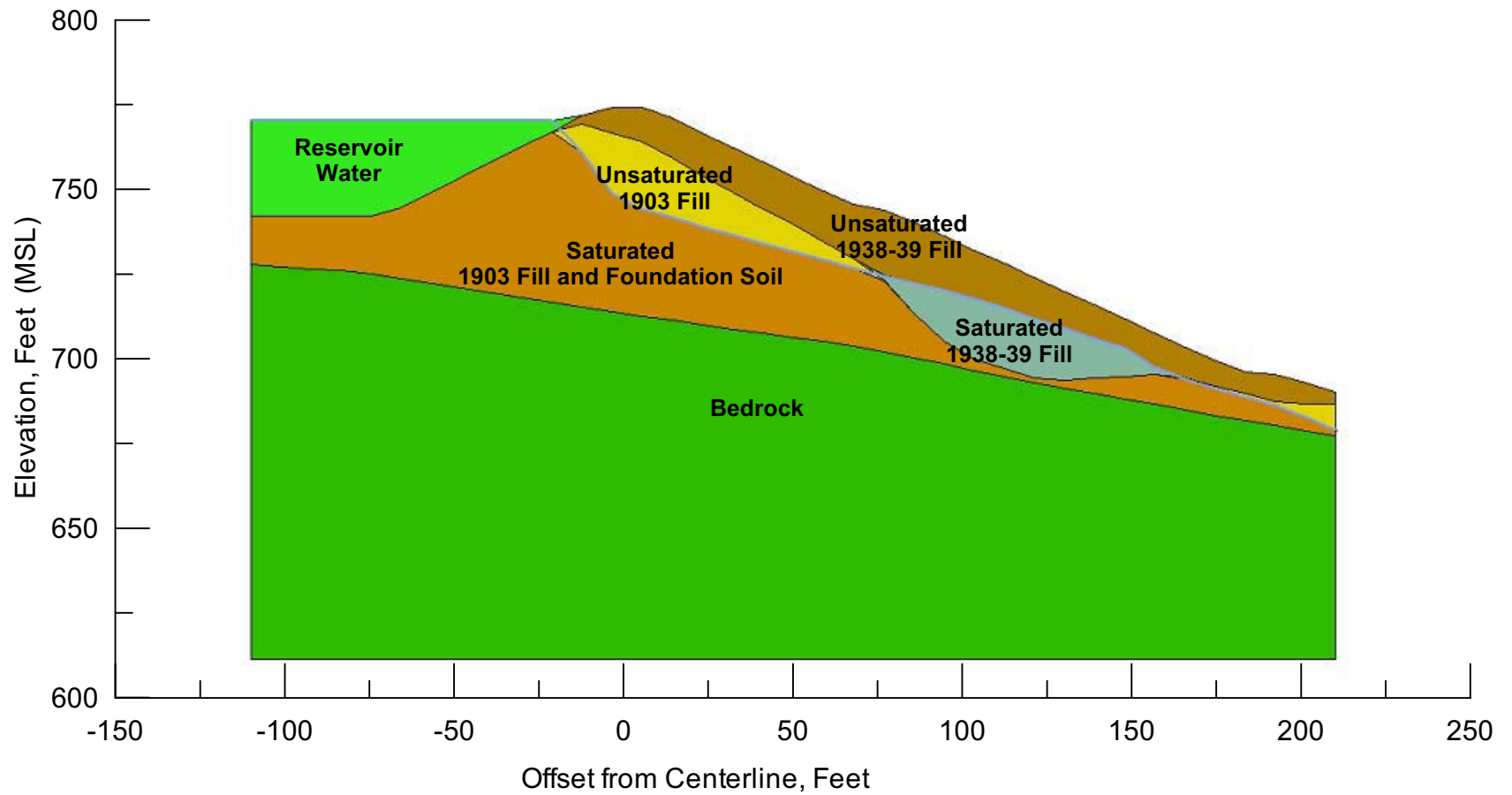
- █ Clays
(CH; CL; CL/Shale; CL/GC; CL-ML; CL/CH)
- █ Clayey Sands & Gravels
(GC; SC; SC/Sandstone; SC-SM; SC/SM)
- █ Silty Sands
(SM)
- █ Sands & Gravels
(GP; SP/Sandstone)



URS	Estates Dam Seismic Stability	Isometric View of Dam Geometry and Sections A-A' and C-C'	Figure 13-1
	26814957		



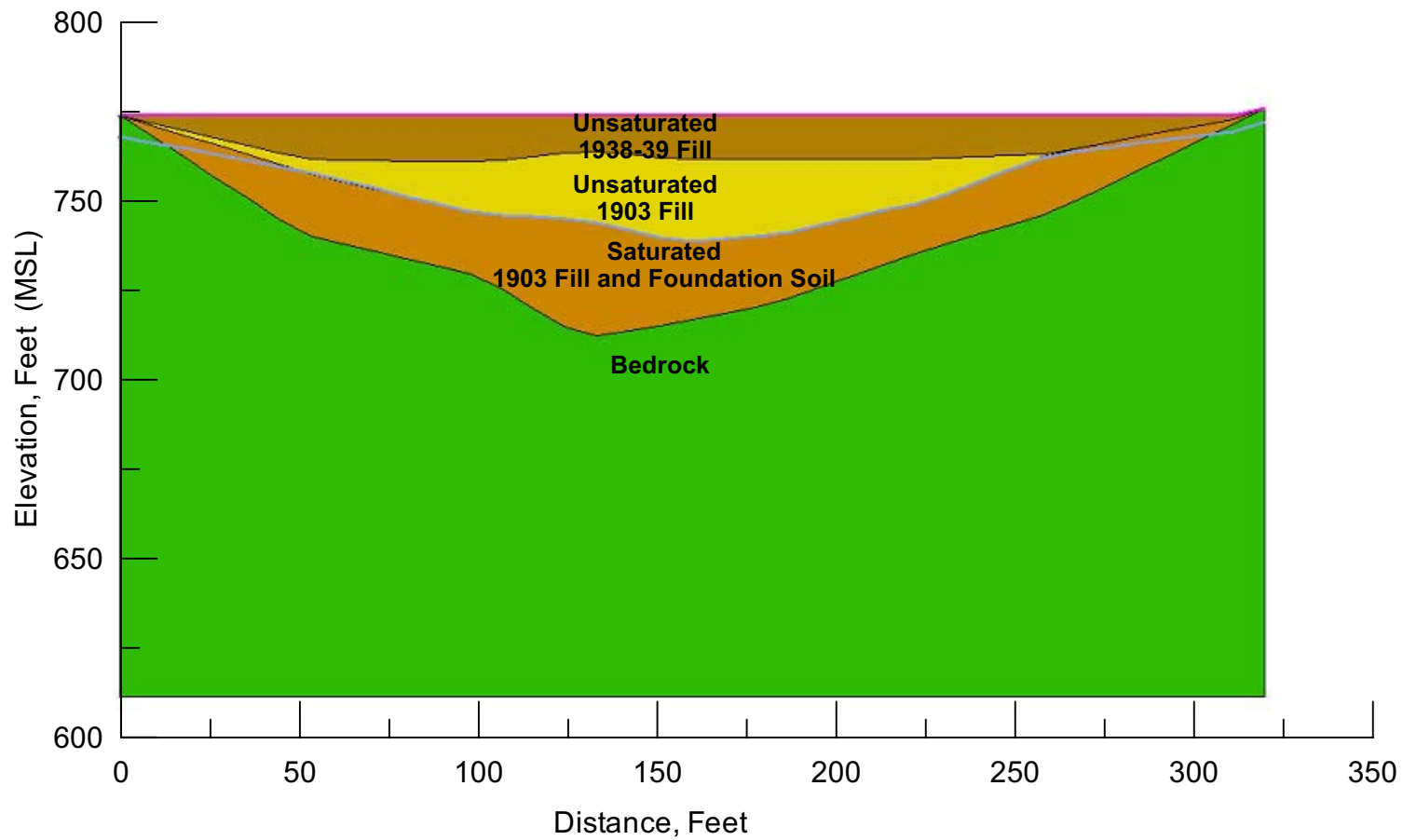
Project No. 26814957	Estates Dam Seismic Stability Analysis	Isometric View of the 3-D Dam Model 3-D Slope Stability Analysis	Figure 13-2
URS			



Note:

Section at Distance = 133 feet in Figure 13-4

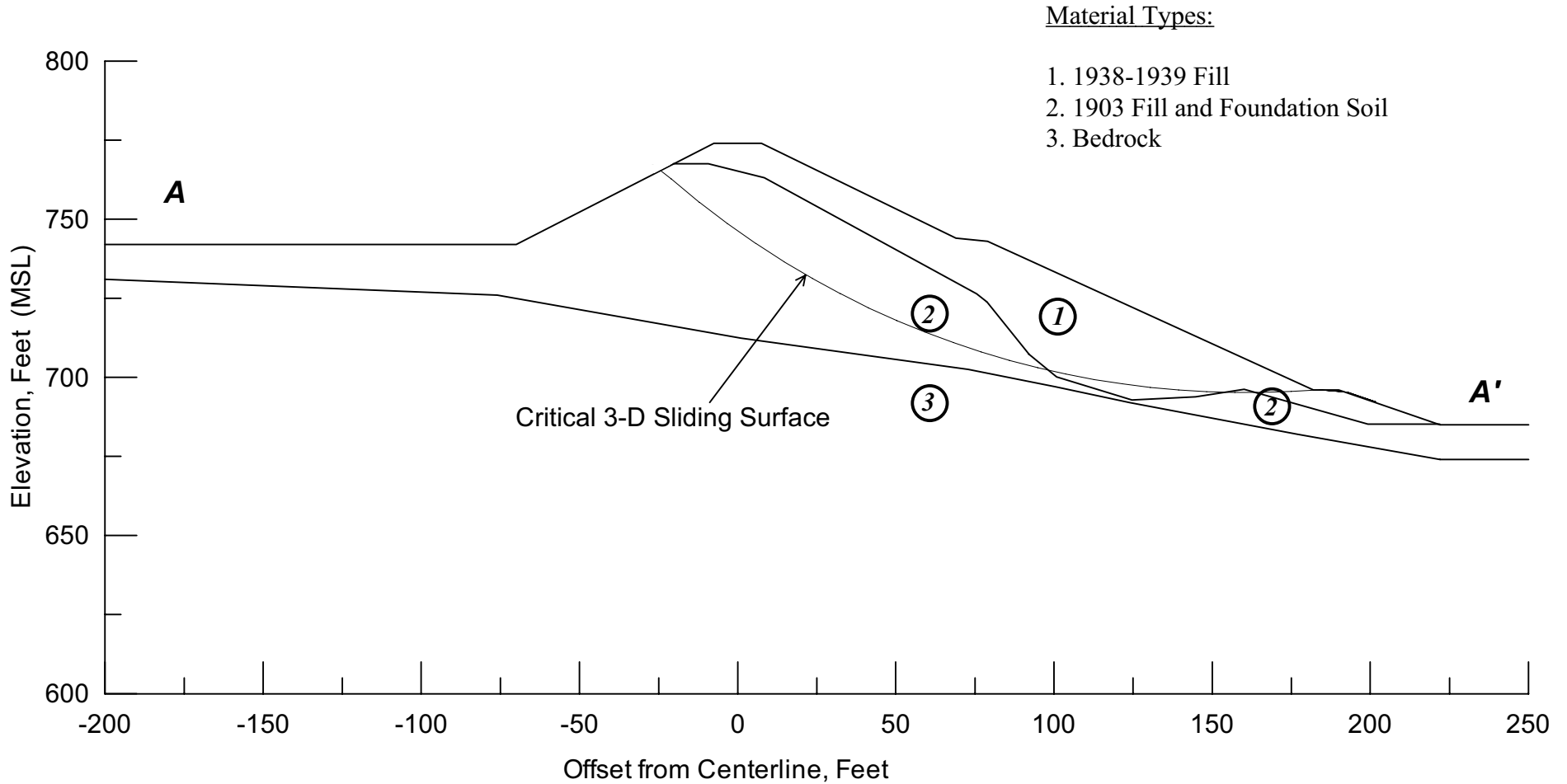
Project No. 26814957	Estates Dam Seismic Stability Analysis	Example of Interpolated Transverse Cross Section From CLARA 3-D Slope Stability Analysis	Figure 13-3
URS			



Note:

Section at Offset = 5 feet in Figure 13-3

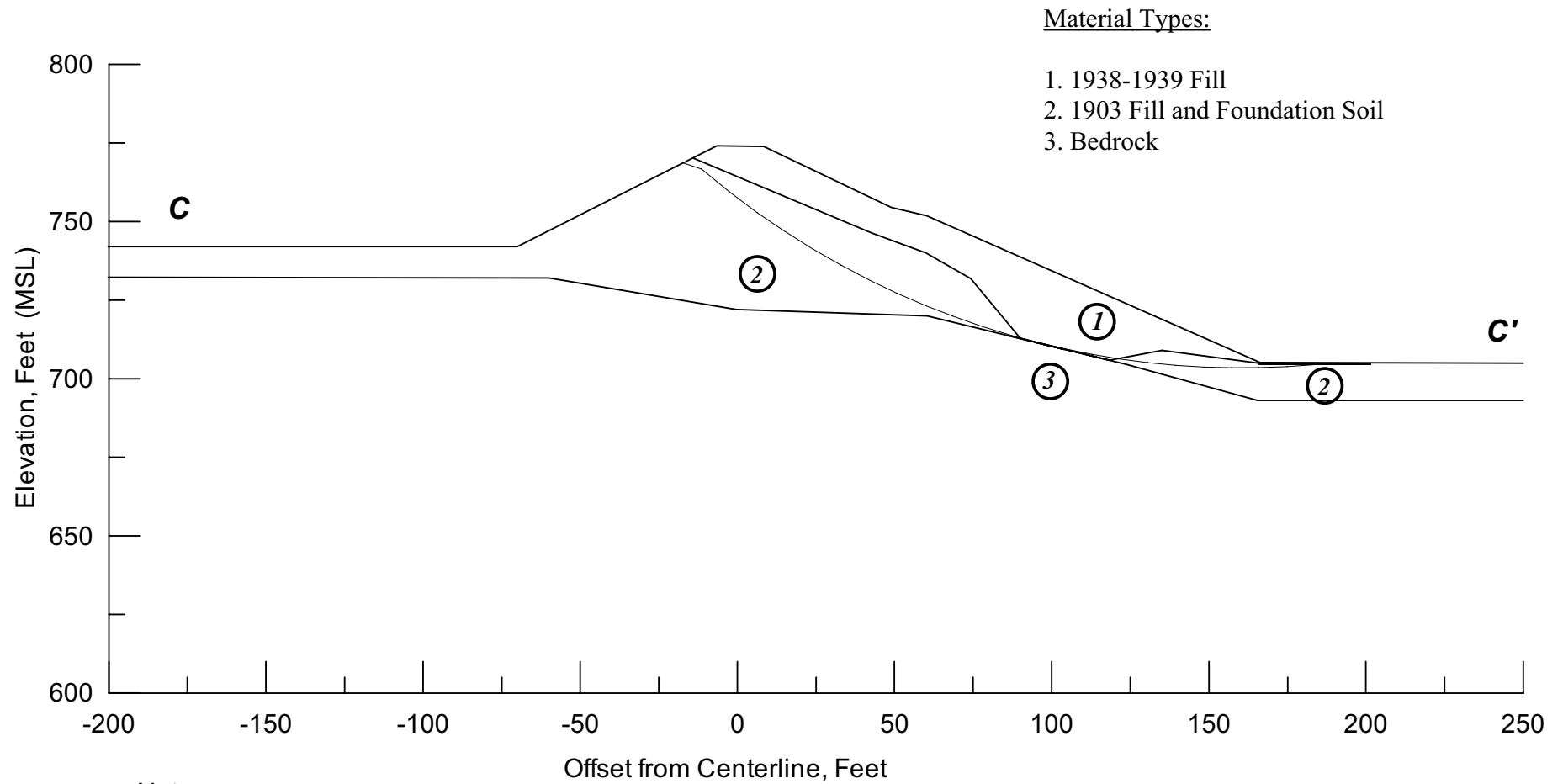
Project No. 26814957	Estates Dam Seismic Stability Analysis	Example of Interpolated Longitudinal Cross Section From CLARA 3-D Slope Stability Analysis	Figure 13-4
URS			



Note:

Section A-A' at Distance = 129 feet in Figure 13-4.

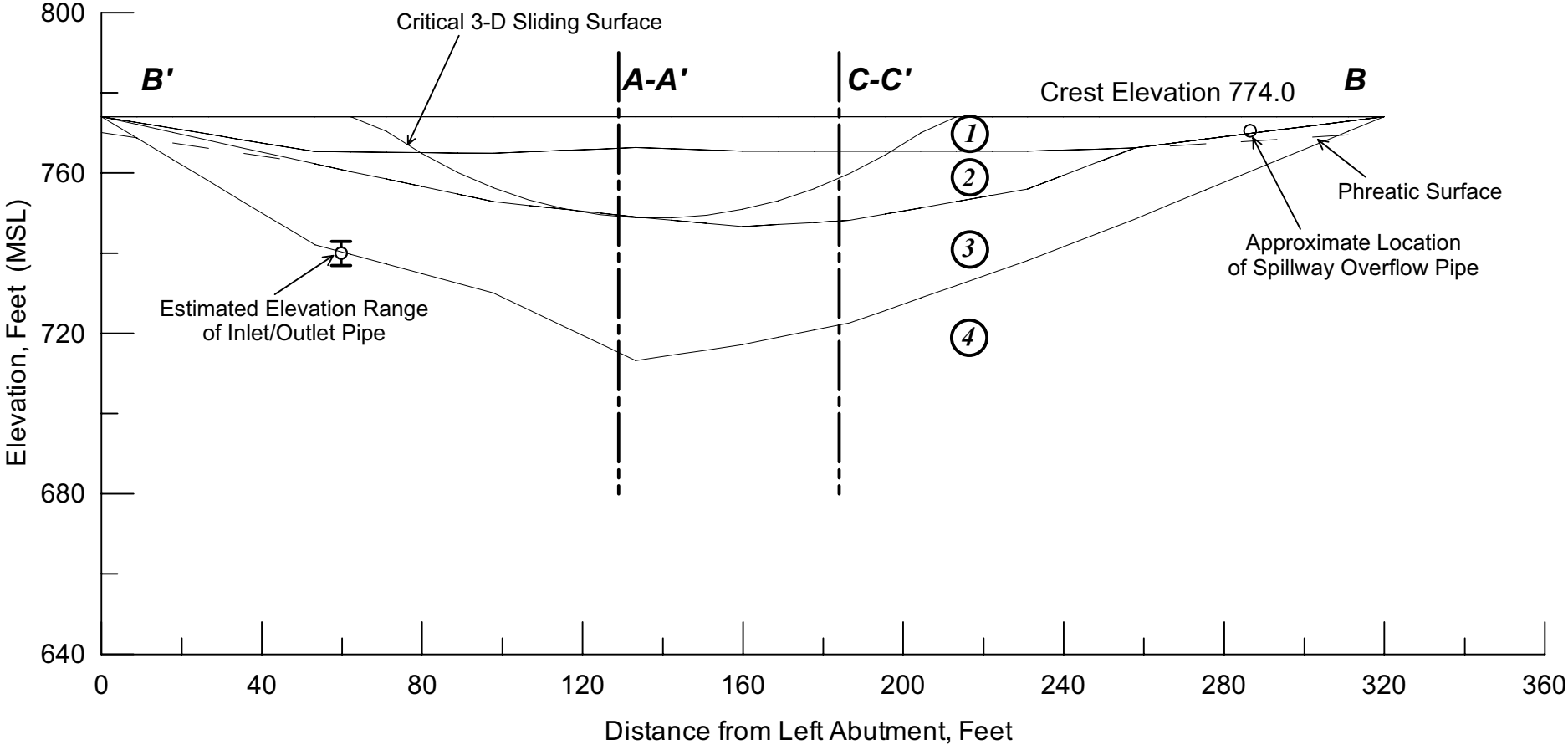
Project No. 26814957	Estates Dam Seismic Stability Analysis	Profile of Critical 3-D Sliding Block on Cross-Section A-A' 3-D Slope Stability Analysis Post-Earthquake Conditions	Figure
URS			13-5



Project No. 26814957	Estates Dam Seismic Stability Analysis	Profile of Critical 3-D Sliding Block on Cross Section C-C' 3-D Slope Stability Analysis Post-Earthquake Conditions	Figure
URS			13-6

Material Types:

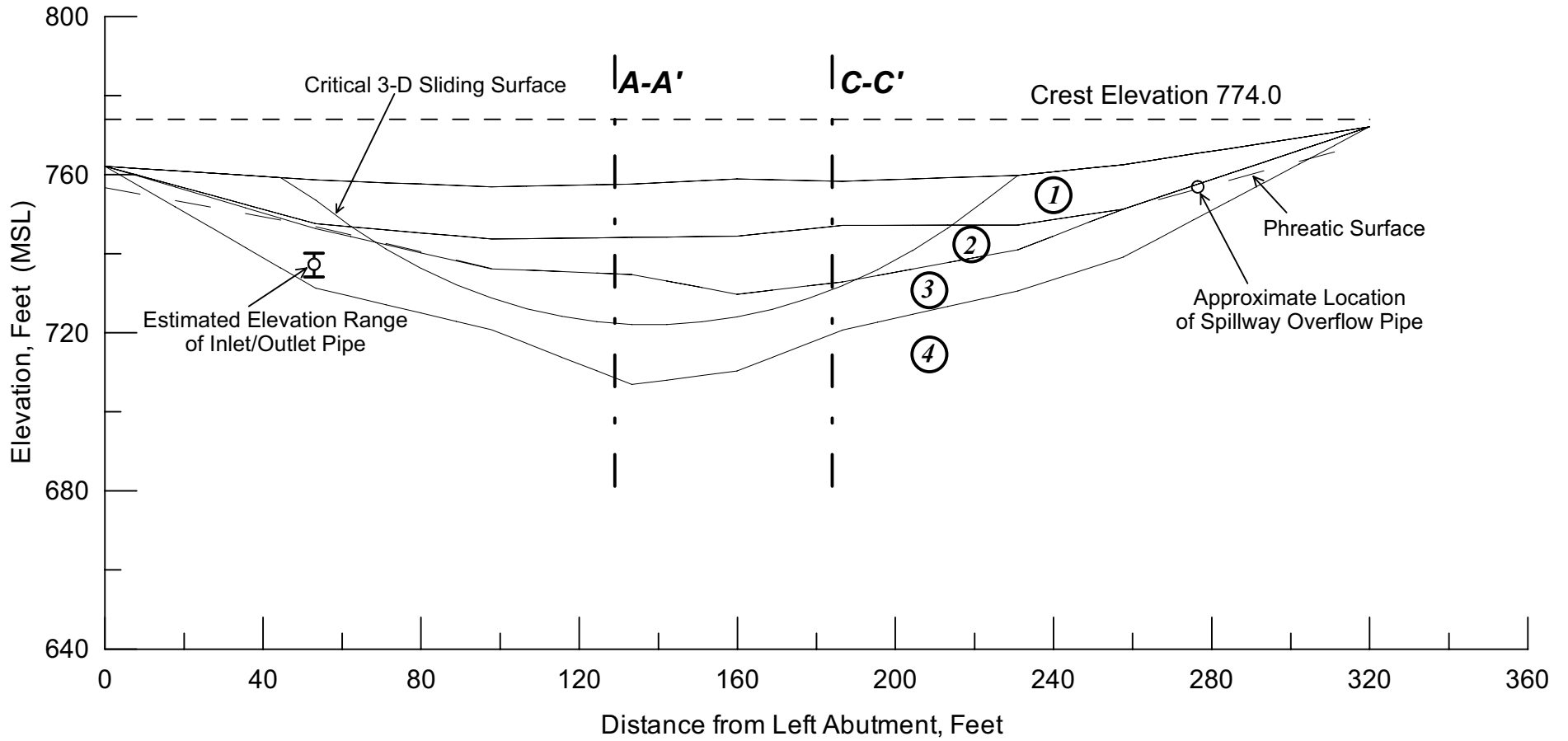
- 1. Unsaturated 1938-1939 Fill
- 2. Unsaturated 1903 Fill
- 3. Saturated 1903 Fill and Foundation Soil
- 4. Bedrock



Project No. 26814957	Estates Dam Seismic Stability Analysis	Profile of Critical 3-D Sliding Block on Longitudinal Section at Offset = 0 3-D Slope Stability Analysis	Figure 13-7
URS			

Material Types:

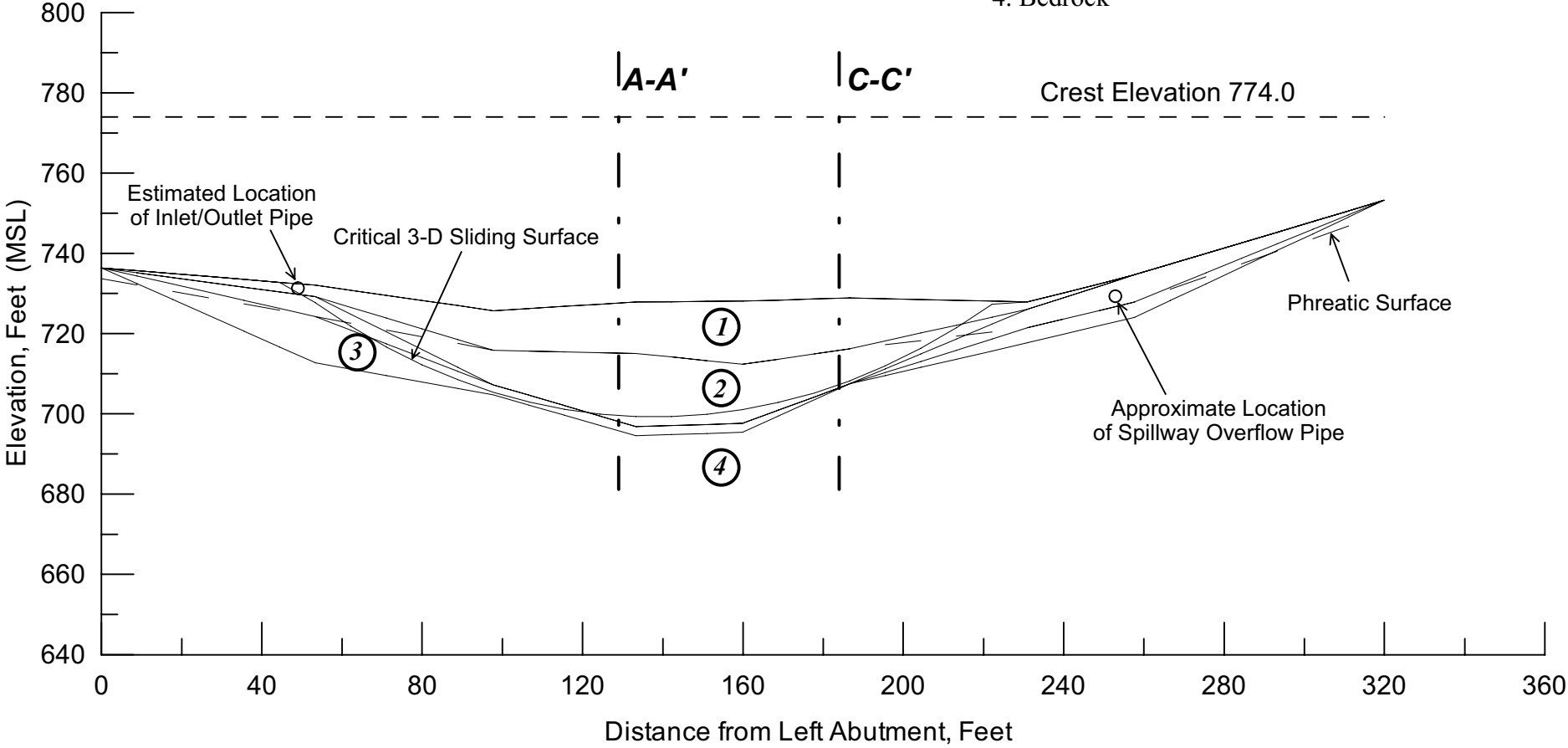
1. Unsaturated 1938-1939 Fill
2. Unsaturated 1903 Fill
3. Saturated 1903 Fill and Foundation Soil
4. Bedrock



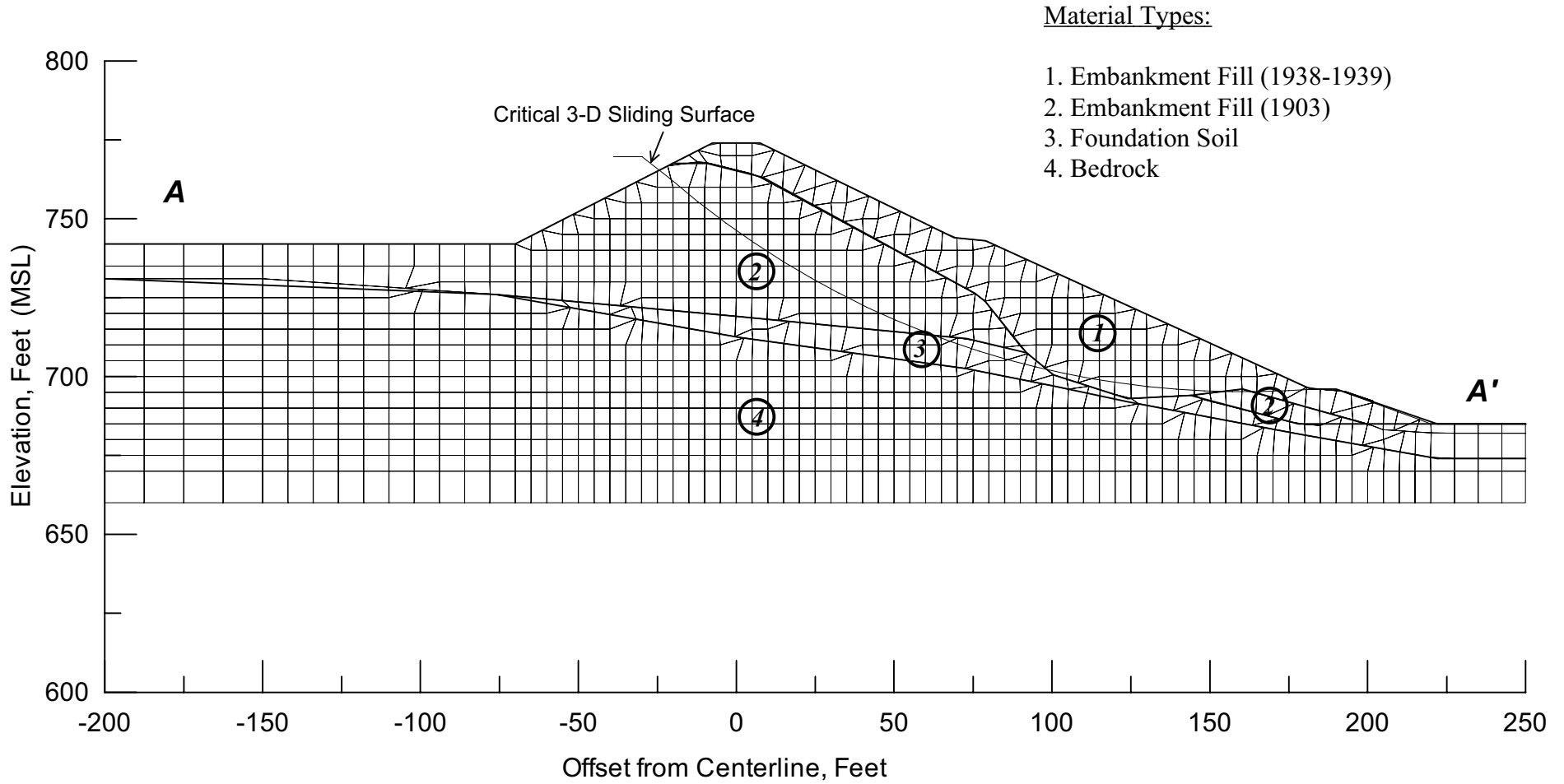
Project No. 26814957	Estates Dam Seismic Stability Analysis	Profile of Critical 3-D Sliding Block on Longitudinal Section at Offset = 40 ft 3-D Slope Stability Analysis	Figure 13-8
URS			

Material Types:

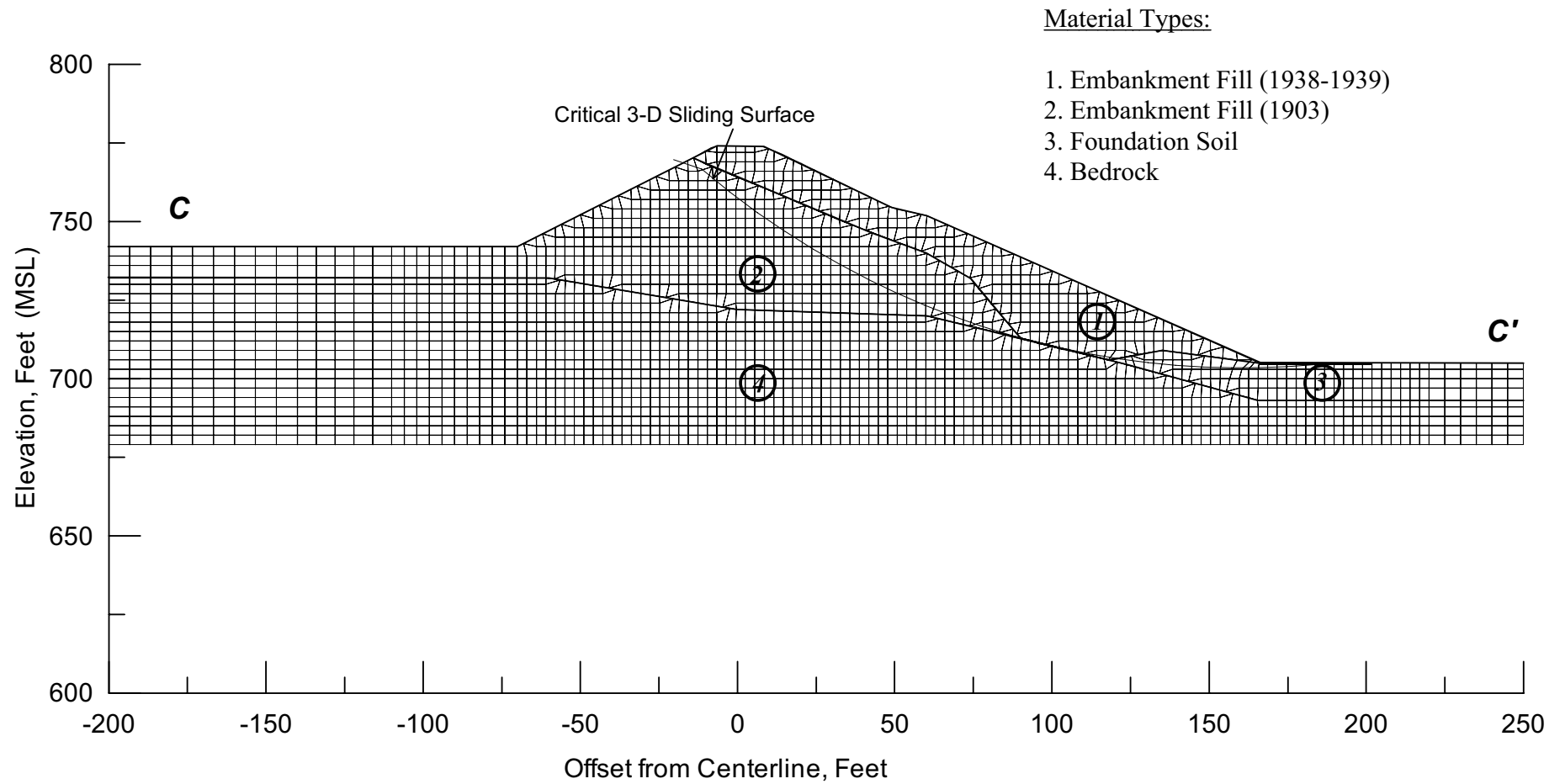
- 1. Unsaturated 1938-1939 Fill
- 2. Saturated 1938-39 Fill
- 3. Saturated 1903 Fill and Foundation Soil
- 4. Bedrock



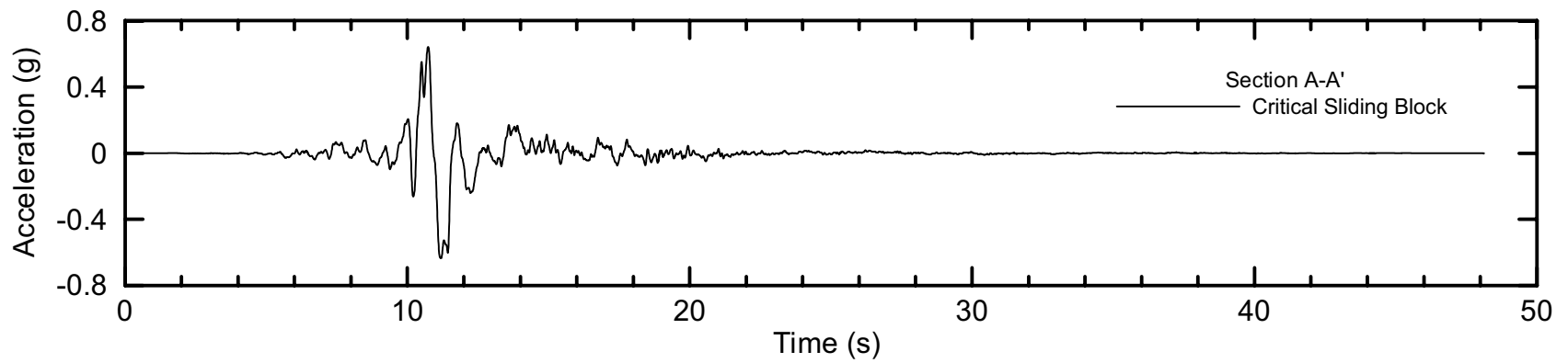
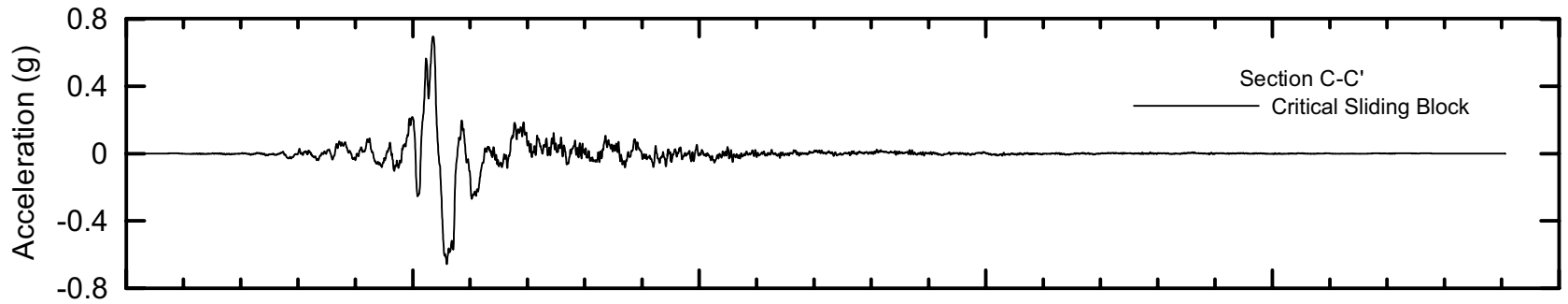
Project No. 26814957	Estates Dam Seismic Stability Analysis	Profile of Critical 3-D Sliding Block on Longitudinal Section at Offset = 110 ft 3-D Slope Stability Analysis	Figure 13-9
URS			



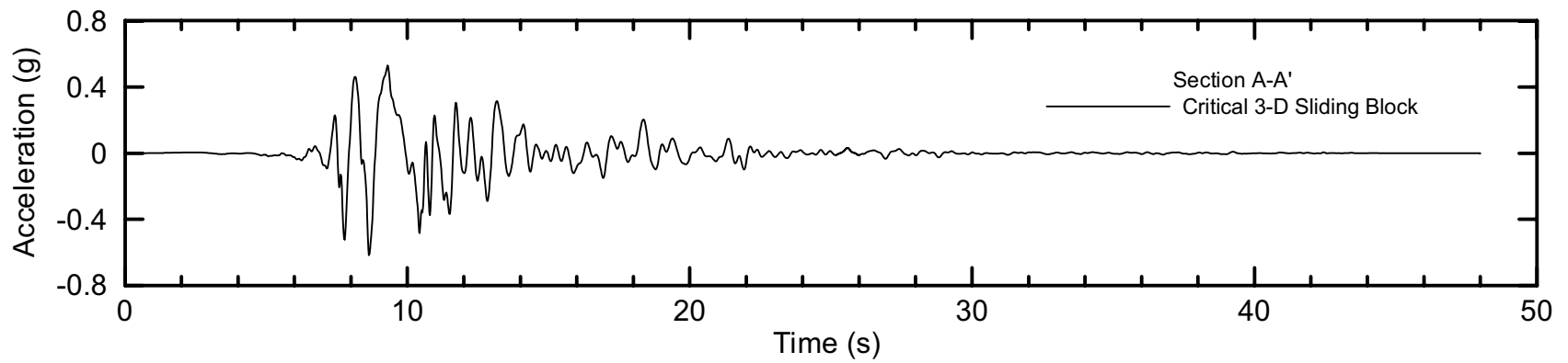
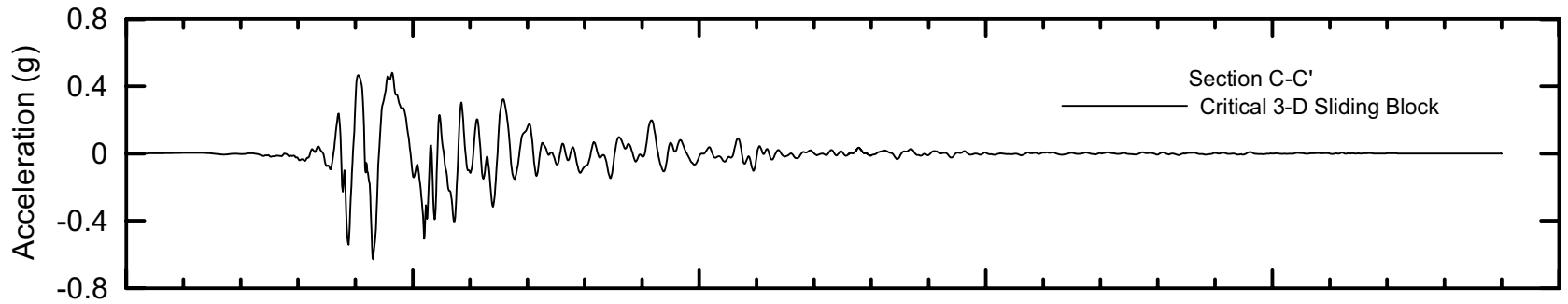
Project No. 26814957	Estates Dam Seismic Stability Analysis	Finite Element Mesh for QUAD4M Analysis Cross-Section A-A' and Critical 3-D Sliding Surface	Figure
URS			13-10



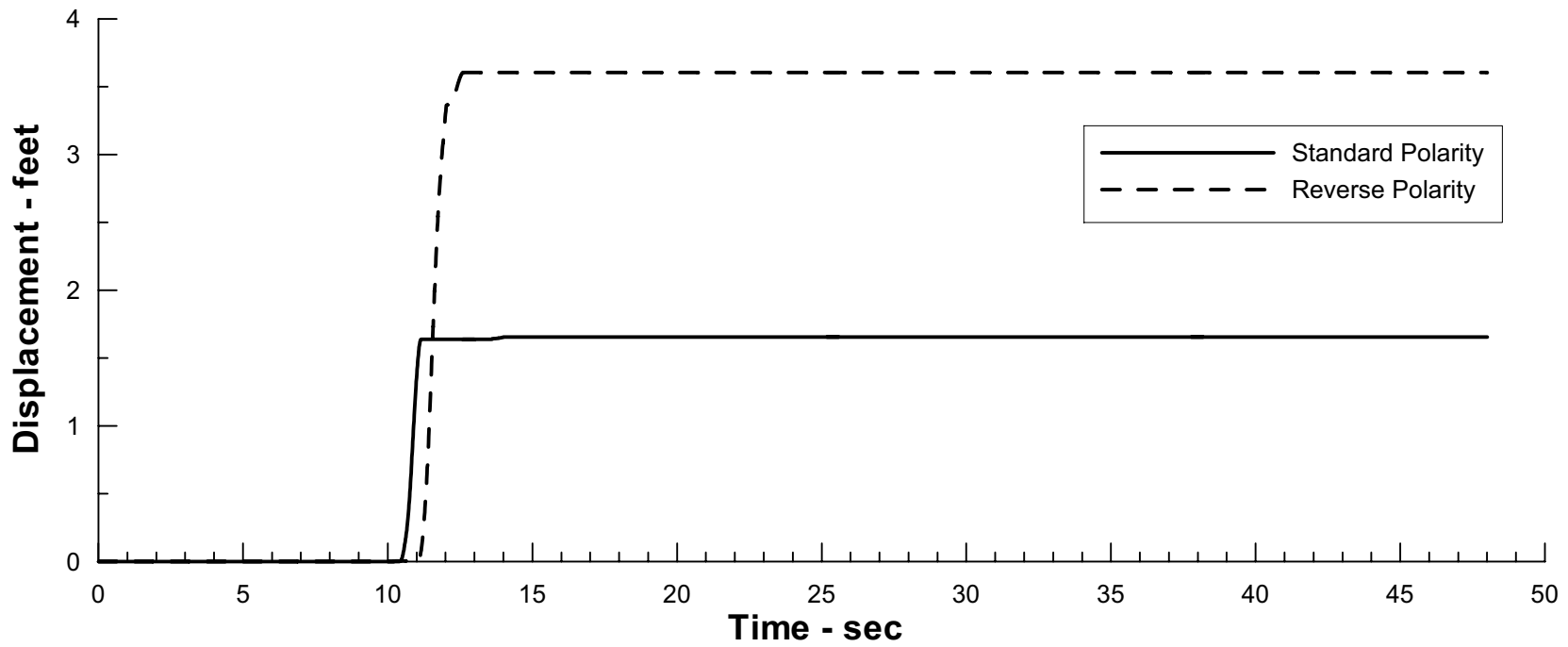
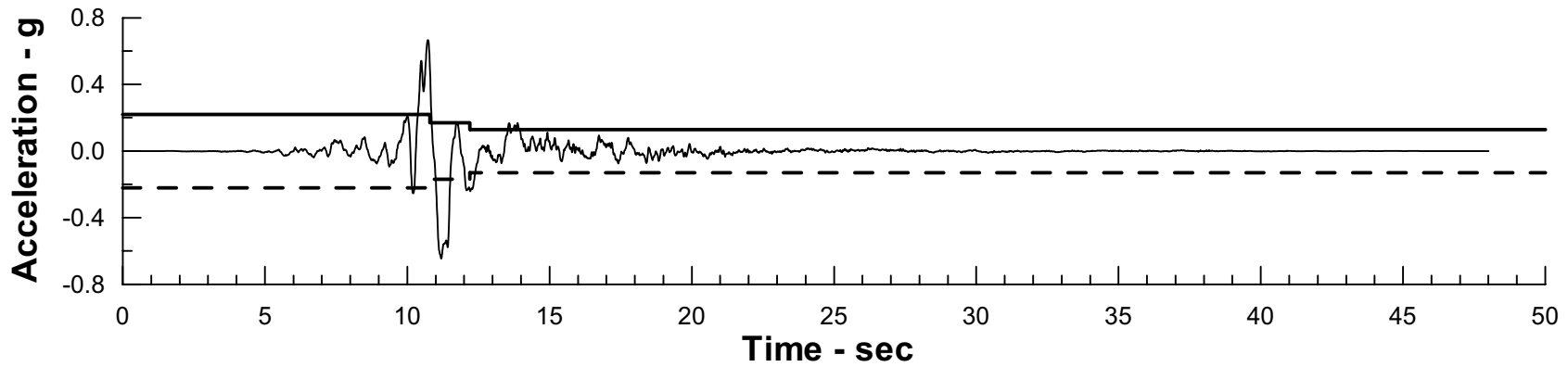
Project No. 26814957	Estates Dam Seismic Stability Analysis	Finite Element Mesh for QUAD4M Analysis Additional Cross-Section C-C' and Critical 3-D Sliding Surface	Figure
URS			13-11



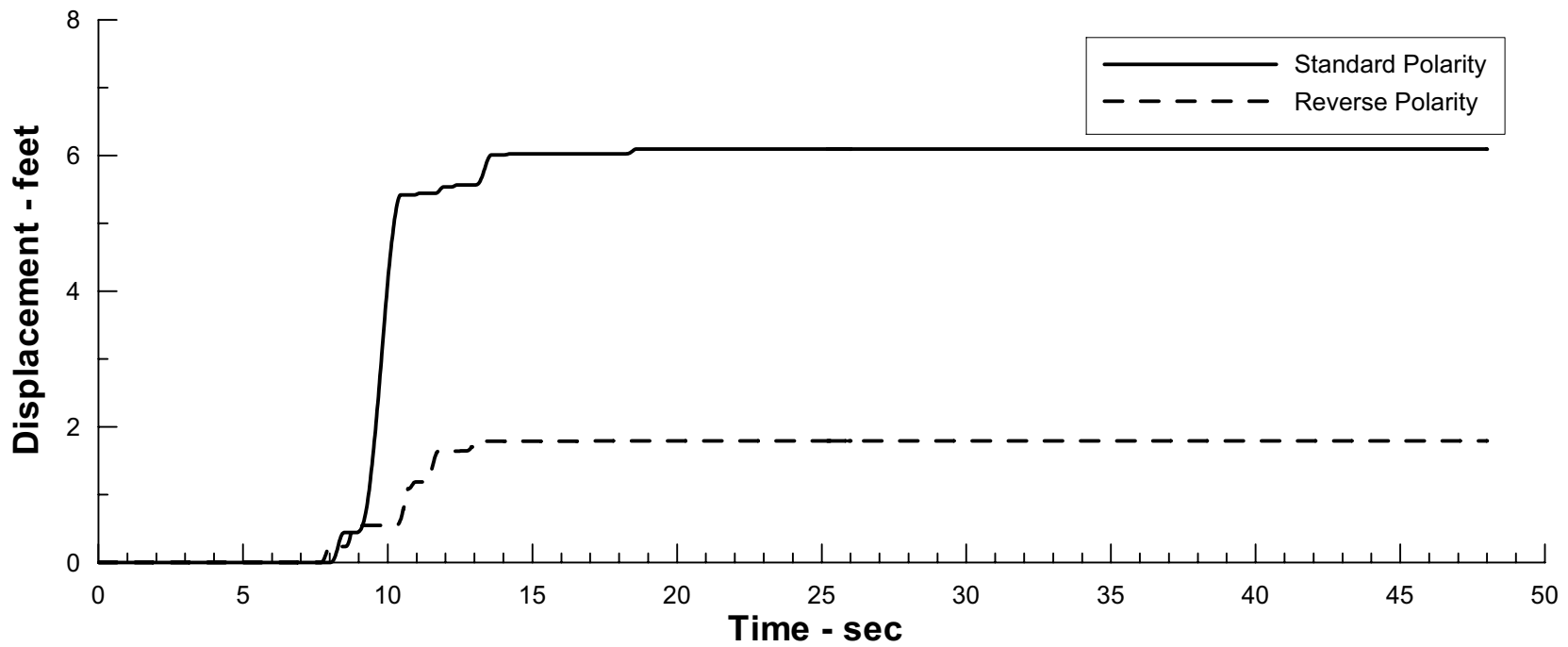
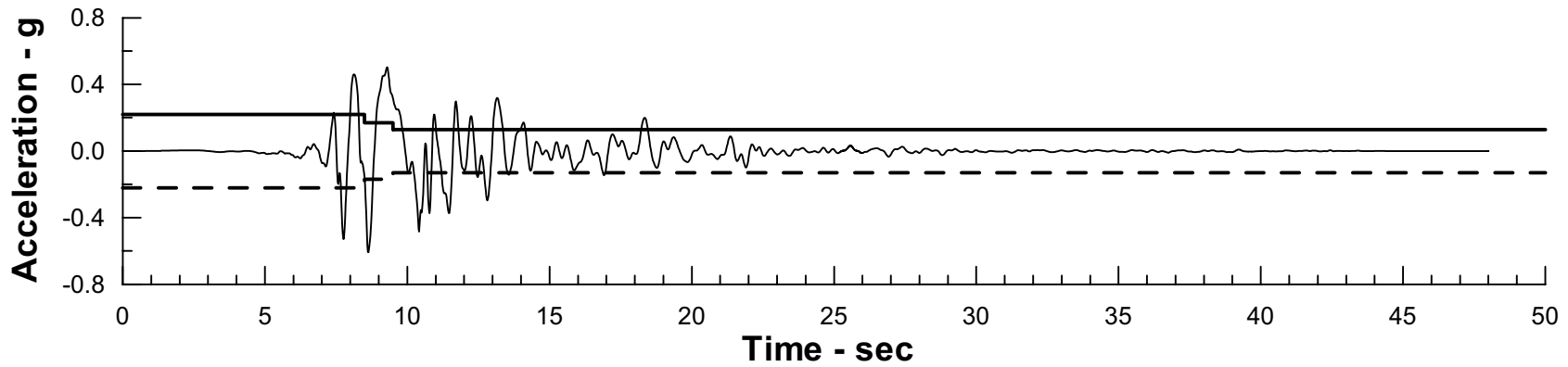
Project No. 26814957	Estates Dam Seismic Stability Check	Average Seismic Coefficient Downstream Blocks QUAD4M Analysis Hayward Fault MCE TH #1	Figure 13-12
URS			



Project No. 26814957	Estates Dam Seismic Stability Check	Average Seismic Coefficient Downstream Blocks QUAD4M Analysis Hayward Fault MCE TH #2	Figure 13-13
URS			



Project No. 26814957	Estates Dam Stability and Deformation Analysis	Newmark Deformation Analysis Calculated Displacement Critical 3-D D/S Sliding Block Hayward Fault MCE TH #1	Figure 13-14
URS			



Project No. 26814957	Estates Dam Stability and Deformation Analysis	Newmark Deformation Analysis Calculated Displacement Critical 3-D D/S Sliding Block Hayward Fault MCE TH #2	Figure
URS			13-15

The expected performance of the dam during the design earthquake was evaluated based on the analyses presented in Sections 11, 12 and 13. The analyses indicate that the design earthquake motions are likely to induce significant deformations of the dam. However, the dam is not expected to undergo gross instability during the shaking.

No liquefaction is expected within the embankment and foundation soils because of their overall clayey nature. However, the earthquake is likely to induce high excess pore water pressures in these materials in zones of limited extent above the bedrock surface. The excess pore water pressures will be accompanied by some reduction in the strength of the materials in those zones.

The dam deformations calculated from the analyses are sensitive to the details of the input ground motion time histories. Accordingly, sensitivity analyses were performed with multiple input time histories to estimate the range of potential deformations and the average deformation response of the dam. Because the dam is located in a relatively narrow ravine, the height and cross-section geometry of the embankment vary markedly across the site between abutments. Thus, analyses were also performed to assess the effects of the dam's three-dimensional geometry on the calculated seismic deformations.

Horizontal displacements of the downstream slope of up to about 11 feet are calculated from two-dimensional Newmark-type analyses. The results of sensitivity analyses indicate that a representative average of the calculated displacements is about 7 feet. The 2-D Newmark-type analyses also result in upstream horizontal displacements of the upstream slope of up to 6 feet.

Two-dimensional finite difference analyses with the computer program FLAC yield downstream horizontal displacements of up to 12 feet with an overall representative average of about 8 feet. A representative average of the calculated crest settlement is about 5 to 6 feet. The FLAC analyses indicate that the principal mechanism of embankment deformation is downstream block displacement resulting from shear within a relatively thin zone in the 1903 fill and foundation soil just above the bedrock contact. This mechanism seems intuitive in view of the fact that the bedrock surface slopes downstream beneath the embankment. Thus, based on the FLAC analyses, no upstream displacements of the embankment are expected to develop. Because the FLAC analyses are significantly more refined than the Newmark-type analyses, they are viewed as offering a greater degree of reliability.

Three-dimensional slope stability analyses result in calculated factors of safety that are significantly higher than those calculated from 2-D analyses. Furthermore, the 3-D analyses result in calculated downstream horizontal displacements that are on the average about two-thirds of those calculated from 2-D analyses. This is because the longitudinal extent of potential failure surfaces within the dam is constrained by the abutments, and deviates considerably from that implicit in 2-D analysis conditions. The limited extent of a failure surface leads to an increase in the forces resisting movement relative to the driving forces, as the thinner side sections of the slide mass provide a restraining effect over its thicker central section.

Based on the analysis results and considering the limitations of the methods of analysis, the best estimate of the maximum crest vertical displacements for the Hayward fault MCE is between 3 and 4 feet. Likewise the best estimate of the maximum horizontal displacements of the downstream slope is about 6 feet. The maximum crest settlements correspond to about 5% to 6.5% of the structural dam height. Such settlement ratios are near the upper end of the range observed in embankment dams during past earthquakes in the absence of gross instability. In view of the estimated crest settlements, the minimum available dam freeboard of 4 feet is not

judged to provide an adequate margin against potential overtopping of the embankment, if the reservoir were to be full during the design earthquake.

The estimated settlements and horizontal deformations will likely result in cracking of the upstream face lining, and possibly of the dam embankment near the crest. Longitudinal cracks may form at the crest in response to the lateral deformation of the embankment. Settlements of the embankment may also lead to transverse cracking at the crest. Although a detailed analysis of potential cracking has not been made, based on past observations of embankment dam earthquake performance (e.g. Fong and Bennett, 1995), the most likely location for transverse cracking, if it occurs, is near the abutments.

The downstream displacements of the embankment will likely disrupt the tile drain system installed between the 1903 and the 1938-39 fills, and may also affect the spillway overflow and inlet/outlet pipes and nearby subsurface drains. Disruption of the tile drain system is unlikely to lead to dam instability immediately after the earthquake, but with time could lead to elevated phreatic levels within the downstream slope. The downstream displacements may also interrupt vehicle access to the Montclair pumping plant, although it is understood from EBMUD that this is not a significant issue.

The spillway overflow pipe is located near the right abutment as shown in Figure 3-2. From manhole No. 1 to manhole No. 2 the pipe runs at a depth of about 5 feet below the ground surface. The estimated location of the pipe in section is shown in Figures 13-7 through 13-9. The foundation conditions beneath the pipe are not well known. Between the dam crest and the bend at the right dam groin (see Figure 3-2), the pipe appears to be founded near the bottom of the embankment fill or in natural ground, whereas downstream of the bend it is founded in natural ground. Based on its location, it seems unlikely that the pipe will be subjected to large ground displacements. However, small displacements are possible in response to the estimated displacements near the center of the downstream slope. Because of its steel construction, the pipe is likely to be capable of withstanding displacements of a few inches, although an in-depth assessment of this issue has not been made.

The inlet/outlet pipe is located near the left abutment as shown in Figure 3-2. The approximate location of the pipe is shown in Figures 13-7 through 13-9. It appears that beneath the dam crest the pipe is founded on bedrock. Downstream of the crest, the pipe foundation appears to transition from bedrock to foundation soil, to possibly embankment fill near the pumping plant. The available construction records indicate that the pipe was laid in a trench through the embankment and foundation materials and was encased in concrete from the reservoir inlet to the pumping plant. Based on the excavation slopes, it appears that the bottom of the trench was cut through competent materials. In view of its location, it seems unlikely that the pipe will be subjected to large displacements. However, small displacements are possible in response to the estimated displacements of the downstream slope, particularly where the pipe approaches the pumping plant. Because the pipe is of cast iron construction, it may not be able to tolerate displacements greater than a few inches without damage. Although rupture of the pipe is possible, the extent of damage to the pipe would be limited by the concrete encasement, and potential erosion from pipe leakage would likely be localized to the near-surface materials in the area of the pumping plant.

There is no evidence of Holocene activity in possible minor faults or shears in the Franciscan rock units at the site, either as independent faults or as structures that exhibit coseismic

movement with earthquakes on the Hayward fault. Accordingly, the potential for fault rupture at the dam site is judged to be very small.

The analyses for the San Andreas fault MCE result in a dynamic response of the embankment lower than that calculated for the Hayward fault MCE. The calculated dam deformations for the San Andreas event are lower than those for the Hayward event. Thus, the results of the analyses indicate that the San Andreas event is less critical than the Hayward event regarding the seismic stability of the dam.

The purpose of this study was to evaluate the seismic stability of Estates Dam. The study included a review of previous engineering investigations and geologic studies of the dam, geologic mapping of the site, field exploration and laboratory testing of the embankment and foundation materials, evaluation of the design earthquake ground motions, analyses of seismic stability and deformations, and assessment of the overall expected dam seismic performance. The main conclusions from the study are summarized as follows.

The dam and reservoir are located at the head of a narrow ravine. The main body of the dam embankment was placed in 1903 and consists predominantly of clayey sands and sandy clays with gravel, placed and compacted by horse-drawn equipment. The dam was raised between 1938 and 1939 to its present configuration using similar materials, compacted with a sheepsfoot roller. The foundation consists of colluvium and residual soils and underlying bedrock of the Franciscan Complex.

Because of their clayey nature, the embankment and foundation soils will exhibit cohesive behavior under earthquake shaking and are not susceptible to liquefaction. However, they may develop excess pore pressures and undergo strength loss under strong earthquake shaking. The foundation soils have similar strength characteristics as the 1903 embankment fill while the bedrock is much stronger.

The dam is located within 0.3 km of the Hayward fault and 29 km of the San Andreas fault. The Hayward-Rodgers Creek fault is judged capable of generating a maximum earthquake of magnitude M_w 7¼. The San Andreas fault is judged capable of a M_w 8 earthquake. In accordance with DSOD guidelines, the ground motions from these earthquakes were estimated at the 84th-percentile level. The ground motions for the MCE on the Hayward fault are associated with a peak horizontal ground acceleration (PGA) of 1.06 g whereas those for the San Andreas fault MCE correspond to a PGA of 0.35 g. No active faults underlie the dam and the potential for sympathetic fault movements beneath the dam is judged to be very small.

The results of the analysis indicate factors of safety for the upstream and downstream slopes that are consistent with the known long-term stability of the dam. The dam should perform satisfactorily during small to moderate earthquakes.

The analyses for the San Andreas fault MCE result in calculated dam deformations that are lower than those for the Hayward event. Thus, the results of the analyses indicate that the San Andreas event is less critical than the Hayward event regarding the seismic stability of the dam. The calculated response of the dam for motions representative of those expected to have occurred at the site during the 1989 Loma Prieta earthquake is in good agreement with the known performance of the dam during that earthquake.

The dam deformations calculated for the Hayward fault MCE are sensitive to the details of the input acceleration time histories used to represent the earthquake motions. Because the dam is located in a relatively narrow ravine, the height and cross-section geometry of the embankment vary markedly across the site between abutments. Accordingly, 3-D analyses were necessary to assess the effects of the dam's three-dimensional geometry on the calculated seismic deformations. Three-dimensional slope stability analyses result in calculated factors of safety that are significantly higher than those calculated from 2-D analyses. Furthermore, the 3-D analyses result in calculated downstream horizontal displacements that are on the average about two-thirds of those calculated from 2-D analyses.

Based on the analysis results and considering the limitations of the methods of analysis, the best estimate of the maximum crest vertical displacement for the Hayward fault MCE is between 3 and 4 feet. Likewise the best estimate of the maximum horizontal displacement of the downstream slope is about 6 feet. The principal mechanism of embankment deformation is downstream block displacement resulting from shear within a relatively thin zone in the 1903 fill and foundation soil just above the bedrock surface. No upstream displacements of the embankment are expected to develop. The maximum crest settlement corresponds to about 5% to 6.5% of the structural dam height. Such settlement ratios are near the upper end of the range observed in embankment dams during past earthquakes in the absence of gross instability.

The estimated settlements and horizontal deformations will likely result in cracking of the upstream face lining, and possibly of the dam embankment near the crest. In view of the estimated crest settlements, the minimum available dam freeboard is not judged to provide an adequate margin against potential overtopping of the embankment, if the reservoir were to be full during the design earthquake.

The downstream displacements of the embankment may affect the spillway overflow and inlet/outlet pipes and nearby subsurface drains. Based on its location, it seems unlikely that the spillway pipe will be subjected to large ground displacements. However, small displacements are possible in response to the estimated overall displacements of the downstream slope. Because of its steel construction, the pipe is likely to be capable of withstanding displacements of a few inches, although a detailed assessment of this issue has not been made.

It also seems unlikely that the inlet/outlet pipe will be subjected to large displacements. However, small displacements are possible in response to the estimated displacements of the downstream slope, particularly where the pipe approaches the pumping plant. Because the pipe is of cast iron construction, it may not be able to tolerate displacements greater than a few inches without damage. Although rupture of the pipe is possible, the extent of damage to the pipe would be limited by the concrete encasement, and potential erosion from pipe leakage would likely be localized to the near surface materials in the area of the pumping plant.

In view of the available freeboard, it may be concluded that the potential crest settlements and horizontal embankment displacements during the design earthquake represent a significant risk regarding the safety of the structure. Damage to the embankment is likely to require drawdown of the reservoir immediately after the earthquake.

- Abrahamson, N.A. (1993). "Non-Stationary Spectral Matching Program RSPMATCH," Unpublished Report, July.
- Abrahamson, N.A. and Silva, W.J. (1997). "Empirical response spectral attenuation relations for shallow crustal earthquakes," *Seismological Research Letters*, v. 68, p. 94-127.
- Abrahamson, N.A. (2000) "Effects of rupture directivity on probabilistic seismic hazard analysis," Proceedings of the 6th International conference on Seismic Zonation, Palm Springs, California.
- Boore, D.M., Joyner, W.B., and Fumal, T.E. (1997). "Equations for estimating horizontal response spectra and peak acceleration from western North American earthquakes: A summary of recent work," *Seismological Research Letters*, v. 68, p. 128-153.
- Boulanger, R.W. and Idriss, I.M. (2004). "Evaluating the potential for liquefaction or cyclic failure of silts and clays," Center for Geotechnical Modeling, Report No. UCD/CGM-04/01, University of California, Davis, December.
- Duncan, J.M., Wright, S.G. and Wong, K.S. (1990) "Slope stability during rapid drawdown," Proc., H.B. Seed Memorial Symp., BiTech, Vancouver, B.C., (2), 253-272.
- Fong, F.C. and Bennett, W.J. (1995) "Transverse cracking on embankment dams due to earthquakes," presented at the Association of State Dam Safety Officials (ASDSO) Western Regional Seminar and Conference, Red Lodge, Montana, May.
- Fraser, W.A. and Howard, J.K. (2002), "Guidelines for use of the Consequence-Hazard Matrix and selection of ground motion parameters," The Resources Agency, Department of Water Resources, Division of Safety of Dams.
- Hudson M., Idriss, I.M. and Beikae, M. (1994) "User's manual for QUAD4M," Department of Civil and Environmental Engineering, University of California, Davis, California, May.
- Hungr, O. (1988) "User's manual, CLARA, slope stability analysis in two or three dimensions for IMB compatible microcomputers," December.
- Idriss, I.M. (1985) "Evaluating seismic risk in engineering practice," Proceedings 11th International Conference on Soil Mechanics and Foundation Engineering, San Francisco, August.
- Itasca, (2000). "FLAC, fast lagrangian analysis of continua, version 4.0, user's guide," Itasca Consulting Group, Inc., Thrasher Square East, 708 South Third Street, Suite 310, Minneapolis, Minnesota.
- Jones, S. (2003) "Seismic stability, Estates Dam, No. 31-10, Alameda County," Memorandum of design review, Division of Safety of Dams Memorandum, September.
- Lee, K.L. and Focht, J.A. (1976) "Strength of clay subjected to cyclic loading," *Marine Geotechnology*, Vol 1, No. 3, pp 165-185.
- Lienkaemper, J.J. (1992) "Map of recently active traces of the Hayward fault, Alameda and Contra Costa Counties, California," USGS Miscellaneous Field Studies Map MF-2196.

- Lilhanand, K. and Tseng, W.S. (1988). "Development and application of realistic earthquake time histories compatible with multiple-damping design spectra," Proceeding of the 9th World Conference on Earthquake Engineering, Tokyo-Kyoto, Japan, August.
- Mejia, L.H. (1989) "Three-dimensional stability of an old dam," Proceedings 12th International Conference on Soil Mechanics and Foundation Engineering, Rio de Janeiro, August.
- Sadigh, K., Chang, C.Y., Egan, J.A., Makdisi, F., and Youngs, R.R. (1997). "Attenuation relationships for shallow crustal earthquakes based on California strong motion data," Seismological Research Letters, v. 68, p. 180-189.
- Schnabel, P.B., Lysmer, J. and Seed, H.B. (1972) "SHAKE: A computer program for earthquake response analysis of horizontally layered sites," Report No. UC/EERC-72/12, Earthquake Engineering Research Center, University of California, Berkeley, December.
- Seed, H.B., and Idriss, I.M, (1970). "Soil moduli and damping factors for dynamic response analyses," Report No. EERC 70-10, Earthquake Engineering Research Center, University of California, Berkeley.
- Seed, H.B. (1979) "Soil liquefaction and cyclic mobility evaluation for level ground during earthquakes," Journal of the Geotechnical Engineering Division, ASCE, Vol. 105 No. GT2, pp 201-255.
- Seed, H.B. (1979) "Considerations in the earthquake-resistant design of earth and rockfill dams," Geotechnique, 29(3), Sept., pp 215-263.
- Seed, H.B. and Idriss, I.M. (1982) "Ground motions and soil liquefaction during earthquakes," EERI Monograph, Earthquake Engineering Research Institute.
- Seed, R.B., Cetin, K.O., Moss, R.E.S., Kammerer, A., Wu, J., Pestana, J., Riemer, M., Sancio, R.B., Bray, J.D., Kayen, R.E. and Faris, A. (2003) "Recent advances in soil liquefaction engineering: a unified and consistent framework," Report No. EERC 2003-06, (originally presented at 26th Annual ASCE Los Angeles Geotechnical Spring Seminar, Keynote Presentation, H.M.S. Queen Mary, April 30, 2003, Long Beach, CA), Earthquake Engineering Research Center, University of California, Berkeley, June.
- Shannon and Wilson, Inc. (1965)a "Review of Stability of Estates Reservoir, Oakland, California," report prepared for EBMUD, October.
- Shannon and Wilson, Inc. (1965)b "East Bay Municipal Utility District Piedmont No. 1 Reservoir Embankment Stability Evaluation," report prepared for EBMUD (field and laboratory data), May.
- Somerville, P.G., Smith, N.F., Graves, R.W., and Abrahamson, N.A. (1997). "Modification of empirical strong ground motion attenuation relations to include the amplitude and duration effects of rupture directivity," Seismological Research Letters, V. 68, n.1, pp. 199-222.
- Thiers, G.R. and Seed, H.B. (1969) "Strength and stress-strain characteristics of clays subjected to seismic loads," Symposium on Vibration Effects of Earthquakes on soils and Foundations, ASTM STP 450, pp 3-56.

- URS (2005) "Dynamic stability analysis of Chabot Dam, Alameda County, California," Client report prepared for EBMUD, October.
- Wells, D.L. and Coppersmith, K.J., (1994) "New empirical relationships among magnitude, rupture length, rupture width, rupture area, and surface displacement," Bulletin of the Seismological Society of America, v. 84, p. 974-1002.
- Wahler Associates (1980) "Seismic reevaluation of Estates Reservoir Dam," report prepared for EBMUD, June.
- Woodward-Clyde Consultants (1989) "Seismic Safety Evaluation, Lake Madigan Dam, Solano County, California," Client report prepared for City of Vallejo, July.
- Wright, S.G. (1991) "UTEXAS3, a computer program for slope stability calculations," Shinoak Software, Austin, Texas.



URS

URS Corporation
1333 Broadway, Suite 800
Oakland, CA 94612

26814957.E0000